ACCESSIBLE MICROFLUIDIC DEVICES FOR STUDYING ENDOTHELIAL CELL BIOLOGY

by

Edmond Wai Keung Young

A thesis submitted in conformity with the requirements

for the degree of Doctor of Philosophy

Graduate Department of Mechanical & Industrial Engineering

University of Toronto

Your file Votre référence
ISBN: 978-0-494-59169-7
Our file Notre référence
ISBN: 978-0-494-59169-7

Thesis Title: Accessible Microfluidic Devices for Studying Endothelial Cell Biology

Degree and Year: Doctor of Philosophy, 2009

Name: Edmond Wai Keung Young

Department: Mechanical & Industrial Engineering

University: University of Toronto

Abstract

Endothelial cells (ECs) form the inner lining of all blood vessels in the body, and coat the outer surfaces of heart valves. Because ECs are anchored to extracellular matrix proteins and are positioned between flowing blood and underlying interstitium, ECs are constantly exposed to hemodynamic shear, and act as a semi-permeable barrier to blood-borne factors. *In vitro* cell culture flow (ICF) systems have been employed as laboratory tools for testing endothelial properties such as adhesion strength, shear response, and permeability. Recently, advances in microscale technology have introduced microfluidic systems as alternatives to conventional ICF devices, with a multitude of practical advantages not available at the macroscale. However, acceptance of microfluidics as a viable platform has thus far been reserved because utility of microfluidics has yet to be fully demonstrated. For biologists to embrace microfluidics, engineers must validate microscale systems and prove their practicality as tools for cell biology. Microfluidic devices were designed, fabricated, and implemented to study properties of two EC types: aortic ECs and valve ECs. The objective was to streamline experimentation to reveal phenotypic traits of the two types and in the process demonstrate the usefulness of microfluidics. The first task was to develop a protocol

to isolate pure populations of valve ECs because reported methods were inadequate. Dispase and collagenase in combination for leaflet digestion followed by clonal expansion of cell isolates was optimal for obtaining pure valve EC populations. Using a parallel microfluidic network, we discovered that valve ECs adhered strongly and spread well only on fibronectin and not on type I collagen. In contrast, aortic ECs adhered strongly on both proteins. Both aortic and valve ECs were then exposed to shear and analyzed for cell orientation. Morphological analyses showed aortic and valve ECs both aligned parallel to flow when sheared in a macroscale flow chamber, but aortic ECs aligned perpendicular to flow when sheared in a microchannel. Finally, a microfluidic membrane device was designed and characterized as a potential tool for measuring albumin permeability through sheared endothelial monolayers. Overall, these studies revealed novel EC characteristics and phenomena, and demonstrated accessibility of microfluidics for EC studies.

Acknowledgements

The last three years of my Ph.D. program (and my stay in Toronto) have been the most memorable, fun, and enlightening years of my life, and many people are to thank for their part in making it an unforgettable experience. First and foremost, I am indebted to my supervisors, Drs. Craig Simmons and Aaron Wheeler, for whom I have the highest regard and utmost respect. I especially thank Craig for taking a chance on me and on my project when I most needed support, for providing countless opportunities through collaborations, conferences and other offers, and for his guidance, encouragement and friendship. I believe it is dedicated and talented people like Craig who truly make a difference in the world, and I am grateful we shared this experience together. I thank Aaron for always having an open door, bringing positive energy and showing limitless enthusiasm everytime we meet. I have learned invaluable lessons from you both, academic and otherwise, and I feel privileged to have been a part of your groups and your research. I look forward to hearing your many successes in the very near future.

I thank all my labmates, past and present, "Simmonsonians" and "Wheelerites" alike. The camaraderie I shared with many of you was special, and I would not have survived graduate school without your support, friendship, and good humour; I hope our friendships last forever. I especially thank Jan, Chris, Derek, Kristine, and Cindy, who were a part of the Simmons Group from the very beginning. To Jan – remember, live to eat; to Chris – thank you for being the microfabrication guru, and I agree that size does matter; to Derek – my "heart" goes out to you; and to Kristine and Cindy – you are my bad idea bears. To Kelly,

Krista, Ruogang, Morakot, and Zahra – thank you for making the Simmons Group dynamic what it is.

To the Wheeler Group, I especially thank Mohamed, not only for his assistance with microfabrication and for stimulating discussions on engineering and teaching, but also for taking every step of this journey with me for the last three years. I cannot help but feel we were meant to walk this path together. I thank Beth for lending an ear, sharing a beer, and just being Beth. To Mike, I thank you for unleashing the analytical chemist in me, for being a partner on the permeability work, and for teaching me how to display "levity in all situations" (only Mike will really know what I mean). To Sergio, Irena, Lindsey, Mais, Vivienne, Nikoo, Steve, Mark, Sam and Andrea, thank you for being great citizens of the Wheeler Lab.

I wish to thank the undergraduate students who worked with me: Baosen, Maged, Wing-Yee, Suthan, George, and Rachel. Some of you have gone on to bigger and better things already, and the rest of you will no doubt do so in the near future. To Wing-Yee and Suthan especially, I thank you for all your hard work and dedication to the cause. Your efforts are seen throughout this thesis, and I could not have done it without you. I only hope that you have learned as much from me as I have learned from you.

I thank all the collaborators I have worked with, especially Dr. Lowell Langille for serving on my committee, generously donating cells to my cause, and supporting the microfluidics work with passion. I thank Marc Chrétien and Dan Trcka for sharing lab space, microscopes, and endothelial cell know-how. I also thank Dr. Axel Guenther for offering microfabrication facilities and serving on my committee, Dr. Myron Cybulsky for agreeing to step into the committee on short notice, and Dr. Dana Spence for taking time to

act as the external examiner. And I thank Dr. Christopher McCulloch, Dr. Eugenia Kumacheva, Dr. Rita Kandel, Wei Li, and Caroline Spiteri for involving me in their research work.

I wish to thank Frances Yeung, who provided wonderful illustrations for the thesis, and helped inject some much-needed colour into the work. And I thank all my wonderful friends in Toronto for providing me a life in Toronto outside of the lab, and for caring about my research (once in a while).

And last but not least, I thank my family: Mom and Dad; Eva, Wally, and Amanda; Sandra, Stan, Olivia, and Quinton; and Helen, Ray and Sabrina, for their love, unwavering support and faith in me. I do not know how to fully express my gratitude for everything you have done and everything you mean to me. I know you will understand me even when I am lost for words.

Overview of Contributions

The work presented in this thesis would not have been possible without the help, support, and guidance from many labmates and collaborators. They devoted many long hours to help me along the way, and it was a privilege working with all of them. In this section, I present a detailed record of all their contributions, as well as my own, in developing methodologies, setting up instrumentation, and running experiments.

Chapter Four describes experiments completed during the development of a technique to isolate and purify porcine aortic valve endothelial cells. This work was largely carried out by Wing-Yee Cheung, whom I supervised together with Dr. Craig Simmons from May 2006 to April 2007 when she was an undergraduate thesis student. I proposed the use of dispase in combination with collagenase as a possible solution to previously high levels of interstitial cell contamination, and she performed all the isolation experiments that resulted in published data. I was responsible for purification using MACS cell sorting, while Wing-Yee did all the work on clonal expansion, with guidance from Jan-Hung Chen. Together, Wing-Yee and I wrote and published an article in the *Journal of Heart Valve Disease* in the summer of 2008 summarizing this work.

Chapter Five describes the development of a microfluidic system for studying endothelial cell adhesion, and a series of experiments to test adhesion of two endothelial cell types. I was responsible for all aspects of this study, including design and fabrication of masters and microfluidic devices, endothelial cell culture, experimental design, protocol development, microchannel characterization by flow visualization, fluid flow analyses,

experimental setup, and statistical and all subsequent data analyses. This work was also published, in *Lab on a Chip* in the summer of 2007.

Chapter Six describes experiments for testing shear stress response of endothelial cells in macroscale parallel plate flow chambers, and in microfluidic channels. All experiments with parallel plate flow chambers were carried out by Suthan Srigunapalan, whom I supervised together with Dr. Craig Simmons from May 2007 to August 2008 when he was an undergraduate thesis student. Parallel plate flow chambers were fabricated at the University of Toronto Mechanical and Industrial Engineering machine shop by Jan-Hung Chen and Samir Raza in 2005, and were tested rigorously by Jan and Samir. I helped test and troubleshoot the flow chambers in a series of preliminary experiments prior to Suthan's arrival. Suthan carried out all macroscale flow chamber experiments and post-shear analyses presented in this thesis. For microfluidic experiments, I was responsible for designing and implementing the microflow recirculatory experiment, with helpful discussions from Omar Khan. I made microfluidic channels for all experiments, set up flow experiments, designed the experimental protocol, fixed and immunostained cells within microchannels and performed all subsequent analyses. Live-cell imaging experiments were carried out in the laboratory headed by Dr. Lowell Langille using his microscope setup. Marc Chrétien was the resident graduate student in the Langille Lab responsible for setting up the microscope and imaging procedures. Suthan and I were responsible for culturing cells in microchannels, transporting samples to the Langille Lab, and setting up the flow experiments.

Chapter Seven describes the development and implementation of a membrane-based microfluidic device for studying endothelial permeability. This work would not have been possible without the collaboration, support, and insight of Mike Watson, a graduate student

in the Wheeler Lab. I designed and fabricated all membrane microfluidic devices for this study, with assistance from Suthan Srigunapalan, Rachel Tonelli-Zasarsky, and Mike Watson for PDMS casting. I used established membrane fabrication procedures from the literature and I made minor modifications for my own work. I performed experiments to characterize membrane adhesion, and devised perfusion protocols for maintaining long-term cell culture in microfluidic devices. Mike Watson was solely responsible for assembling the microscope and laser-induced fluorescence setup. Together, Mike and I devised the experimental protocol for applying flow rate ratios to the top and bottom microchannels, monitored fluorescence measurements, and troubleshooted experimental issues. I developed the analytical model that involves combining Darcy's law with a mixing equation, while Mike and I were both involved in all other aspects of data interpretation and experimental design.

Finally, I would like to acknowledge the regular helpful discussions I had with Christopher Moraes, Mohamed Abdelgawad, Lindsey Fiddes, and Yali Gao for all microfabrication-related issues.

Table of Contents

List of Figures

List of Tables

To Mom and Dad,

for always believing in me.

Chapter 1

1 Introduction

The endothelium is a single layer of cells that lines all blood-contacting surfaces of the cardiovascular system. The endothelial cells (ECs) that compose the endothelium form cell-cell contacts with their neighbours and organize into a contact-inhibited cellular lining that is selectively permeable to nutrients and molecules of the blood. ECs are exposed to flowing blood on their luminal side and are anchored to a basement membrane (*basal lamina*) on their abluminal side. Because of their anatomic location, ECs experience a multitude of mechanical forces from the surrounding microenvironment. Hemodynamic forces from the luminal blood and adhesive forces between cell-surface anchoring proteins (*integrins*) and the basal lamina are part of a complex set of signals that are known to regulate vascular function through a myriad of mechanotransduction pathways. Mechanical cues from the local EC environment are thus responsible for biological responses at the molecular level, and ultimately, changes in cellular structure and function that include

adjustments in cell morphology, cytoskeletal arrangement, cell-cell adhesion properties, cell permeability, and the release of specific cytokines. The particular combination and the nature and magnitudes of the mechanical stimuli together play a major role in determining whether vascular homeostasis is maintained, or whether cardiovascular pathologies such as atherosclerosis and aortic valve sclerosis will eventually develop.

Understanding mechanobiology of the endothelium requires engineered tools that can maintain ECs in a healthy and controlled culture environment while exposing them to mechanical stimuli. Such controlled *in vitro* experimentation is necessary to complement *in vivo* approaches that are often less effective at isolating specific causal factors, even though they more closely represent physiological conditions. Over the last quarter century, many *in vitro* systems have been developed to study ECs under physical force. The majority of these systems incorporate fluid flow over adhered, confluent EC monolayers to mimic the hemodynamic shear stress experienced by ECs in their native environments. These *in vitro* cell culture flow (ICF) systems form a broad class of tools with varied designs tailored to answer specific questions about EC behaviour under physical stress. Much of our current understanding of endothelial mechanotransduction is attributable to the research work performed using a handful of well-characterized shear flow devices that have become mainstays in typical endothelial cell biology laboratories.

Despite their widespread usage, current ICF systems have significant drawbacks. ICF systems are typically custom-designed and require precision machining, so designs cannot be easily modified once the system has been fabricated. Some systems are available from commercial machine shops (e.g., parallel plate flow chambers from Whitehaus Precision Machining, Hummelstown, PA), but stringent tolerances of these devices can lead to high

manufacturing costs. ICF systems also require connections to a fluid flow circuit that typically include components such as pumps, controllers, tubing, and fluid reservoirs. Thus, these systems have large footprints, and either take up valuable space in temperature-controlled incubators or in some cases require dedicated rooms with controlled ambient conditions. Finally, limitations in available biological assays and cell culture techniques necessitate large EC populations to be grown and studied, which ultimately lead to large consumption of chemicals and reagents during experiments as well as during post-experiment processing. Altogether, these issues make efficient large-scale experimentation formidable because of cost and space limitations. Inability to experiment in a high-throughput manner is likely a major reason why scientific progress continues to be largely incremental, and significant research findings are not discovered sooner than what is currently achievable.

In the past decade, microfluidics has emerged as an advanced technology with wide-ranging capabilities for chemical, biological, and biomedical applications. Microfluidics is the study of fluid flow phenomena in micron-sized channels or capillaries. Fluid flow at the small length scale is dominated by viscous, interfacial, and diffusional forces that typically do not dominate at larger length scales. These forces allow for predictable laminar flow in complex channel networks, and introduce new strategies for manipulating, handling, detecting, and analyzing small discrete fluid samples and elements within these samples. The most notable advantages of microfluidics are its suitability for miniaturization and its potential to integrate multiple fluid handling processes on a single platform or *microchip* for high-throughput analyses, i.e., a "*lab-on-a-chip*". Thus, microfluidics can vastly improve

efficiency of experimentation, and bring forth new scientific discoveries in less time than by conventional large-scale methods.

The advantages of microfluidics can be exploited to study effects of mechanical forces on ECs. Laminar flow in microchannels is suitable for generating flow-induced shear stress on EC monolayers. Also, complex microfluidic networks can be designed to mimic the *in vivo* microenvironment of small capillary beds. The small length scales and minute sample volumes within microfluidic systems translate to reduced consumption of reagents. Furthermore, fabrication of microfluidic devices by soft lithography is efficient and economical. Short design-to-device turnaround times allow multiple configurations to be tested, making rapid prototyping an affordable option. Therefore, microfluidic systems have the potential to eliminate many of the aforementioned drawbacks associated with macroscale setups.

Reports on the application of microfluidics for EC biological studies have emerged from the vast body of microfluidics literature in the last few years. However, the reports to date have mostly focused on proof of principle, and often require special instrumentation and technical expertise for proper operation of the microfluidic systems. This has hindered acceptance from the biological research community that microfluidic tools are indeed practical alternatives to their macroscale counterparts. It is necessary to bridge this gap between microfluidics and EC biology so that developed technologies can be accessible to the intended end user. Thus, the main objective of this thesis is to demonstrate the flexibility and accessibility of microfluidic devices for endothelial cell biology, and to help assimilate microfluidics technology into the laboratories of endothelial cell biologists.

Chapter 2 reviews the literature on established macroscale ICF systems that have become standard equipment for EC biologists. The current state of the art in microfluidic systems for EC studies is also reviewed, and a comparison between macro- and microscale devices is presented. Chapter 3 summarizes the thesis objectives and lists the specific aims and hypotheses that were investigated. Chapter 4 presents techniques for isolating porcine aortic valve ECs, a cell type known to be important in regulating the development of aortic valve calcification leading to sclerosis. Isolating pure populations of aortic valve ECs allowed direct comparison to neighbouring ECs from the aortic root, and permitted the discovery of subtle but important differences between the two cell types. Chapter 5 discusses the first of a series of three microfluidic applications for EC biology, namely the use of a parallel multichannel microfluidic device to study cell adhesion between aortic and aortic valve ECs. The results of this study demonstrated how discovery of subtle cell type differences can be facilitated by high-throughput experimentation using microfluidics. Chapter 6 investigates morphological adaptations of ECs in macro- and microscale shear stress systems. Interesting findings on both platforms revealed new exploratory research directions that may have an impact on design of microfluidic devices as well as in fundamental mechanobiology. Chapter 7 proposes a multilayer membrane-based device for measuring albumin permeability through endothelial monolayers. The potential for this design to develop into a high-throughput screening platform have made this an interesting research endeavour. Lastly, Chapter 8 provides conclusions from this study, and recommendations for future work to further advance microfluidics technology for EC studies.

Chapter 2

2 Background – Literature Review

The main purpose of this review is to provide a comparison between different ICF systems used to study effects of mechanical forces on ECs. The focus is to discuss the basic principles of macro- and microscale systems, compare their advantages and disadvantages, and uncover new opportunities for developing novel technologies that have potential to both improve efficiency of experimentation (and ultimately scientific progress) as well as answer important biological questions that otherwise cannot be tackled with existing systems. To help understand the need for various designs of ICF systems, we first review briefly main properties of ECs and their native environments. We then divide the review into macro- and microscale systems, and categorize each apparatus by the endothelial characteristic for which the system was designed to study. In the end, we discuss outlook for technological advancements and propose studies that could have immediate impact on how biologists in the research community perceive the usefulness of microfluidic systems.

2.1 Endothelial Cells

Endothelial cells (ECs) form the intimal lining of all blood vessels, from arteries and veins to arterioles, venules and capillaries. ECs also cover outer surfaces of other cardiovascular tissues such as heart valves. Because of the diversity of locations, and the distinct physical properties of the local microenvironments in which ECs reside within the vasculature, ECs display well known structural and functional heterogeneity to suit the local needs of tissues within the body [1]. In this brief overview of the endothelium, we discuss the importance of phenotypic heterogeneity as an endothelial property, and demonstrate how heterogeneity pervades other important endothelial characteristics, such as adhesion strength, response to shear stress, and permeability.

2.1.1 Endothelial Heterogeneity

ECs *in vivo* display phenotypic heterogeneity in both structure and function [1, 2]. In arteries, ECs align parallel to the direction of blood flow, elongate to different aspect ratios depending on region, and are known to be less permeable to blood-borne factors than capillaries and veins [3]. In contrast, ECs in veins are polygonal instead of elongated in shape, lack specific orientation and are generally more permeable than those in the arterial system [2]. These distinguishable traits are closely correlated to differences in both the hemodynamic environments in which ECs reside and the functional purpose of the vessels to which they belong. Arteries are thick-walled and compliant, properties that allow them to deliver oxygenated blood directly and efficiently to capillary beds that require nutrients. Arterial ECs are thus exposed to higher average flow rate and shear stress compared to other ECs, but must maintain low permeability for blood to reach capillaries without depletion of

nutrient supplies. Veins on the other hand are thin-walled and are responsible for carrying deoxygenated blood back to the heart after blood has flown through highly resistive capillary networks. Venous ECs are therefore exposed to lower flow rate and shear stress compared to arterial ECs. Furthermore, ECs from post-capillary venules and veins have higher permeability due to fewer occluding and tight junctions [4], and are the primary sites for leukocyte trafficking and inflammatory responses [5]. Clearly, these distinctions between arterial and venous ECs demonstrate that heterogeneity is a function of location within the vasculature. As an added complication, ECs also display differences across species (e.g., human versus rat versus mouse), even when they are derived from similar vascular locations [6]. The notion of endothelial heterogeneity existing between locations and across species suggests that experimental findings from one EC type must be interpreted with caution when attempting to generalize to other EC types. These issues are discussed further through a specific example of endothelial heterogeneity in Section 2.1.6.

Endothelial heterogeneity has a large impact on *in vitro* experimentation of ECs. Because of the diversity of the endothelial population, specialized isolation techniques and characterization studies are necessary for each EC type, and a large body of work on such methods has been accumulated [7-11]. Perhaps the clearest example of endothelial heterogeneity *in vitro* was a comparative study of various ECs isolated from different organs of fetal pigs, which showed that typical markers of ECs, such as von Willebrand factor, Weibel-Palade bodies, uptake of acetylated low density lipoprotein (diI-ac-LDL), and cobblestone morphology were all organ- and tissue-specific [12]. Indeed, some eminent discoveries on the effects of mechanical stimuli on the endothelium can be generalized to all

ECs [13], but the above example of marker specificity between cell types is clear evidence of the diversity of the endothelium, even in *in vitro* systems.

Heterogeneity in endothelial structure inherently leads to similar diverseness in endothelial function. Three important biological properties of ECs that will be discussed in more detail throughout this thesis are adhesion properties, shear stress-induced responses, and permeability. Each topic itself provides an example of the multiformity of the endothelial population.

2.1.2 Adhesion and Integrins

ECs are anchorage-dependent cells that only function when adhered to a substrate. *In vivo*, ECs adhere to a basement membrane, or basal lamina, composed of various extracellular matrix (ECM) proteins that include varying amounts of fibronectin, vitronectin, type IV collagen, and laminin [14]. Adhesion is mediated at the cell surface by integrins, a family of transmembrane heterodimeric glycoproteins that physically link the ECM, the cell surface, and the intracellular cytoskeleton (Figure 2.1). Integrins are not only important for establishing focal adhesions as physical anchors to the ECM, but are also responsible in part for transducing mechanical signals generated by blood flow-induced shear stress [15]. Integrin expression levels and their distributions on the cell surface are cell type-specific. Immunohistochemical staining of different regions of the heart showed that ECs from distinct anatomic locations expressed integrins to varying degrees [16]. Because of this specificity, focal adhesions likely have varying strengths, and mechanical signals are likely transduced distinctly for different EC types. Mapping integrin expression of the diverse endothelial population is therefore of fundamental importance for understanding mechanisms of

mechanotransduction. Furthermore, adhesion strength of ECs to matrix proteins is particularly important for tissue engineering applications that require vascular endothelialization of scaffold materials or other biocompatible surfaces for potential implantation. Without proper EC adhesion on scaffold surfaces, tissue-engineered constructs may lack endothelial monolayer integrity, leading to loss of function and ultimately poor long-term performance [17]. Adhesion assays using ICF systems to measure binding affinity and strength of cells on a specific surface have been devised to measure adhesion properties so that we can better understand cell-matrix interactions between cell types and matrix protein components.

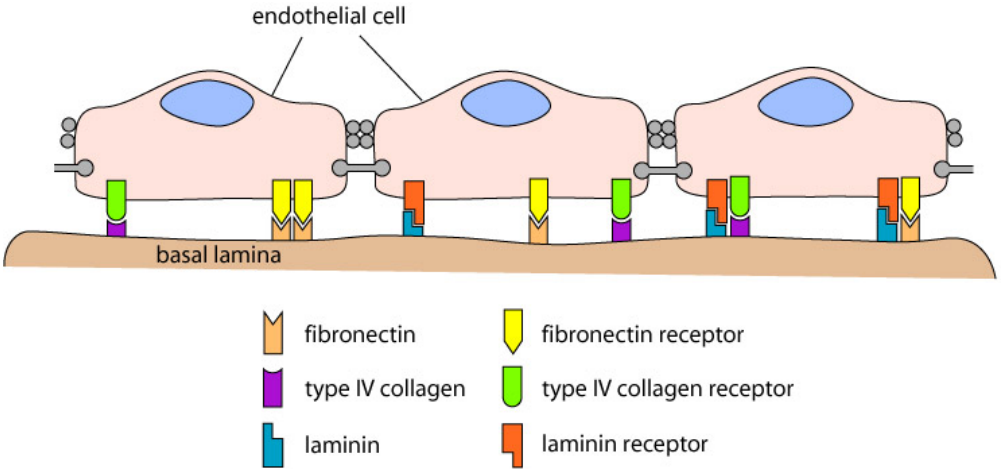

Figure 2.1. Endothelial cells anchored via cell-surface receptors (integrins) to extracellular matrix proteins of the basal lamina.
Fibronectin, type IV collagen, and lamina shown.

2.1.3 Shear Stress Response

All ECs *in vivo* are exposed to blood flow-induced shear stress. These forces are imposed directly on the apical surfaces of the ECs, and are transmitted to the cell cytoskeleton via transmembrane mechanosensors at the surface [13, 18]. As mentioned, the

cytoskeleton is also linked to integrins found on the basal surface of ECs [18]. The cytoskeleton therefore forms a bridge between mechanosensors on the luminal side and mechanotransducers (in the form of integrins) on the abluminal side. Shear stress has been shown to mediate endothelial morphological adaptations [19-21], endothelial permeability [22], vasoregulation [23], arterial remodeling [24, 25], and pathophysiological processes leading to atherosclerosis and other cardiovascular diseases [26]. Due to its importance, shear stress effects on endothelial function have been studied extensively in the last forty years, both *in vivo* and *in vitro*.

In vivo, morphological adaptations of the endothelium were first observed when Flaherty et al. [21] demonstrated that endothelial nuclei from a cell patch that had been rotated 90 degrees from its original orientation (i.e., long axis aligned perpendicular to flow) had the ability to realign their long axis in the direction parallel to flow. Since then, others have found evidence that link distinct *in vivo* flow patterns (laminar versus disturbed) to endothelial cell shapes [18, 20] as well as to focal genesis of atherosclerotic lesions [27].

Although *in vivo* experimentation provides unique insight into shear stress responses of ECs, fundamental studies of shear stress effects have mostly been facilitated by controlled *in vitro* experimentation using ICF systems that mimic physiological conditions while reproducing trends observed in *vivo*. Alignment and elongation of ECs in the direction of flow have been thoroughly demonstrated *in vitro* [28-32], and these morphological responses have since become standard validation measures for ensuring that ICF systems such as parallel plate flow chambers can reproduce *in vivo* observations with fidelity. Biochemical responses of ECs related to protein synthesis [33], and production and secretion of vasodilators [34, 35], vasoconstrictors [36], thrombogenic factors [37], and other cytokines

[38] have also been extensively studied with controlled fluid flow. In most of these studies, shear stress magnitudes and waveforms are carefully chosen to mimic physiological conditions. Laminar steady flow is the most common mode because it is simple and provides the most direct assessment of the effect of shear in comparison to static culture conditions. Because blood flow during the cardiac cycle is pulsatile, other experiments have incorporated various types of unsteady flow (e.g., oscillatory, non-reversing pulsatile) to evaluate the dynamic effects of pulsatility, such as frequency, amplitude, and degree of flow reversal [39, 40]. Because shear stress waveforms are so complex and varied between vascular locations as well as across species, choice of which shear stress pattern to use *in vitro* becomes an important consideration.

2.1.4 Permeability

The endothelium acts as a semi-permeable barrier between flowing blood and the underlying tissue matrix. As one of its primary functions, the endothelium selectively traffics fluid, solutes, and macromolecules from lumen to interstitium in an effort to maintain specific protein gradients or molecular balances between the two sides. Selective permeability depends on both molecular size and the location within the vasculature. Smaller molecules less than three nanometres in radii pass between intercellular endothelial junctions via a paracellular mechanism, while larger macromolecules require vesicular carriers within ECs to carry them through the cell in a transcellular fashion [41]. Within the vasculature, capillary beds and post-capillary venules are more permeable than large arteries [1], and this reemphasizes the heterogeneity of the endothelial population. Permeability controls the passage of molecules through highly regulated transport pathways [41]. Because overall

permeability is dependent on junctional integrity as well as density of surface-bound proteins, it is not surprising that permeability is also tightly regulated by cytoskeletal mechanisms [42, 43] and the glycocalyx [44]. Furthermore, loss of junctional integrity and barrier function results in increased permeability, and usually signifies a breach in the endothelial monolayer accompanied by subsequent inflammatory responses. Thus, understanding permeability of ECs is imperative to elucidating pathogenic processes of the vasculature.

Permeability studies *in vitro* are paramount to the pharmaceutical industry where pharmacokinetic properties of drug compounds need to be screened for their ability to absorb through an endothelial layer such as the blood-brain barrier [45]. In these studies, ECs are typically grown on membrane inserts seated in well plates, and albumin usually serves as a model protein whose movement is tracked across the endothelium. Albumin plays a central role in permeability because of its abundance in plasma and its interactions with ECM proteins and the glycocalyx [41]. In shear response studies, it was demonstrated that albumin permeability increases at the onset of shear stress, and decreases to baseline values at the cessation of shear [46]. This important finding suggests that flow-induced shear regulates permeability, and that ICF systems that incorporate flow with permeability measurement are valuable to our experimental repertoire.

2.1.5 Neighbouring Cells of ECs

All cardiovascular tissues contain cells within the interstitium below the basal lamina on which ECs reside. These neighbouring cells of ECs generally help maintain cardiovascular homeostasis. For example, smooth muscle cells (SMCs) reside in the tunica

media of blood vessels, and are largely responsible for contraction and dilation of the vessel walls (Figure 2.2). In the aortic valve, valve interstitial cells (VICs) reside in the leaflet interstitium and are responsible for regular maintenance of the surrounding matrix as well as valve repair and remodeling [47, 48]. However, the role of SMCs and VICs as mediators of vascular health also implicates them as sources of disease initiation. Lesions form in the artery wall due to proliferation of and excessive matrix protein synthesis by SMCs, usually initiated by endothelial dysfunction [49]. Calcific nodule formation on valve leaflets also involves matrix remodeling by activated VICs, leading to thickened leaflets with stiffened matrix properties [47].

ECs are naturally involved in the regulation of SMC/VIC function due to their location as a barrier between flowing blood and the interstitium. Perhaps the best example of EC-SMC communication leading to SMC function is the role of nitric oxide (NO) in smooth muscle contraction [14]. Activated nitric oxide synthase (NOS) within ECs produces NO gas that readily diffuses across EC membranes and into SMCs where it produces cyclic GMP and ultimately relaxes the SMCs. Because NO, and many other cytokines and secreted factors that are important to tissue function, have short half-lives, their ability to induce an SMC response via paracrine signaling is dependent on the proximity between communicating cells. Thus, recreating spatial relationships in *in vitro* models is imperative to study transfer of molecular signals from one cell to another. Coculture models provide a method to bring both ECs and SMCs/VICs into the same culture where they can share certain biological products within the same media while still maintaining sufficient separation from each other (so as not to have a mixed aggregate of cells).

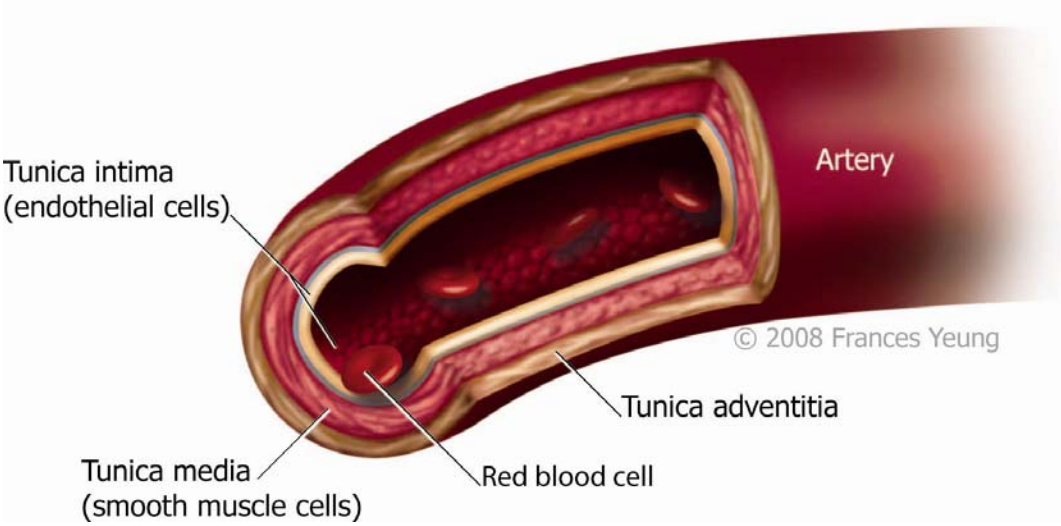

Figure 2.2. Anatomy of large artery.
The tunica intima is lined with endothelial cells while the tunica media consists of smooth muscle cells. (*Source*: Illustrated by and used with permission from Frances Yeung).

2.1.6 An Example of Heterogeneity: Aorta versus Aortic Valve

To illustrate the uniqueness of structural and functional properties between different ECs, we compare two neighbouring endothelial phenotypes: aortic ECs and aortic valve ECs.[1] Aortic ECs across a variety of species have been used for *in vitro* experimentation [30, 32, 34, 38, 39], and have become a standard cell type for understanding shear stress effects on the endothelium. Its popularity is due in part to commercial availability and accessibility of well-established isolation protocols, but also because the aorta is a prime model of other arteries within the cardiovascular system. Valve ECs, on the other hand, have been studied to a much lesser extent. Valve ECs are not commercially available, established isolation

[1] Henceforth, aortic valve ECs will simply be referred to as valve ECs for brevity. Other valve ECs (i.e., mitral, pulmonary, and tricuspid) will be specified explicitly for clarity if and when necessary.

techniques are scant, and the tissue on which they reside is not representative of any other in the cardiovascular system. Despite these differences, there has been a growth in interest surrounding the characterization of the valve EC phenotype, largely attributable to some recent studies that have revealed some profound and distinct differences in cell structure and molecular level expression [50, 51]. Given the current interest in valve ECs and the relative scarcity of published work on their characterization, it is of potential benefit to carry out direct comparative studies between ECs from the valve and those from a well-characterized EC type, such as those from the aorta.

The aorta is the largest artery in humans, and is the first vessel carrying blood from the heart to the rest of the body (Figure 2.3). The main parts of the aorta include the ascending aorta, aortic arch, and thoracic aorta. The straight sections of the ascending and thoracic regions are characterized by smooth laminar blood flow and are consequently lesion-free [18, 52]. Endothelia from these sections are often chosen for isolation and investigation *in vitro* because ECs from these locations have been exposed to relatively calm and uniform flow patterns, resulting in well-characterized morphologies that can be recapitulated *in vitro*. In contrast, the aortic arch consists of major branches where the subclavian and carotid arteries bifurcate, leading to a geometry that promotes disturbed blood flow, specifically in regions that correlate with focal development of atherosclerotic lesions [52].

The aortic valve is a dynamic yet delicate tissue of the cardiovascular system consisting of three membranous leaflets arranged circumferentially around the base of the aortic root (Figure 2.4). The aortic valve is positioned just upstream of the ascending aorta (Figure 2.3), and mainly functions as a blood flow regulator, directing blood from the heart to the rest of the body while preventing regurgitation. It achieves this by shutting its three valve

leaflets during diastole, when positive transvalvular pressure maintains leaflet coaptation. Because the leaflets open and close in concert with the cardiac cycle, the leaflet surfaces are exposed to unsteady local flow environments while also simultaneously undergoing continuous flexure. Thus, the aortic valve is constantly exposed to stressful dynamic loading conditions.

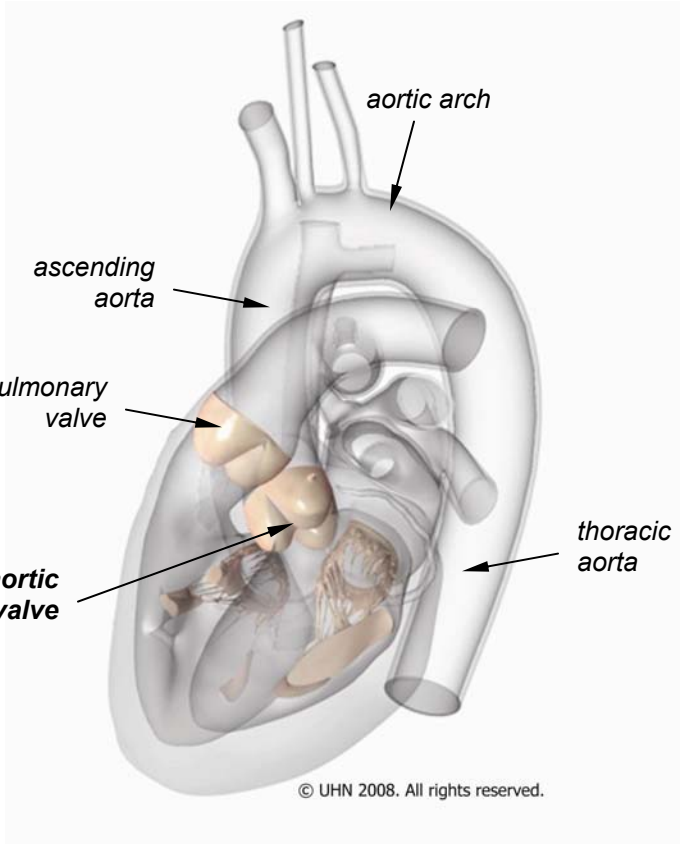

Figure 2.3. Three-dimensional transparent model of heart illustrating anatomy of the aorta and location of heart valves.

The aortic valve is situated posterior to the aorta. Blood flows through the aortic valve, up the ascending aorta, around the aortic arch, and down the thoracic aorta. (*Source*: [53], used with kind permission from Dr. Gordon Tait at Toronto General Hospital).

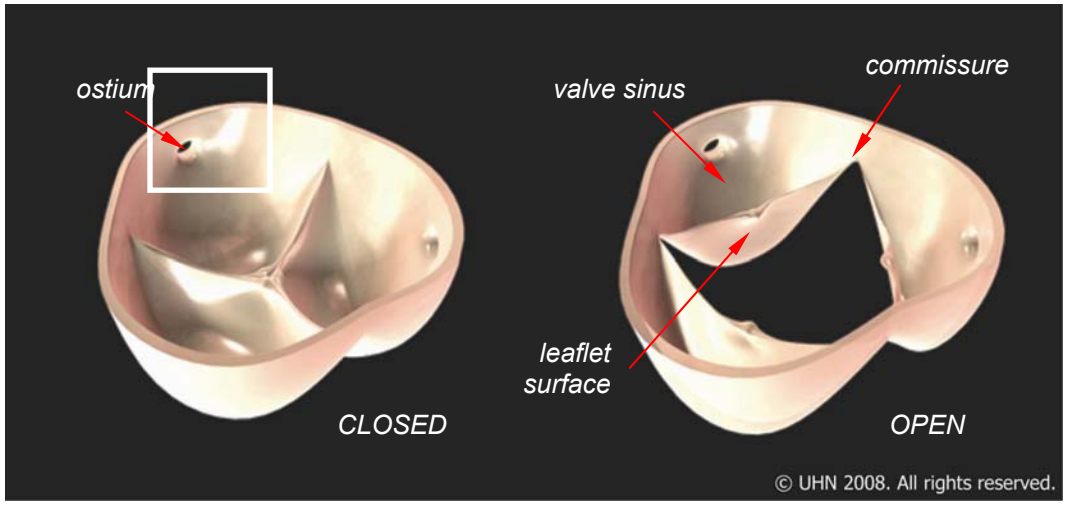

Figure 2.4. Anatomy of the aortic valve.

The aortic valve consists of three membranous leaflets symmetrically arranged in the circumferential direction. Leaflets are attached to the valve wall at commissures. (*Source*: [53], used with kind permission from Dr. Gordon Tait at Toronto General Hospital).

Valve leaflets are composed of three separate layers of tissue. The fibrosa faces the aortic root and consists mostly of load-bearing collagen fibres; the ventricularis faces the left ventricle and is composed mainly of elastin fibres; and the spongiosa lies between the other two layers, and is made of mostly water and glycosaminoglycans [54]. The two major cell types are the valve ECs, which line both the aortic side and ventricular side leaflet surfaces, and the valve VICs, which are spaced throughout the layers of the valve matrix (Figure 2.5).

Because of the geometry of the valve, and the complex hemodynamics around the leaflets during the cardiac cycle, the aortic and ventricular sides of the leaflet experience vastly different shear stresses (Figure 2.6). Rough estimates of average shear stress on the ventricular side are on the order of ~ 100 dyn/cm^2 where a high velocity, yet relatively laminar jet of blood passes the surface. On the aortic side, estimates are closer to ~ 1 dyn/cm^2 as a result of recirculating flow in the valve sinus [55, 56].

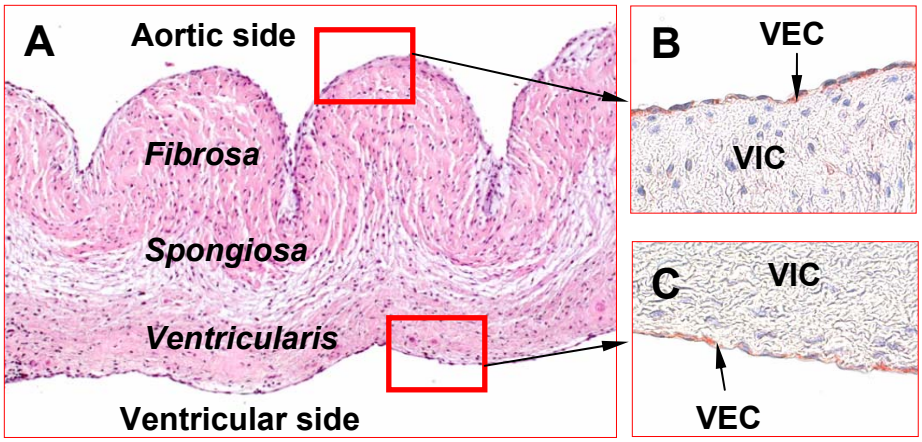

Figure 2.5. Histological cross section of aortic valve leaflet.

(A) Valve leaflet consists of three distinct tissue layers. The aortic side is corrugated while the ventricular side is smooth. (B and C) Immunostaining of vWF shows valve endothelial cells (VECs) on the surface of the valve leaflet. Hematoxylin staining (blue) shows nuclei of valve interstitial cells (VICs). (*Source*: Adapted from Simmons et al., *Circ Res* (2005); 96(7):792-799 [51], with permission from Lippincott, Williams & Wilkins).

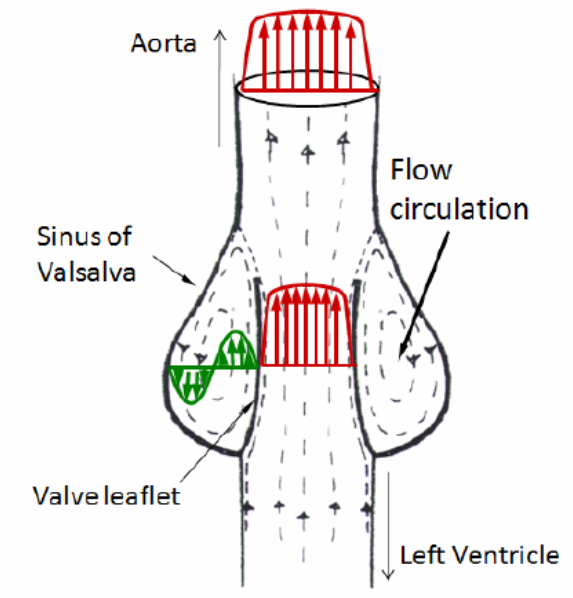

Figure 2.6. Fluid mechanics of the aortic valve.

Laminar flow exits the left ventricle and imposes high shear stress on ventricular side ECs. Geometry of valve sinus induces flow circulation that imposes low shear stress on aortic side ECs.

Recent work on the valve endothelium of pigs has revealed phenotypic differences between porcine aortic ECs (PAECs) and porcine aortic valve ECs (PAVECs). PAVECs appear to be more proliferative than PAECs in regular culture conditions on a variety of different protein coatings [57]. When transcriptional profiles were analyzed, the two cell types displayed distinct sets of expressed genes. Furthermore, in a separate study, side-dependent gene expression profiles appeared to show site-specific susceptibility to aortic valve disease that correlated with local hemodynamic environments, implicating the valve endothelium as a mechanosensitive layer likely involved in the disease process [51]. When shear stress was applied, PAECs elongated and aligned in the direction of flow, while PAVECs were reported to align perpendicular to flow [50] (Figure 2.7), further demonstrating the heterogeneity between the two populations.

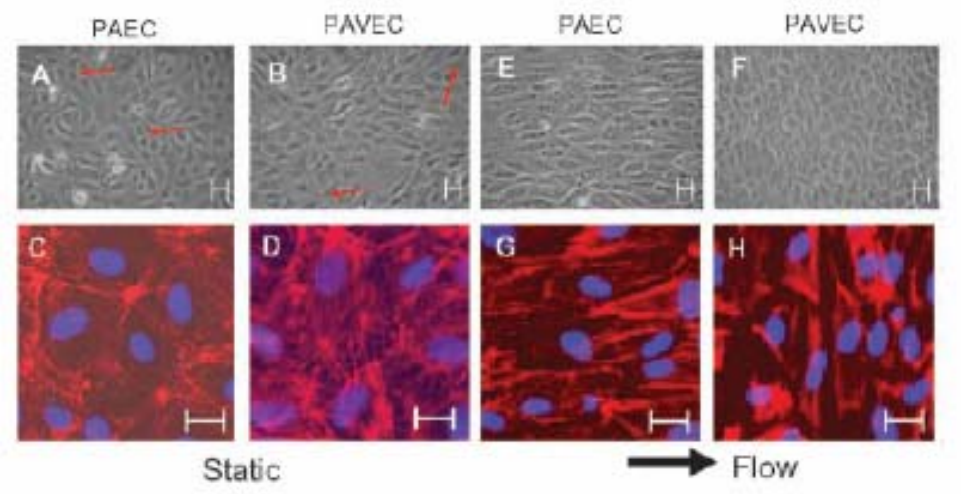

Figure 2.7. PAECs and PAVECs exposed to shear stress.

PAECs (A, C, E, G) and PAVECs (B, D, F, H) in static and steady fluid flow environments. (A-D) static; (E-H) after 48 hours of steady shear at 20 dyn/cm^2. PAECs aligned parallel to flow (G), while PAVECs aligned perpendicular to flow (H). Cells stained for f-actin (red) and cell nuclei (blue). Flow direction from left to right. Scalebar = 50 μm. (*Source*: Butcher et al. *Arterioscler Thromb Vasc Biol* (2004); 24(8):1429-1434 [50], with permission from Lippincott, Williams & Wilkins).

Altogether, these findings suggest that valve ECs need to be more fully characterized and studied more extensively in concert with aortic ECs in order to differentiate their phenotypes. Furthermore, broadening our knowledge of valve EC biology will likely help our understanding of their specific role in the regulation of normal valve function and the development of valve disease.

2.2 Fluid Flow Principles

ICF systems are designed to provide an enclosed and controlled culture environment where ECs can be exposed to *in vivo*-like hemodynamic conditions. Because fluid flow must be predictable to properly control shear stress on the endothelial monolayer, the geometries of the systems are usually simple, and have analytical solutions for velocity and pressure fields that are based on the theory of viscous flow in ducts.

The Reynolds number, Re, is an important dimensionless parameter in viscous flows, particularly when different length scales are involved and inertial and viscous forces dominate. Re is calculated by

$$\mathrm{Re} = \frac{\rho U L}{\mu} \tag{2.1}$$

where ρ is the fluid density, U is a representative velocity of the flow, L is the characteristic length, and μ is the fluid viscosity. Re is derived from non-dimensionalization of the Navier-Stokes equations, and represents a ratio between inertial and viscous forces. Low Reynolds number ($\mathrm{Re} < 10^3$) signifies viscous laminar flow where fluid streamlines are steady and predictable; high Reynolds number ($\mathrm{Re} > 10^4$), on the other hand, signifies chaotic turbulent flow where fluid motion is random and unpredictable, and where analyses are only possible

by time-averaged approaches. Between these two regimes lies a third ($10^3 < \mathrm{Re} < 10^4$) where flow transitions from laminar to turbulent [58]. For the purpose of designing well-characterized ICF systems, flows are usually restricted to $\mathrm{Re} < 10^3$ (and often times $\mathrm{Re} < 100$) to ensure that laminar streams are maintained, and predictable shear stresses can be applied at the walls of flow sections.

Most flows in ICF systems are steady pressure-driven flows, and because of the dominance of viscous terms, the Navier-Stokes equation simplifies to

$$0 = -\nabla p + \mu \nabla^2 \vec{u} \tag{2.2}$$

where p is the pressure field and $\vec{u}$ is the velocity field. As an example of an application of Eq. (2.2), we derive wall shear stress for the simplest of ICF systems: the parallel plate flow chamber (PPFC). In a PPFC, flow is treated as a standard pressure-driven flow problem between two parallel infinite flat plates (Figure 2.8). The steady velocity profile $u(y)$ is uniform along the length of the plate in the x-direction, and Eq. (2.2) becomes

$$0 = -\frac{dp}{dx} + \mu \frac{d^2 u}{dy^2} \tag{2.3}$$

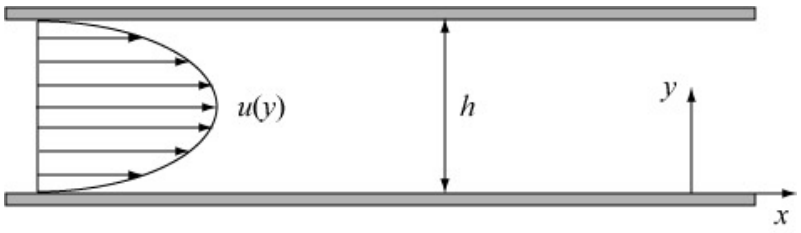

Figure 2.8. Pressure-driven flow between two infinite flat plates in the x-z plane. Parabolic velocity profile $u(y)$ between the flat plates separated by a gap height h.

Integration of Eq. (2.3) yields

$$u(y) = -\frac{1}{2\mu}\frac{dp}{dx}\left(hy - y^2\right), \tag{2.4}$$

and this represents a parabolic velocity profile that satisfies no slip at the walls and maximum velocity at the midplane between the plates, $y = h/2$. Since wall shear stress τ_w is defined as

$$\tau_w = \mu\frac{du}{dy}, \tag{2.5}$$

the slope of the velocity profile from Eq. (2.4) can be calculated to obtain τ_w at the wall via Eq. (2.5):

$$\tau_w = \mu\frac{du}{dy} = -\frac{h}{2}\frac{dp}{dx} \tag{2.6}$$

For a PPFC with channel width w, the volumetric flow rate Q can be determined by integrating the velocity profile over the gap height h:

$$Q = w \times \int_0^h u(y)dy = -\frac{dp}{dx}\frac{wh^3}{12\mu} \tag{2.7}$$

Combining Eqs. (2.6) and (2.7) yields a simple algebraic equation for wall shear stress in terms of volumetric flow rate, fluid viscosity, and flow chamber dimensions:

$$\tau_w = \frac{6\mu Q}{wh^2} \tag{2.8}$$

Eqs. (2.1) to (2.5) outline the basic principles used to determine wall shear stress within pressure-driven flows. Although ICF systems have varying geometries, all are governed by

the same basic flow principles, and thus result in equations for shear stress having similar form to Eq. (2.8) with minor variations.

Eq. (2.8) applies to the channel region where flow is fully developed. Near the channel inlet, a region of developing flow is characterized by non-parabolic velocity profiles where Eq. (2.8) does not apply. For flow between plates, this entrance length, L_e, can be calculated based on channel height h and Re:

$$L_e = a \cdot h \cdot \mathrm{Re} \tag{2.9}$$

where a is an empirical proportionality constant. It is important to determine L_e prior to experimentation to allow proper delineation of the developing and fully developed regions. This ensures that the uniform section of the sheared surface can be appropriately analyzed.

Because Eq. (2.8) was derived from an ideal case of infinite flat plates, and because flow in PPFCs is confined by side walls, the near-wall regions experience flow that deviates from the above model. The extent of this deviation depends on the cross-sectional aspect ratio, $\alpha = h/w$, where $0 \leq \alpha \leq 1$. Low α signifies wide plates and a slit-like geometry that closely mimics the two-dimensional model. In contrast, high α (e.g., $\alpha = 1$) signifies a square-like geometry where wall effects substantially alter flow profiles. An exact solution to the three-dimensional velocity profile in rectangular ducts can be derived via Fourier series expansions [59]. To avoid the computational rigour inherent in solving Fourier series expansions, a simple approximation has also been derived, resulting in a modified version of Eq. (2.8) in algebraic form [59]:

$$\tau_w = \frac{2\mu Q}{wh^2}\left(\frac{m+1}{m}\right)(n+1) \tag{2.10}$$

In Eq. (2.10), m and n are empirical constants, with $m = 1.7 + 0.5\,\alpha^{-1.4}$ and $n = 2$ for aspect ratios $\alpha < 1/3$ (see Appendix C for detailed derivation). It is prudent to note that although wall effects are typically negligible for the majority of macroscale systems, these effects have become more important in microfluidic geometries because of the desire to increase parallelization, and hence reduce microchannel widths. In the process, aspect ratios are higher, and wall effects more pronounced.

The basic fluid flow principles apply to all ICF systems, regardless of physical scale. For microscale flows, Reynolds number is usually less than unity, guaranteeing laminar flow in all microchannels. Because of the convenience of soft lithography, it is straightforward to design and fabricate multi-channel networks of various configurations. This opens the door for highly organized and integrated fluidic circuits for multi-level on-chip processing. Although flow analyses for networks are inherently more complex, calculations can be simplified by treating individual channel sections as resistances within the flow circuit (i.e., analogous to an electrical circuit). This was previously demonstrated in an analysis of fluid flow within multi-channel microfluidic droplet generators [60]. Eq. (2.7) simplifies to

$$Q = \frac{\Delta p}{R} \tag{2.11}$$

where R is the fluidic resistance, and Δp is the pressure drop across a particular section of length L. This simplification applies for a constant pressure gradient, i.e. $-dp/dx = \Delta p/L$. For rectangular channel sections,

$$R = \frac{12\mu L}{wh^3} \tag{2.12}$$

The simplest multi-channel configurations involve channel sections either in series or in parallel (Figure 2.9). Higher complexity networks can be achieved by simply combining these two simple configurations. For multiple channels in series (Figure 2.9A), flow rate Q remains constant through all sections such that pressure drop varies according to resistance:

$$Q = \frac{(\Delta p)_i}{R_i} \quad \text{for section } i,\ i = 1, 2 \ldots, n \tag{2.13}$$

Rearranging and summing over all n sections in series yields total pressure drop:

$$\Delta p = Q \sum_i R_i \tag{2.14}$$

In the case of multiple channels in parallel (Figure 2.9B), flow rates in each branch of the network are summed such that for similar pressure drops between inlet and outlet (i.e., pressure drops between a and b, a and c, and a and d are equal in Figure 2.9B), total flow rate equates to

$$Q = \Delta p \left(\sum_i \frac{1}{R_i} \right) \tag{2.15}$$

Other important physical phenomena pertinent to microfluidics include diffusion, surface tension, capillary forces, and surface area-to-volume ratios. These topics are discussed in detail in a review by Beebe [61].

We now focus on introducing existing ICF systems designed to study endothelial properties in the form of adhesion, flow-induced mechanotransduction, and permeability. Excellent comprehensive reviews on these topics from a biological perspective are available in the literature, and interested readers are directed to them [18, 41, 43, 44, 62]. The purpose of this overview is to consolidate the various macro- and microscale designs under a single

review in an effort to facilitate comparisons focused on experimental procedures, protocols, measurement methods, and analyses as opposed to the interpretation of biological outcomes (we leave that for the aforementioned topical reviews).

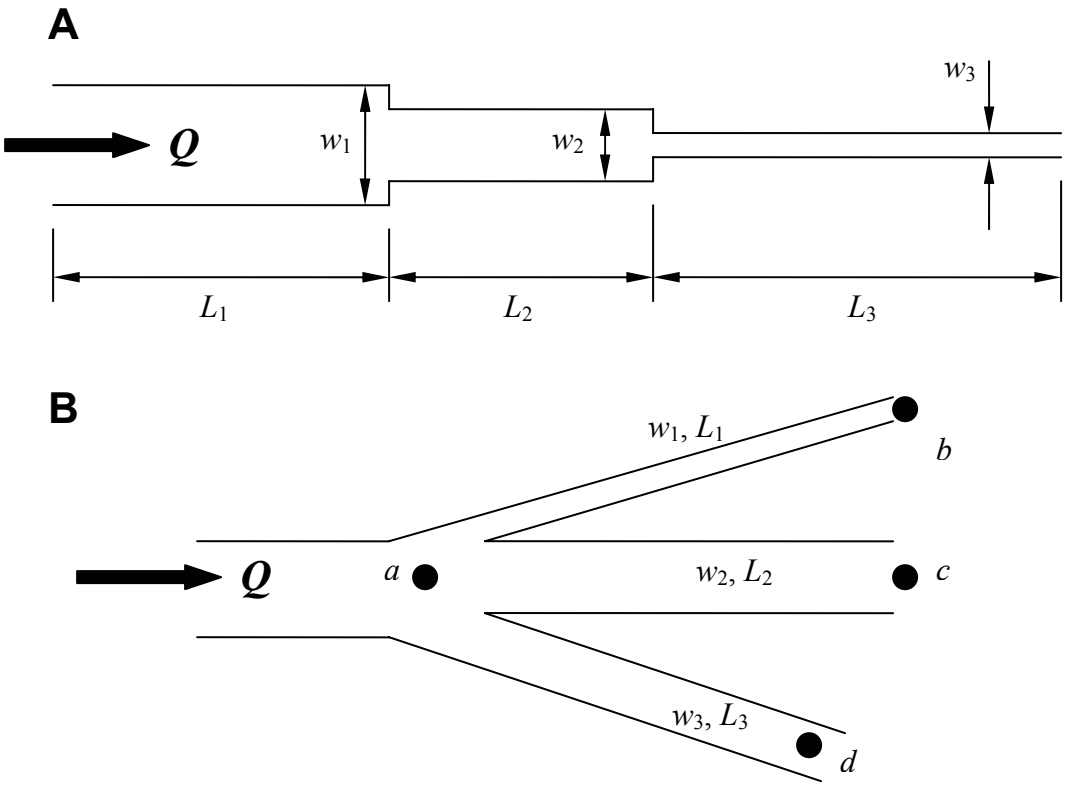

Figure 2.9. Channel networks in series and in parallel.

(A) Three channel sections of different w and L, and therefore different resistances, connected in series. Flow rate Q is constant in each section such that pressure drop varies according to fluidic resistance. (B) Three channel sections of different w and L connected in parallel. Flow rate at point a is equal to the sum of the flow rates at b, c and d.

2.3 Macroscale Systems

2.3.1 Adhesion

Adhesion assays are designed to measure the strength of attachment between anchorage-dependent cells and their underlying substrates. There are two main ways to quantify adhesion strength: (1) count the fraction of cells that detaches when exposed to a specific shear stress, or (2) determine an estimate of the total force per bond between cell and substrate. The first method is a global measure of adhesion that assesses overall preference of a cell type for a particular surface; the second is a fundamental measure of bond strength that requires determining number of bonds present in each cell, cell contact area, and models for bond and force distributions. In bioengineering studies, the global measure is sufficient and ideal for testing overall suitability of a biomaterial for cell attachment, spreading, growth, proliferation, and migration, as well as for determining the limits of forces which the cell population can resist. ICF systems designed to study adhesion can easily allow cell counting under different shear stresses and at different timepoints, but may require certain modifications to the system to allow proper visualization via microscopy to permit accurate predictions of individual cell-to-surface bond strengths.

The simplest system for studying adhesion is the parallel plate flow chamber (PPFC) [63]. PPFCs are the most commonly used apparatus for EC shear stress response studies (as discussed below), but can also be used for adhesion assays. Adhered cells are loaded into the flow chamber, and applied shear stress is incrementally increased to produce a ramped shearing protocol. Because flow chamber geometry is uniform throughout the device and samples of adhered cells are treated with the same conditions for a given experiment, the PPFC is limited to studying only one experimental condition at once. To apply different

shear rates, the flow rate must be adjusted manually during the ramping procedure. Thus, to obtain a graph of adhered cell fraction versus applied shear stress, the user is required to constantly monitor and operate the system. Because of the tedium associated with using PPFCs for adhesion, most researchers have designed other more robust systems.

Most other adhesion systems allow the same flow rate to simultaneously generate different shears at different locations. This reduces the tedium associated with adjusting flow rates to vary shear stress, as in the case of PPFCs. The difference between these systems is usually a matter of geometry. Variable-height flow chambers [64] rely on a sloped top plate such that shear stress varies as a function of height, $h(x)$, along the x-direction of the bottom plate (Figure 2.10A). In a single experiment with one flow rate, an entire curve of adherent cell fraction versus applied shear stress can be obtained because each x position along the bottom plate corresponds to a different shear stress. Xiao and Truskey [64] used this system to efficiently obtain adherent cell fraction curves of bovine aortic endothelial cells (BAECs), and used curve fits to determine critical wall shear stresses (defined as the shear stress corresponding to 50% adherent cell fraction) on various functionalized surfaces.

Rather than vary channel height, an alternative is to vary channel width along the flow chamber. Usami et al. [65] designed a tapered channel where side walls followed an inverse function, resulting in a flow chamber that produced a linear shear stress gradient from inlet to outlet (Figure 2.10B). In addition to having the same advantage as the variable-height flow chamber in permitting simultaneous application of a range of shear stresses, this design is also easier to fabricate because of the uniform height, and thus lends itself well to other fabrication techniques. Indeed, as discussed below, the tapered design has recently been replicated using microscale soft lithography techniques (see Section 2.4.1).

Another method of generating a range of shear stresses at one time is to take advantage of non-uniform velocity fields associated with radial and circumferential flows. Radial flow can be generated by either divergence from a single point source, or convergence to a sink. In either case, if flow is confined by parallel plates, velocity is dependent on radial position from the source or sink, and shear stress varies from one radial position to another (i.e., constant shear stress in concentric circles). Circumferential flows may also be developed to generate similar shear stress gradients in the radial position. These fluid flow principles have been implemented for cell adhesion studies in a myriad of designs, including radial flow chambers [66, 67], spinning disc apparatuses [68], and cone-and-plate viscometers [69] (Figure 2.10C).

Although variable shear stress devices can produce a range of shear rates using a single volumetric flow rate, they suffer from one major drawback. In all cases, adhered cells represent a single sample condition consisting of one cell type on one specific surface. Many bioengineering studies involve investigation of multiple cell types on different surface functionalizations to screen for appropriate biomaterials and surface coatings that provide optimal adhesion of a given cell type. Thus, although one experiment can generate enough data to determine critical wall shear stresses, none of these devices can screen for multiple critical wall shear stresses at once. From a bioengineering perspective, such a device would have a distinct advantage over the existing systems reviewed here.

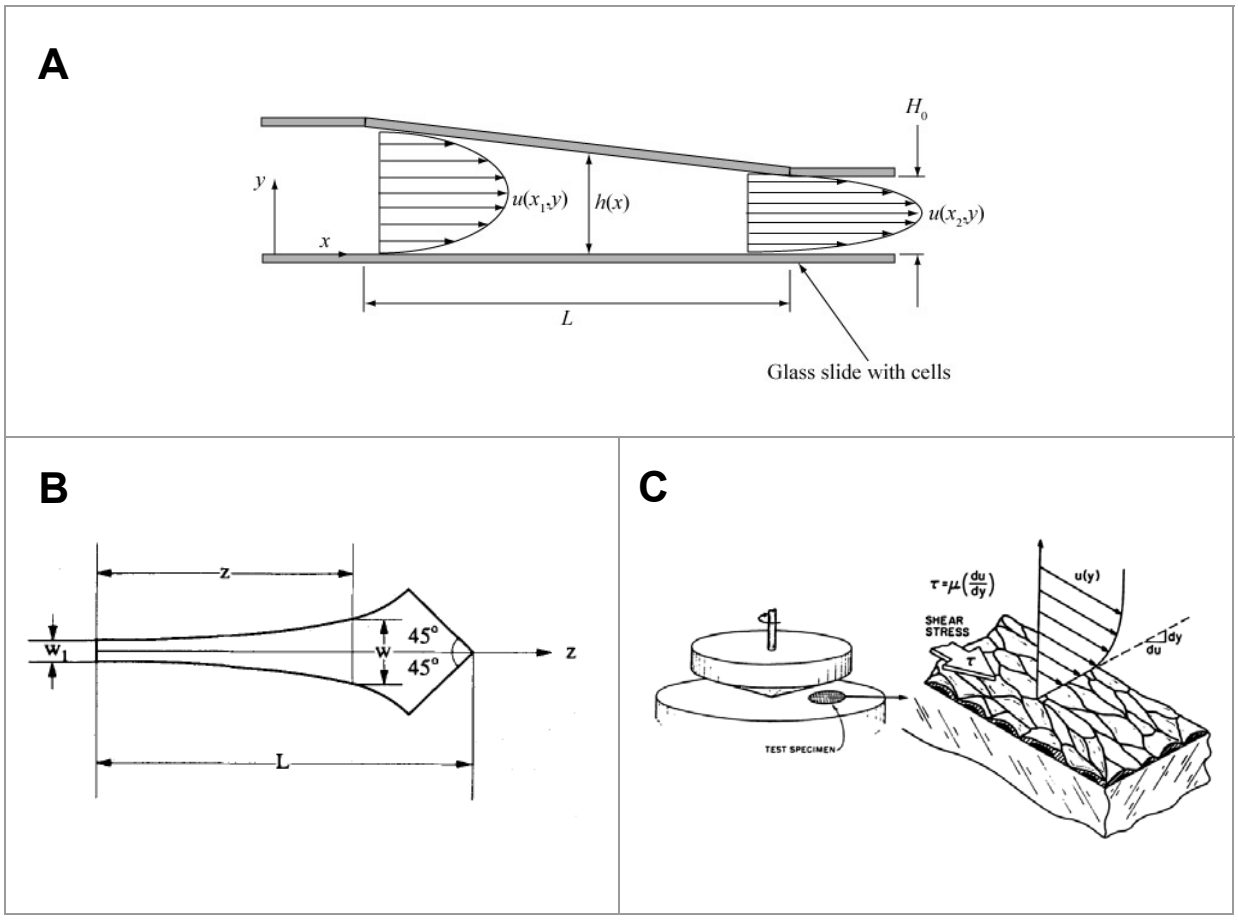

Figure 2.10. Various macroscale ICF systems for adhesion assays.

(A) Variable-height flow chamber used by Xiao and Truskey [64]. (B) Variable-width linear shear stress flow chamber (*Source*: Usami et al., *Annals Biomedical Eng* 1993; 21(1); 77-83 [65], with kind permission from Springer Science and Business Media). (C) Cone and plate viscometer (*Source*: Journal of Clinical Investigation by Davies, P.F. et al. [70]. Copyright 1983 by American Society for Clinical Investigation. Reproduced with permission of American Society for Clinical Investigation in the format Dissertation via Copyright Clearance Center.)

2.3.2 Shear Stress Response

The objective in shear stress response studies is to expose endothelial monolayers to uniform shear forces while maintaining sterile cell culture conditions. This is achieved by applying well-characterized flow fields on sufficiently large endothelial surfaces. Monolayer

size dictates the amount of material, e.g., secreted factors, proteins, or mRNA, that can be extracted for analysis at the end of experiments. Knowing endpoint measures and having an estimate of the amount of material needed for analysis aids in choice of flow chamber size.

Because the goal is to expose ECs to uniform shear stress, many of the variable shear flow chambers designed for adhesion assays are not suitable for shear response studies. The applicable systems are the PPFCs and the cone-and-plate viscometers [71-73]. The others generate shear stress gradients undesirably, leading to varied levels of mechanical stimuli across the endothelial sample, and ultimately local variations in cellular response that cannot be easily isolated. To ensure uniform shear stress across the monolayer, some designs employ baffles [31, 74] or perforated plates [75] to produce laminar streams upstream of the test region. Most of the time, however, laminar shear flow is produced without difficulty, as long as the inlet geometry is properly designed.

Once a uniform shear stress is established, the next step is to choose appropriate experimental parameters such as flow rates and duration of experiment, with due consideration for the output measure of interest. A typical first metric of endothelial response to shear is cell morphology and structure. Morphological responses in the form of cell elongation and preferential orientation to flow have been shown to require 24 to 48 hours before the response can be detected [29, 30, 32]. In some cases, such as the full restoration of linear adherens junctions at borders of sheared ECs, the response may need up to 96 hours [76]. For other applications, such as studying the regulation of specific shear stress response elements (SSREs), responses may occur in less than six hours [77]. Thus, although the duration of adhesion assays is short and appears to only depend on the time needed to ramp

through a range of shears, duration in shear stress response assays is a more important consideration and depends on the output measure of interest.

The majority of studies use steady shear stress in the range of 10 to 40 dyn/cm^2 to mimic physiological conditions [29, 32, 50, 76, 78]. Steady continuous shear is a natural starting point for understanding EC responses to shear *in vitro*. However, to model more closely the *in vivo* hemodynamic environment, particularly in the arterial system, consideration should be given to unsteady pulsatile flow, where past studies have demonstrated unique time-dependent adaptations to cell morphology depending on whether flow is steady, purely oscillatory, or pulsatile (with and without reversing patterns) [39]. A further advance was replacing simple sinusoidal patterns with accurate arterial waveforms that were generated by precision microstepper motor technology on a cone-and-plate device, resulting in accelerations and decelerations of fluid with high temporal resolution [71]. For the majority of studies, steady shear remains the simple, reliable choice for inducing shear-related responses unique from static conditions, and the subtle differences afforded by more accurate waveforms are usually of minor consequence.

A number of studies have attempted to recreate turbulent flow patterns *in vitro* that mimic vascular regions of disturbed flow where atherosclerotic lesions are known to originate. The simplest way is to introduce a lateral protruding step or "trip bar" across the flow chamber to perturb the laminar fluid stream, and in the process create shear stress gradients in the direction of flow [79, 80]. The design is far from an accurate depiction of vascular geometry, but it provides a simple solution to a complex fluid problem, i.e., the controlled and predictable generation of recirculation zones and reattachment points that model aspects of the turbulent regime.

Many of the systems reviewed thus far fully enclose the sample in large contraptions to provide a leak-proof seal and contamination-free environment. As a consequence, access to the sample during experimentation is limited to before and after the application of flow. Real-time monitoring of live cells via video microscopy can provide unparalleled insight into the dynamics of EC response to shear [81], and studies have demonstrated the power of this technique through novel quantitative morphodynamic analyses of cultured and sheared ECs [82]. Live cell imaging setups have become increasingly sophisticated over the years, incorporating features such as direct heating, and perfusion ports within systems designed for optimal optical performance (Bioptechs).

In choosing an appropriate ICF system, or designing a new one for a specific application, the first priority is to determine the endpoint measure and the amount of material needed to carry out the desired analyses. Some morphological studies rely heavily on post-shear immunostaining to determine localization of specific intracellular proteins associated with cytoskeletal remodeling [30, 32, 76, 78]. In these cases, it may be a simple matter to divide the tested glass slide into separate compartments to allow staining of multiple markers. For measurement of secreted factors and proteins, e.g., nitric oxide [83], prostacyclin (PGI_2) [35], tissue plasminogen activator (tPA) [37], or fibronectin [33], it is pertinent to estimate the amount of substance needed to detect differences between experimental samples. This is important when choosing assays with the appropriate level of sensitivity. More importantly, however, it impacts experimental design because it necessitates proper selection of media volumes and endothelial surface area such that suitable levels of protein are produced and secreted for analyses.

Though the variety of ICF systems for shear stress response studies is mostly limited to PPFCs and cone-and-plate viscometers, there is no shortage of variations on these two themes. Simple modifications to existing systems and more sophisticated implementations are available to the end user using either platform.

Figure 2.11 illustrates some of the noteworthy designs reviewed here. A clear shortcoming, however, is one previously stated for adhesion devices, i.e., that these systems test only one condition at a time. As an example, immunostaining of sheared ECs under different chemical or mechanical stimuli and for multiple timepoints would require a single PPFC for each condition. Clearly, more high-throughput means are needed to expedite the experimental process.

2.3.3 Permeability

The goal in permeability assays is to assess the integrity of a given endothelial monolayer by determining the flux of molecules from luminal to abluminal sides. Two main methods are usually employed: (1) tracking the movement of molecules from one side to the other by labelling and detecting the permeate using fluorescence or other means [46, 84, 85]; and (2) measuring transendothelial electrical resistance (TEER) by passing a current, measuring a voltage across the monolayer, and using Ohm's law [86-88]. The first method is more direct in that actual flux of particles are tracked and counted; the second method relies on the concept that the endothelial monolayer can be treated as an impedance layer or "barrier". In either case, endothelial permeability can be tested against various chemical and mechanical stimuli to induce a differential response that sheds light on underlying mechanisms related to endothelial barrier function.

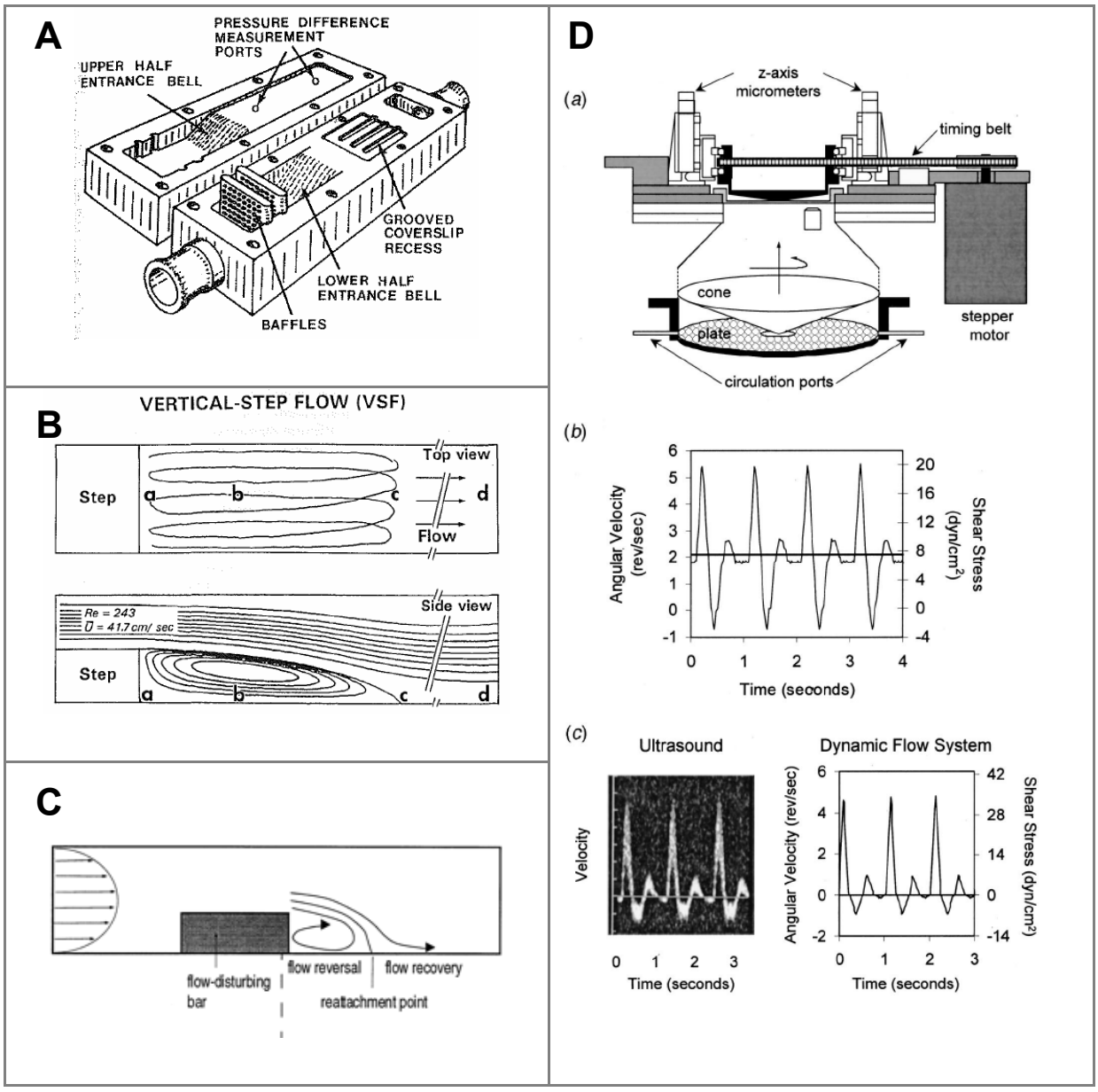

Figure 2.11. Shear stress flow chambers and various modifications.

(A) Parallel plate device with inlet baffles (*Source*: Viggers et al. (1986) [31]). (B) PPFC with inlet step to produce recirculation zone (*Source*: Chiu et al. (1998) [80]). (C) PPFC with trip bar to produce recirculation zone, (*Source*: Tardy et al., *Arterioscler Thromb Vasc Biol* (1997); 17(11):3102-3106 [79], with permission from Lippincott, Williams & Wilkins). (D) Cone-and-plate viscometer with microstepper motor for mimicking arterial waveforms (*Source*: Blackman et al. (2002) [71]). Figures A, B, and D reprinted with kind permission from the Americal Society of Mechanical Engineers (ASME), Journal of Biomechanical Engineering, copyright © by ASME.

Regardless of the measurement technique, the first priority in permeability experiments is to culture ECs on a supporting porous membrane. This is most conveniently done using Transwell cell culture inserts that can be seated in well plates while bathed in culture media. Inserts, or the membrane alone, can then be transferred to a setup that holds the membrane in media and contains both upper and lower compartments where abluminal and luminal sides are exposed for interrogation. For electrical resistance measurements, current passing electrodes are placed on either side; for fluorescence detection of labelled molecules, a specified concentration of solutes is added to the luminal side, and the concentration on the abluminal side is measured to determine flux across the monolayer.

Most permeability measurements are done while ECs are in static conditions. However, knowing the effects of shear stress on ECs, and the role of shear-regulated EC components in endothelial permeability (e.g., cytoskeleton and glycocalyx; see Section 2.1.4), it is not surprising that endothelial permeability is shear-dependent. Only a few reports have incorporated shear stress on ECs with their permeability measurements. Since our focus here is on different ICF system designs, we review two apparatuses that incorporate flow with measurement of endothelial permeability for comparison.

The first, developed by Jo and co-workers [46], consisted of a shear chamber that housed the membrane containing the endothelial monolayer, and two separate loops that included an abluminal non-circulatory loop and a luminal circulatory loop (Figure 2.12). The purpose of the luminal flow loop was to provide shear stress over the endothelial monolayer and supply a constant stream of fluorescently-labelled albumin molecules. The purpose of the abluminal loop was to maintain a prescribed transmembrane pressure across the membrane while providing access to the sampling region in the lower compartment under the

monolayer. The second, from Sill and co-workers [85], employed a rotating cylindrical disk on the luminal side to produce circumferential flow patterns and corresponding shear stress on the endothelial monolayer (Figure 2.13). In this case, volume flux of fluid (rather than solute flux) was measured in real-time by tracking the motion of a bubble in a glass tube through spectrophotometric measurements.

These two examples provide us with a glimpse of the complexities involved in shear-dependent permeability experiments. Shear stress can be produced using similar concepts as before, with either linear flow through parallel plates, or circumferential flow via cone-and-plate setups. In both cases, control of pressure on luminal and abluminal sides is critical to proper detection of permeability. The size of these apparatuses limits them to laboratories dedicated to understanding specific problems of the endothelium, where targeted molecules can be analyzed in detail and high-throughput is not necessary.

2.3.4 Coculture

Coculture of ECs with either SMCs or VICs is important for understanding cell-cell communication and how it affects homeostasis and pathogenesis within the cardiovascular system. Allowing interaction of two cell types within the same environment adds a level of experimental sophistication that has the potential to capture paracrine-dependent effects that otherwise would be lost in the absence of either cell type. Coculture models can be configured in a number of ways depending on the desired amount of contact between cells. Using membrane cell culture inserts, ECs can be grown on the top of the membrane while SMCs or VICs are grown inside the wells in a fully separated configuration suitable for conditioned media testing [89]. Alternatively, SMCs or VICs can be grown on the bottom of

the membrane opposite the ECs, permitting extension of cell processes through membrane pores and allowing controlled physical contact via myoendothelial bridges [90, 91]. Finally, SMCs or VICs can be seeded directly on EC monolayers in a model that allows full contact between the two cell types without segregation [92]. Each option offers its own advantages, and answers different questions (e.g., separated coculture examines paracrine signaling and effects of conditioned media, whereas controlled contact coculture examines cell-cell communication via physical bridging); the choice is dependent on application.

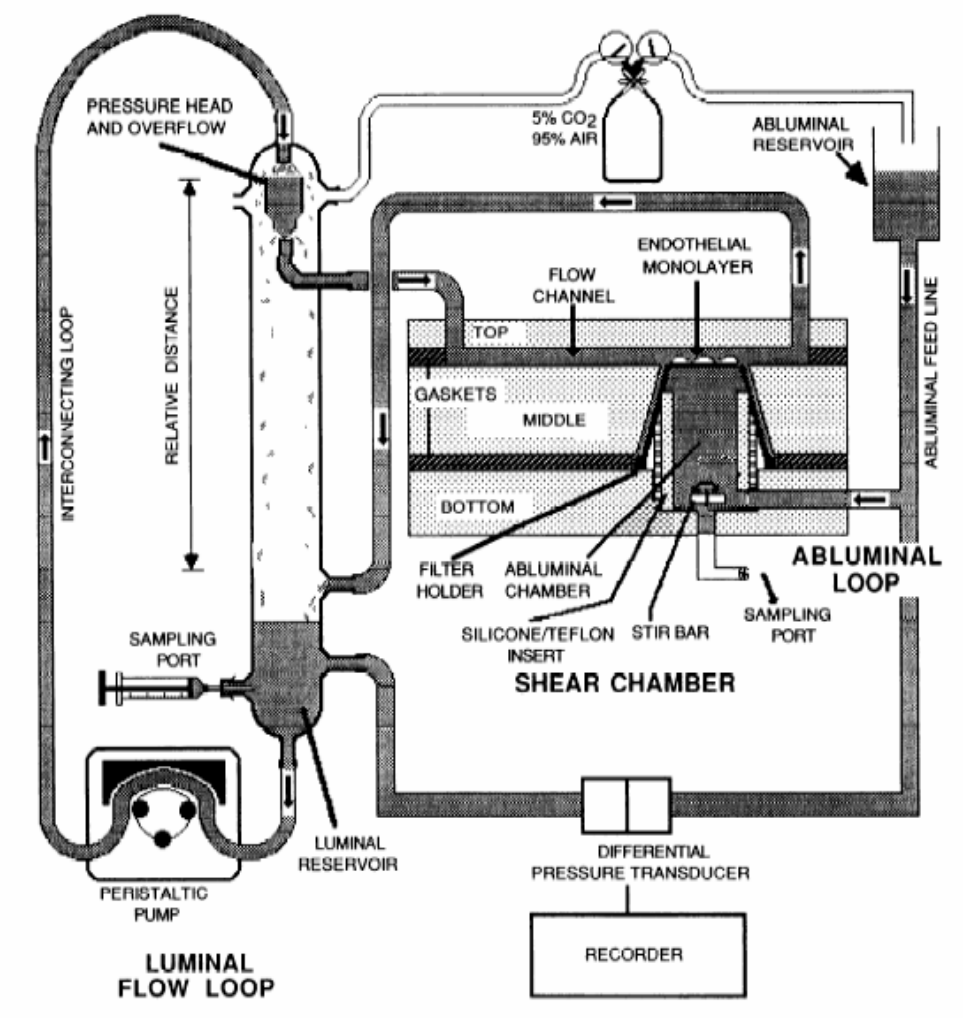

Figure 2.12. Permeability apparatus with shear stress through parallel plates.
(*Source*: Jo et al., *American J Physiol* 1991; 260(6): H1992-H1996 [46]; used with permission from the American Physiological Society).

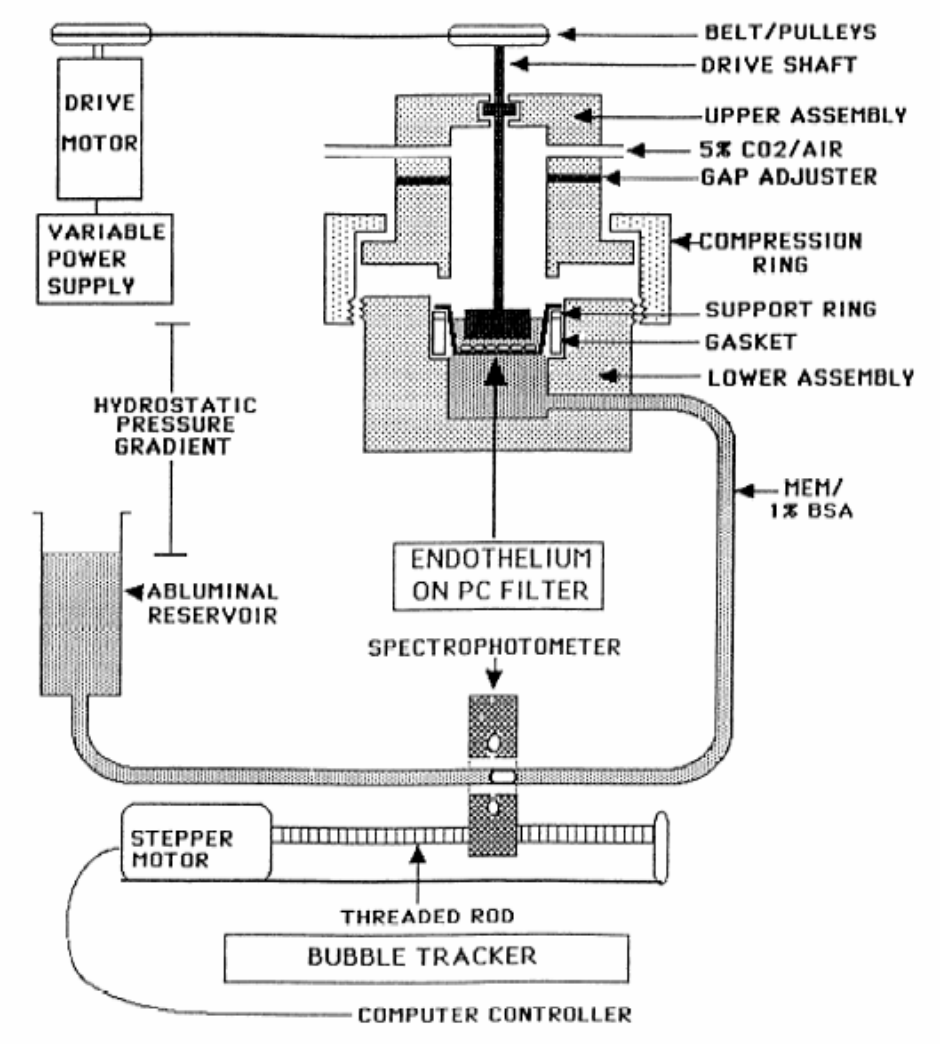

Figure 2.13. Permeability apparatus with shear stress from rotating cylindrical disk. (Source: Sill et al., *American J Physiol* 1995; 37(2): H535-H543 [85]; used with permission from the American Physiological Society).

Many of the early coculture studies simply focused on ensuring viable coexistence of both cell types in the same vicinity [90, 91]. Proliferation rates and cell counts were determined to ensure cell viability, and scanning electron micrographs were taken to assess cell shapes and possible extension of cell processes through membrane pores. Others investigated secretion rates of certain molecules in the presence of the second cell type. One specific example was the report of C-type natriuretic peptide (CNP) production by ECs in the

presence of SMCs [92]. Interestingly, in this work Komatsu and co-workers discovered marked increases in CNP production when high densities of SMCs were grown directly on ECs, but no significant increases when SMCs were seeded at low densities or in separated coculture.

To more closely mimic *in vivo* conditions, shear stress of ECs in any coculture system is a desirable feature. Although the majority of coculture studies are conducted with ECs in static condition, a number of coculture systems that incorporate shear have also been reported in the last decade. Three major types of systems have emerged. A series of papers published by Redmond and co-workers reported cocultured semipermeable capillary tubes featuring ECs grown inside the tubes and SMCs grown on the outer walls of the tubes [93-95]. ECs were sheared and perfused with media flown through the tube "lumen". In this setup, cells were separated by the tube wall such that there was no physical contact between cell types. One shortcoming of this system involves the many challenges related to post-experimental analyses of cells grown on curved tubes.

A coculture technique that has gained widespread popularity involved growing ECs and SMCs on opposite sides of a membrane insert (similar to that discussed above), and mounting the insert to a parallel plate flow chamber such that the ECs were exposed to flow [96-99] (Figure 2.14). This has several advantages over the capillary systems of Redmond, including simple assembly and disassembly to access either cell layer, and easy conventional coculture maintenance prior to inducing flow.

A third class of coculture systems that employed shear flow was an adaptation of the coculture using PPFCs above. Instead of growing both cell types on the same membrane, Ziegler and co-workers embedded SMCs in a matrix of collagen gel before seeding the gel

surface with ECs [100]. The cocultured gel layer was then inserted into a PPFC where the ECs were sheared. Interestingly, Butcher et al. have recently used a similar coculture model to investigate aortic valve ECs with VICs [101], and found perpendicular alignment of valve ECs to flow.

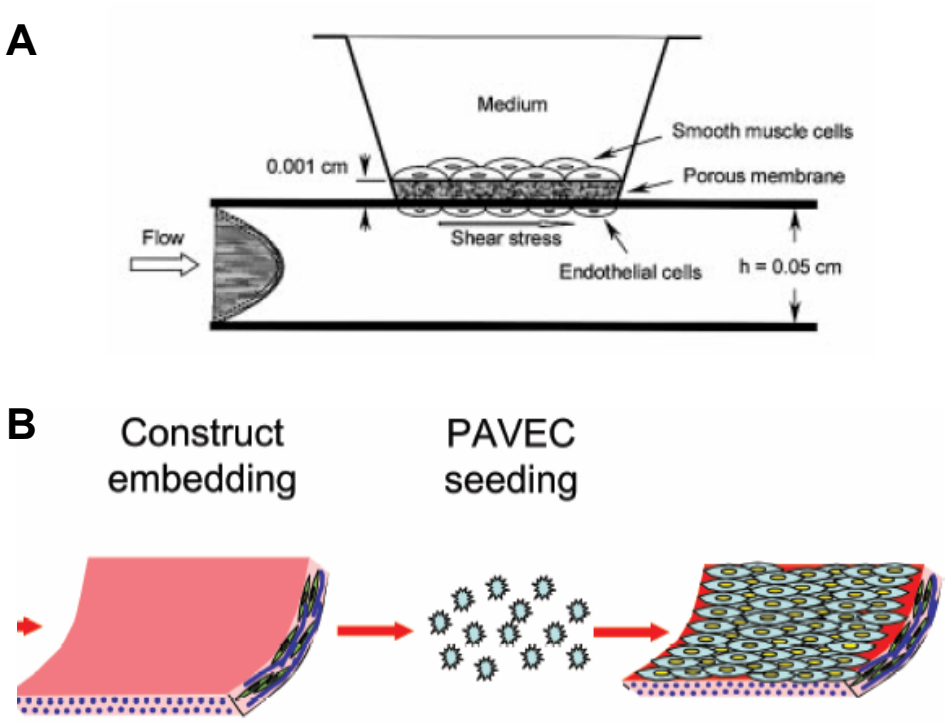

Figure 2.14. Shear-based coculture systems.

(A) PPFC with coculture of ECs and SMCs on opposite sides of membrane insert. (*Source*: This research was originally published in Blood. Chiu et al. Shear stress inhibits adhesion molecule expression in vascular endothelial cells induced by coculture with smooth muscle cells. *Blood*. 2003; 101(7): 2667-2674 [96]. © the American Society of Hematology.) (B) Coculture of matrix-embedded VICs and surface-seeded valve ECs, exposed to shear in PPFC. (*Source*: Butcher et al. [101]. Figure reproduced with permission from Mary Ann Liebert, Inc. publishers.)

2.4 Microscale Systems

2.4.1 Adhesion

One of the first adhesion studies to take advantage of parallelization in microfluidics and the convenience of soft lithography was the study by Kantak and co-workers who investigated platelet adhesion to different fibrinogen-coated substrates [102]. By fabricating four individual straight microchannels on the same chip and applying different surface coatings in each, Kantak and co-workers demonstrated one of the most basic advantages of microfluidics, i.e., increased efficiency of experimentation by parallelizing multiple conditions. Though simple in channel design and fabrication, it was rather impractical because it required separate injection into each microchannel using individual syringes mounted on a multi-syringe pump (Figure 2.15A). However, keeping the microchannels separate ensured no cross-contamination between samples.

To further streamline experimentation, Lu and co-workers designed parallel multi-microchannel networks to study adhesion of fibroblasts [103]. In each of two separate designs, Lu employed a single inlet port that required only one syringe to feed four interconnected microchannels, obviating the need for multiple syringe hookups (Figure 2.15B). Flow analyses in these networks relied on principles of hydraulic resistance (see Section 2.2). While these designs reduced the number of connections, they introduced the possibility of cross contamination between connecting branches of the network. When care is taken to ensure that hydraulic resistances are equal between parallel branches, cross contamination can be largely avoided.

The examples thus far are essentially PPFCs in parallel on a single chip. While these designs have benefited from parallelization, they still suffered from the same drawback as

mentioned for PPFCs, i.e., that shear stress must be manually adjusted by changing flow rate in the system, in this case via the syringe pump. Gutierrez and Groisman [104] designed a microfluidic network that incorporated variable shear stress flow chambers in a parallel configuration, combining the efficiency of multiple shear rates within one chamber with the flexibility of multiple experimental conditions across separate chambers of the same network. In addition, the design integrated pressure-actuated membrane valves that added an extra level of sophistication and permitted the simultaneous loading and experimentation of two separate cell populations. To date, this is perhaps the best demonstration of the benefits of microfluidics for testing adhesion: increased functionality coupled with simultaneous application of a range of shears over several different experimental conditions.

Several reports by Murthy and co-workers have employed linear shear stress flow chambers for studying adhesion strength as well as for selective enrichment of cell populations [105-107]. The design is identical to the tapered chamber of Usami (Figure 2.10B), and based on channel sizes, the devices implemented by Murthy are in fact physically larger than the original Usami design. Although this potentially illegitimizes their claim that their studies were microfluidics-based, it should be noted that Murthy fabricated devices using soft lithography, and this provides the benefit of allowing future parallelization of multiple linear shear stress chambers.

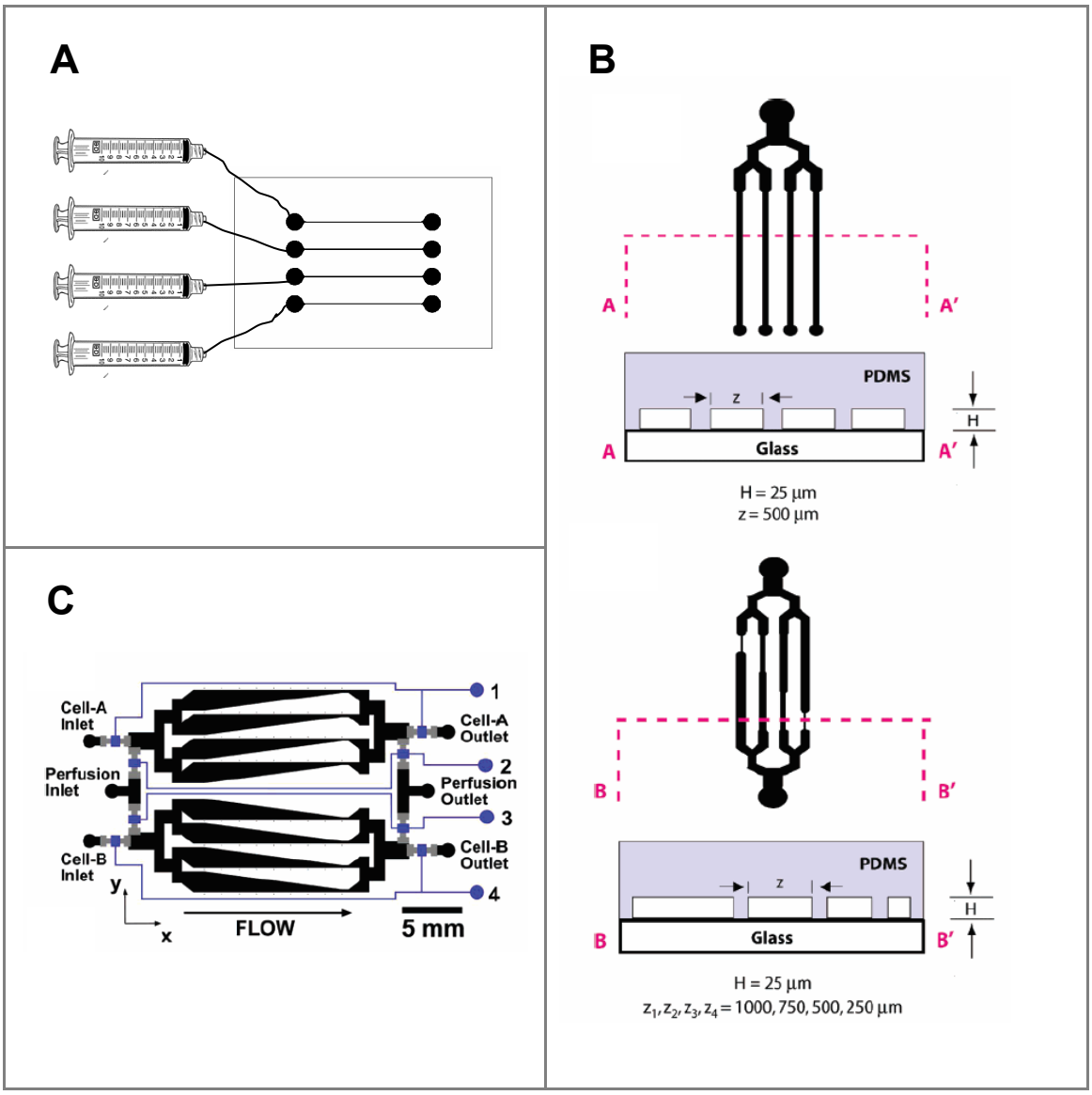

Figure 2.15. Various microfluidic systems for adhesion assays.

(A) Four separate microchannels in parallel from Kantak et al. [102]. (B) Parallel microfluidic networks with uniform shear flow chambers. (*Source*: Reprinted with permission from Lu et al. [103]. Copyright 2004 American Chemical Society.) (C) Parallel microfluidic networks with variable shear flow chambers. (*Source*: Reprinted with permission from Gutierrez et al. [104]. Copyright 2007 American Chemical Society.)

2.4.2 Shear Stress Response

Although a multitude of microfluidic cell culture devices have been reported, only a select few have focused on shear stress-induced responses of ECs. Many more studies have directed their attention to investigating other cell types including neurons, hepatocytes, osteoblasts, fibroblasts, and others, and this is understandable given the suitability of microdevices for all cellular scale studies [108-112]. The major challenge in these studies is the need for long-term culture of cells and the assurance of their viability, which was not necessary for the short duration of experiments in microfluidic adhesion assays. The challenge of culturing ECs is amplified by the need to achieve a confluent monolayer with proper cell-cell contacts, the absence of which has been shown to impact normal cell response. In terms of fluid mechanics, microfluidics is suited for shear stress studies because Reynolds numbers are low and almost guaranteed to be laminar. Consideration, however, must be given to channel aspect ratios to ensure wall effects on velocity profiles are minimized.

To my knowledge, the first shear response study of ECs in microfabricated channels was conducted by Gray et al. [113] who fabricated a device from silicon by deep reactive ion etching (DRIE), and cultured ECs to confluence to assess cell shape in varying channel widths. Bovine aortic ECs aligned with the direction of flow in a 200 micron wide microchannel after 16 hours of shear at 20 dyn/cm^2, demonstrating the feasibility of converting macroscale experimentation to the microscale. Perhaps a more interesting result from the study, however, was the natural tendency for ECs to elongate and align with channel lengths even in the absence of flow (for widths less than 200 microns). Thus, to

maintain proper EC morphology under static conditions in microenvironments, channel width was shown to be an important design parameter.

One of the often cited advantages of microfluidics and soft lithography is the ability to produce micropatterned surfaces. As one example of micropatterning for EC culture, Rhee and co-workers created adhesive patches on glass with a poly(dimethylsiloxane) (PDMS) patterning piece, and bonded a second microfluidic PDMS piece over the patches to form enclosed channels where ECs were seeded [111] (Figure 2.16). They were able to demonstrate adhesion and spreading of ECs on the patterns over a five-hour culturing period, but did not apply shear stress to the cultured cells. Although the culturing time was relatively short and no shear was applied, this was nevertheless an important study that demonstrated in-channel micropatterns could be generated to spatially control growth of ECs.

One of the most novel advances in microfluidics technology with biological relevance was the work of Spence and co-workers who fabricated an inline carbon ink microelectrode [114] for amperometric detection of nitric oxide (NO) production from pulmonary artery ECs [115]. A general concern of microfluidics is the low volume, and thus, low numbers of detectable analytes. NO measurements at the macroscale are typically performed by sampling millilitres of media over specified time periods (on the order of tens of minutes), but volume limitations make this impractical at the microscale. Inline amperometric detection allows real-time monitoring of NO production and reduces the amount of NO lost due to autooxidation to NO_2^-. Oblak and co-workers have since used fluorescent microscopy for NO detection as an alternative technique with improvements over amperometry [116]. Further investigation is needed to ensure EC behaviour is directly scalable from macro- to microscale so that no loss in biological activity is introduced. If this is the case, on-chip

measurements of secreted factors would be a large step toward advancing microfluidics for EC studies.

Finally, we discuss one of the most innovative techniques for generating flow-induced shear on ECs in microfluidic channels. Microchannels cast in PDMS were used to culture ECs to confluence before recirculating flow was introduced via Braille pin actuation [117] (Figure 2.16). On-chip valves were incorporated by fabricating thin film PDMS membranes that were deflectable by computer-programmed actuating pins to pump fluid in a pulsatile fashion through the microchannels. Using this device, Song and co-workers measured EC morphological response and obtained data on elongation and orientation consistent with the literature, i.e., low shear of 1 dyn/cm^2 did not align cells while high shear of 9 dyn/cm^2 aligned cells parallel to flow. One caveat of this system is that only peristaltic pressures can be generated, and although this is sometimes desirable for mimicking physiological environments more closely, data cannot be easily compared to the large body of literature on steady shear EC responses.

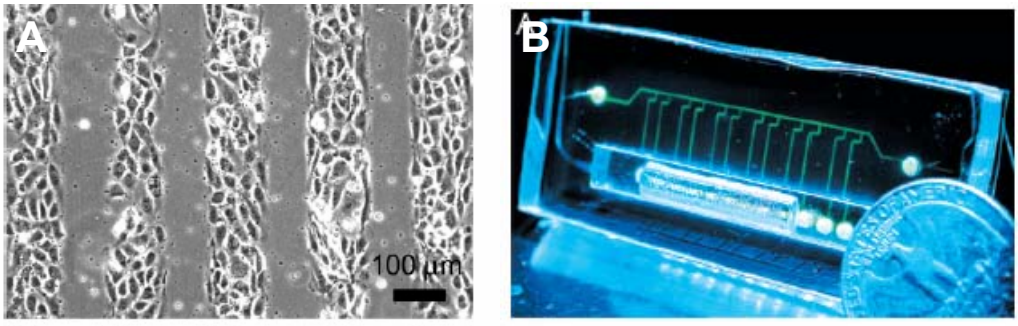

Figure 2.16. Microfluidic devices for shear stress application on ECs.

(A) Micropatterned substrates for HUVEC culture in microfluidic channels. (*Source*: Rhee et al. [111] – reproduced by permission of The Royal Society of Chemistry.) (B) PDMS-based EC shear device with flow actuated by Braille pins. (*Source*: Reprinted with permission from Song et al. [117]. Copyright 2005 American Chemical Society.)

2.4.3 Permeability

To date, no studies have measured permeability of ECs in microfluidic channels. Despite the absence of specific studies pertaining to permeability, advances in microfluidics have helped introduce practical fabrication methods suited for endothelial permeability experiments. The most important feature of a permeability measurement system, based on macroscale setups, is a porous membrane that supports endothelial cell growth while also allowing passage of molecules from luminal to abluminal sides of the endothelium. In microfluidic systems, the simplest way to incorporate membranes is to sandwich a commercially available track-etched membrane between two pre-cured PDMS slabs each containing their own microfluidic channel patterns, as reported by Ismagilov et al. [118]. At the time of this paper, this approach introduced new opportunities for multilayer fabrication in which microchannels could be separated by a permeable layer to communicate in a three-dimensional microfluidic network. Others have since adopted this technique for their own applications [119-121]. Indeed, there are other fabrication options available for introducing membrane layers within microfluidic devices, and these are critically reviewed by de Jong et al. [122]. The incorporation of commercially-available membranes, however, is the most direct and economical of the alternatives.

It is worth mentioning here the novel work of Huh et al. [120], who used a membrane-based microfluidic device to culture small airway epithelial cells and study the effects of rupturing liquid plugs in a liquid-air two-phase flow system. The study demonstrated the feasibility of culturing ECs on membranes for long term within microfluidic environments. More importantly, however, the work was a reminder that once

cells are properly cultured on the membrane, microfluidics is a natural platform for imposing shear stress on the endothelial monolayer.

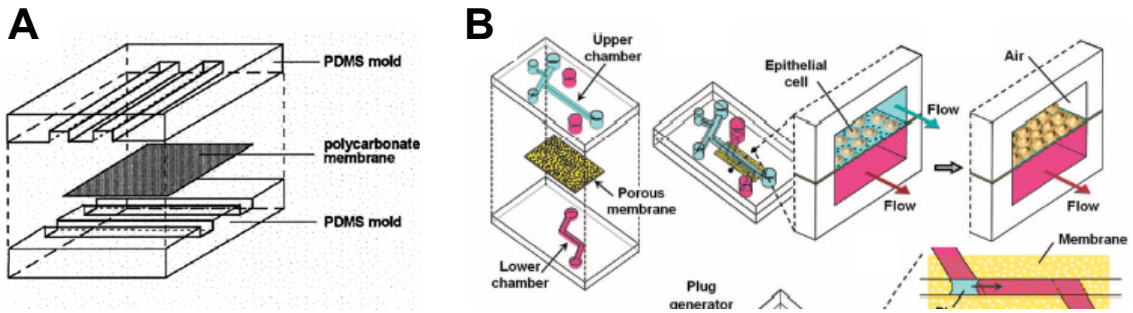

Figure 2.17. Microfluidic devices incorporating commercial membranes.
(A) Fabrication of microfluidic device by sandwiching membrane with PDMS slabs. (*Source*: Reprinted with permission from Ismagilov et al. [118]. Copyright 2001 American Chemical Society.) (B) Application of membrane device for modeling the lung airway system. (*Source*: Huh et al. [120]. Copyright 2007 National Academy of Sciences, U.S.A.)

2.4.4 Coculture

Microfabrication technology has recently aided advances in coculture studies. However, none of the reports to date have discussed a microfluidic system for coculture of ECs and SMCs/VICs while the ECs are exposed to shear stress. Published reports of coculture have mainly focused on controlling spatial relationships of cells and chemical gradients of reagents in a microscale platform consisting of culture arrays and perfusion networks [112, 123, 124]; none of these involved ECs. Others who have studied ECs in coculture have utilized the benefits of laminar flow in microfluidics to assemble a model of a blood vessel consisting of three separate layers of cells in distinct matrices [125]. Perhaps the closest demonstration of ECs in coculture was the work of Genes and co-workers who cultured ECs on one side of the membrane in a microchannel and streamed red blood cells on the opposite side of the membrane to stimulate NO production from the ECs [126]. Although

demonstrative of the coculture capabilities of microscale systems, these reports have yet to take advantage of the inherent benefits of microfluidic geometry to apply shear stress over EC monolayers to induce a proximal SMC/VIC response. With the membrane-bound devices described in the previous section, such a coculture system appears to be within reach in the near future.

2.5 Macro- versus Microscale

Macroscale ICF systems are built for long-term reliable use, and materials chosen for their construction are usually autoclavable, chemically resistant, and optically transparent to aid visualization. Designs are usually based on well-characterized two-dimensional steady fluid flow patterns so that known theoretical solutions are available to aid analyses (e.g., cone-and-plate viscometers and parallel plate flow chambers). Because of the size of the platform, large populations of cells are studied at once, and this is advantageous for global population-based studies where it is desirable to smooth out heterogeneities and also make available enough biological products for gene and protein expression analyses. Many of these claims are still regarded as advantages of conventional ICF systems. And because much of the current literature on ECs was established using conventional systems, it is easy to resist change and continue with traditional methods so that results between different studies can be objectively and conveniently compared. However, over the last five to ten years, developments in microfluidics have presented a compelling case for a revolutionary change in the systems that should be used for endothelial cell biology, and a change in the way we approach scientific experimentation in general.

The majority of microscale ICF systems are currently fabricated by soft lithography and replica molding of elastomeric materials. This fabrication technique is convenient, versatile, and relatively economical, meaning new designs of complex channel networks can be implemented quickly over short concept-to-device turnaround times. Elastomeric materials are not ideal for all applications, but serve as good materials for rapid prototyping of different designs for proof-of-principle experiments. Also, the technique easily allows feature sizes as small as five microns, offering high spatial resolution for micropatterning, and high density of microchannels for parallelization and integration with other on-chip processes. Microchannel sizes for cell-based studies often do not need to be smaller than 100 microns, but the flexibility to pattern the internal surfaces of larger microchannels is an added bonus. Naturally, small microchannel cross-sections mean high surface area-to-volume ratios and a significant reduction in reagent consumption. Because length scales are small, low Reynolds number laminar flows dominate, and this can be exploited to generate controllable concentration gradients of soluble factors. Thus, the cellular microenvironment in terms of chemical, mechanical, and topographic cues can be tailored to researchers' needs. These advantages are simply not available at the macroscale.

The aforementioned "advantages" of macroscale setups, including its durability and its capacity for large population-based studies, are in fact becoming less favourable when one considers the new options available to us through microfluidics. Macroscale ICF systems may be durable, but often require regular maintenance and repair. Microfluidics offers an affordable option that can be made disposable and at the same time amenable to existing infrastructure, so that microfluidic cartridges akin to Petri dishes and well plates can be employed to streamline experimentation. The argument that macroscale ICF systems can

study large populations of cells and smooth out heterogeneities is also weakening with advancements in small population-based studies and single cell analyses [127]. For example, the research group led by Stephen Quake at Stanford has demonstrated single cell mRNA isolation and analysis [128], while Ginsberg has reported methods to amplify RNA from a single cell [129]. Microfluidic systems give us the option of obtaining information from single cells when needed, while population averages can be reassembled from the single cell data if so desired. Therefore, previous claims to macroscale benefits are perhaps simply misconceptions stemming from the time when these technological advances had yet to mature.

2.6 Future Outlook

For over twenty years, macroscale ICF systems have been important laboratory instruments for basic research in endothelial cell biology. Yet, within just the last five years alone, developments in microfluidics have revolutionized the way we approach cell-based research, and called into question the utility and efficiency of existing setups. To realize the promise of microfluidic technology, however, it is imperative for the research community to bridge the gap between engineers, who design novel devices that often do not translate to user-friendly systems, and biologists, who are the end users of these devices and ultimately want accessibility in the design. In the next ten years, the true measure of whether microfluidics has made significant impact on biology will be the number of biologists who have accepted microfluidics as an alternative to macroscale formats, and the number of significant findings originating from microfluidic-based studies, which otherwise would not

have been discovered with macroscale experiments. The role of the engineer is to facilitate this revolution by designing for true accessibility.

Chapter 3

3 Thesis Objectives

Microfluidic systems offer a new platform for studying endothelial cell biology, and promise to streamline experimentation, increase throughput, and reduce reagent consumption. To date, the design, fabrication, and use of microfluidic devices have remained largely the focus of a dedicated community of experts in the areas of microscale engineering, chemical analyses, and biomolecular applications. Although reports of microfluidic cell culture studies are growing rapidly worldwide, the acceptance of this technology among cell biologists has been gradual and reserved. In view of this current divide between technology and basic cell science, the main goal of this thesis is to demonstrate the usefulness and convenience of microfluidics for studying EC biology, and to provide evidence of novel biological findings that illustrate the practicality of integrating microfluidics technology into existing cell biology laboratories.

To achieve this goal, we focused on developing a toolbox of accessible microfluidic devices for examining properties of EC types. Two EC types were of particular interest: ECs from the porcine aorta (PAECs) and ECs from the porcine aortic valve (PAVECs). The motivation behind studying PAECs and PAVECs was discussed above, and will be re-emphasized in the subsequent chapter. Briefly, studying two related but distinct EC phenotypes allowed direct comparison of their properties, and offered an opportunity to assess sensitivity of microfluidic systems for detecting subtle phenotypic differences. Furthermore, aortic valve ECs have not yet been fully characterized, owing partly to a lack of reliable methods in the literature for isolating and purifying valve ECs for *in vitro* experimentation. The list of objectives reflects the need to first obtain pure populations of the cells prior to examining their unique properties within microfluidic environments.

The objectives (Roman numerals) and specific aims (Arabic numerals) of this thesis are:

I. To investigate techniques for isolating and purifying PAVECs

1. Measure yield and purity of PAVECs obtained from different enzymatic digestions
2. Compare feasibility and economy of magnetic-based cell sorting and clonal expansion techniques for purification

II. To study EC adhesion properties in microchannels

1. Design, fabricate, and implement a microfluidic system for measuring adhesion and spreading of ECs
2. Utilize system to compare adhesion and spreading between cell types
3. Develop integrin blocking and immunostaining techniques in microchannels

III. To study shear stress response of ECs in microchannels

1. Investigate long-term culture of ECs within microchannels
2. Design flow loop that can incorporate microchannels into recirculatory experiments
3. Determine morphological response of ECs in microchannels and compare to macroscale results

IV. To design and implement a microfluidic device to measure EC permeability

1. Design, fabricate, and implement a multi-layer membrane-based microfluidic device to facilitate controlled communication between channels
2. Devise and implement setup for sample detection and measurement of permeability
3. Measure permeability of ECs on membranes

V. To design a coculture microfluidic device to study EC

1. Design and fabricate a multi-layer microfluidic device suitable for studying cell-cell communication and for high resolution microscopy for imaging applications.

Throughout the thesis, accessibility of the developed technology will be emphasized, and novel or significant biological findings will be highlighted when appropriate to demonstrate the potential impact of microfluidics on the cell biology community at large. When needed, caveats to microfluidic systems will also be discussed, and recommendations for future directions and improvements will be provided. These technologically-driven themes will be presented through investigations of EC properties that reflect the importance of endothelial heterogeneity, as well as the other endothelial characteristics outlined in the background literature.

Chapter 4

4 Isolation and Purification of Valve Endothelial Cells[2]

Although many different types of ECs have been studied extensively in the past thirty years, valve ECs specifically have received little attention. Examples of standard ECs chosen for *in vitro* experimentation include bovine aortic ECs and human umbilical vein ECs, simply because they are readily available, easy to isolate, have well-known properties in culture, and are obtained from blood vessels that many would consider representative of the vasculature in general. Valve ECs, on the other hand, are not as readily available. And because they reside on leaflet tissues with vastly different matrix composition and structure from other tissues in the vascular system, they are far less representative of other endothelial phenotypes. As a result, isolation techniques for valve ECs are scarce, and documentation of their properties is relatively thin.

[2] I thank Wing-Yee Cheung for her contributions to the work presented in this chapter, which resulted in an article published in the Journal of Heart Valve Disease [130. Cheung, W., E.W.K. Young, and C.A. Simmons, Techniques for isolating and purifying porcine aortic valve endothelial cells. *Journal of Heart Valve Disease*, 2008: p. (in press)..

As mentioned, recent progress in valve EC biology [50, 51] has sparked interest in characterizing and examining the valve endothelium in more detail. Performing rigourous characterization of valve ECs, however, requires first and foremost high purity EC populations that are not contaminated with other cell types. From past experience, techniques used to isolate vascular ECs, including enzymatic digestion of the subendothelial matrix and gentle scraping to release cells [50, 57], have not yielded valve EC populations that were sufficiently pure for long-term culture experiments. Rather, these approaches often resulted in release of both ECs and a minor but significant proportion of ICs from within the valve matrix. When undesired ICs are left in culture with ECs, ICs have the potential to overpopulate the culture, particularly once the ECs reach confluence and are contact-inhibited. Improvements in isolation techniques are therefore desirable to increase both the yield and purity of ECs for *in vitro* culturing and subsequent experimentation.

In this chapter, we describe experiments that examined various conditions for enzymatic digestion and determined isolation parameters that yielded large numbers of valve ECs. Two separate methods were employed to further purify these initial isolates: a magnetic bead-based technique for separation of immuno-labelled cells, and a clonal expansion technique that yielded a pure EC population from culturing of single cells. The purification techniques were subsequently compared for quality, efficiency, and economy.

4.1 Materials and Methods

Unless stated otherwise, chemicals and reagents for cell isolation and culture were purchased from Sigma-Aldrich Canada (Oakville, ON, Canada); fluorescent dyes were from

Invitrogen (Burlington, ON); and all other materials were purchased from Fisher Scientific (Ottawa, ON).

4.1.1 Valve Endothelial Cell Isolation

Porcine hearts were obtained from a local abbatoir (Quality Meat Packers, Toronto, ON) and were transported and stored in phosphate buffered saline (PBS) containing Ca^{2+} and Mg^{2+} until isolation. Within two hours of death, aortic valves were excised from surrounding heart tissue and cut open between the commissures of the leaflets to facilitate removal of the leaflets. After excision, leaflets were rinsed thoroughly with PBS containing 1% penicillin-streptomycin (P-S) and 1% amphotericin B.

Leaflets were treated by enzymatic digestion in a solution containing collagenase and dispase (Invitrogen) of various concentrations (as indicated in results of this chapter) diluted in PBS. This step dissociated ECs from the extracellular matrix and released them into suspension. After digestion, leaflets were further treated to detach residual ECs from the matrix. Several treatment methods were attempted, including (1) rinsing without physical agitation, (2) gentle scraping of leaflet surfaces, and (3) vortexing of leaflets (1 minute on 'high' setting) using a Mini Vortexer (VWR Scientific Products, Mississauga, ON). Vortexing was found to be the more effective method for dislodging more ECs from the matrix while leaving the matrix intact. Scraping, on the other hand, often led to excessive removal of subendothelial matrix debris that polluted the isolated cell population.

Primary isolated cells (P0) were resuspended in EGM-2 basal medium with SingleQuots (Cambrex Clonetics, East Rutherford, NJ) supplemented with 20% fetal bovine serum (FBS; Hyclone, South Logan, UT) and 1% P-S (supplemented EGM-2), and cultured on tissue culture-treated polystyrene (TCP) coated with 3% (w/v) gelatin (room temperature,

15 min) for 3-4 days, at which point the primary cells were ready for passaging. Higher passage ECs (P1 or higher) were cultured in M199 media containing 10% FBS and 1% P-S (supplemented M199). Media was changed after two days in all cases. For cell yield and EC purity experiments, cells were resuspended in supplemented M199. Isolated cells were then either counted (Vi-CELL Analyzer, Beckman Coulter, Mississauga, ON) for total cell yield, or deposited onto microscope slides by cytocentrifugation (Shandon Cytospin, Thermo Scientific, Waltman, MA) for immunostaining and quantification of EC purity. (See Appendix A for detailed protocol).

4.1.2 Magnetic Cell Sorting (MACS)

Subcultured cells (P1) were cultured for approximately one week before purification using magnetic cell sorting (MACS). Briefly, cells were dislodged from culture with 0.25% trypsin containing 2 mM EDTA, centrifuged at 284 × *g* for 10 minutes, and resuspended in MACS buffer (PBS containing 0.5% (w/v) bovine serum albumin (BSA) and 2 mM EDTA) at 1 million cells per 100 µL. ECs were labelled (4°C, 40 min) with a primary mouse anti-porcine antibody for CD31 (Clone LCI-4; Serotec, Raleigh, NC) a recognized EC marker not expressed by valve ICs. ECs were then magnetically labelled (4°C, 40 min) with MACS goat anti-mouse IgG Microbeads (Miltenyi Biotec, Auburn, CA). The entire cell suspension was loaded onto the MACS magnetic column to capture labelled cells within the column while eluting the unlabelled cells. Captured cells were flushed out of the column, counted with a hemocytometer, and subsequently seeded onto gelatin-coated glass slides for immunostaining, or onto gelatin-coated polystyrene flasks for subculturing. Cells prepared for immunostaining were cultured for ~1-2 days to ensure proper cell adhesion, and were less than 50% confluent to facilitate quantification.

4.1.3 Single Cell Clonal Expansion

Valve ECs were isolated as described above, followed by serial dilution of the primary cell suspension to obtain a final concentration of 1 cell/mL in supplemented EGM-2. 200 μL of this cell suspension was pipetted into each of the 3% (w/v) gelatin-coated wells of a 96-well plate to yield a nominal cell seeding density of 0.2 cells/well. This density was found to be optimal for obtaining a high number of wells containing a single cell. Five 96-well plates were used in total for each isolation. Cells were incubated at 37ºC for one week before the first morphological screening and feeding of pure EC colonies. ECs were distinguished from ICs by their cobblestone morphology and monolayer organization. Wells that were initially identified as containing ECs were fed with 100 μL of supplemented EGM-2 every two days. Cells were frequently monitored until they reached 70% confluence so that any wells suspected of containing ICs would be properly discarded.

EC colonies from selected wells were trypsinized and plated onto gelatin-coated 24-well plates, and expanded in supplemented M199. To reduce likelihood of IC contamination (in the event that EC colonies were misidentified during initial screening), cells from selected wells were not pooled together when seeding into larger wells. Cells at P3 were plated on gelatin-coated glass coverslips for immunostaining to determine EC purity.

4.1.4 Indirect Immunostaining

Cells plated on gelatin-coated coverslips were fixed with 10% neutral buffered formalin (NBF), permeabilized with 0.1% Triton X-100, and stained for CD31 and alpha-smooth muscle actin (α-SMA, Clone 1A4) to identify ECs and ICs, respectively. Briefly, samples were blocked (37ºC, 20 min) with 3% (w/v) BSA diluted in PBS, and incubated (4ºC

overnight) with mouse anti-porcine CD31 primary antibody or mouse anti-human α-SMA primary antibody at a dilution of 1:100 in 3% (w/v) BSA. The samples were blocked (room temperature, 30 min) with 10% goat serum diluted in PBS, and were subsequently incubated (room temperature, 1 h) with goat anti-mouse AlexaFluor 568 secondary antibody for conjugation to CD31, or goat anti-mouse AlexaFluor 488 secondary antibody for conjugation to α-SMA at a dilution of 1:100 in 10% goat serum. Once excess secondary antibodies were removed with PBS, the samples were incubated (room temperature, 5 min) with Hoescht 33342 nuclear dye at 1:1000 dilution in PBS. Samples were mounted on microscope slides with Permafluor mounting media (Fisher) and analyzed with a fluorescence microscope (Olympus IX71) to identify CD31-positive or α-SMA-positive cells.

4.1.5 Image Analysis

Fluorescent images were taken with a CCD camera (QImaging Retiga, Surrey, BC) connected to the fluorescent microscope. Images were analyzed with ImageJ software (NIH), and quantification of EC purity was based on counts of cells expressing only Hoechst nuclear dye (all cells) or both Hoechst and their respective cell-specific stains. Three viewfields were imaged, counted, and averaged for each sample, and three to four samples were analyzed for each condition.

4.1.6 Statistical Analysis

All values are presented as mean ± standard error (independent samples $n = 3$ or 4). Single-variable analysis of variance (ANOVA) was used for multiple comparisons within a study, and Tukey's method was used for post-hoc pair-wise comparisons. Differences were considered significant for $P < 0.05$.

4.2 Results

4.2.1 Effect of Enzymatic Digestion Protocol on Yield and Purity

Three different collagenase concentrations of 20, 40, and 60 U/mL were tested to determine the concentration that provided the highest yield of ECs. All collagenase concentrations were tested in a solution with 0.5 U/mL dispase for six hours in an incubator (37°C, 5% CO_2). Cell yield increased with increasing collagenase concentrations (Figure 4.1A), but this trend was not statistically significant ($P = 0.14$). Increasing the collagenase concentration from 20 U/mL to 60 U/mL had no effect on EC purity, which remained relatively low (49 ± 7% to 68 ± 9% ECs) (Figure 4.1B).

Three different dispase concentrations of 0.5, 1.0, and 2.0 U/mL were also tested to determine the dispase concentration that gave the highest yield of ECs. All dispase concentrations were tested in a solution with 60 U/mL collagenase (based on above results for high yield), and incubated for six hours as before. Although varying dispase concentrations did not affect total cell yield (Figure 4.1C), EC purity was significantly higher with high dispase concentrations (1.0 and 2.0 U/mL) than with low dispase concentration (0.5 U/mL) ($P < 0.05$, Figure 4.1D).

To obtain high yields of ECs efficiently, incubation times of one, two, and three hours were also tested using 60 U/mL collagenase and 2.0 U/mL dispase. Although total cell yield appeared to increase with longer incubation times, the differences were not statistically significant ($P = 0.23$, Figure 4.1E). However, cell yields and EC purity for two and three hours of incubation were comparable to one another and to the cell yields and purity obtained for six hour incubations (~ 1 million cells, 98% purity) (Figure 4.1F).

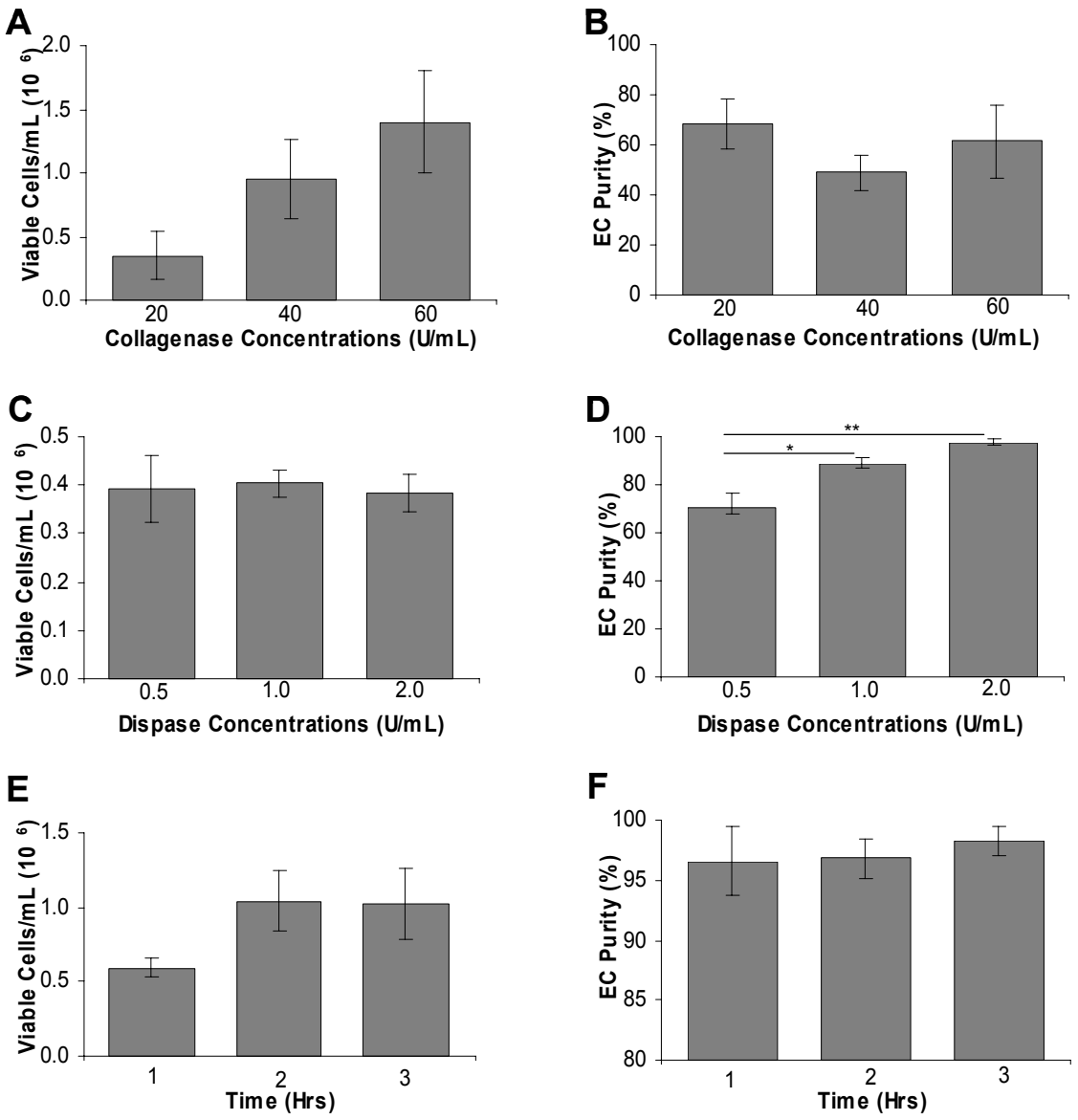

Figure 4.1. Optimization of enzymatic digestion and incubation times for viable cell yield and EC purity.

All cell yields represent totals collected from three aortic valves. (A) Increasing collagenase concentration increased cell yield, but data was not statistically significant ($P = 0.14$). (B) Increasing collagenase concentration did not affect EC purity (~60%). (C) Increasing dispase concentrations did not affect cell yield. (D) Increasing dispase concentrations from 0.5 U/mL to 1.0 U/mL and 2.0 U/mL increased EC purity. (* $P < 0.05$, ** $P < 0.01$). (E) Increasing incubation times from one hour to two and three hours increased cell yield, but data was not statistically significant ($P = 0.23$). (F) EC purity was not affected with increasing incubation times, but remained high at ~ 97%.

4.2.2 Magnetic Cell Sorting

Despite the relatively high purity of the primary isolates, many cells appeared fibroblast-like, had overlapping processes (Figure 4.2A), and did not express CD31 (Figure 4.2B) only 24 to 72 hours after plating, suggesting significant IC growth and contamination. To improve EC purity further, primary isolated cells were cultured for one week to obtain ~20 million cells and then magnetically sorted to isolate CD31-positive cells. Samples of cells taken before and after sorting were immunostained for Hoescht nuclear dye and CD31, and analyzed to compare EC purity. Whereas the pre-sort population was significantly contaminated with non-ECs (Figure 4.2A and B), most of the sorted cells displayed cobblestone morphology after 72 hours in culture (Figure 4.2C), and expressed CD31 (Figure 4.2D). The marked improvement in EC purity was statistically significant, with EC purity increasing from 40 ± 6% before sorting to 96 ± 3% after sorting ($P < 0.01$) (Figure 4.2G).

Although magnetic cell sorting markedly improved cell purity after initial isolation, it suffered from two drawbacks. First, separation efficiency of the MACS system was strongly dependent on antibody labelling conditions (concentration, temperature, and duration) because of the different protein binding affinities between cell surface markers, primary antibodies, and antibody-bound magnetic microbeads. In some cases, separation efficiency was as low as ~ 10% (based on a final separation of 1×10^6 labelled cells from an initial suspension of 25×10^6 cells of ~ 40% EC purity). Secondly, although confluent EC cultures appeared to be free of IC contamination, ICs began to reappear in cultures grown one day post-confluent (Figure 4.2E and F). These cells then populated the culture on top of the contact-inhibited EC monolayer, resulting in cultures having properties similar to pre-sorted cultures when left for one to two extra days.

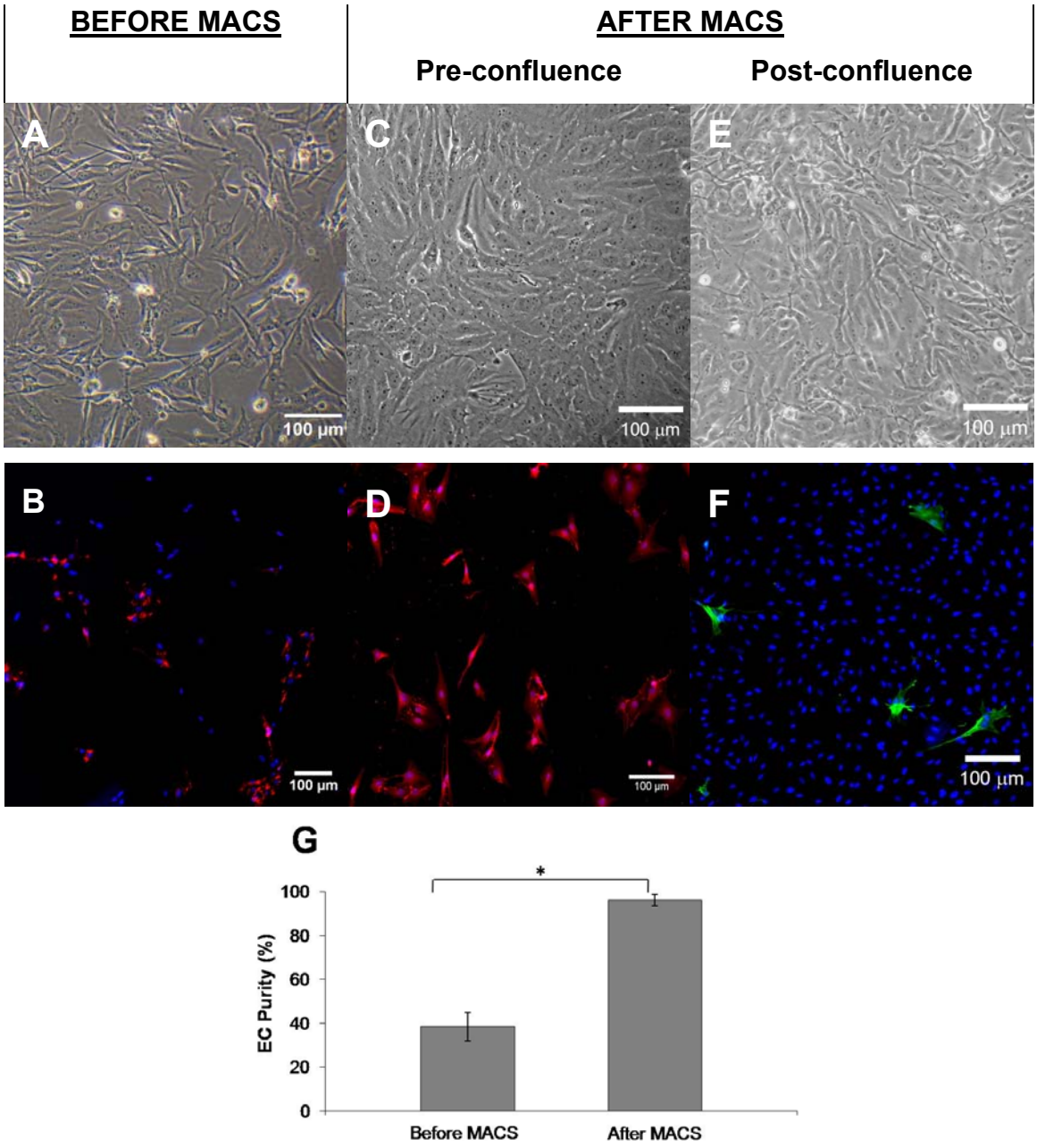

Figure 4.2. Phase contrast images (A,C,E) and fluorescent immunostaining (B,D,F) of valve ECs at different confluencies purified by magnetic cell sorting.

Hoechst (blue), CD31 (red), and α-SMA (green). (A) 72 h after seeding, before sorting, with noticeable IC growth. (B) 24 h after seeding, before sorting. Cells expressing Hoechst but not CD31 were considered ICs. (C) 72 h after sorting. Culture reached close to confluence with no noticeable IC growth. (D) 24 h after sorting, with improved EC purity, demonstrated by CD31 expression. (E) 24 h after confluence, with noticeable IC contamination reappearing on top of underlying ECs. (F) 24 h after confluence, with ICs fluorescently-labelled with α-SMA. (G) EC purity before (24 hr before isolation) and after (24 h after sorting) magnetic cell sorting, showing significant statistical difference (* $P < 0.01$).

4.2.3 Single Cell Clonal Expansion

As an alternative method to improve EC purity, freshly isolated cells were cultured as single cells in 96-well plates. Cells cultured from single cell colonies were determined to be ECs based on morphology (Figure 4.3). During identification, cell colonies that displayed cobblestone morphology and contained cuboidal cells in close contact with one another were considered EC colonies (Figure 4.3A). Colonies that lacked these characteristics, but instead were elongated, spread apart from one another, and contained extended cell processes were considered IC colonies (Figure 4.3B). In each of three separate isolations, 480 wells (five 96-well plates) were seeded at 0.2 cells/well, yielding 60 ± 20 wells contained a colony, of which 15 ± 4 wells were identified conservatively to be EC colonies. The cells were expanded from these wells to T-75 flasks in three passages over the course of three weeks, corresponding to a consistent doubling rate of ~15 - 21 hours.

When cultured to confluence, cells displayed cobblestone morphology typical of ECs (Figure 4.4A), and expressed CD31 without IC contamination (Figure 4.4B), even over several passages. When cultures were maintained at confluence for an additional two weeks without passaging, cultures remained free of ICs.

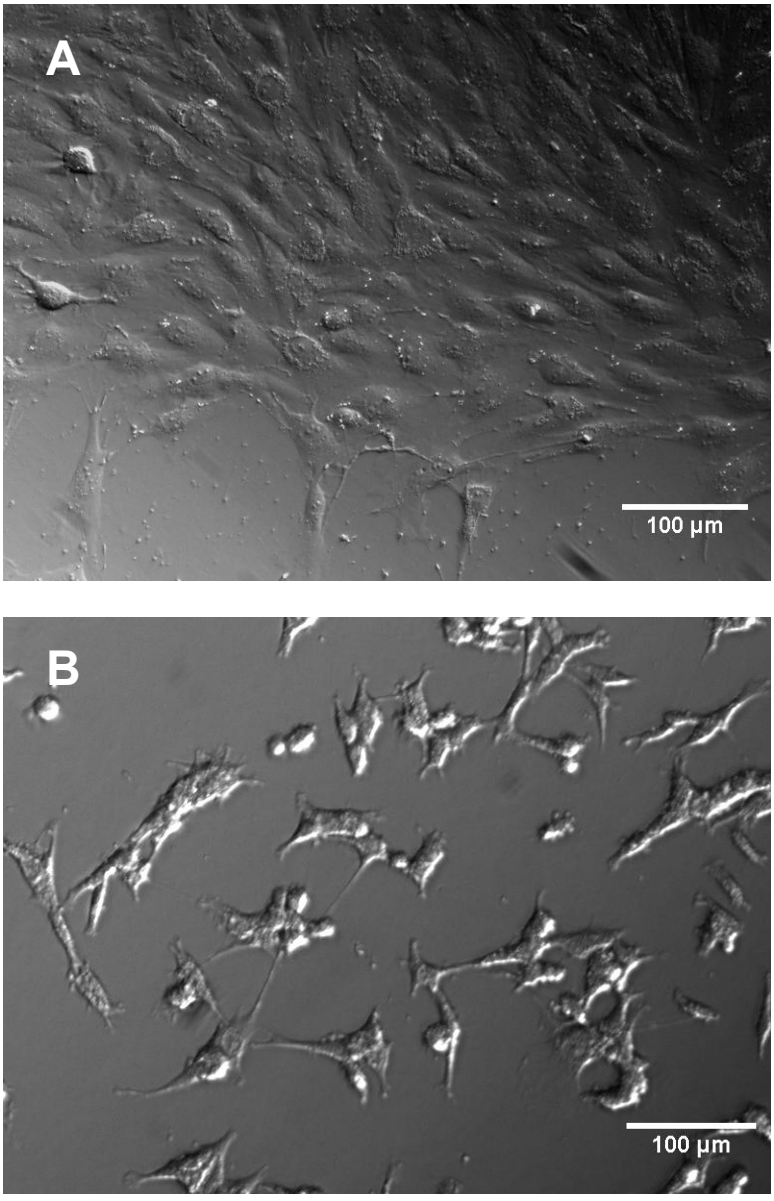

Figure 4.3. Identification of endothelial cell colonies.

(A) Cells identified as ECs under relief contrast. Cells appeared cuboidal and formed networked islands that were locally confluent. (B) Cells identified as ICs under relief contrast. These cells displayed elongated cell bodies, developed processes, and were found to be separated by several cell diameters from each other during initial growth. These characteristics were consistent with typical IC morphology.

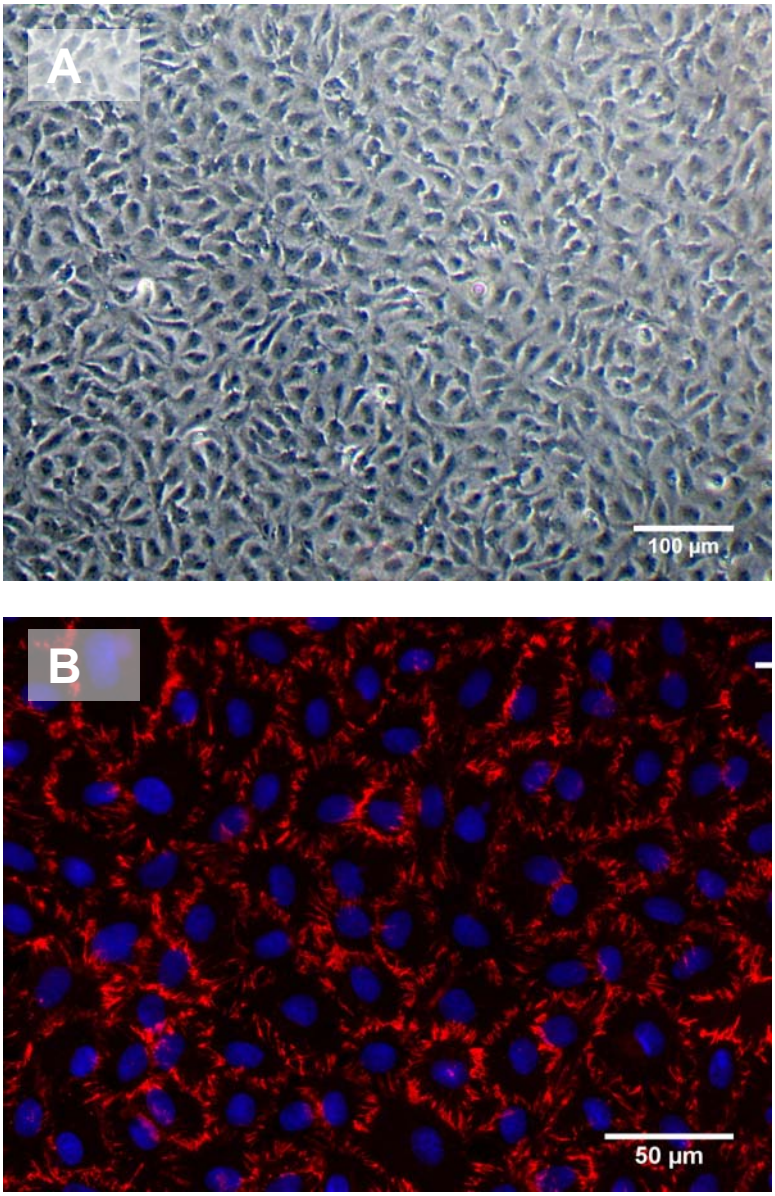

Figure 4.4. Endothelial cell culture at confluence, derived from clonal expansion.

(A) P2 ECs imaged under phase contrast after approximately 14 days from initial isolation. **(B)** Immunostaining of P3 ECs grown to 100% confluence, with no IC contamination. Hoechst nuclear dye (blue) and CD31 (red).

4.3 Discussion

Recent evidence indicates that aortic valve ECs are phenotypically distinct from their counterparts in the vasculature [50, 131, 132] and play important roles in homeostasis and the initiation of valve disease [1, 2]. Accordingly, there is increasing interest in studying aortic valve EC biology. To facilitate *in vitro* studies of aortic valve ECs, we tested different isolation and purification techniques. Our goal was to provide a direct and objective comparison of methods so that other researchers can choose a suitable isolation method based on their application. We found that enzymatic digestion of leaflets with 2.0 U/mL dispase and 60 U/mL collagenase for two hours of incubation yielded the best combination of EC purity, yield, and isolation time. Further purification was achieved by magnetic cell sorting or single cell expansion. The latter method provided pure EC populations that could be maintained post-confluent for weeks without being overgrown with contaminating ICs.

Published protocols for valve EC isolation have used collagenase solutions of various concentrations to gently loosen ECs from the leaflet surfaces before applying mechanical means to dislodge the cells [132, 133]. However, enzyme cocktails for the isolation of other types of ECs often contain dispase in combination with collagenase for improved viability and purity of the isolates [134-136]. Dispase is a metalloprotease that specifically cleaves type IV collagen and fibronectin, two main constituents of the basement membrane on which the endothelium is anchored. By specifically targeting digestion of the basement membrane (as opposed to using only collagenase to digest the type I collagen of the interstitial matrix), we hypothesized that a higher number of ECs would be dislodged from the valve surface more quickly such that there would be less time for the collagenase to release undesired ICs. Our results confirmed that the purity of isolated ECs is improved with the use of 2.0 U/mL

dispase in combination with collagenase; this dispase concentration is reported to be appropriate for isolation of other ECs [135]. The total yield of valve ECs increased with higher collagenase concentrations, as expected. The yield, however, was independent of incubation time for times longer than two hours. Based on these observations, we concluded that the optimal parameters for enzymatic digestion of leaflets for isolating valve ECs were 2.0 U/mL dispase for best purity, 60 U/mL collagenase for highest yield, and two hours of incubation for the shortest time required to obtain high cell yield.

High yield and purity were important to the success and efficiency of the subsequent purification steps. High yield was critical for successful purification by magnetic cell sorting because the procedure was hindered by low capture efficiency due to the multiple immunolabelling steps. Approximately 10 million cells needed to be harvested after the first passage in order to obtain ~1-2 million captured endothelial cells, enough for subsequent subculturing and expansion without driving the cells to high passage. On the other hand, high purity was critical for efficient purification by clonal expansion because success of the technique depends on how frequently one obtains a single endothelial cell in one well. This frequency drops proportionately with any reduction in EC purity of the seeding suspension.

The MACS cell sorting system substantially improved EC purity in passages after isolation. However, we observed that even in cultures that were high in purity (97 ± 2 %) upon isolation, contaminating ICs released during digestion overtook the cultures once the ECs reached confluence and proliferation was abrogated due to contact inhibition (Figure 4.2A and B). Although IC overgrowth happened to a lesser extent for MACS-purified cells, it still occurred after a few passages or in post-confluent cultures (Figure 4.2E and F). This was especially apparent for purified subcultures that were maintained for ~1-2 days post-

confluent for long-term experiments, such as those requiring proper actin reorganization before exposure to fluid-induced shear stress for up to 48 hours [76]. Therefore, magnetic cell sorting was found to be an effective method for purification only for the first few passages, and for cultures not requiring post-confluence.

Clonal expansion of single cells eliminated the problems associated with IC contamination because the technique ensured only pure endothelial colonies were selected for expansion. This method was demonstrated previously to be successful in obtaining pure populations [133]. Here we report the efficacy and efficiency of this approach. Based on our observations, the frequency of wells with single ECs was slightly lower than that expected theoretically, but still large enough to generate over a quarter million ECs by first passage from a single 96-well plate. This technique is readily scalable, only limited by the number of multiwell plates and the number of population doublings tolerable. We observed that even after 20 doublings, cryopreservation, and further expansion, the ECs isolated by the single cell technique retained their purity and original morphological and phenotypic characteristics.

The populations of cells obtained by the single cell isolation technique are clonal and therefore may not be representative of the overall valve EC population. If heterogeneous populations are desired, populations from multiple wells can be pooled once endothelial phenotype has been confirmed. Additionally, it is likely that even clonally-derived populations will exhibit significant heterogeneity after multiple doublings [137]. The ability to grow large numbers of pure ECs from very few isolated cells with this technique makes region-specific EC isolation possible. Aortic valve ECs exhibit distinct site-specific phenotypes *in vivo* [51]. By isolating pure ECs from small spatially-defined regions, one may

test *in vitro* whether regional valve EC phenotype is pre-programmed or environmentally regulated [51, 138]. This technique also lends itself to isolation of ECs from the small leaflets of mice and rats, and will therefore significantly increase the model systems available to investigate valve EC biology.

Between the two purification methods, clonal expansion is clearly the better option for obtaining a pure EC population. In terms of financial costs and time, however, magnetic cell sorting is a slightly less expensive and faster option (Table 4.1). To obtain a purified population of ~10 million cells using magnetic cell sorting, one would need ~100 mL of supplemented EC media and additional antibodies and microbeads over a culturing period of one week. To obtain a pure population of ~10 million ECs using clonal expansion, one would need ~200 mL of the same supplemented media while culturing for more than two weeks. Depending on the supplemented media chosen for culturing, the extra volume needed for longer culturing periods in the clonal technique may or may not offset the costs from the additional reagents needed for magnetic cell sorting. In our case, the MACS cell sorting system was slightly more economical.

Table 4.1. Comparison of cost and time for purification methods*

Purification Method	*Culturing Time, days*	*Doublings*	*Volume EGM-2 media used, mL*	*Additional reagents needed*	*Total cost per assay, USD*
Magnetic cell sorting	7	~ 6	~ 100	CD31 Ab, 50 µL Microbeads, 20 µL MS Columns, 1 unit	~$ 50
Clonal expansion	16	~ 20	~ 200	None	~ $ 60

** Numbers based on obtaining 10 million purified cells from 1 million primary isolated cells.*

In summary, we investigated various parameters and purification techniques to obtain high yield of pure valve EC populations for culturing and experimentation. We reported for the first time use of dispase as an additional enzyme to be used in conjunction with collagenase for isolation of large numbers of relatively pure valve ECs. Two separate purification techniques were considered to further increase purity: a magnetic bead-based cell sorting technique and clonal expansion of single cells. Magnetic cell sorting markedly improved the quality of the cell population during the first few passages after purification, but the potential for IC contamination and overgrowth was inherent in the method, particularly after several passages or in post-confluent cultures. In contrast, the clonal expansion technique ensured a pure population of ECs, though at the cost of longer culturing periods and higher expense compared to magnetic cell sorting to produce the same number of purified cells. The selection of a suitable isolation and purification method therefore depends on the requirements of the intended application and the resources available.

Chapter 5

5 Adhesion[3]

Comparative studies between PAECs and PAVECs have begun to reveal important differences between the two neighbouring endothelial phenotypes [50, 57, 139]. Their uniqueness has raised questions regarding the use of aortic ECs instead of more regionally compatible valve ECs for endothelialization of tissue-engineered (TE) valve scaffolds ([101]). Given that proper endothelialization of biomaterial surfaces depends on suitable anchorage of cells to the matrix (via integrins), it is beneficial to investigate adhesion properties of ECs to understand the effect of cell-matrix interactions, as well as to further reveal distinguishing features of aortic and valve cells. In addition, integrins that mediate cell attachment are also involved in flow-induced mechanotransduction [15], so examining adhesion may concomitantly improve our understanding of the effects of hemodynamic environment on the performance of native and TE valves *in vivo*.

[3] The work presented in this chapter was published in Lab on a Chip in 2007 [131].

The motivation is clear from a biological perspective: study adhesion to uncover differences between aortic and valve ECs that may impact tissue engineering design. An equally important motivation, however, stems from the need to understand the engineering of microfluidic systems for cell biology. The ability for cells to attach in microfluidic systems is likely to affect their ability to spread, migrate, proliferate, and respond to chemical and mechanical stimuli while in culture. And since macro- and microscale systems differ in their local microenvironments [140, 141], subtle differences in a cell's ability to adhere due to both phenotype and physical scale of their surroundings may impact downstream biological responses. Thus, to aid in development of microfluidic systems for studying ECs and to ensure proper interpretation of biological outcomes at the microscale, understanding the subtleties of adhesion in microchannels is a critical first step.

In this chapter, we investigate adhesion of PAECs and PAVECs in microchannels. Two model ECM proteins, fibronectin (FN) and type I collagen (Col-I), were chosen for study, based on their abundance in the basement membrane and interstitium, and on their popularity in the literature as substrate coating proteins. We were interested in finding an optimal protein concentration for cell adhesion, and therefore tested six different concentrations for each protein and each cell type, resulting in a total of 24 experimental conditions. Given that each condition requires a different surface, the majority of ICF systems available for studying adhesion are unsuitable (i.e., they offer a range of shear stress but not a range of surface conditions). We chose to expand the design of Lu et al. [103], employing a parallel microfluidic network of test channels to facilitate experimentation and increase throughput from conventional parallel plate flow chambers.

5.1 Materials and Methods

5.1.1 Device Design and Fabrication

The microchannel pattern of the shear devices used in this study was similar to the multi-sample device design by Lu et al. [103]. In our design, eight identical parallel microchannels of 516-μm width and 59-μm depth were connected to a single inlet reservoir via a symmetric branching network (Figure 5.1). The branches were designed to ensure the same hydrodynamic resistance through all eight fluidic paths.

The microfluidic shear devices were formed from PDMS and glass using the rapid prototyping technique [142] (See Appendix B). Briefly, channel patterns were drawn in AutoCAD (Autodesk, San Rafael, CA, USA) and printed at high resolution on a transparent photomask. Masters were fabricated by spin-coating SU-8-25 negative photoresist (Microchem, Newton, MA, USA) on glass slides that had been cleaned in piranha solution (70% sulfuric acid, 30% hydrogen peroxide, 30 min). After pre-baking, exposure, and post-exposure baking, the photoresist layer was developed by gentle agitation in SU-8 developer (Microchem). After development, masters were examined by profilometry (WYKO) at nine different random locations, and the feature depth was found to be 58.5 ± 4.2 μm, thus confirming the uniformity. Poly(dimethylsiloxane) (PDMS) (Sylgard 184, Dow Corning, Midland, MI, USA) in a 10:1 base/curing agent ratio was poured over the masters, exposed to vacuum to remove air bubbles, and cured at 70°C for at least four hours. A piranha-washed glass slide and a PDMS cast of the microchannel pattern were both rinsed in isopropyl alcohol (IPA), plasma-treated for 90 seconds (Harrick Plasma, Ithaca, NY, USA), and then assembled with polyethylene tubing as inlet ports for eventual microfluidic injection and withdrawal.

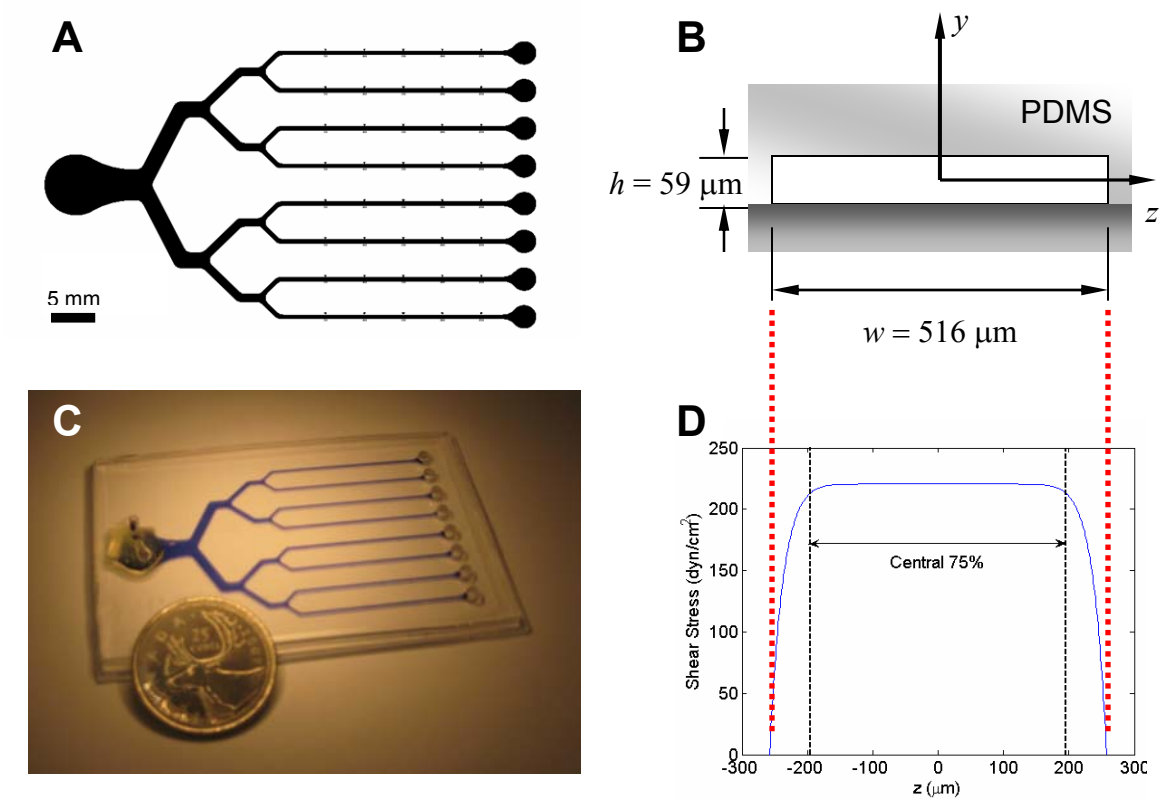

Figure 5.1. Design of microfluidic shear device with eight parallel microchannels.

(A) Parallel microfluidic shear device pattern, consisting of eight microchannels of 516-μm width. Scale bar = 5 mm. (B) Cross section of one microchannel with width w = 516 μm and height h = 59 μm. (C) Photograph of assembled PDMS-glass microfluidic shear device. (D) Shear stress distribution on microchannel surface (y = - h/2) from side wall to side wall (-258 μm ≤ z ≤258 μm). The central 75% is exposed to approximately constant shear stress (less than 5% difference from shear stress at z = 0).

5.1.2 Cell Culture

Unless otherwise stated, all chemicals and reagents for cell isolation and culture were purchased from Sigma-Aldrich Canada (Oakville, ON, Canada); fluorescent dyes were from Invitrogen (Burlington, ON); and all other materials were purchased from Fisher Scientific Canada (Ottawa, ON).

Primary PAVECs were isolated from valve leaflets as described in Chapter 4. Within four hours of acquiring fresh pig hearts from a local abattoir, PAVECs were treated by enzymatic digestion in a solution of 60 U/mL collagenase and 2.0 U/mL dispase for 2.5 hours at 37°C, followed by scraping to dislodge the cells. These concentrations and incubation times were found to be optimal for yield. Isolated cells were cultured for three to four days in EGM-2 basal medium with SingleQuots (Cambrex Clonetics, East Rutherford, NJ, USA) supplemented with 20% fetal bovine serum (FBS) and 1% penicillin-streptomycin (P-S). For all adhesion experiments reported in this study, PAVECs were purified by magnetic cell sorting. Purified endothelial cells were subsequently expanded in M199 supplemented with 10% FBS and 1% P-S in flasks pre-coated with 3% (w/v) gelatin, and frozen for later use. PAVECs between passages 4 and 7 were used in all reported experiments.

As a model of vascular endothelial cells, we used primary PAECs generously donated by Lowell Langille (University of Toronto). Cells were thawed and expanded in M199 supplemented with 5% FBS, 5% calf serum (CS), and 1% P-S. All reported experiments used PAECs between passages 4 and 7.

5.1.3 Experimental Preparation

For a detailed description of the adhesion assay protocol, see Appendix D. Three hours prior to experimentation, cells (PAVECs or PAECs) were labelled with vital nuclear and cytoplasmic fluorescent dyes to aid in their visualization. Cells were incubated with Hoechst 33342 nuclear dye (2 μg/mL in supplemented M199 medium appropriate to the cell type) for 30 minutes at 37°C and 5% CO_2, and then with CellTracker Green cytoplasmic dye

(5 μM in serum-free M199 medium) for an additional 30 minutes at 37°C and 5% CO_2. Finally, cells were maintained in fresh supplemented M199 medium until experimentation.

Prior to protein loading, the microchannels were sterilized by rinsing with 70% ethanol (10 min), followed by PBS (10 min). PBS was then pushed out of the microchannels by flushing with sterile air from the inlet port. Two proteins were used in this study, human plasma fibronectin (FN) (Invitrogen – Gibco, Carlsbad, CA, USA) and rat-tail type I collagen (Col-I) (Becton Dickinson, Mississauga, ON, Canada). FN was diluted to desired concentration with supplemented medium (appropriate for cell type), while Col-I was diluted with sterile 0.02 N acetic acid. Five solutions of each protein were prepared: 500, 200, 100, 50, and 10 μg/mL. To coat the microchannels with proteins, 15 μL of each solution was added to the outlet reservoir of a microchannel on the device (i.e., circular reservoirs on the right side of Figure 5.1A). The remaining reservoirs were filled with various controls, i.e., 0 μg/mL protein. After loading, suction was applied from the inlet port to draw the protein solutions from each reservoir into their respective microchannels. To prevent mixing of protein solutions, suction was ceased before the interface of the solutions reached any branch in the network. Thus, it was important to clear the microchannels with sterile air before coating to track this process. Compared to previous methods of coating microchannels with proteins [103], this method resulted in considerable reduction in solution use, representing a concrete example of the often-cited advantage of low reagent consumption on microscale platforms.

After the proteins were drawn into the microchannels, the device was incubated at room temperature for 30 min to allow sufficient protein adsorption onto the underlying glass surface. After rinsing with ~1 mL of supplemented medium, 1% (w/v) BSA in PBS was

flushed through the network and incubated (37°C, 30 min) to block non-specific cell adhesion. Microchannels were rinsed and maintained in supplemented medium until analysis.

5.1.4 Cell Spreading and Adhesion Strength Assays

Cells labelled with Hoechst and CellTracker Green vital dyes were trypsinized from the flasks and suspended at 10 million cells/mL. Using a syringe, the concentrated cell suspension was injected into the protein-coated microchannel network where the cells dispersed uniformly (Figure 5.2). The device was incubated at 37°C with 5% CO_2 for two hours to allow initial cell attachment and spreading on channel surfaces. Observations were made immediately after the two-hour incubation using an inverted fluorescent microscope (Leica), and fluorescent images were taken with a CCD camera (Hamamatsu). Cell areas were quantified using the ImageJ software package (NIH) to trace cell cytoplasmic borders.

To investigate adhesion strength, attached cells were subjected to increasing levels of flow-induced shear stress over a 12-minute period. Culture medium was dispensed using a syringe pump (Harvard Apparatus series 11, Harvard, Holliston, MA, USA) at 12 mL/hr for the first four minutes, 120 mL/hr for the next four minutes, and 240 mL/hr for the final four minutes. These flow rates translated to shear stresses of 11, 110, and 220 dyn/cm^2, respectively, based on the Purday approximation [59],

$$\tau_w = \frac{2\mu Q}{wh^2}\left(\frac{m+1}{m}\right)(n+1) \tag{5.1}$$

where τ_w is the wall shear stress, Q is the volumetric flow rate, m and n are empirical constants related to channel aspect ratio (see Appendix C), width w = 516 μm, height h = 59

μm, and viscosity of the culture medium at 37°C is $\mu = 0.72 \times 10^{-3}$ kg/m·s, as measured with a Cannon-Fenske capillary viscometer. Note that Eq. (5.1) is similar in form to the parallel plate approximation of $\tau_w = 6\mu Q / wh^2$. Fluorescent images were taken after each four-minute shear period, at three separate locations, x = 10, 15, and 20 mm from the start of each straight 30-mm long microchannel section. Cell counting (based on nuclear staining) was performed using ImageJ, and cell counts from the three locations were averaged to give a mean cell count for each microchannel.

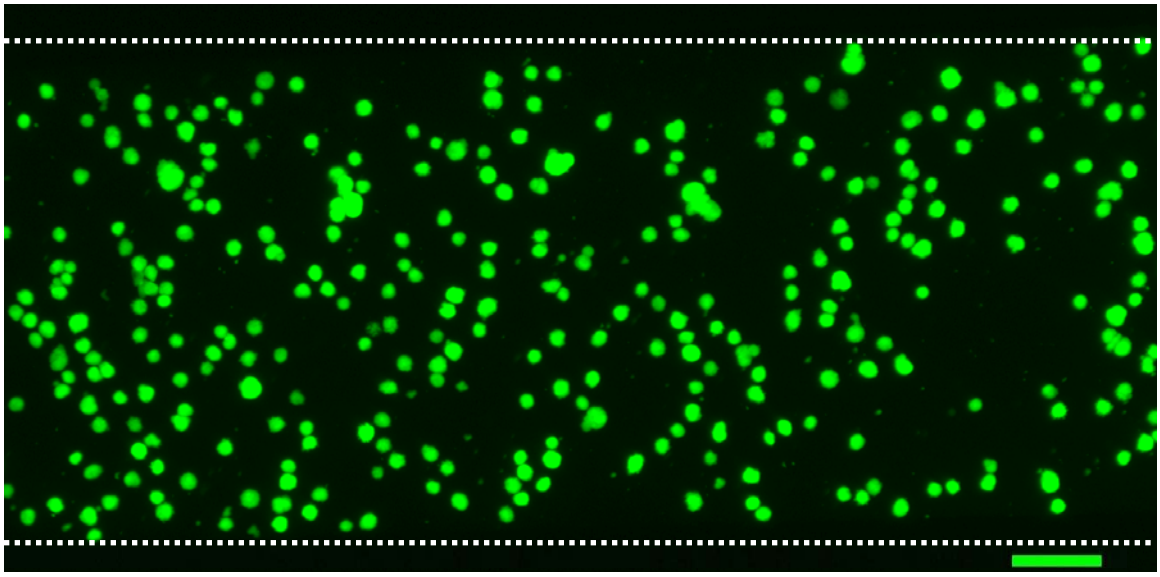

Figure 5.2. PAECs after initial injection into microchannels at 10 million cells/mL. Cells were uniformly dispersed and labeled with brightly fluorescing CellTracker Green cytoplasmic dye. Dotted lines indicate side walls of microchannel. Scale bar = 100 μm.

Two control experiments were also performed to examine how quickly cells detached over time, and to evaluate whether initial low shear stress levels preconditioned cells for detachment at higher shear stresses in the approach outlined above. The first experiment involved repeating the standard shear assay of 11, 110, and 220 dyn/cm^2 at four-minute

intervals and capturing images every 30 seconds over the 12-minute period to obtain intermediate timepoints. The second experiment involved applying 220 dyn/cm^2 for 12 minutes, also with images captured every 30 seconds. Results are presented for experiments performed with PAVECs on 50 μg/mL FN (see Appendix C). Similar results were observed with other combinations of cell type, protein type, and coating concentration.

To facilitate statistical analyses of acquired data, we created an adhesion strength parameter (ASP), ϕ, defined as

$$\phi = \frac{1}{3}\left(F_1 + F_2 + F_3\right) \tag{5.2}$$

where F_1, F_2, and F_3 are the normalized fractions of remaining cells at t = 4, 8, and 12 minutes, respectively. ASP averages the percentage of remaining cells over the course of the shear assay, and therefore, accounts for adhesion strength at all three nominal shear stress levels. Each adhesion strength time profile can thus be represented by a single metric measuring the propensity for a given cell type to remain adhered to a specific protein.

5.1.5 Flow Characterization

To confirm that flow rates were uniformly distributed throughout the network, particle streak velocimetry [143] was used to measure velocities in each microchannel. Briefly, 1-μm fluorescent microspheres (FluoSpheres F8819, Molecular Probes) diluted in ethanol were pumped through microchannels at prescribed flow rates using a syringe pump. As illustrated in Figure 5.3, images of particle streaklines were focused on the midplane between the top and bottom channel surfaces and captured using a CCD camera mated to an inverted fluorescent microscope (Olympus IX-71). The length of the longest streakline in

each image was measured, and the average of these lengths determined the maximum velocity, u_{max}, for a given channel. We found measured maximum velocities to be consistent with theoretical predictions from the Purday approximation [59]. Furthermore, variability between channels within the same network was less than 10%. We note that ~12% of the channel width along each of the side walls was predicted to be lower than 95% of the shear stress found in the rest of the channel (see Figure 5.1D). Therefore, only cells in the central 75% of the microchannels were counted during analysis of cell adhesion. A detailed description of the flow characterization is provided in Appendix C.

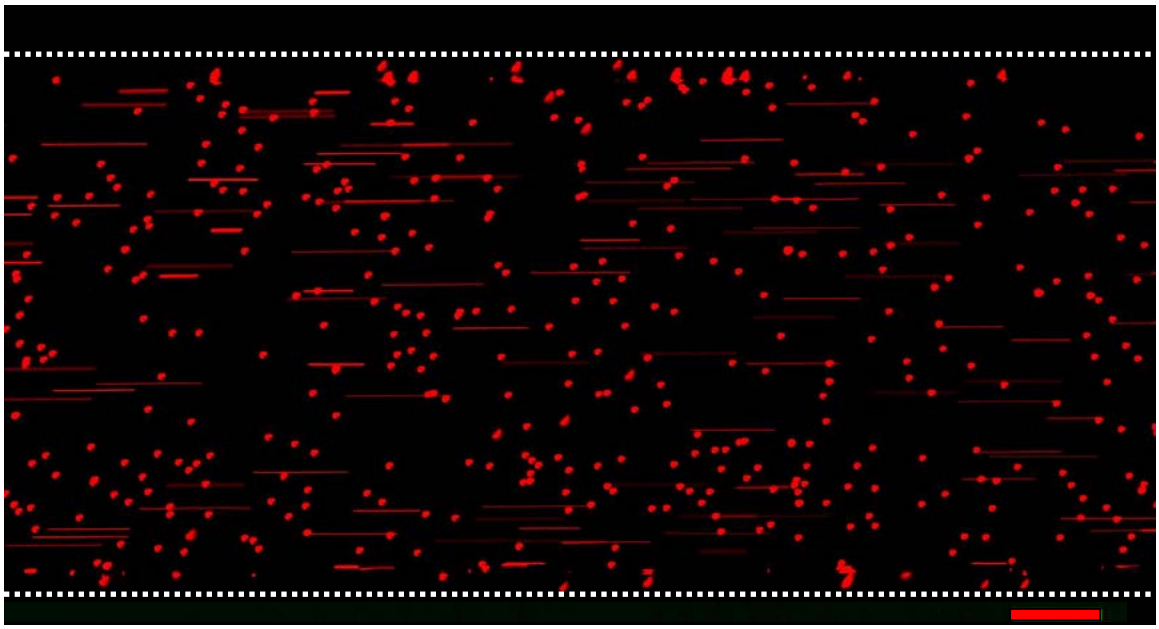

Figure 5.3. Streaklines from 1-μm fluorescent microspheres.
Flow rate Q = 1.2 mL/hr from syringe pump. Measured maximum velocity in microchannels was u_{max} = 2.38 mm/s (c.f. theoretical prediction of u_{max} = 2.24 mm/s). Scale bar = 100 μm.

5.1.6 Statistical Analysis

In total, three experiments (n = 3) were conducted for each condition, i.e., three microdevices were tested for each combination of cell type and protein. Three-way analysis of variance (ANOVA) was performed using Prostat 3.01 (Poly Software International, Inc., Pearl River, NY, USA) to analyze the effects of cell type (PAVECs or PAECs), protein type (FN or Col-I), protein coating concentration (500, 200, 100, 50, 10, or 0 μg/mL), or any interaction between the three factors for both cell spreading area and cell adhesion strength. Since no significant three-way interaction was found for either spreading area or adhesion strength, two-way ANOVAs were performed for each combination of two factors (collapsing over the third factor) to elucidate the main effects of each factor separately. For example, two-way ANOVA was performed for protein type and protein coating concentration for all PAEC data first, then for all PAVEC data (i.e., collapsing over cell types). If statistical significance was found between protein types, it was deemed a *main effect* of protein types averaged over all protein concentrations.

Simple effects were also analyzed using one-way ANOVAs for each factor at all different combinations of the remaining two factors. For example, for the combination of PAVECs on FN, one-way ANOVA was performed for all coating concentrations. Statistical significance in this case was then considered a *simple effect* in concentration, but only for PAVECs on FN. When necessary, multiple comparisons were performed using Tukey's method. Data was considered statistically significant only if $P < 0.01$.

5.2 Results

5.2.1 Cell Spreading Area

We first compared the ability of PAVECs and PAECs to spread and adhere to different ECM proteins over a range of protein concentrations. In general, PAECs spread well on both FN and Col-I, covering large regions of the microchannel surface and forming visible networks with neighbouring cells. In contrast, PAVECs spread well on FN, but not on Col-I (Figure 5.4). Interestingly, PAVECs tended to be uniformly dispersed throughout the microchannel, and spread as individual cells without networking with their neighbours (see Figure 5.4A and B), while PAECs maintained contact with adjacent cells, forming networked islands in confined regions of the microchannel (see Figure 5.4E and F).

Morphological analyses confirmed that there was significant difference in cell spreading for PAVECs on FN versus Col-I (main effect, $P < 0.0001$), especially for 500, 200, and 100 μg/mL where FN resulted in larger cell areas (Figure 5.5). Even at the highest Col-I concentration, PAVECs did not spread much more than on the control condition with no protein coating (240 ± 21 μm^2 vs. 199 ± 29 μm^2, respectively). For PAECs, a significant difference also existed between FN and Col-I (main effect, $P < 0.005$), but a simple effect was observed only for 500 μg/mL FN, which led to modestly larger cell areas (Figure 5.5). By segregating the data based on protein type, comparisons were also made between cell types. For the FN coatings, no significant difference was found in spreading area between PAVECs and PAECs ($P > 0.05$). In contrast, for Col-I, there was a significant difference in spreading area between the cell types ($P < 0.0001$), with PAECs spreading much more than PAVECs. Thus, the level of spreading was cell type-dependent on Col-I, but not on FN.

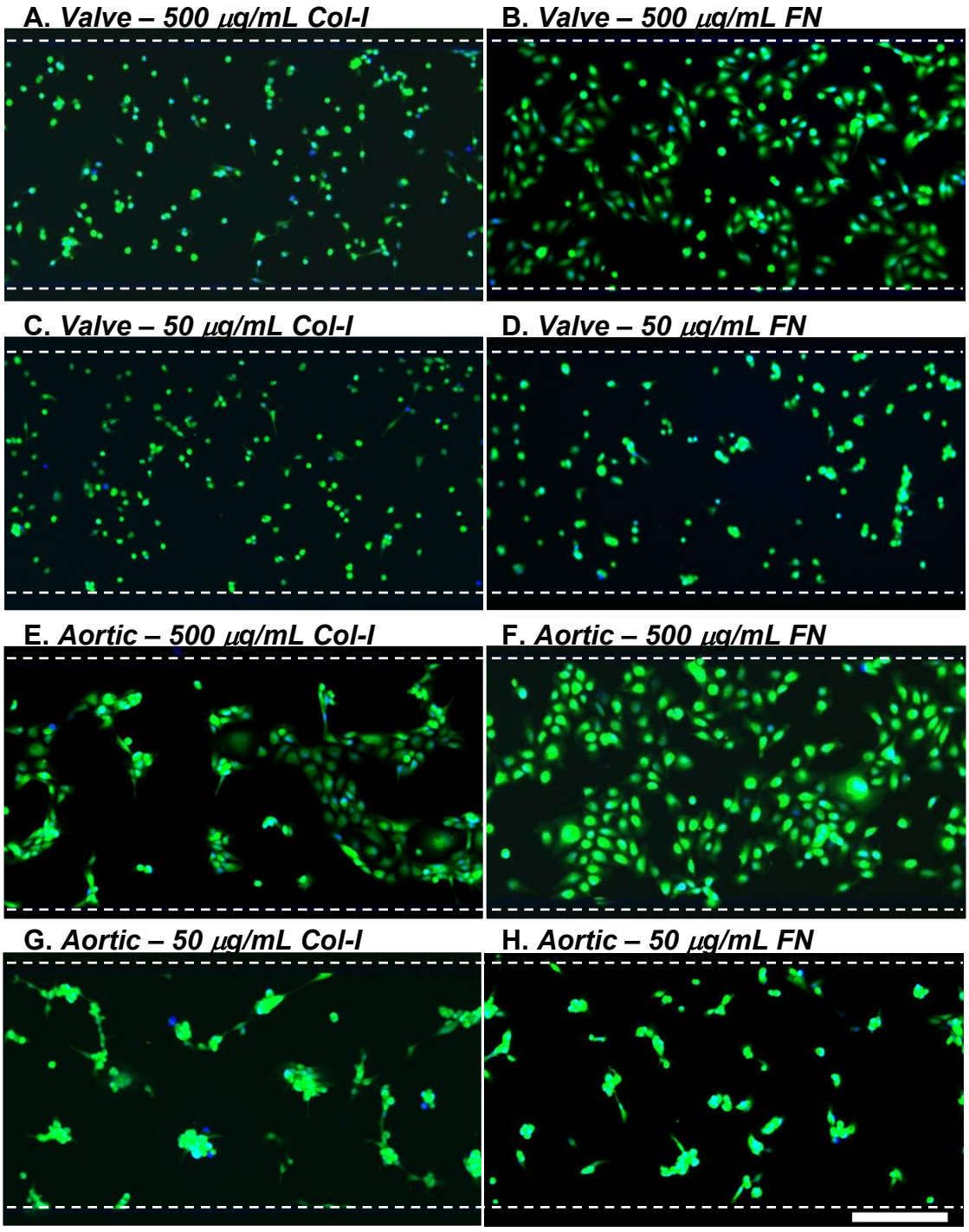

Figure 5.4. Fluorescent images of cells on different proteins after two hour incubation.

Valve ECs (A-D) and aortic ECs (E-H). At high protein coating concentration (500 μg/mL), valve ECs spread more on FN than Col-I (A and B) while aortic ECs spread well on both FN and Col-I (E and F). Neither valve nor aortic ECs spread well at low protein coating concentration (50 μg/mL) (C, D, G, H). Scale bar = 200 μm.

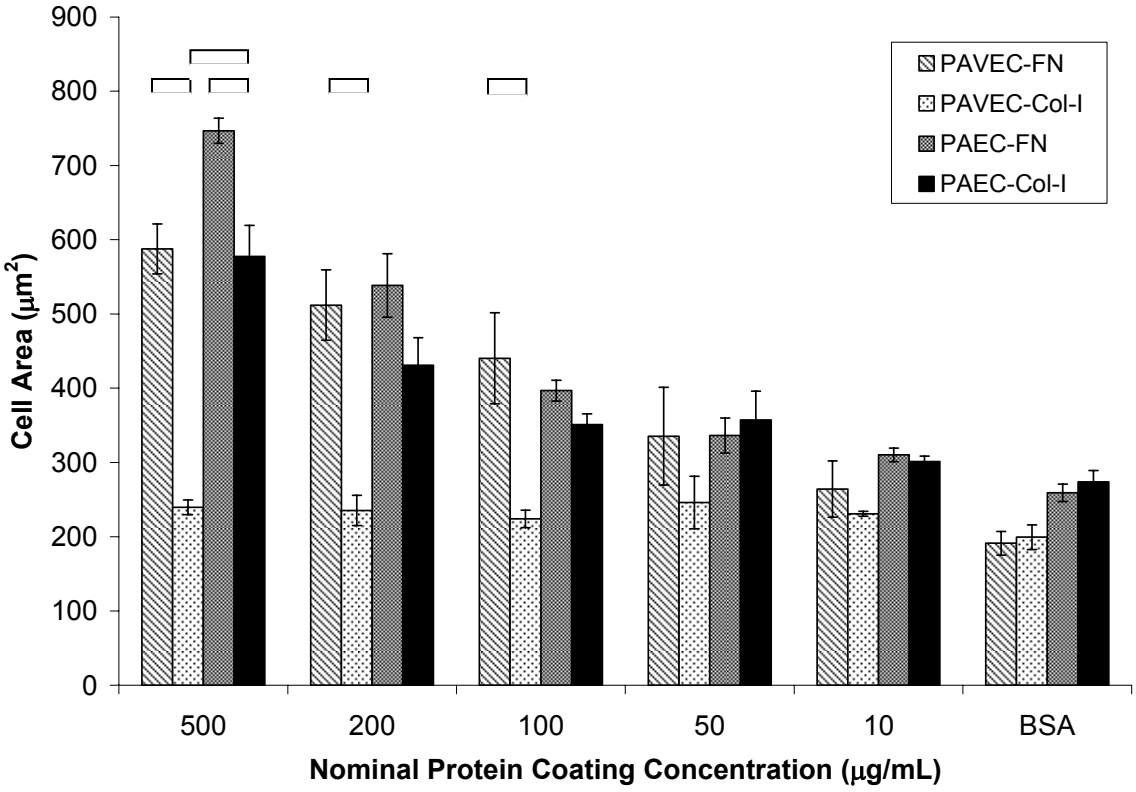

Figure 5.5. Cell spreading area (μm^2) for cell-protein combinations at various levels of protein coating concentration.

Data presented as mean ± SE (n = 3). Brackets indicate statistical significance, $P < 0.01$ (For clarity, some significant comparisons have not been shown).

5.2.2 Cell Adhesion Strength

Using the microfluidic device, we measured adhesion strength time profiles for all four cell-protein combinations at six levels of protein coating concentration (Figure 5.6). Qualitative evaluation of these profiles shows that PAVECs were strongly attached to FN at 500 and 200 μg/mL, with almost 100% of all cells remaining after the entire shear assay (Figure 5.6A). Likewise, PAVECs were moderately well attached at 100 μg/mL FN, with ~60% of the original number of cells remaining after the assay. In contrast, PAVECs were

poorly attached to Col-I at all coating concentrations (Figure 5.6B), with no significant difference in adhesion strength between concentrations ($P > 0.5$). For PAECs, excellent adhesion strength was observed for 500 μg/mL FN (Figure 5.6C), while only moderate strength was observed for Col-I, even at 500 μg/mL (Figure 5.6D). Equally poor adhesion strength was found for PAECs at all other concentrations for both protein types.

The dynamics of cell detachment were further investigated to confirm that cells detached abruptly at a given shear level and were not simply slowly peeling off as the shear stress was increased with each step. We observed that for each steady shear stress level in the stepped approach, the number of attached cells always decreased quickly in the first 30 seconds to a steady value (see Appendix C). The number of attached cells then remained constant for the remaining 3.5 minutes of each interval, until the next shear stress level was applied. In addition, when 220 dyn/cm^2 was constantly applied for 12 minutes, the number of attached cells decreased abruptly to a steady value within the first 90 seconds, and then remained constant for the remaining 10.5 minutes (see Appendix C). Moreover, this steady value matched that from the ramped shear experiment after exposure to 220 dyn/cm^2. This confirmed that cells did not gradually detach over time, but instead responded immediately to shear at each level.

Figure 5.7 shows the average adhesion strength parameter (ASP, defined above) for each cell-protein condition. For all FN coatings, PAVECs were more strongly attached than PAECs (main effect, $P < 0.0005$); however, no significant difference between cell types was found for Col-I data ($P > 0.05$). When data were segregated by cell type, significant difference was found between FN and Col-I only for PAVECs on 500 μg/mL ($P < 0.01$); data was not significant at all other protein concentrations for both cell types.

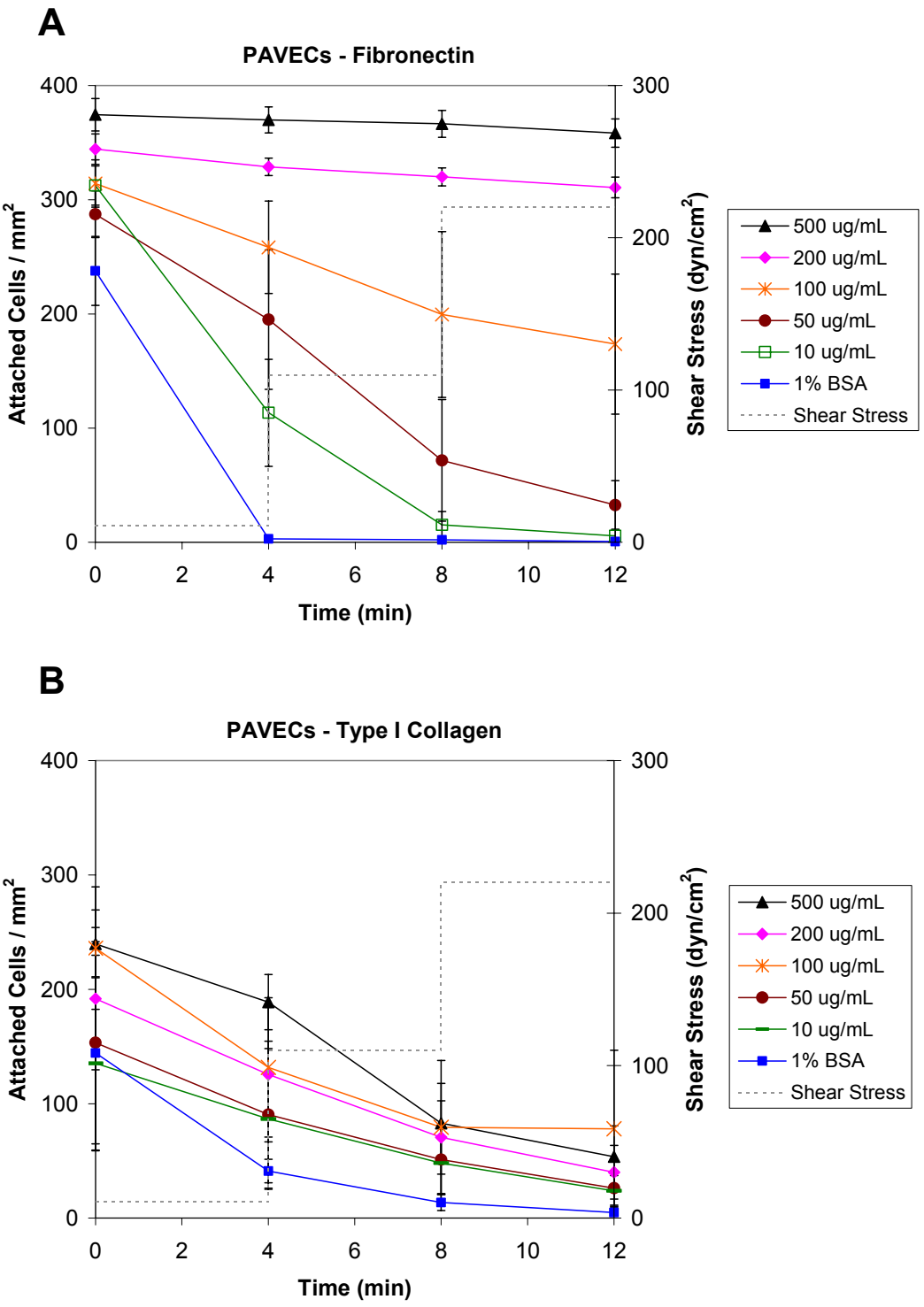
A
PAVECs - Fibronectin
Attached Cells / mm2
Shear Stress (dyn/cm2)
Time (min)
500 ug/mL
200 ug/mL
100 ug/mL
50 ug/mL
10 ug/mL
1% BSA
Shear Stress
B
PAVECs - Type I Collagen
Attached Cells / mm2
Shear Stress (dyn/cm2)
Time (min)
500 ug/mL
200 ug/mL
100 ug/mL
50 ug/mL
10 ug/mL
1% BSA
Shear Stress

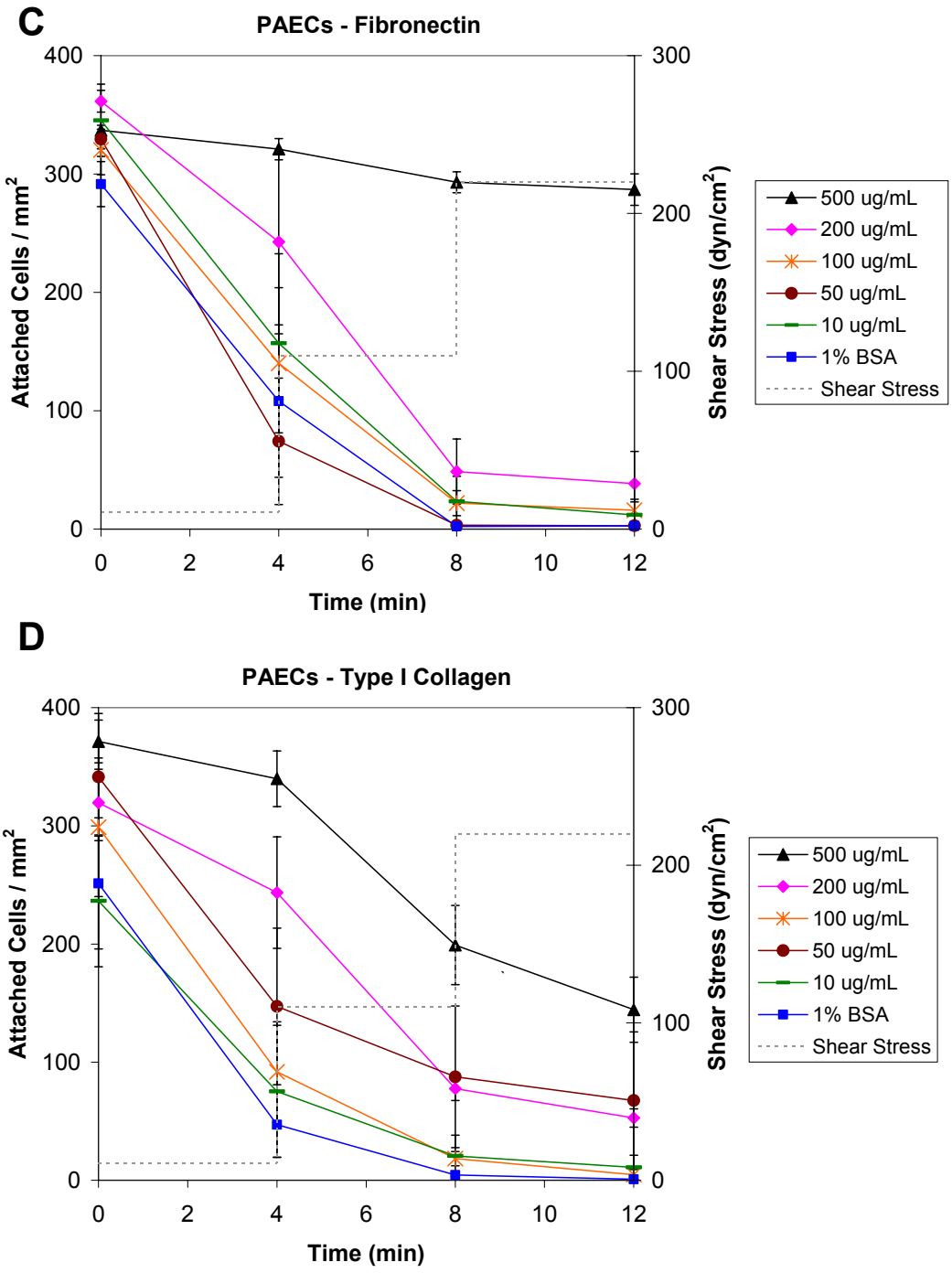

Figure 5.6. Adhesion strength time profiles.

Number of attached cells per mm^2 of microchannel surface plotted versus time exposed to shear (left axis). Dotted lines represent shear stress level applied, 4 min each at 11 dyn/cm^2, 110 dyn/cm^2 and 220 dyn/cm^2 (right axis). (A) PAVECs on FN; high adhesion strength for 500, 200, and 100 μg/mL. (B) PAVECs on Col-I; poor adhesion strength for all concentrations. (C) PAECs on FN; high adhesion strength for 500 μg/mL. (D) PAECs on Col-I; moderate adhesion strength for 500 μg/mL only. Data presented as mean ± SE (n = 3).

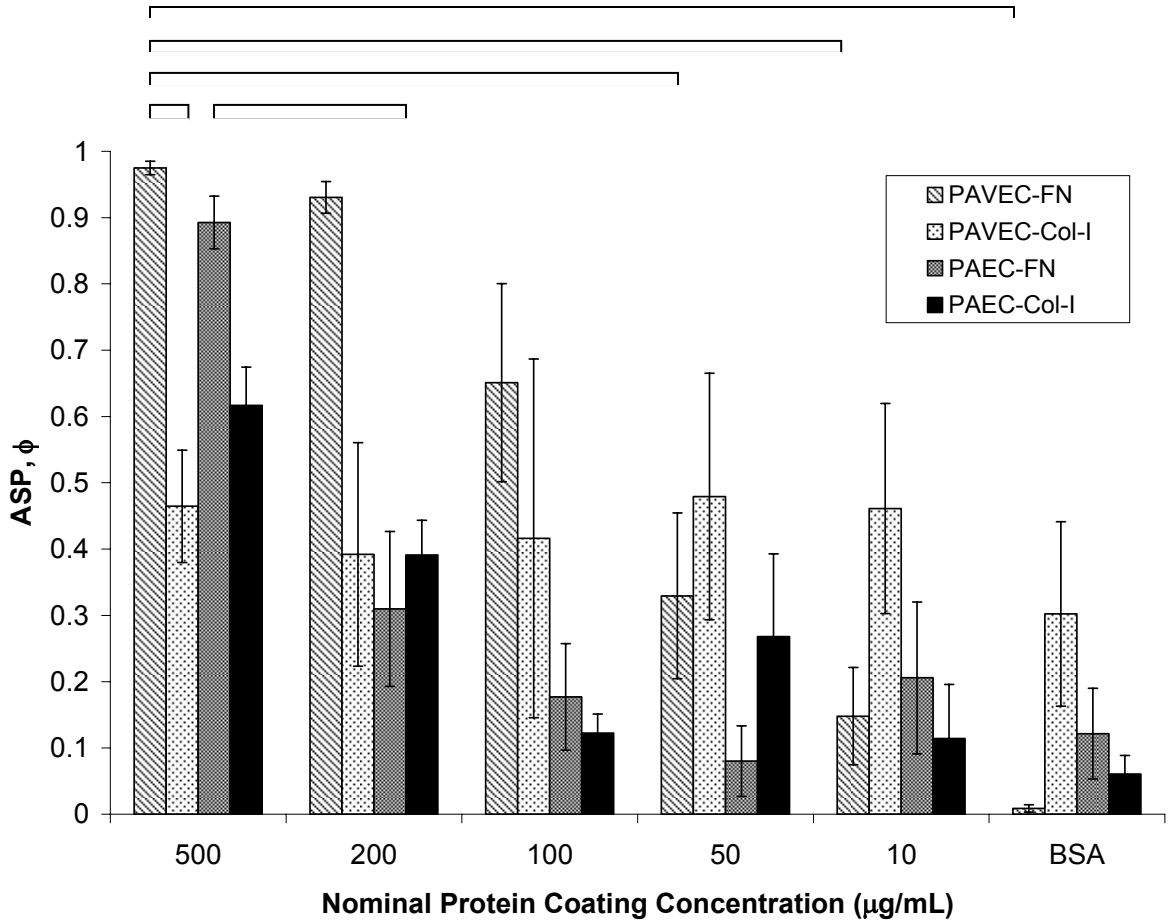

Figure 5.7. Adhesion strength parameter, ϕ, for different cell-protein combinations at various levels of protein coating concentration.

Data presented as mean ± SE (n = 3). Brackets indicate statistical significance, $P < 0.01$ (For clarity, some significant comparisons have not been shown).

5.3 Discussion

It has been previously reported that vascular and valvular endothelial cells exhibit distinct morphologies and develop unique reorganization of focal adhesion complexes under dynamic shear conditions [50]. When grown to confluence on Col-I and exposed to long-term shear stress at approximately physiological levels, aortic endothelial cells elongated and aligned parallel to the flow direction, and focal adhesion components were found to cluster at

the tips of the major axis upstream and downstream of flow. In contrast, aortic valve endothelial cells elongated and aligned perpendicular to the flow direction, and while focal adhesion components also clustered at the tips of the major axis, these locations coincided with a perpendicular polarization neither upstream nor downstream of flow. These observations provided preliminary evidence that the two closely-related and neighbouring cell types are in fact phenotypically different.

In this work, we have shown for the first time quantitative comparisons between the interaction of vascular and valvular endothelial cells with their matrix. These data provide novel evidence in support of phenotypic heterogeneity between vascular and valvular endothelial cell populations [138]. While PAECs were well spread on both FN and Col-I, PAVECs were only well spread on FN and not at all on Col-I. And while PAECs adhered strongly to high concentrations of both FN and Col-I, PAVECs adhered strongly only to FN at moderate to high concentrations, but not at all on Col-I. From these observations, it is evident that the extent of spread and the strength of attachment depend not only on the type of ECM protein, but also on the cell type.

It is likely that the dissimilarities in adhesion properties between the two cell types reflect differences in integrin expression, activation, and distribution. Integrin expression in healthy human hearts is distinct between the aorta and the aortic valve [16]. Notably, the integrin receptor for Col-I ($\alpha 2\beta 1$) is expressed in the aorta, but not the aortic valve, whereas the integrin that binds FN ($\alpha 5\beta 1$) is equally expressed in the two tissues. This expression pattern *in vivo* is consistent with our current observations that PAVECs attach only to FN *in vitro*, whereas PAECs are able to bind to both FN and Col-I. These observations not only provide new evidence that PAVECs and PAECs are phenotypically different, but also

suggest that the matrix protein may differentially modulate the biological responses of vascular versus valvular endothelial cells when exposed to long-term shear stress. Shear stress regulates a number of important endothelial responses that are mediated through pathways involving integrins and the extracellular matrix components to which they are attached. The availability of different matrix components for attachment can therefore alter the response of a particular cell type [144, 145]. This has implications for the selection of matrix proteins in endothelialized microdevices and engineered tissues. It may also explain the differences observed between vascular and valvular endothelial cells in response to shear when grown on Col-I [50].

The current results should be interpreted with due consideration of the physical environment within which the cells were cultured. The microfluidic environment presents a vastly different cell culture milieu compared to conventional culturing platforms such as Petri dishes and flasks [140]. One of the most important microscale-dominant phenomena is diffusion [140, 141]. In our experiments, during the two-hour incubation when cells spread and attached, the cells were in a static microenvironment where soluble factors traveled to neighbouring cells by diffusion alone. This is in contrast to conventional macroscale cell culture where convective transport plays a greater role. Because of the high cell surface density achieved in the present experiments, the local accumulation of biological factors was likely much higher than what would occur at the macroscale, even for a shorter time of culture. The effects of higher concentrations of soluble factors produced by endothelial cells during microscale culture, particularly in promoting or inhibiting the spreading and attachment of nearby cells through paracrine and autocrine signaling, is largely unknown.

Research in this area would benefit our understanding of microscale cellular studies, and potentially improve current methods for culturing cells in the microenvironment.

Our procedure for coating the microchannels with proteins was rapid and required less reagent volume than previous methods [103]. Using indirect immunostaining with anti-FN and anti-Col-I antibodies and measuring fluorescence intensity, we confirmed that higher inoculated protein concentrations indeed led to higher levels of protein adsorption to the glass substrate (data not shown). Since PDMS is hydrophobic and permissive to protein adsorption, we also observed some adsorption to the side walls. Although adsorption of proteins from the culture medium was also a consideration because of the high surface-to-volume ratio at the microscale [140], this effect was likely minor because we blocked with BSA after protein coating. Considering the simplicity and effectiveness of our protein loading and coating procedure, it may find widespread utility in many other microfluidic cell culture studies. Further, as demonstrated here, the use of parallel networks of microchannels provides a simple method to rapidly determine the optimal protein type and coating density required for cell adhesion, which will be useful for both conventional and microfluidic cell culture.

Understanding cell adhesion at the microscale allows us to extend current methods to long-term culture for fundamental studies of endothelial cell biology. Furthermore, the current results apply not only to cell culture, but also to the endothelialization of biomaterials for the regeneration of tissues such as heart valves [146]. While some researchers have specifically examined *valve* endothelial cell growth and morphology on different biomaterials [147, 148], the majority of efforts to engineer heart valves have used *vascular* endothelial cells [149-151]. It has been suggested that failures of current tissue engineered

heart valves stem in part from the use of vascular endothelial cells instead of more regionally compatible valve endothelial cells [101]. Our data provide new evidence of phenotypic and functional heterogeneity in endothelial cells and suggest that the adhesion and function of endothelial cells on tissue engineered valves (and consequently the success of the valves) is strongly dependent on the type of cell used and the nature of the biomaterial substrate.

Chapter 6

6 Shear Stress[4]

In the previous chapter, we showed that aortic and valve ECs adhered and spread differently on two different ECM proteins. Differences were especially noticeable between PAECs and PAVECs on Col-I. Interestingly, the study by Butcher et al. [50], which showed differential orientation of aortic and valve ECs under flow, was also conducted with Col-I as the underlying matrix protein. Taken together, this collective evidence of differential adhesion and alignment on Col-I suggests a possible correlation between the two behaviours, i.e., it is reasonable to hypothesize that the differences in alignment observed by Butcher and co-workers are in fact a downstream effect of cell-specific integrin-mediated adhesion and spreading on Col-I. Furthermore, since PAECs and PAVECs adhered and spread similarly on FN (as opposed to dissimilarly like on Col-I), it is questionable whether the same differential alignment would be observed had the two cell types been sheared on FN-coated

[4] I thank Suthan Srigunapalan and Marc Chrétien for their contributions to this chapter. Without their help and insight, this chapter would not have been possible.

surfaces. In other words, if the nature of matrix proteins mediates cell adhesion, it is also possible for it to mediate cell orientation given the connections between integrin signaling, adhesion, and cell shape [15, 18, 152]. A more fundamental question is why any EC (valve or otherwise) would align perpendicular to flow, given the biophysical preference for cells and nuclei to orient in a parallel manner to reduce hemodynamic drag on their bodies [153]. Answering such fundamental questions regarding cell morphological response to shear would have important implications on how we approach studying mechanisms of endothelial mechanotransduction.

Although the majority of studies on endothelial shear stress response have been conducted with conventional ICF systems, microfluidic channels have promised to provide two important advantages. First, as previously stated, a main goal of microfluidics technology is to streamline experimentation by increasing throughput and lowering reagent consumption. Some shear studies have already reported achieving these objectives [117]. However, continued research is needed in this area to make this technology more accessible to end users. In addition, validation studies comparing macro- and microscale systems are necessary to ensure that the change in physical scale alone does not inadvertently impact biological responses, i.e., that experimental outcomes are indeed transferable across length scales.

Second, microscale geometries can potentially reveal important clues about fundamental endothelial mechanobiology. For instance, Gray et al. [113] reported EC elongation and alignment in narrow microchannels, even in the absence of flow. Also, Nelson et al. [154] demonstrated that ECs were more proliferative at monolayer edges, suggesting that endothelial monolayers with varied length-to-width ratios may respond

uniquely to mechanical stimuli because of differential edge effects. Studying shear stress effects on ECs in microchannels, therefore, has important fundamental implications in addition to the practical advantages stated.

In this chapter, we compare some interesting preliminary findings on aortic and valve ECs under shear stress, using both macro- and microscale recirculatory systems. The large system employed a conventional parallel plate flow chamber, while the microscale system used microchannel devices fabricated by soft lithography. We focus on describing the advantages and disadvantages of the microscale system, its potential development, and the likelihood of its acceptance by the research community. Post-shear immunostaining and morphological analyses of the two studies revealed unexpected but potentially consequential results regarding preferred orientation. Though preliminary, these observations were found to be important for introducing new exploratory research directions, both in practical engineering design aspects as well as in fundamental biology.

6.1 Materials and Methods

Two systems were used to compare results from different geometries and physical scales: the parallel plate flow chamber system (*the macroflow system*), and the microfluidic recirculatory flow system (*the microflow system*). Experimental methods for each system are presented in succession.

6.1.1 Macroflow System

6.1.1.1 Parallel Plate Flow Chamber

The parallel plate flow chamber (PPFC) is a standard system used for studying flow-induced shear stress response of ECs. The PPFCs used in this study were custom-built, and

were based on similar designs reported in the literature [155, 156]. Details of the design are described by Chen [157]. Briefly, the chamber consisted of a polycarbonate base with a machined rectangular cavity. A small lip bordered the cavity to create an edge where a glass slide (75 mm × 38 mm) was seated. A silicone gasket and top polycarbonate block were secured to the base using copper screws, sealing the glass slide in a leak-proof assembly (Figure 6.1).

As described in Chapter 2, the PPFC forms a small gap of height *h* that forces fluid to flow in a laminar fashion from inlet to outlet, creating a parabolic velocity profile with a well-characterized wall shear stress τ_w determined by Eq. (2.8)

$$\tau_w = \frac{6\mu Q}{wh^2} \tag{2.8}$$

Endothelial cell monolayers grown on glass slides were exposed to prescribed shear stress through the application of an appropriate flow rate, *Q*.

6.1.1.2 Recirculatory Loop

The PPFC was connected to a closed-loop recirculatory flow system (Figure 6.2). A peristaltic pump forced fluid from the media reservoir to the damper, which converted pulsatile flow coming from the pump into steady continuous flow entering the chamber. The flow entered the inlet from the side, and passed through a narrow slit in the polycarbonate base that spanned the width of the rectangular cavity where laminar flow was generated. Media then exited the flow chamber through the outlet and re-entered the media reservoir. The recirculatory loop was contained in a temperature-controlled environment (37°C) while 5% CO_2 was continuously bubbled into the media reservoir.

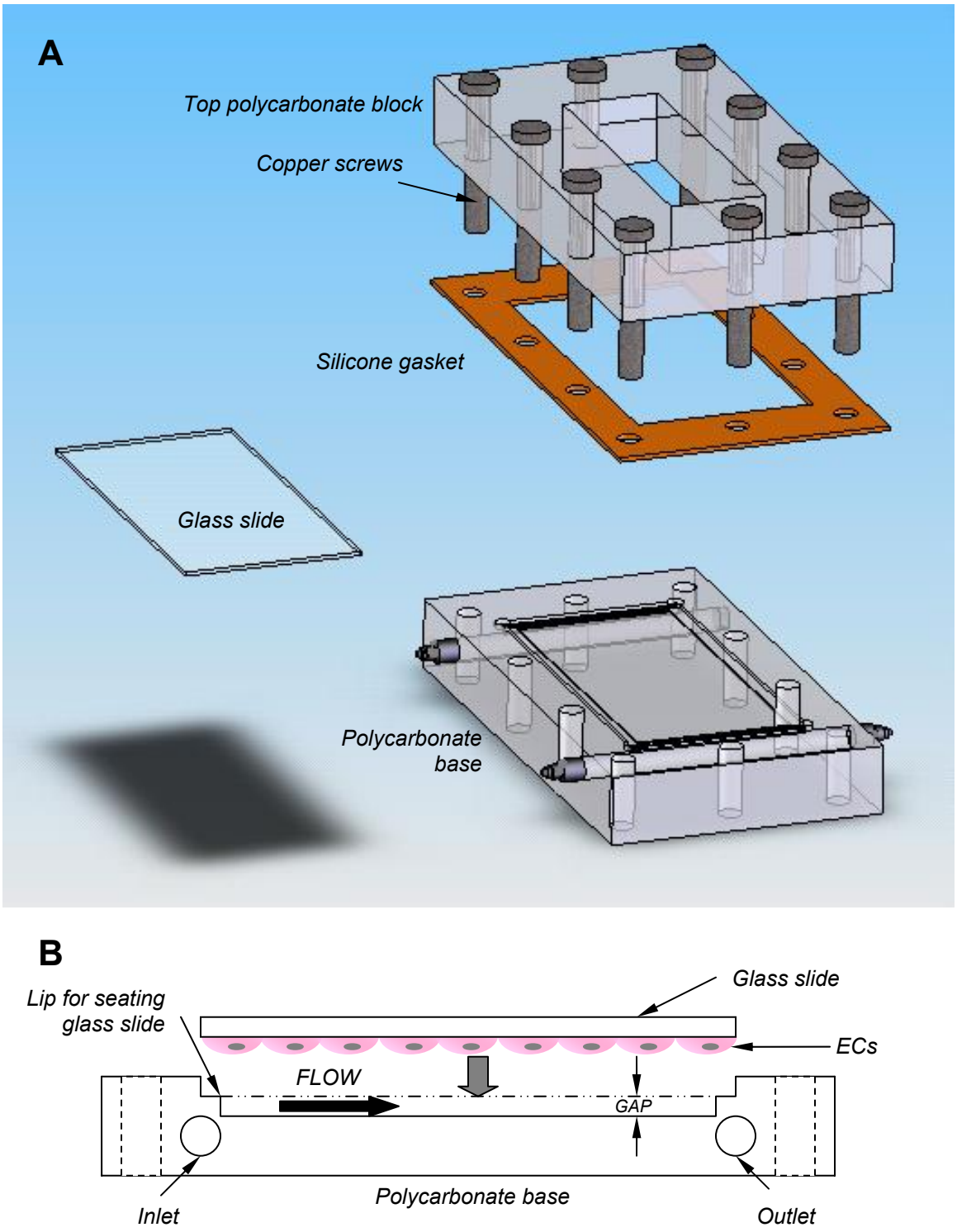

Figure 6.1. Design of the parallel plate flow chamber.

(A) Exploded three-dimensional view of the parallel plate flow chamber [158]. (B) Side view of flow chamber showing inlet and outlet ports, position of cells on glass slide with respect to polycarbonate base, and lip for seating of glass slide.

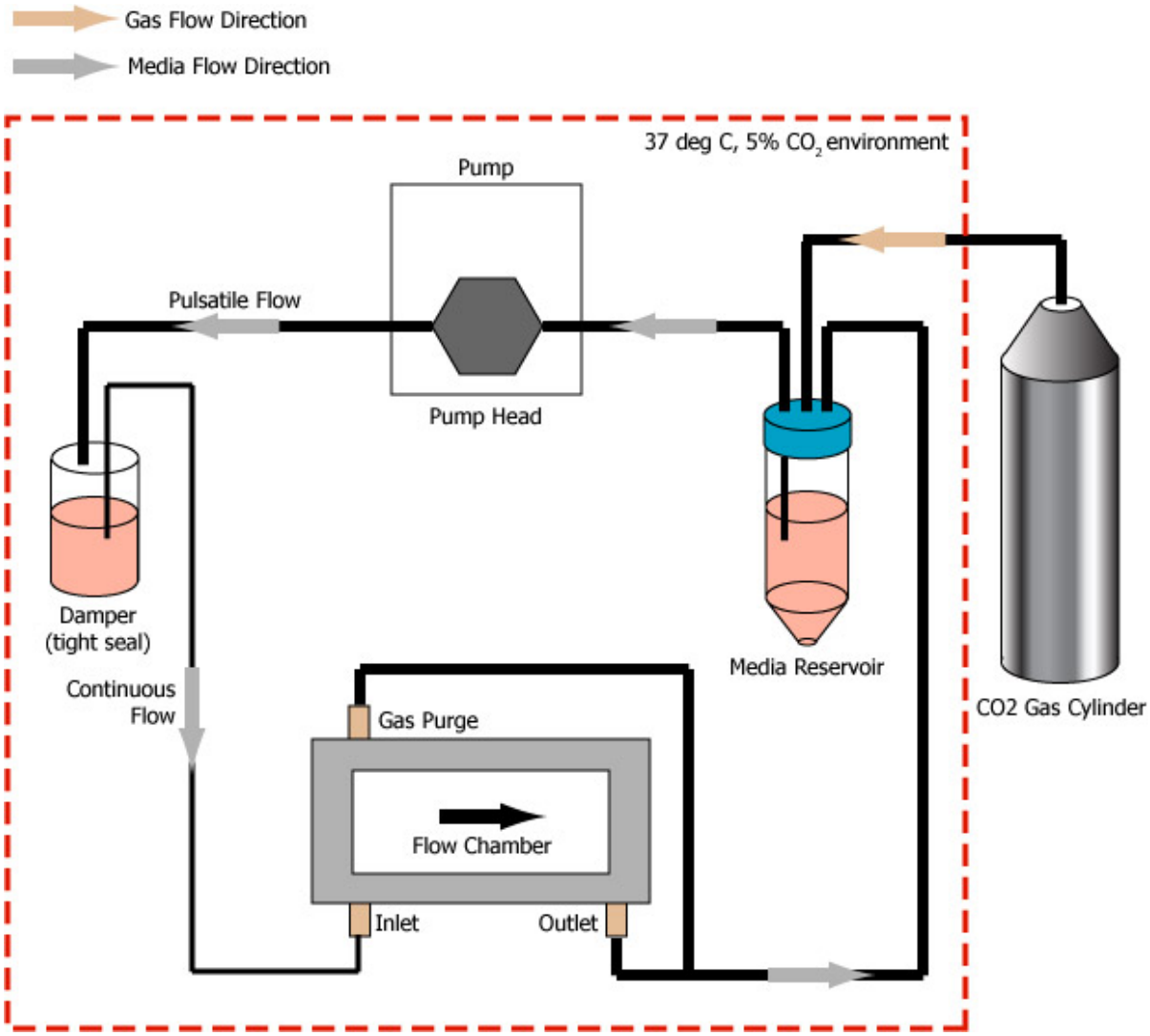

Figure 6.2. Schematic of closed-loop macroflow system.

Flow was driven by a peristaltic pump from the media reservoir to the damper. The damper converted pulsatile flow from the pump to continuous flow before entrance of media into the flow chamber. The system was contained in an enclosed environment maintained at 37°C (dotted line). 5% CO_2 was continuously pumped into the environment.

6.1.1.3 Cell Culture

PAECs were generously donated by Lowell Langille, and PAVECs were isolated and purified as described in Chapter 4. PAECs were maintained at 37°C and 5% CO_2 in Petri dishes containing 10 mL of M199 media supplemented with 5% FBS, 5% CS, and 1% P-S. PAVECs were maintained with 10 mL of M199 supplemented with 10% FBS and 1% P-S. Cells were fed every two days, and subcultured every 3-4 days. Passages 4 to 7 were used in all shear stress experiments reported.

For experimentation in PPFCs, glass slides (75 mm × 38 mm) were coated with FN at a concentration of 77 μg/mL (8.8 μg/cm^2) (room temperature, overnight). Cells were seeded at a density of approximately 75,000 cells/mL (12,500 cells/cm^2), and cultured on the glass slides until cells had reached two days post-confluence, at which point the monolayers were subjected to flow-induced shear stress.

6.1.1.4 Fixation and Immunostaining

At the end of the shear experiment, flow was stopped, and cells were immediately fixed and permeabilized in 10% neutral buffered formalin (NBF) and 0.1% Triton X-100, respectively. Glass slides were cut into three sections using a glass cutting pen, and one section was used for immunostaining. Cells were immunostained for filamentous actin stress fibres (phalloidin) and nuclei (Hoechst), and imaged for subsequent alignment analysis.

6.1.2 Microflow System

6.1.2.1 PDMS-glass Microchannel Devices

Microfluidic devices were fabricated in a similar manner to those for adhesion assays, with minor modifications (see Appendix E). The hybrid PDMS-glass structure was

advantageous for long-term culture and shear stress studies because (1) the bottom glass surface permitted protein adsorption and cell attachment, and provided good optical properties for microscopy and imaging; and (2) the PDMS was gas-permeable, and therefore permitted proper gas exchange while cells were cultured within the microchannels. For simplicity, all trials used straight microchannels of 20-mm length, 1.6-mm width, and 320 μm height (see Appendix B for SU-8 fabrication procedure for 300 μm high microchannels).

6.1.2.2 Recirculatory Loop for Microchannels

For convenience and accessibility, the recirculatory flow loop used for microchannels was designed purposely to mimic the flow loop for the macroflow system so that equipment and accessories could be reused (see Appendix E). The peristaltic pump, damper, and media reservoir were arranged in a similar manner to the macroflow system. A combination of tygon and polyethylene tubing was used instead of the C-Flex tubing used in the macroflow system (see [157]). Low pressure union adapters were also added to provide leak-proof seal at the inlet and outlet of the microfluidic device (Figure 6.3).

6.1.2.3 Live Cell Imaging and Video Capture

To monitor dynamic changes in EC morphology, a live-cell imaging system was employed in conjunction with digital image acquisition software (Langille Lab, MaRS Centre, Figure 6.4). The live cell imaging system consisted of an inverted fluorescent microscope (Nikon Eclipse TE2000, Nikon Canada, Mississauga, ON, Canada) surrounded by a temperature-controlled enclosure, and connected to a CCD camera (Hamamatsu). During a live cell imaging experiment, the microflow system was assembled as in Section 6.1.2.2 with the peristaltic pump placed next to the microscope, outside of the temperature-

controlled environment (Figure 6.4B). Damper and media reservoir were placed within the enclosure to maintain temperature at culture conditions. Tubing was extended out of the enclosure to reach the pump. The microfluidic device was secured to the microscope stage insert with scotch tape (Figure 6.4C).

6.1.2.4 Cell Culture in Microchannels

PAECs and PAVECs were maintained in Petri dishes as described above in their specific supplemented M199 media. Prior to introducing cells into microchannels, the microfluidic devices were rinsed sequentially with 100% ethanol, 70% ethanol, and sterile PBS (see Appendix E). Microchannels were coated with 250 ug/mL FN, chosen based on results from adhesion tests (room temperature, 90 min incubation). Cells were trypsinized, resuspended in media, and injected at a cell concentration of 500,000 cells/mL. Cells were allowed to attach and spread for 3-4 hours (37°C, 5% CO_2) before fresh media was introduced at a flow rate of ~0.5 mL/min. Fresh media was replenished after another 8 hours (t = 12 hours after seeding). Subsequent media changes took place every 12 hours over the next 3-7 days until confluence.

6.1.2.5 Fixation and Immunostaining in Microchannels

At the end of the shear experiment, cells were immediately fixed and permeabilized with 10% NBF and Triton X-100, respectively. Unlike macroscale glass slides, fixation, permeabilization, and all subsequent immunostaining procedures were performed directly on-chip within the microchannels by fluid injection via syringe. For a microchannel of 20 mm length, 1.6-mm width, and 320-μm height (equivalent to 10 μL volume), 200-μL volumes of

reagents at working concentrations were injected at each step of the fixation and immunostaining procedure to completely replace the solution resident in the microchannel.

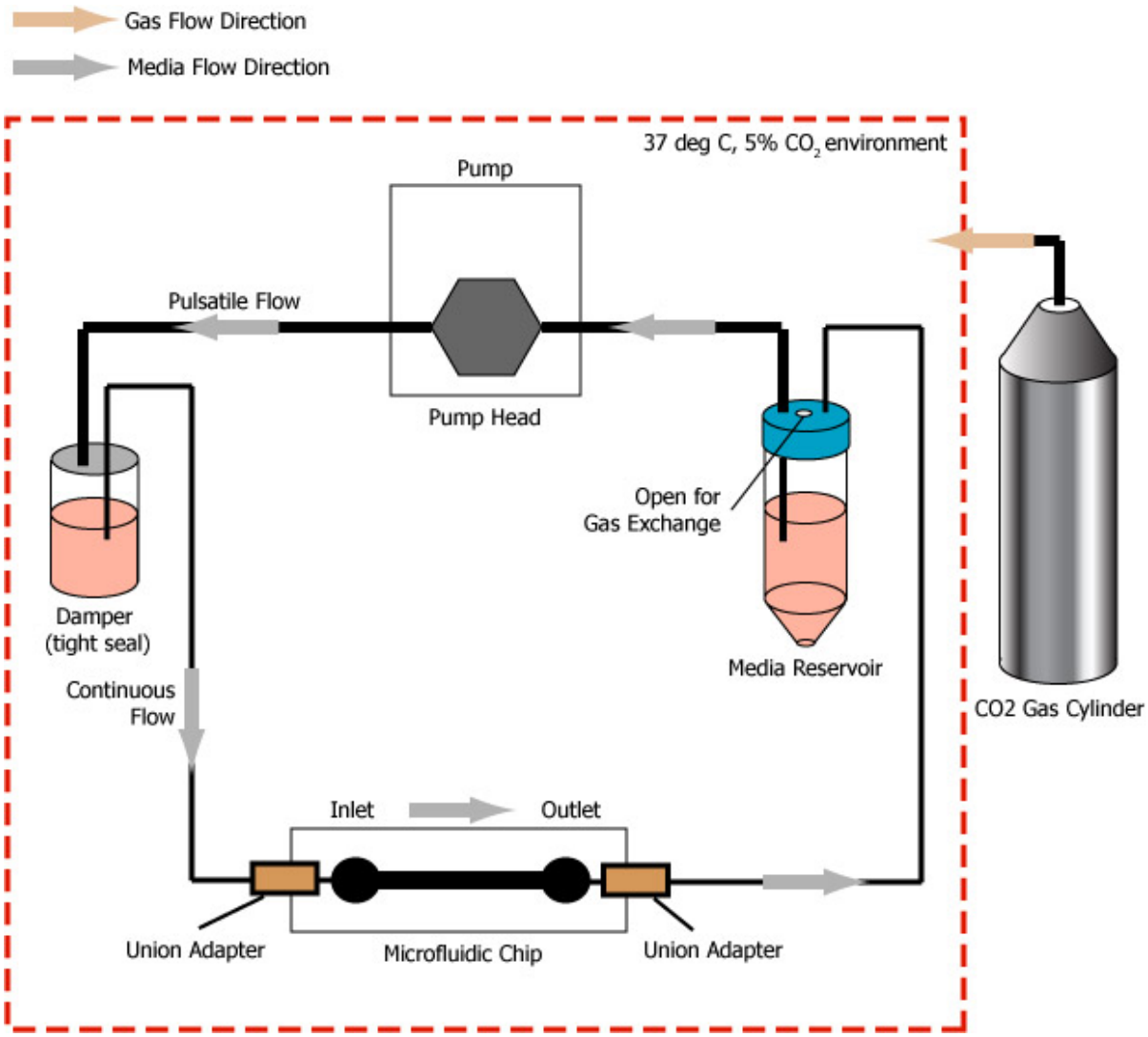

Figure 6.3. Schematic of closed-loop microflow system.

Flow was driven by a peristaltic pump from the media reservoir to the damper similar to the macroflow system. The damper converted pulsatile flow from the pump to continuous flow before entrance of media into the flow chamber. The system was contained in an enclosed environment maintained at 37°C (dotted line). 5% CO_2 was continuously pumped into the environment. Low pressure union adapters were needed to ensure leak-proof seals at the inlet and outlet of the microchannel.

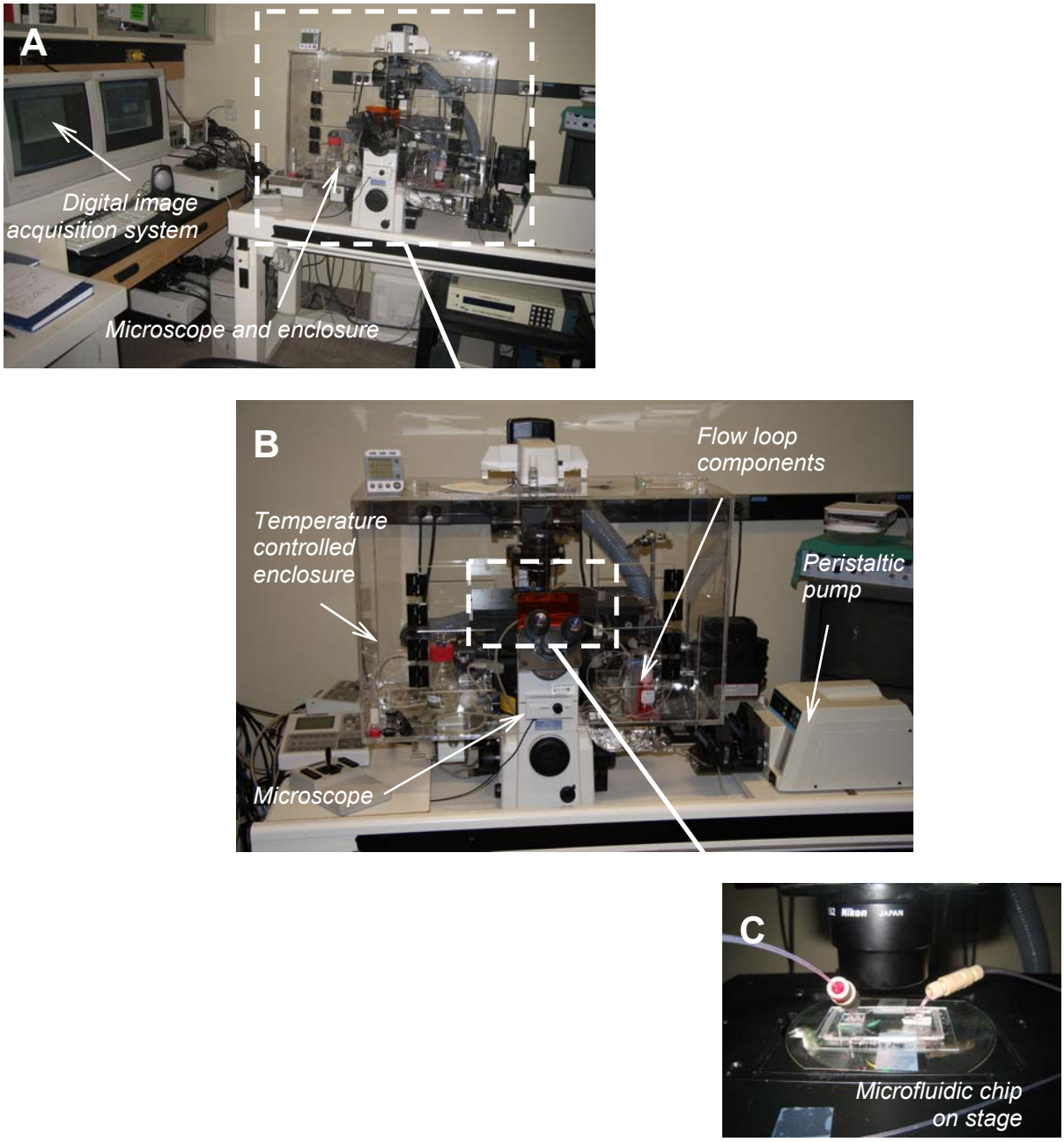

Figure 6.4. Live cell imaging system (Langille Lab, MaRS, Toronto, Canada).

Live cell imaging system for capturing real-time video of PAECs in microchannel over 48 hours of shear. (A) Digital image acquisition software controls rate of frame capture. (B) Microscope setup (Nikon TE-2000) with temperature-controlled enclosure to maintain environment for EC culture. (C) Microfluidic chip secured to microscope stage and connected to flow loop via pressure union adapters. (Images courtesy of Marc Chretien).

6.1.3 Morphological Analysis

Cell alignment of static and sheared ECs in both macro- and microflow systems were assessed by measuring angle of orientation θ of phalloidin-stained stress fibres from the direction of flow (the positive *x*-axis) (Figure 6.5A). Averaged cell orientation $\overline{\theta}$ was considered (1) parallel to flow when $0 \le \overline{\theta} < 30$ degrees; (2) perpendicular to flow when $60 \le \overline{\theta} \le 90$ degrees; and (3) neither parallel nor perpendicular when $30 \le \overline{\theta} < 60$ degrees. Generally, this intermediate range represented random cell orientation indicative of static cultures (Figure 6.5A); most other reports in the literature have used a similar interpretation [50]. Note that these delineations are applicable only when the *sign* of the orientation angle is removed before averaging such that there is no distinction between, for example, $\theta = +15$ or -15 degrees in the parallel alignment case, or between $\theta = +75$ or -75 degrees in the perpendicular case.

Although the average angle of orientation is usually sufficient as a first metric to assess overall alignment trends, its simplicity under certain circumstances may lead to misinterpretation of actual morphological tendencies. In particular, $\overline{\theta}$ values in the intermediate range ($30 \le \overline{\theta} < 60$ degrees) do not necessarily represent random orientation when individual cells all preferentially orient with a positive (or negative) sign. Figure 6.5B illustrates two specific scenarios where cells align at +45 degrees (quadrant I) or -45 degrees (quadrant IV) to the direction of flow. To distinguish between these non-random alignment cases, we introduced a second metric for orientation, the global orientation factor ϕ, that assesses the preference for cells to align in either a northeasterly (quadrant I) or southeasterly (quadrant IV) fashion:

$$\phi = \frac{1}{n}\sum_{i=1}^{n} \mathrm{sgn}(\theta_i) \qquad (6.1)$$

Eq. (6.1) utilizes the signum function to extract the sign from each measured cell angle. The average of sgn(θ) for a particular angular distribution provides an indication of the tendency to orient in a particular quadrant. ϕ = 1 means a northeasterly orientation whereas ϕ = -1 means a southeasterly orientation. ϕ = 0 likely indicates a random orientation.

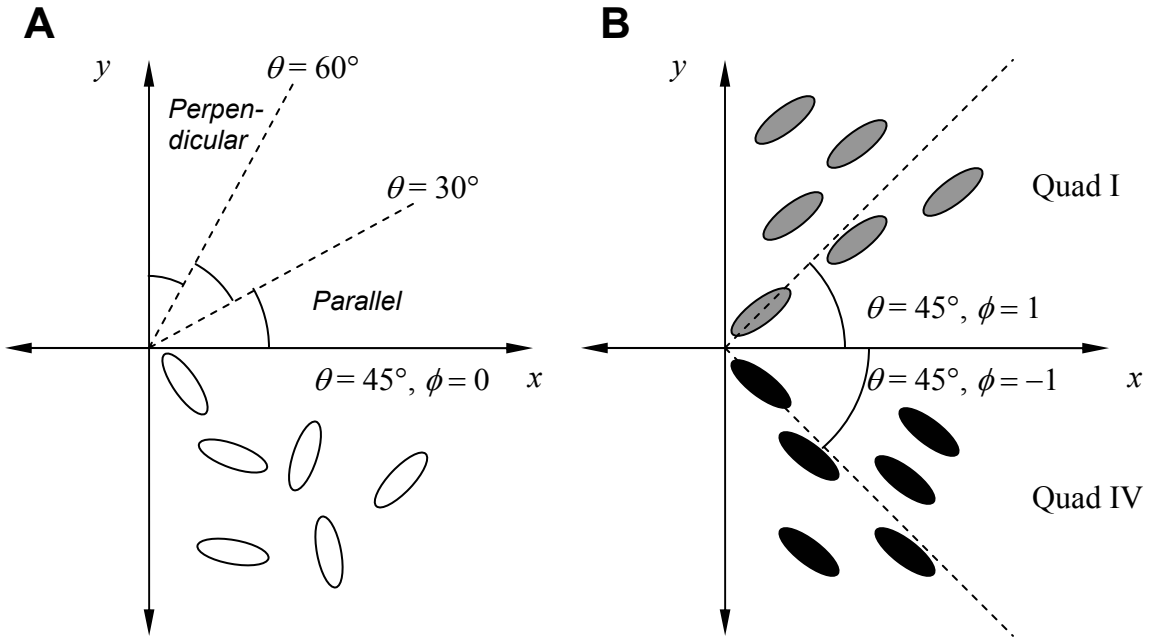

Figure 6.5. Cell alignment scenarios.

(A) In quadrant I, delineations of parallel and perpendicular orientation based on unsigned individual angle measurements. In quadrant IV (hollow ellipses), typical case of random orientation where θ = 45°, ϕ = 0. (B) In quadrant I (gray ellipses), θ = 45°, ϕ = 1. In quadrant IV (black ellipses), θ = 45°, ϕ = −1 .

6.2 Results

6.2.1 Macroflow System

PAECs and PAVECs seeded on FN-coated glass slides were either kept in static culture conditions or exposed to shear in a PPFC at 20 dyn/cm^2 for 48 hours. All monolayers were cultured for two days past confluence before the start of shear experiments. At the beginning of shear, static samples were given fresh media, and then maintained in culture without any additional media changes during the subsequent 48 hours of experimentation.

PAECs in static condition maintained cobblestone morphology and displayed a dense peripheral band of actin stress fibres near the cell border, typical of cultured, non-sheared endothelial monolayers (Figure 6.6A and B). PAECs were generally polygonal in shape, and randomly oriented throughout the culture. On the other hand, PAECs exposed to shear were elongated in shape and aligned parallel to the flow direction as expected (Figure 6.6C and D).

Similar results were obtained in the case of PAVECs. Static samples displayed cobblestone morphology and random cell orientation (Figure 6.7A and B) while samples exposed to shear elongated and aligned in the direction of flow (Figure 6.7C and D). Note that this parallel alignment of PAVECs grown and sheared on FN is unique from the perpendicular alignment of PAVECs on Col-I observed by Butcher and co-workers [50].

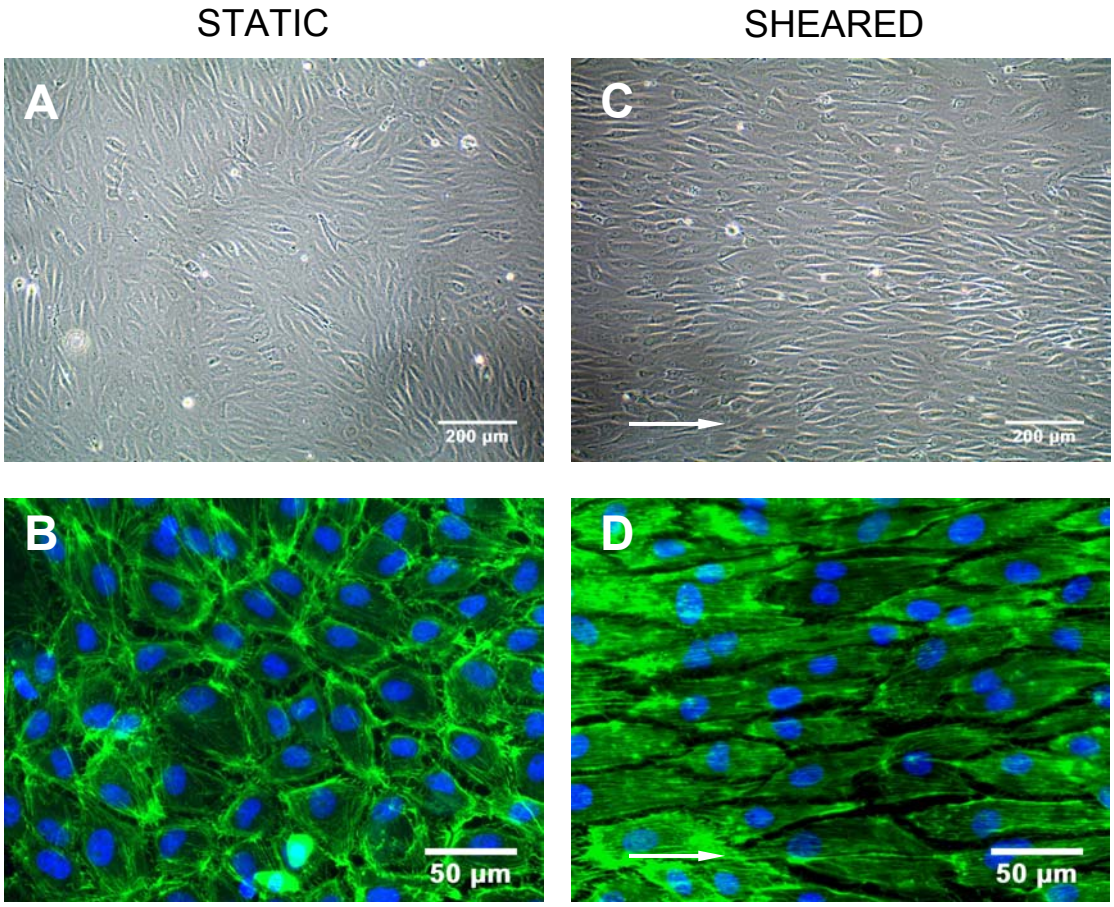

Figure 6.6. PAECs cultured on FN, static versus sheared.

Phase contrast images (A and C) and immunostained images (B and D) of FITC-labelled phalloidin for PAECs cultured on FN. For static condition (A and B), cells were cultured for 48 hours post-confluence. For sheared condition (C and D), cells were exposed to 20 dyn/cm^2 for 48 hours before fixation.

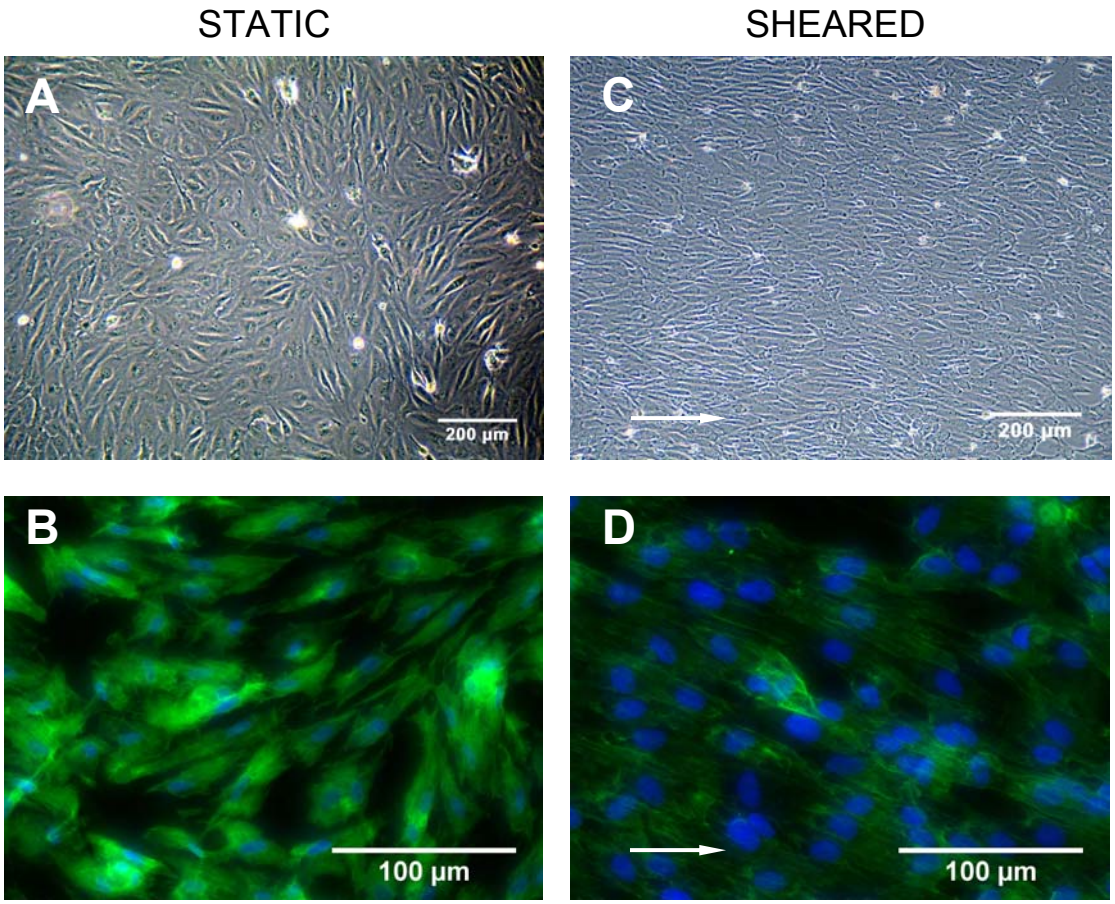

Figure 6.7. PAVECs cultured on FN, static versus sheared.

Phase contrast images (A and C) and immunostained images (B and D) of FITC-labelled phalloidin for PAVECs cultured on FN. For static condition (A and B), cells were cultured for 48 hours post-confluence. For sheared condition (C and D), cells were exposed to 20 dyn/cm^2 for 48 hours before fixation.

As preliminary analysis, angle of orientation was quantified for one representative sample in each of the four cases (PAECs and PAVECs; static and sheared for each cell type) (Figure 6.8). Observations of a second sample for each case verified the reported results. For both cell types, static samples fell in the intermediate range of $30 \le \overline{\theta} < 60$ degrees. Specifically, PAECs in static condition yielded $\overline{\theta} = 31 \pm 24$ degrees and $\phi = -0.12$; PAVECs in static condition yielded $\overline{\theta} = 43 \pm 27$ degrees and $\phi = 0.25$. In both cases, the global

orientation factor was closer to zero than to unity, indicating random orientation of cells. When sheared samples were quantified, PAECs were found to have $\overline{\theta}$ = 5.0 ± 4.2 degrees and ϕ = 0.16, while PAVECs had $\overline{\theta}$ = 12 ± 15 degrees and ϕ = -0.19. Both are indicative of preferential alignment in the direction of flow.

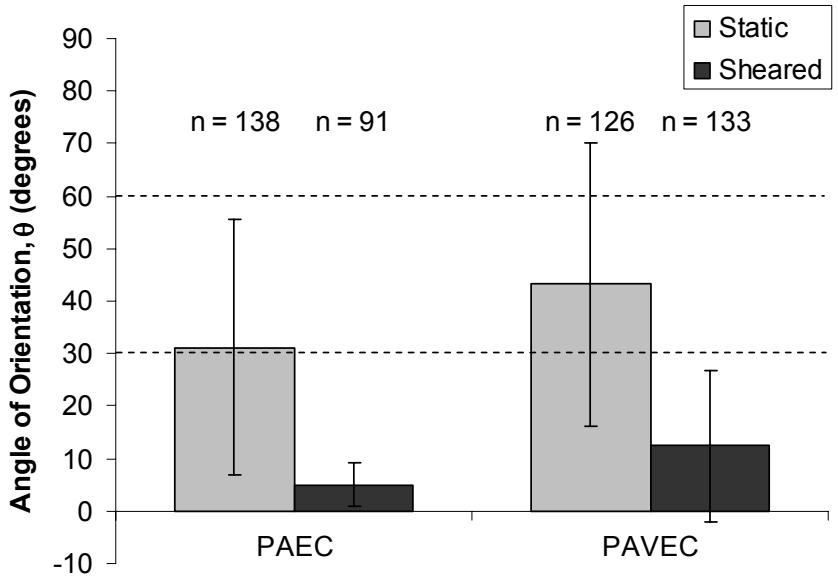

Figure 6.8. Angle of orientation for PAECs and PAVECs, static versus sheared.
Angle measurements of one representative sample for each condition. Static conditions for both cell types fell in the intermediate range (between dotted lines), indicative of random orientation. Sheared samples for both cell types had orientations below θ = 30 degrees, indicative of parallel alignment. *n* is the number of cells analyzed for each condition.

6.2.2 Microflow System

Both PAECs and PAVECs were cultured directly in microchannels until confluence. PAECs seeded at 500,000 cells/mL in microchannels coated with 250 μg/mL FN proliferated uniformly over the first three days, and reached confluence in 3.5 to 4 days. Cells displayed typical cobblestone morphology at confluence (Figure 6.9). PAVECs seeded at the same cell

concentration on the same protein coating displayed similar morphology at confluence, but required up to a week to reach confluence (Figure 6.10).

Different seeding densities were tested in preliminary trials, and it was found that 0.5 to 2 × 10^6 cells/mL provided the most consistent and uniform cultures for subsequent experimentation. Cells seeded at 100,000 cells/mL also displayed cobblestone morphology, but needed an extra two to three days of culture to reach confluence. On the other hand, cells seeded at > 2 × 10^6 cells/mL appeared to stretch into elongated shapes and aggregate prematurely with neighbouring cells, forming tubule-like networks in the microchannel that did not resemble EC monolayers.

Cells cultured in microchannels were more sensitive to pH changes in media than cells cultured in conventional Petri dishes. We monitored pH levels of supplemented media stored at 4°C, and noticed that pH slowly increased from 7.4 to 8.0 over 3 to 4 days. When cells in Petri dishes were maintained in media with this range of pH, cells proliferated and remained viable. However, when cells in microchannels were cultured with media having pH deviating from 7.4 substantially, cells did not grow and appeared to change in morphology. To eliminate changes in pH levels and prevent deterioration of media over the course of the experiment, fresh media was always made prior to each experiment, aliquoted into separate 1 mL vials, and frozen at -20°C. This procedure largely eliminated the problems associated with pH change, and resulted in improved EC cultures within microchannels.

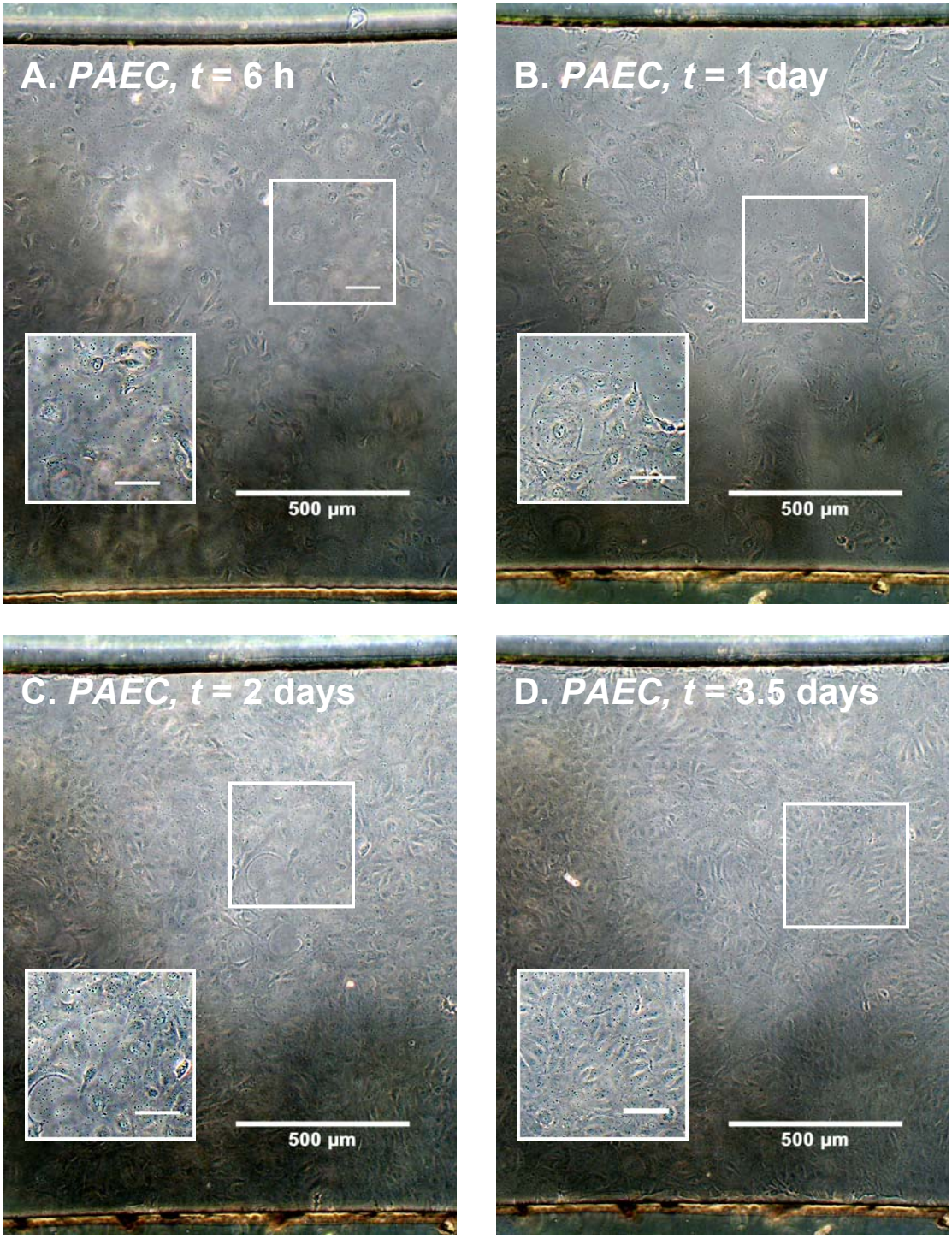

Figure 6.9. PAECs cultured in microchannels until confluence.

PAECs proliferated uniformly over the first three days, and reached confluence at 3.5 to 4 days after seeding. Cells displayed typical cobblestone morphology. Insets show close-up of local EC confluence (inset scalebar = 100 µm).

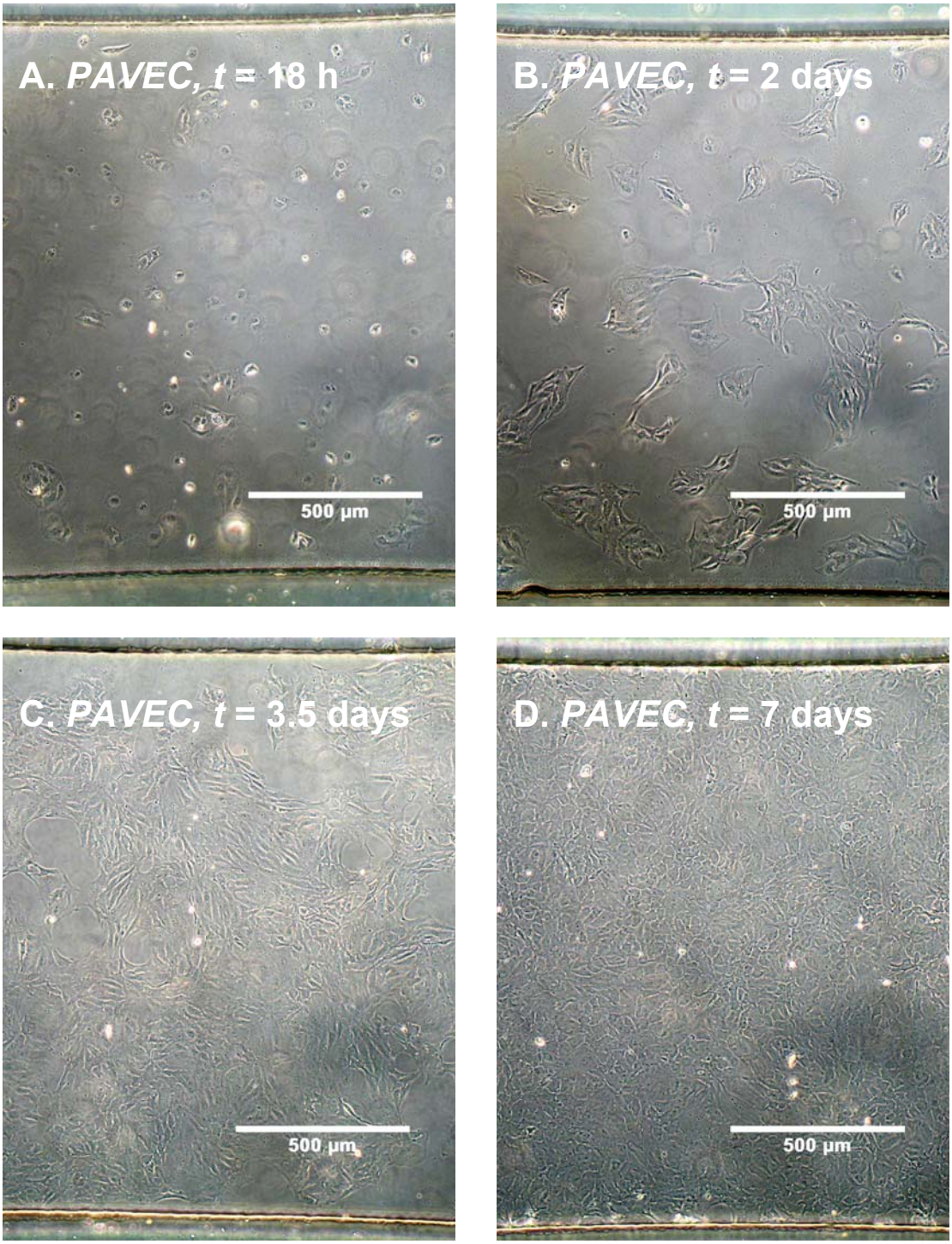

Figure 6.10. PAVECs cultured in microchannels until confluence.

PAVECs proliferated over the first three days, and reached confluence at seven days after seeding. Cells displayed typical cobblestone morphology.

PAECs cultured on FN in microchannels were exposed to shear for 48 hours within 24 hours of reaching confluence. Control samples of PAECs cultured on FN in microchannels were maintained in static condition while the sheared samples were connected to the recirculatory microflow system. Static samples were fed with fresh media every 12 hours during the 48 hour experimental period. After 48 hours of shear, both static and sheared samples were fixed in 10% NBF and immunostained for actin stress fibres (phalloidin), cell adhesion molecules (CD31), and nuclei (Hoechst). Fluorescent images were captured at multiple locations along the length of the microchannel. These images showed that for experiments in microchannels, PAECs in static condition displayed cobblestone morphology and polygonal shapes with no preferential orientation (Figure 6.11). Dense peripheral bands of actin stress fibres in the cortical shell were apparent within the cell borders, and CD31 was prominently stained at cell-cell junctions. This type of morphology is indicative of static cultures, well documented in the literature, and was observed previously for PAECs in PPFCs in the current study.

For PAECs exposed to shear, cells were discovered to align perpendicular to the direction of flow (Figure 6.12). Actin stress fibres were oriented from side wall to side wall, and cells appeared elongated in the transverse direction, orthogonal to flow. CD31 staining indicated proper cell-cell contacts throughout the monolayer. A subsequent experiment exposed PAECs to shear in a microchannel for 96 hours (data not shown). Cells were monitored every 24 hours; perpendicular alignment was apparent again at 48 hours, and persisted till the end of the experiment. The observation of perpendicular alignment was unexpected, and unique from the parallel alignment of PAECs found in PPFCs.

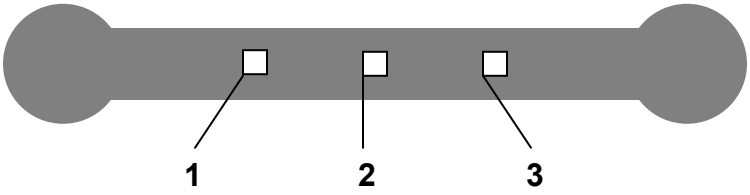

PAECs – static control

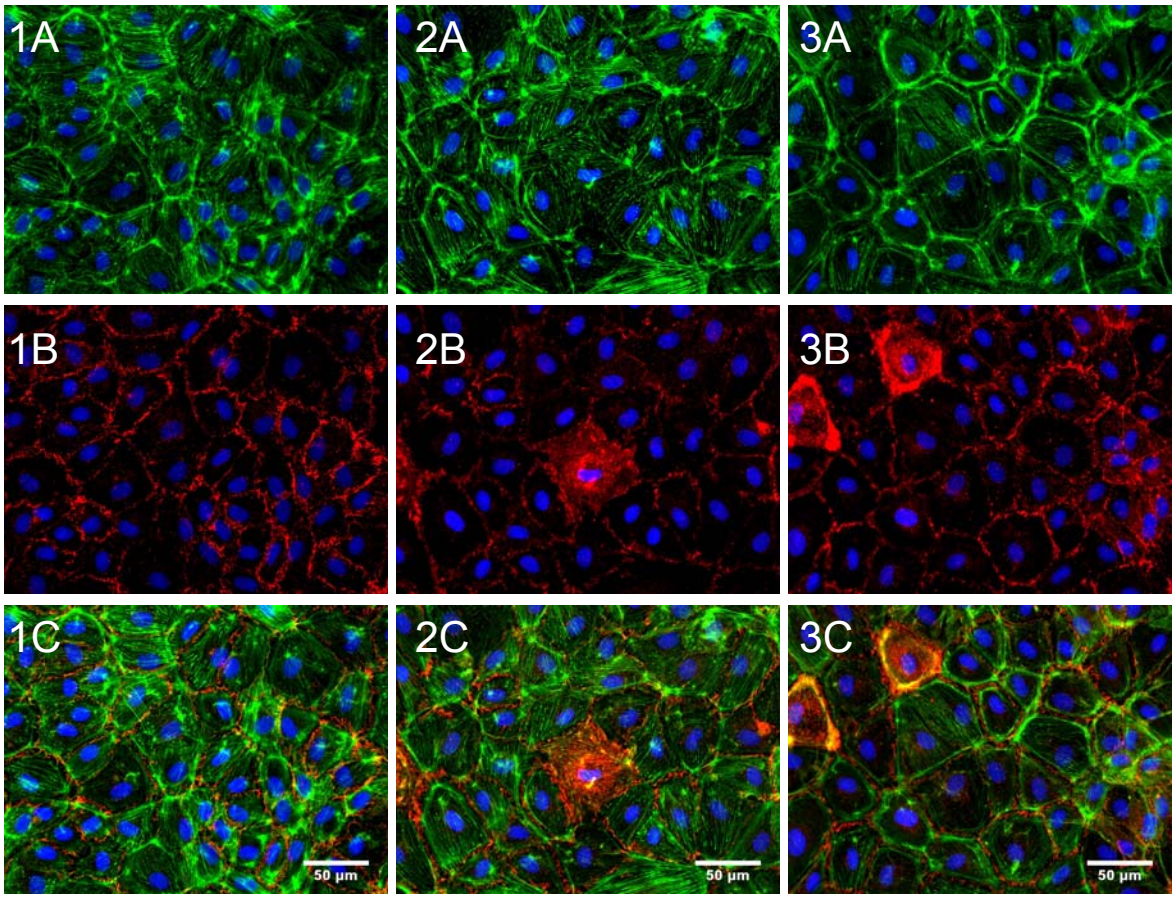

Figure 6.11. PAECs in static condition, cultured in microchannels.

PAECs were cultured in microchannels coated with FN, and maintained past confluence for 48 hours. Cells displayed cobblestone morphology, dense peripheral actin bands (green) (A), and proper cell-cell contacts through CD31 (red) (B). Overlaid images (C) showed that the cortical cytoskeleton was located just within the cell borders. Three locations are shown. Scalebar = 50 μm.

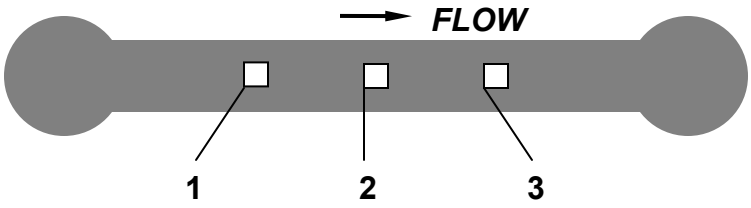

PAECs – sheared at 20 dyn/cm^2 for 48 h

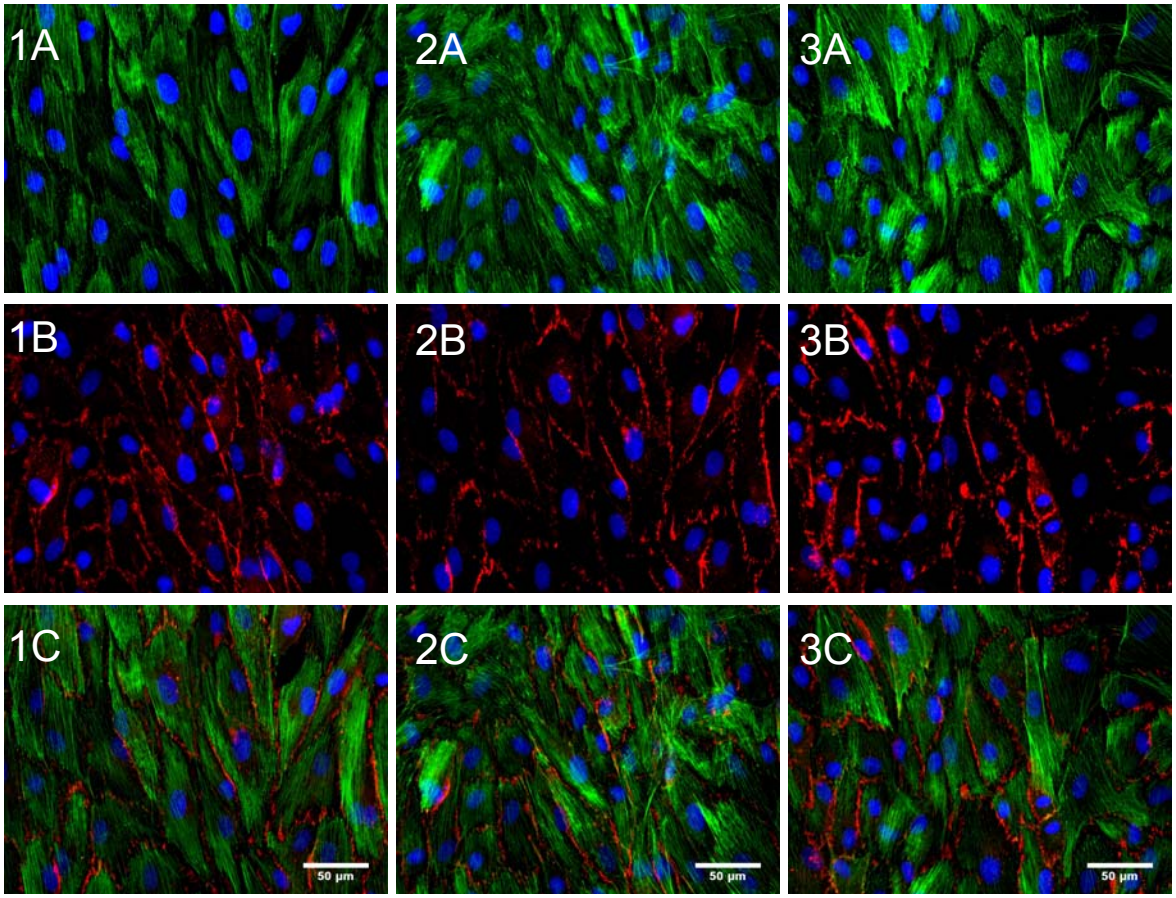

Figure 6.12. PAECs cultured in microchannels and sheared at 20 dyn/cm^2 for 48 hours.

PAECs were cultured in microchannels coated with FN, and sheared at 20 dyn/cm^2 for 48 hours. Cells elongated and aligned perpendicular to flow, as shown in the immunostaining of actin stress fibres (green) (A), and CD31 (red) (B). Overlaid images are labeled as (C). Scalebar = 50 µm.

For preliminary analysis, angle of orientation was quantified for one representative sample of the static and sheared conditions of PAECs in microchannels, and compared to the previous results for PAECs in PPFCs (Figure 6.13). Static PAECs in microchannel culture had an average angle of orientation of $\overline{\theta}$ = 43 ± 27 degrees and ϕ = 0.03, indicative of random orientation. Sheared PAECs in microchannel yielded $\overline{\theta}$ = 64 ± 20 degrees and ϕ = -0.54. This represented a perpendicular alignment, with tendency for cells to point to the southeast quadrant.

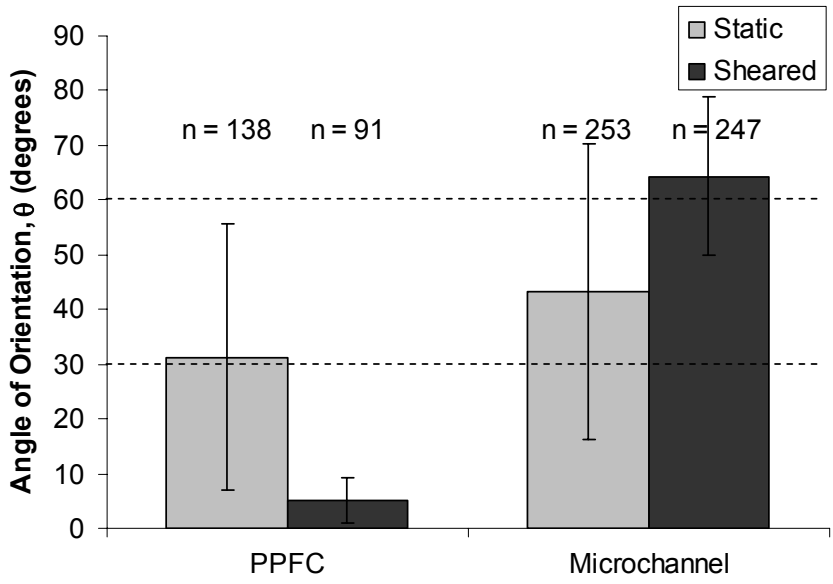

Figure 6.13. Orientation for PAECs in PPFC and microchannel, static versus sheared. Angle measurements of one representative sample for each condition. Static conditions for both cell types fell in the intermediate range (between dotted lines), indicative of random orientation. Sheared sample in PPFC had orientations below θ = 30 degrees, indicative of parallel alignment. Sheared sample in microchannel had orientation above θ = 60 degrees, indicative of perpendicular alignment. *n* is the number of cells analyzed for each condition.

The discovery of unique perpendicular orientation of PAECs in microchannel shear flow prompted further investigation by live cell imaging and real-time video capture. PAECs grown in microchannels were exposed to 20 dyn/cm^2 for 48 hours, and monitored using the live cell imaging system (Figure 6.4). A location at mid-length near the centre of the microchannel (away from side walls) was chosen for the 48-hour study. Phase contrast images were captured every two minutes for the duration of the experiment at the location of interest, and at the end of the test prior to fixation, images were captured at every location along the length of the microchannel. These images were photo-stitched (Adobe Photoshop CS2) to create a full-length map of sheared PAECs within the microchannel. A small section of this map near the mid-length region is shown in Figure 6.14. The map spans the entire channel width, providing a clear view of the endothelial monolayer while also providing possible insights into the effect of side walls on endothelial morphology under shear flow.

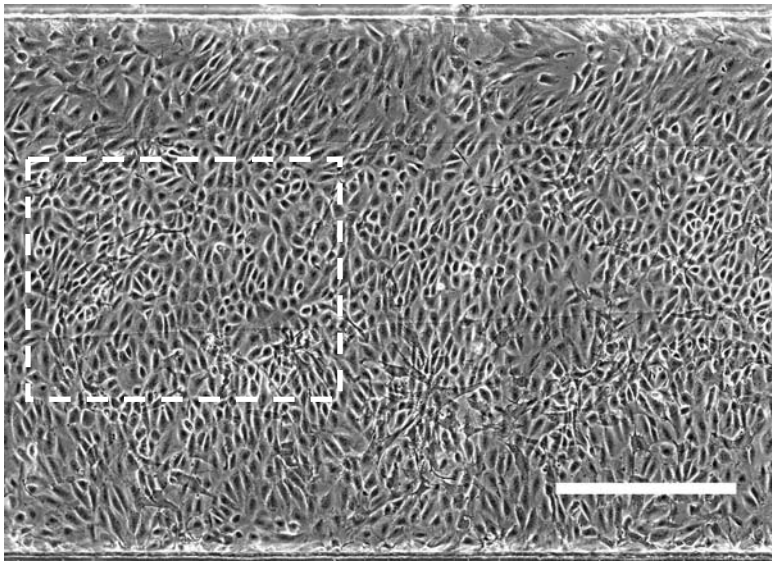

Figure 6.14. Photo-stitched map of PAECs in microchannel, full width at mid-length.
PAECs were exposed to shear of 20 dyn/cm^2 for 48 hours prior to imaging at every location along the entire length of the microchannel. Dotted white line indicates location and viewfield of live-cell video capture. Scalebar = 500 μm.

Real-time video capture provided qualitative evidence of the morphodynamic nature of ECs under flow. Figure 6.15 shows individual frames from the video at select times during the flow experiment. Over the 48 hour period, PAECs constantly migrated with respect to neighbouring cells while maintaining cell-cell contacts. Presumably, cell-cell contacts in the form of adherens and tight junctions were constantly turning over as new junctions formed to replace old ones in a highly dynamic process. A noticeable trend was the overall tendency for cells to migrate toward the centre of the microchannel, away from the side walls. Over time, cells near the top and bottom edges of the images moved into the central region of the frame, resulting in an overall increase in cell density near the channel centre. Qualitative examination of the photo-stitched map verified this observation: cell density appeared to be much less near the side walls than near the microchannel centre. As additional verification, simple quantification can be performed by dividing the microchannel into equal thirds in the longitudinal direction (top wall, centre, and bottom wall), and counting the number of cells with stained nuclei.

The full-channel map revealed a slight tendency for cells near the top wall to align in the northeast direction, while cells near the bottom wall tended to align in the southeast direction. It is possible that these tendencies originated from the side walls and were then propagated toward the centre of the microchannel during cell migration. Interestingly, preliminary analysis of the global orientation factor also indicated a slight preference for perpendicularly-aligned cells to tend toward a specific quadrant (ϕ = -0.54, see above).

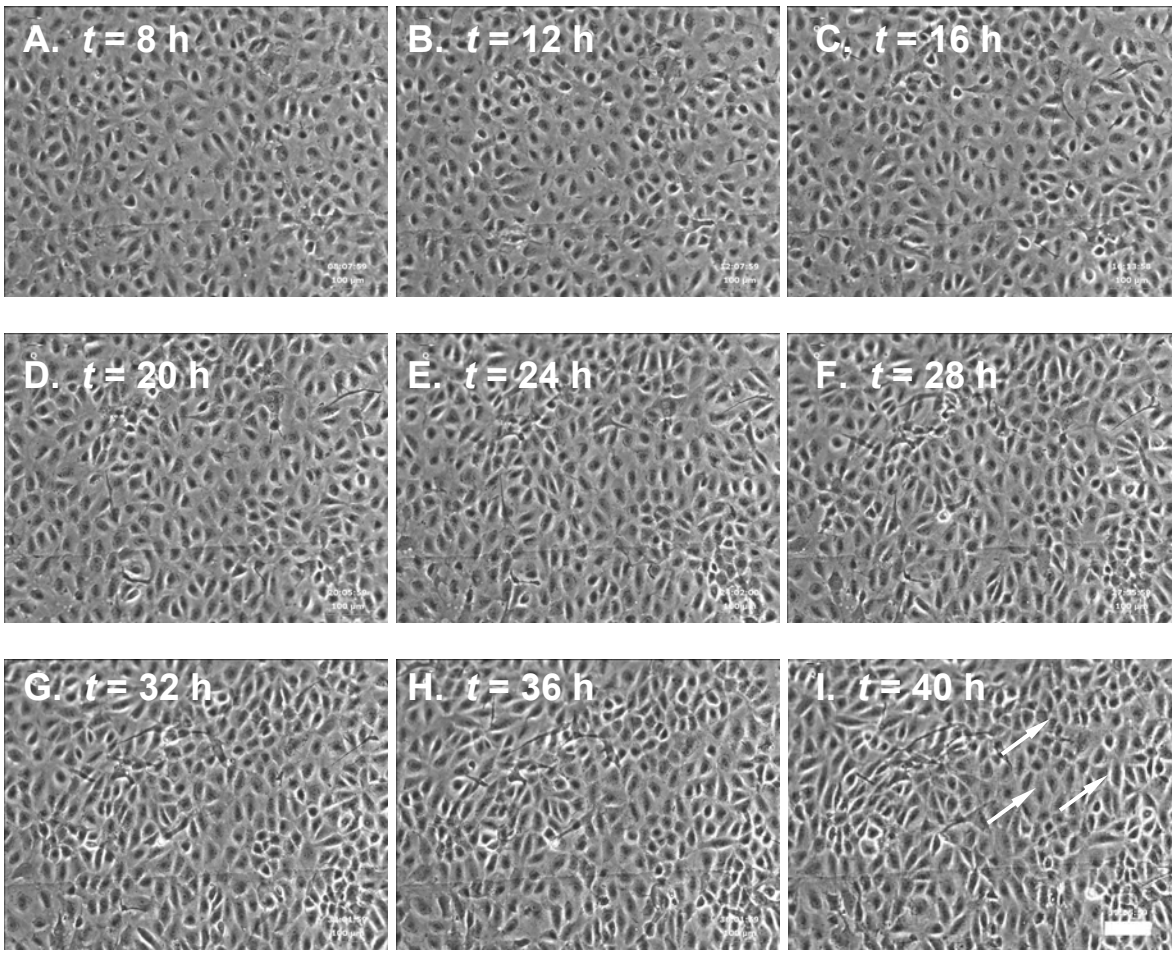

Figure 6.15. Individual frames from real-time video capture of PAECs under shear.

Select images from real-time video capture, from t = 8 to 40 hours. Image sequence indicated regular cobblestone morphology at t = 8 h with cells having cuboidal shape and random orientation. By t = 40 h, cell shape and orientation were less uniform and random, and cell density of the viewfield increased. Perpendicular alignment of cells was also apparent at this point (Panel I, white arrows).

6.3 Discussion

Shear stress acts universally on all ECs lining the vascular system. Thus, to understand how ECs maintain vascular homeostasis and influence pathological development, it is natural to begin with an understanding of how ECs respond to shear. Although *in vitro* shear stress studies are plentiful, and many established tools are available for applying shear

to ECs, there is considerable interest in streamlining experimentation to increase throughput and efficiency. Microfluidics offers a platform that promises improved throughput and possible integration of additional on-chip functionalities for post-shear processing. To realize its potential, it is imperative to demonstrate that shear stress studies of ECs performed in conventional devices can be reproduced with fidelity at the microscale, both as a validation of *in vitro* culture techniques in general, and as a validation of microfluidics as a feasible technology for biological applications. This study provided the first side-by-side comparison of macro- and microscale shear systems, and offered some insight into how physical scales may alter biological response of ECs under shear. We focused on morphological response of ECs as a logical first measure of endothelial adaptation to shear. Though these results were preliminary, the reported observations have since been reproduced, and will help direct future experimental work.

It was important to first establish a working macroscale system that could reproduce past results reported in the literature. It has generally been accepted that vascular ECs align parallel to flow on glass surfaces [30]. This behaviour has been demonstrated on a variety of protein coatings and for various EC types [32, 76, 78, 156]. Specifically, it has been noted for porcine aortic ECs [50, 78]. We studied PAECs on FN in the macroflow system by applying shear flow at 20 dyn/cm^2 for 48 hours, and confirmed this preferential parallel alignment, thus validating our macroflow system with previously published data.

Recent work on the aortic valve endothelium has raised considerable interest in understanding the valve EC phenotype. The recent report from Butcher et al. [50] compared alignment of PAECs and PAVECs, and found distinct morphological changes between the two EC types when both were grown and sheared on glass surfaces coated with Col-I. As

mentioned, PAECs aligned parallel to flow; PAVECs, on the other hand, aligned perpendicular to the flow direction. We hypothesized that if preferential orientation to flow was an adaptive response intrinsic to cell phenotype alone, PAVECs would align perpendicular to flow regardless of surface protein. We applied shear at 20 dyn/cm^2 for 48 hours to PAVECs seeded on FN-coated glass slides, and discovered for the first time that PAVECs aligned parallel to flow, contrary to our hypothesis. This somewhat surprising finding suggested that orientation was perhaps not simply an inherent phenotypic trait, but was more likely a combination of phenotype and extracellular environmental conditions. In this case, the use of a different ECM protein for coating glass may have resulted in a differential alignment for the same cell type.

Specific evidence supports this proposed explanation that cell-matrix interactions are likely involved in the differential alignment of PAVECs observed in these separate reports. In Chapter 5, we demonstrated that PAVECs and PAECs spread and adhered differently when seeded and cultured on FN and Col-I. *In fact, the pattern of preferential adherence appears to correlate with the pattern of preferential alignment.* Recall that PAECs were found to spread and adhere similarly well on both FN and Col-I, whereas PAVECs spread and adhered significantly more on FN than on Col-I. Likewise, PAECs were observed to orient with flow for both FN and Col-I, while PAVECs showed differential alignment by orienting parallel to flow on FN but perpendicular to flow on Col-I. Thus, the two patterns of behaviour suggest that parallel alignment is associated with strong adhesion, whereas the one notable case of perpendicular alignment (PAVECs on Col-I) can be associated with poor adhesion. This is rather speculative, and more research is needed to determine whether

perpendicular alignment is not just associated with, but can be *attributed to* poor adhesion and differential integrin expression.

Validation of the macroflow system also provided a reference by which results from microfluidic systems could be compared. We studied PAECs seeded on FN-coated glass surfaces in straight rectangular microchannels and exposed to shear stress of 20 dyn/cm^2 for 48 hours, and we hypothesized that these cells would align parallel to the flow direction, as demonstrated on macroscale PPFCs. To our surprise, we observed perpendicular alignment of cells. This somewhat paradoxical observation appeared to contradict our hypothesis and our other findings in the current study. However, with the aid of video microscopy to capture continuous real-time footage of endothelial monolayer adaptations to shear, and upon further analysis of fluid mechanics within the microchannel, we made additional observations that suggested a possible explanation.

There were clear differences between the macro- and microflow systems, including (1) material properties of flow chamber surfaces, (2) pre-shear culturing conditions, and (3) physical dimensions of the channel section. Of these three differences, physical dimensions of channel section are likely more influential in its effect on morphological adaptations than the other two. First, the macroscale PPFCs consisted of a polycarbonate base that is relatively stiff (E = 2-2.4 GPa) and completely non-permeable to gas. PDMS, however, is significantly more pliable (E = 1-3 MPa), and more importantly gas permeable. Although such differences were likely important for permitting long-term culture of cells in microchannels (see below), they are unlikely to be related to the differences in morphological responses seen in this study. Cells in both cases were adhered to the same protein and same underlying substrate. The largest possible influence that either material had on these trials

was the attachment of certain cells to the PDMS side walls in the microchannels. Thus, it was reasonable to assume that neither material was responsible for the differences observed.

Secondly, in the microflow case, cells were cultured in a low-volume (less than 100 μL) microenvironment for four to seven days prior to shear. This is different than the macroflow case where cells were maintained in Petri dishes with 10 mL of media before shear was applied. In a microenvironment where surface area-to-volume ratios are much higher than in Petri dishes, cells likely experienced higher concentrations of secreted cytokines and other soluble factors from neighbouring cells [141]. Furthermore, low media volume may have resulted in faster nutrient depletion and waste accumulation, as well as an increase in cellular sensitivity to minor fluctuations in osmolarity and pH, both of which can affect cell growth rates and potential signaling events [159]. Several different feeding schedules were therefore tested to ensure cells were properly maintained in these conditions. Despite these clear distinctions in cell culture maintenance between macro- and microscale systems, live cell imaging of the endothelial monolayer showed typical endothelial motility (albeit in an atypical direction). Presumably, ECs were pre-conditioned in microscale culture, but maintained normal basic cell function throughout the culturing period such that at the onset of shear, ECs were able to adapt morphologically to flow-induced shear stress. The effects of such preconditioning on cellular response to shear and the potential downstream effects are largely unknown, but may be critical for understanding differences between macro- and microscale setups. Thus, preconditioning schemes should be chosen with caution, and their effects should not be discounted.

The most likely explanation for this phenomenon based on our observations is the difference in physical dimensions of the flow section, in particular the channel height-to-

width ratio, α. In the PPFC, the flow section was approximately 38 mm wide and only ~0.2-0.3 mm high, corresponding to an aspect ratio of $\alpha < 0.01$. In contrast, the microchannel flow section was only 1.6 mm wide and 0.3 mm high such that $\alpha = 0.2$. The main effect of high aspect ratio channels is that the walls impose a three-dimensional velocity profile that deviates substantially from the predictions derived from two-dimensional equations where slit geometries are treated as infinite parallel flat plates (Figure 2.8). For three-dimensional velocity profiles in rectangular cross sections, the Purday formula may be used as a simple algebraic approximation to determine the portion of channel near the side walls that deviate from uniform shear stress conditions (see Appendix C). Calculations showed that for $\alpha = 0.2$, approximately 25% of the channel near each side wall experienced a shear stress gradient, and only the middle 50% of the channel was exposed to uniform shear stress of 20 dyn/cm^2. Near the side walls, shear stress on the endothelial monolayer increased monotonically from zero at the wall to maximum shear stress of 20 dyn/cm^2 approximately 400 microns toward the channel center. It should be noted that the live cell imaging experiment monitored the central 40% of the microchannel (600 μm) where shear stress was indeed uniform.

A previous study investigated the effect of shear stress gradients on EC migration, proliferation, and cell loss [79]. The study showed that in a flow chamber with a disturbed flow region, ECs tended to migrate away from the region of highest shear stress gradient toward regions with steady shear stress. From that investigation, it appeared EC migratory response was dependent more on shear stress gradient than on shear stress magnitude. Interestingly, over the 48 hours of live footage captured by video microscopy, we observed continuous cell migration as ECs maneuvered over and around each other in an effort to

reposition themselves in the presence of shear. Cells appeared to consistently migrate from the side walls (high gradient) toward the center of the channel (uniform shear), a direction consistent with the aforementioned study.

Accumulating evidence in past reports [82, 160] and in personal observations and communications with collaborators suggests that a general trend exists between EC migration and cell elongation and orientation. In short, *cells elongate along an axis parallel to the direction of migration.* This tendency is a natural phenomenon related to lamellipodial crawling, where cells move by membrane protrusion and formation of new adhesion sites at the leading edge combined with detachment of adhesion sites at the trailing edge. Cells inherently appear elongated in the direction of migration because it corresponds with the same direction as membrane protrusion and crawling. In time-lapse videos monitoring PAECs in 6-mm wide flow chambers, PAECs aligned parallel to flow after 48 hours of shear at 20 dyn/cm^2 (Marc Chrétien, personal communication). This parallel alignment was preceded by constant EC migration upstream and downstream in the direction of flow. As further evidence, in many wound healing models [160, 161], ECs proliferate and migrate toward the wound edge in an effort to close the unoccupied space between endothelial fronts. In these models, ECs again tended to stretch and elongate in the direction of migration, perpendicular to the wound edge. Clearly, these observations are consistent with current findings that cell migration from side walls toward the centre of the microchannel correlate with cell elongation and orientation in the transverse direction. It is therefore plausible to hypothesize that the perpendicular alignment of PAECs is a manifestation of (1) a migratory response induced by shear stress gradients and (2) the natural tendency of cells to elongate in the direction of migration.

The hypothesis suggests that apparent orientation of ECs is dependent on physical dimensions of the flow section that confine the monolayer and restrict migration to a specific region. To test the hypothesis, different microchannel geometries may be used to investigate the affect of height-to-width as well as length-to-width aspect ratios. Shear stress gradients can also be removed from the problem by eliminating side walls and growing ECs on micropatterns of matrix proteins having the same shape and dimensions as the microchannels tested. Micropatterned slides can then be seeded with ECs, and exposed to shear in a conventional PPFC to apply uniform shear stress without side wall effects.

The current results have reinvigorated interest in understanding mechanisms behind the perpendicular alignment of PAVECs on Col-I as reported by Butcher and co-workers. The authors of that work claimed that differential responses between PAECs and PAVECs were solely due to phenotypic differences between cell types [50]. To my knowledge, the only other report of perpendicular alignment was for bovine carotid artery ECs, which aligned perpendicular to flow after six hours under 128 dyn/cm^2 of shear, but loss this preferential alignment at 12 and 24 hours and reverted to a random orientation [31]. A compelling assertion from a biophysical study by Hazel and Pedley [153] states that alignment of nuclei should always be parallel to flow in order to reduce total hemodynamic drag on the surface of the cell. And given that elongation and orientation of nuclei correlate with those of the whole cell, this solely physical (and mathematical) argument suggests that cells do not align perpendicular to flow unless exposed to specific stimuli "strong" enough to overcome the natural tendency of the cell to streamline itself to flow. Preliminary observations from the current study suggest one possible stimulus: the desire for cells to migrate away from shear stress gradients and crowd into a region of uniform shear.

We conclude the discussion in this chapter by revisiting aspects of microfluidics that are relevant to the current study as well as to future work on the topic of shear stress response of ECs. Culturing cells in microchannels involves overcoming limitations that are inherent to the microscale. One specific limitation is the low volume of media within the channel during static culture. The increase in surface area-to-volume ratio at the microscale results in lower volume of media per cell (Table 6.1). This impacts the balance between nutrient consumption and metabolic waste production, and leads to shifts in pH, osmolarity [159], and oxygen tension [162] that adversely affect long term viability of cultures, and in less time than in conventional platforms. A popular method in microfluidic cell culture is to incorporate a perfusion system. This is effective in ensuring that media volumes are replenished in a timely fashion, and small shifts in culture conditions do not have detrimental effects on cell structure and function. Though additional work is required to choose appropriate perfusion rates [140, 163] and incorporate perfusion channels into the microfluidic network [103], the effort pays off in the form of long-term viability of cells in *in vitro* microscale culture. In the current study, I was able to avoid perfusion and simplify design by using a sufficiently large volume such that intermittent media exchanges (similar to conventional culture) in 12-hour cycles maintained cell viability. However, it is likely that more frequent media changes would be necessary for microchannels of smaller size (see Table 6.1).

The recirculatory microflow system was designed with end-user accessibility in mind. Although the concept of recirculatory flow in microfluidics is not new [117], the current system is one of the few that differs from the regular syringe pump-driven layouts while also keeping the overall setup simple and reliable. Since the majority of system components used

in the microflow system were also used for the macroflow setup, the current apparatus provides cell biologists with a microscale alternative that could be easily integrated into existing laboratory procedures and setups. Although a recirculatory system has its advantages, syringe pumps still offer a robustness and simplicity that makes it an indispensable tool in the laboratory. Both infusion and withdrawal modes have certain advantages over recirculation, and thus, should always be considered as viable options in any microfluidic study.

Live cell imaging was instrumental in providing insight into endothelial cell morphodynamics. A future direction may be to incorporate quantitative morphodynamic measurements and the ability to trace individual cell migration over time [82] together with high-throughput microfluidics and live cell imaging. This would permit large-scale studies of endothelial cell dynamics, particularly for a range of different chemical or mechanical stimuli.

The original goal of this chapter was to validate the use of microfluidics as a platform for studying endothelial shear stress response. The hope was to compare macro- and microscale systems side by side, and demonstrate that microfluidics can produce biological outcomes and conclusions similar to conventional platforms, with the added advantages of high-throughput potential, on-chip integration, and reduced reagent consumption. Instead, we discovered interesting new phenomena at the microscale distinct from the expected results obtained at the macroscale. The finding, that ECs align perpendicular to flow when exposed to shear in a microchannel, may have fundamental implications on understanding endothelial cell phenotype, structure, and function. Although this discovery does not corroborate microfluidics as a simple scaled-down version of a macroscale flow system, it

does emphasize the need for validation studies to ensure artifacts due to physical system geometry alone are eliminated. Despite the differences in biological response shown in the current study, it is important to understand that once these issues are resolved, microfluidics will remain a platform with great potential to streamline experimentation.

Table 6.1. Comparison between macro- and microscale cell culture.

	Cells at confluence	***Culture Area* (mm^2)**	***Volume media* (mL)**	***Cells per mm^2***	***Volume media per cell* (nL)**
***Petri dish* (15 x 100 mm)**	6×10^6	6000	9	1000	**1.5**
***Microchannel h* = 300 μm**	0.03×10^6	30	0.009	1000	**0.3**
***Microchannel h* = 100 μm**	0.03×10^6	30	0.003	1000	**0.1**

(*Based on microchannel width of 1.5 mm, and microchannel length of 20 mm.*)

Chapter 7

7 Permeability[5]

One of the major functions of the endothelium is selective trafficking of solutes and macromolecules from luminal blood to the tissue interstitium, and vice versa. Transport processes through the monolayer occur via transcellular and paracellular mechanisms, and are tightly regulated by local chemical and mechanical microenvironments surrounding the cells [41]. One way to quantify the level of these transport processes is to measure the permeability of the endothelium, a measure of the ease with which soluble factors can penetrate the cellular monolayer. Permeability provides an indication of the structural integrity of the endothelium, which is important for assessing vascular homeostasis or pathogenesis within the cardiovascular system [1] (Section 2.1.4).

[5] I thank Michael Watson for significant contribution to the work presented in this chapter. He masterfully assembled the laser-induced fluorescence microscopy setup, and troubleshooted all analytical chemistry problems.

Because of its fundamental importance and practical significance, endothelial permeability is a widely studied characteristic of ECs. From a fundamental standpoint, measuring and understanding permeability helps characterize phenotypic differences between specific endothelial cell types while also providing insight into the developmental processes related to vascular disease progression. Practically, permeability measurements can help assess the ability of the vascular tissue lining to take up pharmaceutical drugs. Such pharmacological properties are important for evaluating the efficacy of drugs and their suitability for public consumption [45].

Currently, the majority of permeability assays are performed under *static* conditions where EC monolayers are cultured on membrane-based cell culture inserts, and tagged molecules are allowed to permeate through the static monolayer on the luminal side and collect on the abluminal side [45]. An example is the Caco-2 assay [164], generally regarded as the gold standard for measuring permeability. Although such static experiments are informative to a certain extent, and can permit high-throughput drug screening tests in well plate formats, they are not representative of the dynamic *in vivo* conditions where ECs are constantly exposed to shear stress from flowing blood. Shear stress is widely known to be an important mechanical stimulus for regulating EC structure and function [18]. Interestingly (and known to a lesser extent), shear stress has also been shown to effect changes in endothelial permeability [46, 85]. This is an important point from a pharmacological perspective because it suggests that efficient and accurate assessment of drug efficacy depends not only on the ability to carry out high-throughput screening experiments, but also on the ability to mimic the dynamic *in vivo* microenvironment. Without shear stress, *in vitro*

model systems lack an important physical element of the *in vivo* condition that potentially limits their applicability, and brings into question the validity of experimental results.

Although some flow systems have been built to study permeability of endothelial monolayers with shear stress [46, 85], these systems were designed for experimentation of one condition at a time. Also, some of these systems required manual collection of samples that slows experimental procedure. There is a need to design shear-based permeability systems that can potentially support *in vivo*-like high-throughput drug screening for pharmacological applications. Microfluidics is ideally suited for this application because of its miniature scale, potential for parallelization, and natural geometry for laminar fluid flow. Recently, a number of reports have demonstrated the successful incorporation of membranes into microfluidic devices [118, 119]. For an extensive review of membrane-based microfluidic devices, we recommend the review by de Jong and co-workers [122]. Ultimately, these membrane-based systems open the door for a myriad of biological "lab-on-a-chip" applications that could benefit from controlled channel-to-channel communication in a three-dimensional configuration where microchannels are permitted to pass above and below other neighbouring microchannels. In this chapter, we present a novel real-time technique to measure albumin permeability across an endothelium monolayer cultured on a track-etched porous membrane separating two levels of microfluidic channels. Using laser-induced fluorescence (LIF) to detect fluorescently-tagged albumin that permeated through the membrane region, we demonstrated the ability to measure permeability on a microscale platform. This system has the potential for parallelization, and permit measurement of multiple sample streams, opening the door for *in vivo*-like high-throughput drug screening capabilities.

7.1 Materials and Methods

7.1.1 Device Design and Fabrication

A two-layer membrane-based microfluidic system was made from PDMS (Sylgard 184, Dow Corning, Midland, MI, USA), and consisted of north-south (top) and east-west (bottom) microchannels separated by a porous track-etched membrane (Figure 7.1A and B). The cross pattern of the microchannels formed a single intersection where molecular transport from one channel to the other was possible through the membrane (Figure 7.1C). The design is similar to other membrane-incorporated microfluidic devices reported in the literature [118, 119, 121, 165]. PDMS was chosen for its ease of fabrication as well as for its optical properties. PDMS is non-autofluorescent [166], does not affect LIF detection because it does not absorb light [167], and has excellent reflective properties [168].

North-south and east-west channel patterns were drawn in AutoCAD and printed on a transparent photomask (City Graphics, Toronto, Canada). Masters were fabricated by spin-coating SU-8-25 negative photoresist (Microchem, Newton, MA, USA) on glass slides (Corning, Lowell, MA, USA) that had been cleaned in piranha solution (70% sulfuric acid, 30% hydrogen peroxide, 30 min). After pre-baking, exposure, and post-exposure baking, the photoresist layer was developed by gentle agitation in SU-8 developer (Microchem). PDMS in a 10:1 ratio of base to curing agent was poured over the masters, exposed to vacuum to remove air bubbles, and cured at 70°C for at least four hours. PDMS slabs containing the channel features were carefully released from masters, rinsed with distilled water and isopropanol, and sprayed with nitrogen gas before membrane bonding. All microchannels used in experiments were 100 μm high by 800 μm wide.

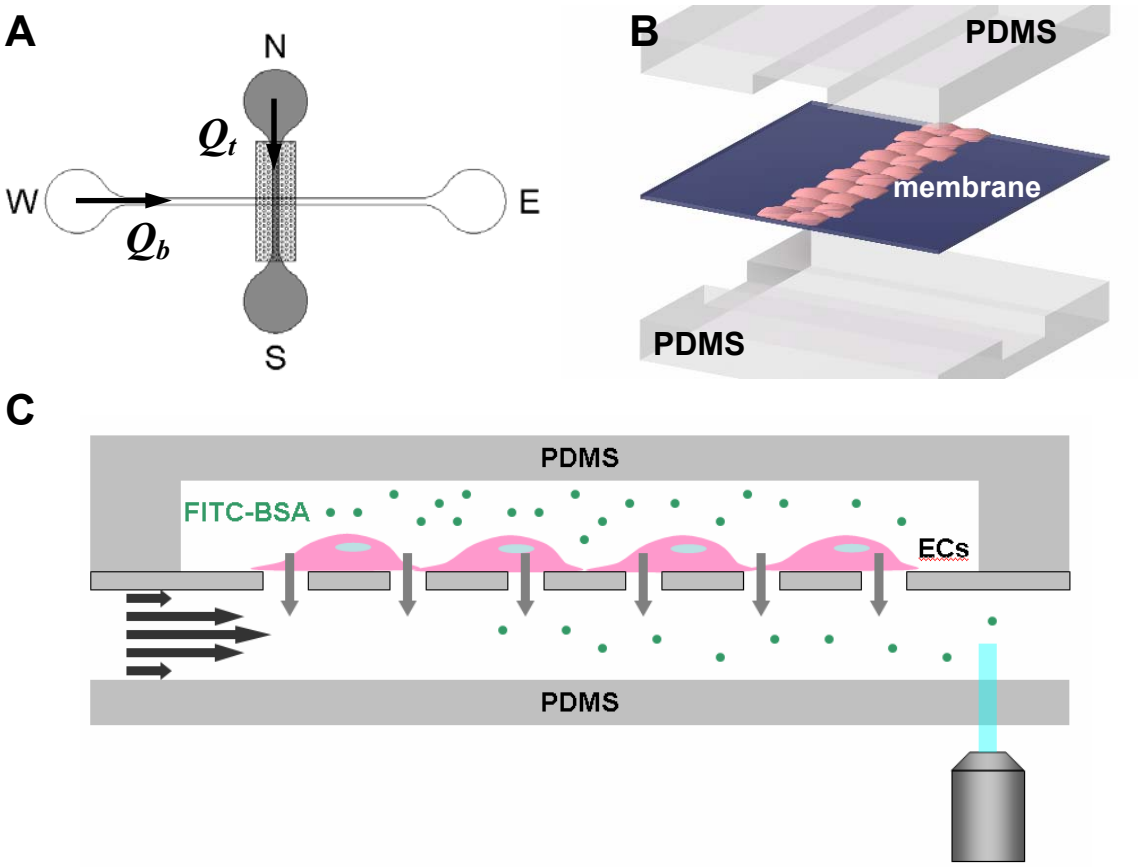

Figure 7.1. Two-layer membrane-based microfluidic system.

(A) Top view of microchannel cross pattern. Polyester membrane (hatched) was sandwiched between top north-south channel (gray) and bottom east-west channel (outline). Top and bottom channel flow rates, Q_t and Q_b respectively, flowed from N to S and W to E. (B) Exploded view of membrane device, consisting of top and bottom patterned PDMS slabs, a membrane between the slabs (blue), and a depiction of endothelial cells grown on the top surface of the membrane (pink). (C) Side view of membrane-separated intersection region. FITC-labelled BSA flowing in the top channel permeated through the endothelial monolayer and membrane into the bottom channel, and was subsequently detected by laser-induced fluorescence downstream of the intersection.

Top and bottom PDMS slabs were bonded to the membrane using the stamping procedure reported by Chueh et al. [119] (Figure 7.2). Briefly, PDMS prepolymer (10:1 ratio of base to curing agent) was mixed with toluene in equal portions, and spin-coated (500 rpm/s ramp for 4 s, 1500 rpm for 60 s) onto a clean glass slide to form a thin PDMS mortar film. Based on the report by Chueh et al., we estimated the mortar layer to be ~2-3 microns thick [119]. PDMS slabs were briefly stamped onto the mortar film (1 min). Membrane edges were gently dipped onto mortar prior to placement at the intersection and bonding of the mortar-coated PDMS slabs. After assembly of the membrane and slabs, the device was placed in an oven at 70°C overnight to cure the mortar. Inlet and outlet ports were inserted to provide connections to top and bottom microchannel reservoirs. See Appendix F for fabrication details.

7.1.2 Cell Isolation and Culture

As before, primary porcine aortic valve endothelial cells (PAVECs) were isolated from fresh pig hearts, and purified using a clonal expansion technique as described previously in Chapter 4. Primary porcine aortic endothelial cells (PAECs) were generously donated by Lowell Langille (University of Toronto). These cells were isolated from porcine thoracic aortas obtained from a local slaughterhouse using an isolation procedure similar to a previously described method [30, 169].

PAVECs were cultured in M199 supplemented with 10% fetal bovine serum (FBS), and 1% penicillin-streptomycin (P-S) (PAVEC media) at 37°C with 5% CO_2. PAECs were cultured similarly using M199 supplemented with 5% FBS, 5% cosmic calf serum (CS), and 1% P-S (PAEC media). Cells were fed every other day, and passaged every 3-4 days. All reported experiments used cells between passages 4 and 7.

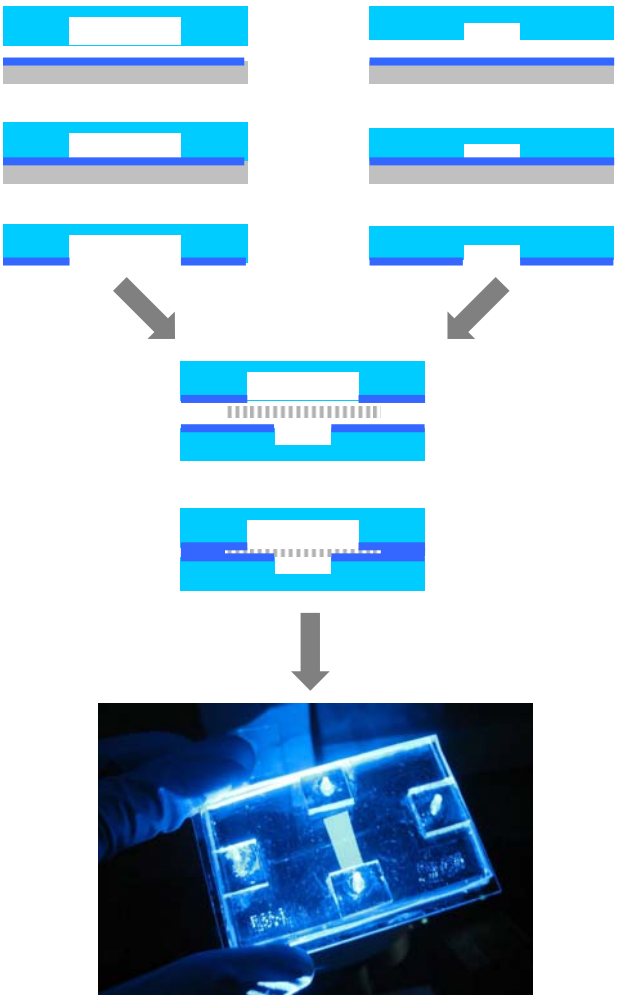

1. Spincoat 1:1 PDMS-toluene on glass
2. Stamp
3. Peel
4. Sandwich the membrane with PDMS slabs
5. Cure at 70 °C overnight
6. Completed device

Figure 7.2. Membrane device fabrication procedure.

(1) Spincoat toluene-PDMS mixture (1:1 volume ratio) onto clean glass slides to form mortar layer. (2) Take cured PDMS slabs containing top and bottom channel features and stamp onto toluene-PDMS mortar. (3) After 1 minute, peel slabs from mortar. (4) Sandwich the membrane between PDMS slabs and (5) cure the device at 70 °C overnight to cure mortar and secure membrane. (6) Photograph of final handheld membrane device.

7.1.3 Cell Adhesion on Membrane

Various membranes were tested to determine the best membrane type for cell adhesion and growth. Cyclopore polycarbonate regular (PC-1), Cyclopore polycarbonate thin clear (PC-2), and Nuclepore polycarbonate (PC-3) track-etched membranes were purchased from Whatman Inc. (Florham Park, NJ, USA) as individual membrane sheets. Polyethylene terephthalate (PET) membranes were obtained by removing the membrane surface from the bottom of cell culture inserts (Becton Dickinson, Mississauga, ON, Canada).

Membranes were trimmed into circular discs of ~ 12 mm diameter (to match the size of a 12 mm diameter coverslip), dipped in 70% ethanol for sterilization, and carefully dried over a small flame. Dried membranes were placed in wells of a 12-well plate, and coated with different matrix proteins for 24 hours. PAVECs were seeded at 7500 cells/cm^2 and cultured for two days prior to fixation with neutral buffered formalin. Media was replaced after the first day of culture to remove unattached cells and replenish nutrients in the media. After fixation, cells were stained with Hoechst nuclear dye and phalloidin (filamentous actin) for cell counting and qualitative assessment of cell spread on the membrane, respectively. PAVECs were chosen as the model cell type for testing adhesion because previous studies suggested PAVECs would adhere more selectively to different substrates and matrix proteins than PAECs (Chapter 5 and [131]). PAVECs grown on 12-mm glass coverslips were used as controls for adhesion tests.

Fluorescent images were captured using a CCD camera (QImaging Retiga, Surrey, BC) connected to an inverted fluorescent microscope (Olympus IX-71). Three random images were taken per sample as representative of the overall coverage of cells on the

membrane, and total number of cells per sample was counted. Three independent samples (n = 3) were analyzed, and the average total cell count was determined.

Two-way analysis of variance (ANOVA) was performed using Microsoft Excel to analyze the effects of membrane type (PC-1, PC-2, PC-3, PET, glass (control)) and protein coating (none, 25 ug/mL FN, 100 ug/mL FN, 100 ug/mL Col-I), or any interaction between the two factors, on total cell count. Since no interaction between factors was found ($P > 0.5$), one-way ANOVAs were performed for each factor to elucidate the main effects. Data was considered statistically significant for $P < 0.05$.

7.1.4 Device Preparation and Cell Seeding

PAECs were cultured directly in membrane-based microfluidic systems for permeability experiments (see Appendix G for details of procedure). Top and bottom microchannels were rinsed successively with ~1 mL of 100% ethanol, ~5 mL of 70% ethanol for sterilization, and ~5 mL of phosphate buffered saline (PBS). Bovine plasma fibronectin (FN) (Sigma-Aldrich Canada) at 100 or 200 μg/mL diluted in supplemented media was injected into the top microchannel and incubated at room temperature for 90 min to allow FN to adsorb onto the membrane surface. PAECs were trypsinized and suspended at a cell density of 0.5 to 4.0 × 10^6 cells/mL. PAECs were seeded into the top channel of the membrane device and allowed to attach to the FN-coated membrane surface during an initial four to six hour static culture stage in an incubator maintained at 37°C with 5% CO_2. Media in the microchannels was replenished by injecting 1 mL of media. Cells were subsequently maintained by perfusing media at 100 uL/hr using a syringe pump for four to five days. Cells

within the microchannels were incubated with 2 μM calcein AM and 4 μM ethidium homodimer-1 for 30 min to distinguish live and dead cells under fluorescence, respectively.

7.1.5 Laser-induced Fluorescence Microscopy Setup

Permeability through membrane and cell layers was measured by flowing fluorescein isothiocyanate-tagged bovine serum albumin (FITC-BSA, 2 μg/mL in buffer unless otherwise noted) into the top channel, and allowing FITC-BSA to pass through the membrane to the bottom channel where it was mixed with a flowing buffer stream. M199 basal medium with 0.1% (w/v) Pluronic F68 (Sigma-Aldrich Canada) was used as buffer for all experiments. Top and bottom channel inlet ports were connected to syringe pumps (Harvard Apparatus, Holliston, MA, USA) via polyethylene tubing. Laser induced fluorescence (LIF) was used to detect FITC-BSA in the bottom channel (Figure 7.3). The 488-nm line of an argon ion laser (Melles Griot, Carlsbad, CA) was focused downstream of the membrane on the bottom channel using a 10X objective on an inverted microscope (Olympus IX-71). Fluorescence was captured by the same objective, filtered both optically (536/40-nm band pass and 488-nm notch filter) and spatially (500 μm pinhole), and imaged onto a photomultiplier tube (PMT, Hammamatsu, Bridgewater, NJ). PMT current was converted to voltage by a picoammeter (Keithley Instruments, Cleveland, OH) and analog-to-digital conversion was performed by a data acquisition pad (National Instruments, Austin, TX) linked to a computer running custom acquisition software in LabVIEW (National Instruments).

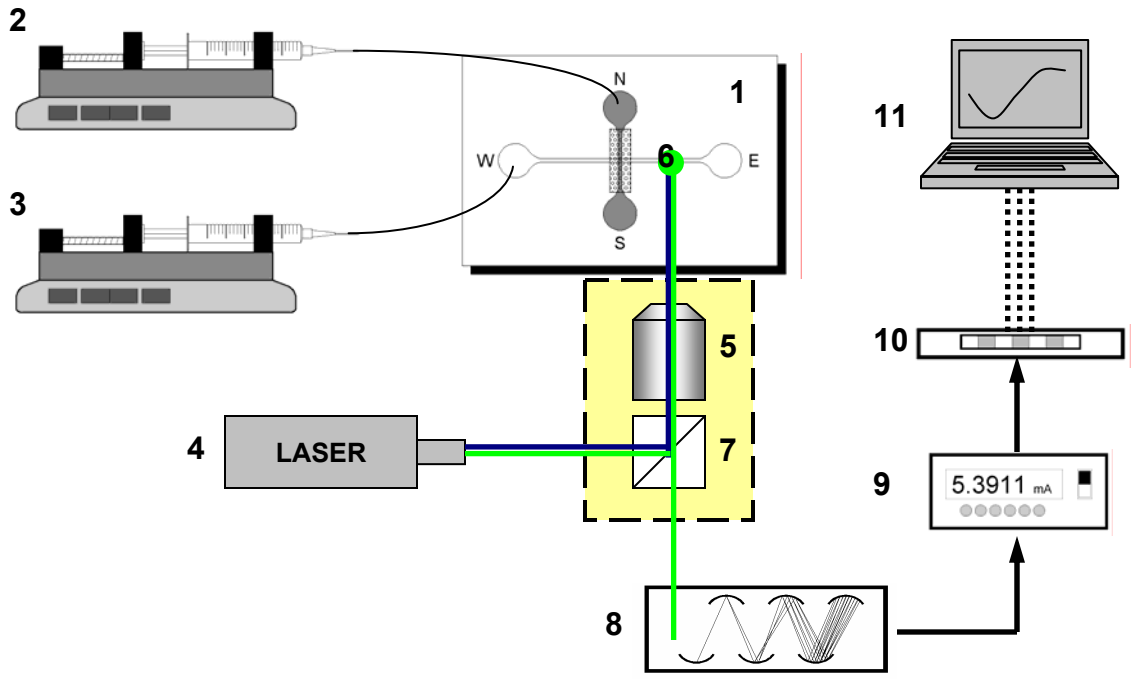

Figure 7.3. Experimental setup for endothelial permeability measurement using laser-induced fluorescence.

Sample and buffer solutions were driven through the top and bottom microchannels of the device (1) using two separate syringe pumps (2,3). A 488-nm line from an argon ion laser (4) passed through a microscope objective (5) and focused on a location in the bottom channel, downstream of the intersection (6). Fluorescence was captured by the same objective and filtered through a dichroic mirror (7) onto a photomultiplier tube (PMT) (8). PMT current was converted to voltage by a picoammeter, converted to a digital signal by a data acquisition card (10), and displayed on a computer running custom acquisition software in LabVIEW (11). Dotted line represents components within the inverted microscope.

7.1.6 Permeability using LIF Detection

The measured inline fluorescence intensity at the point of optical detection was determined by (1) treating the track-etched membrane as a thin porous medium with straight cylindrical pores, (2) solving Darcy's law for porous media flow, and (3) calculating the volume fraction of fluorescent solution (top channel) mixing with buffer solution (bottom channel). Darcy's law predicts that the superficial velocity (i.e., the permeate flux per unit area), v_s, is governed by [170]:

$$v_s = -\frac{k}{\mu}\frac{dp}{dz} = \frac{k}{\mu}\frac{\Delta p_T}{\Delta z} \tag{7.1}$$

where k is the permeability coefficient in (m^2), μ is the dynamic viscosity of the fluid in ($N \cdot s/m^2$), and dp/dz is the pressure gradient across the membrane in (N/m^3).

The pressure gradient is represented by the transmembrane pressure drop Δp_T across the thickness of the membrane Δz. In the cylindrical pore model [170], all pores are considered as straight cylinders of radius r (Figure 7.4). For a porous section with n pores per unit area, and a flow rate q_i through a single pore, v_s is found to be:

$$v_s = nq_i = \frac{n\pi r^4}{8\mu}\frac{dp}{dz} \tag{7.2}$$

Permeability coefficient k is then equivalent to:

$$k = \frac{n\pi r^4}{8} \tag{7.3}$$

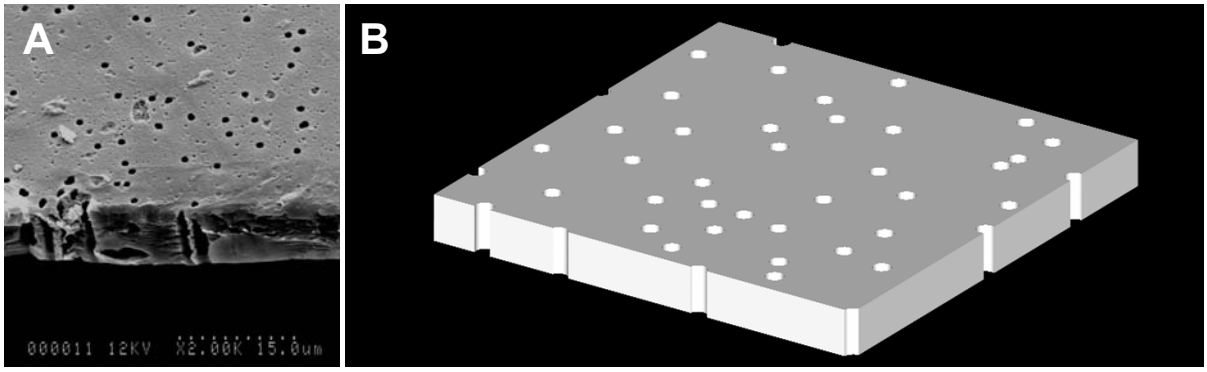

Figure 7.4. PET membrane characterization.

(A) Scanning electron micrograph of PET membrane verifying that pores are 1 μm in diameter and membrane thickness is 10 μm. (B) Cylindrical pore model treats all pores as straight cylinders in a porous media.

To determine the permeability coefficient k experimentally using the LIF setup, a combination of Darcy's law and mixing principles were employed. Transmembrane pressure was calculated by determining the pressure at the half-length of both top and bottom microchannels,

$$\Delta p_T = p_t - p_b = \frac{6\mu}{h^2}\left(L_t v_t - L_b v_b\right) \tag{7.4}$$

where v_t and v_b are the average fluid velocities of the top and bottom channels; L_t and L_b are the top and bottom channel lengths; and p_t and p_b are the top and bottom channel half-length pressures, respectively. Substituting Eq. (7.4) into Eq. (7.1), and rearranging yields the following equation for k:

$$k = \frac{v_s h^2 \Delta z}{6\left(L_t v_t - L_b v_b\right)} \tag{7.5}$$

The superficial velocity v_s is determined by considering the amount of fluorescent material permeating and mixing with the flowing buffer in the bottom channel. If concentration of FITC-BSA in the top channel is considered the maximum fluorescence intensity in the system (C_{MAX}), the concentration of FITC-BSA permeated through the membrane ($C_{membrane}$) and mixed into the buffer stream must be a fraction of the maximum, in a ratio that involves the volume of permeate from the top channel and the total volume of permeate plus buffer being mixed in the bottom channel:

$$\overline{C} = \frac{C_{membrane}}{C_{MAX}} = \frac{v_s w}{v_s w + v_b h} \tag{7.6}$$

Substituting Eq. (7.6) into Eq. (7.5) yields a closed-form solution for k:

$$k = \frac{1}{6}\left[\frac{\overline{C}}{1-\overline{C}}\right]\left[\frac{h^3 \Delta z}{w}\right]\left[\frac{v_b}{L_t v_t - L_b v_b}\right] \tag{7.7}$$

Thus, permeability can be explicitly determined in real-time by simply multiplying parameters of microchannel and membrane geometry, chosen flow rates, and detected fluorescent intensities (represented by normalized concentration values).

7.2 Results

7.2.1 Cell Adhesion on Membranes

Membranes were tested for cell adhesion and growth by culturing PAVECs on protein-coated or non-coated surfaces and counting the number of total viable cells on representative images. Cells were cultured for two days on these surfaces in wells to allow enough time for cells to proliferate after attachment. After fixation, cells were stained with Hoechst nuclear dye to label the nuclei for cell counting, and phalloidin to label the filamentous actin stress fibres for qualitative assessment of overall cell spreading. PAVECs did not attach well to any of the polycarbonate membranes, especially when little or no protein was used (Figure 7.5). For 100 μg/mL FN or Col-I, PAVECs attached and spread only minimally, with only a small area covered by cells. Cell shape on these membranes was also not indicative of typical EC cultures having polygonal cell bodies and cobblestone morphology. On the other hand, PAVECs displayed adhesion and growth on PET membranes for all protein-coated surfaces similar to that seen on glass coverslips. Even without protein coating, cells attached to the membrane and formed EC islands. With 100 μg/mL FN, PAVECs covered large regions of the membrane and reached full confluence in these areas, similar to glass. ANOVA showed no statistical difference between cells grown on PET membrane and glass ($P > 0.5$), but a significant difference between cells grown on PET and polycarbonate membranes ($P < 0.01$, main effect) (Figure 7.6). Thus, we chose PET membranes for all subsequent experimentation involving cell culture on membranes.

Interestingly, PAVECs adhered and grew less on 100 μg/mL Col-I than on 100 μg/mL FN for both glass and PET membranes. This is consistent with previous reports of PAVEC spreading and adhesion where it was found that these cells spread more and adhere more strongly to FN than Col-I (Chapter 5 and [131]).

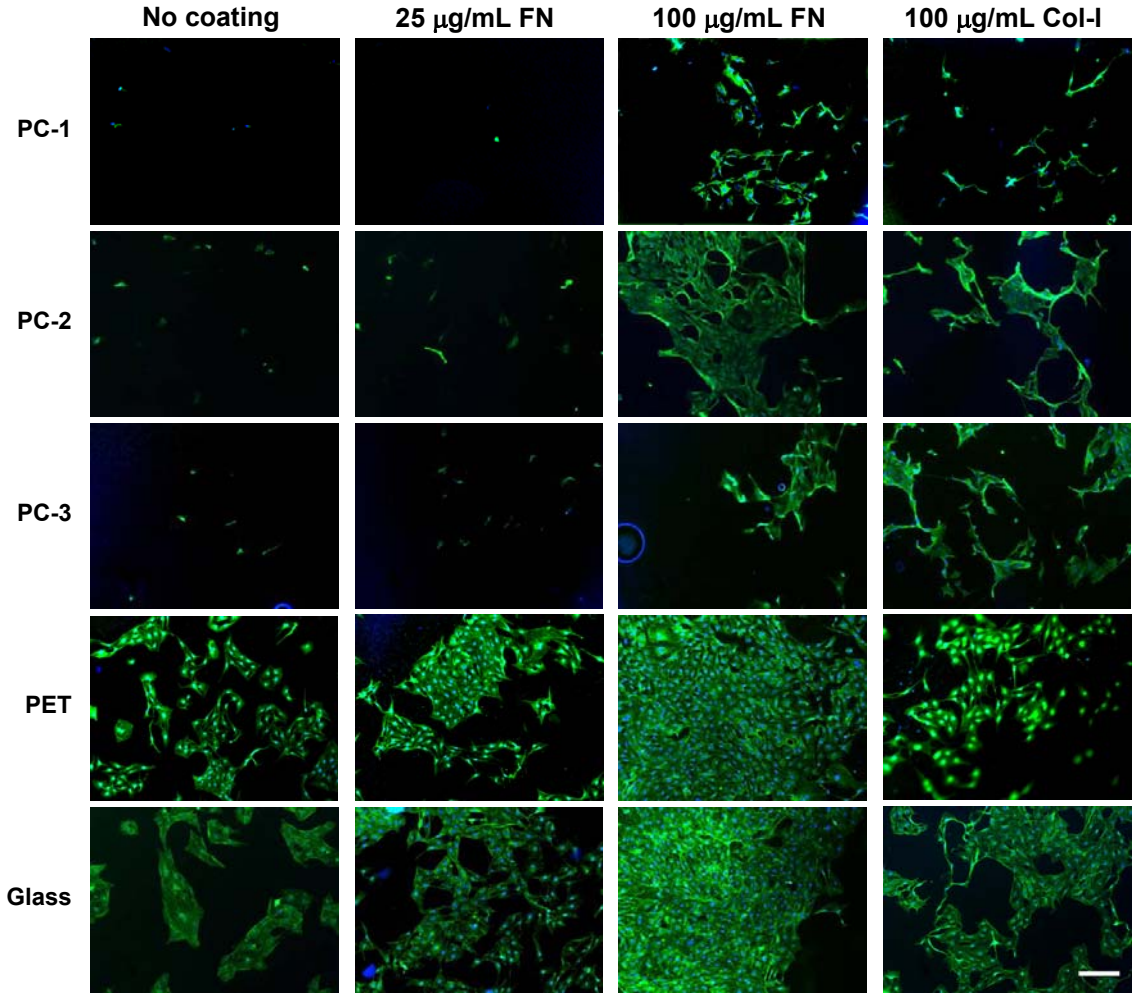

Figure 7.5. Phalloidin-stained images of PAVECs on protein-coated membranes.

Phalloidin-stained (green) PAVECs after 24 hours of static culture on protein-coated membranes. Glass was used as positive control. PET membranes promoted adhesion and growth similar to glass, and yielded the most confluent monolayers among all membranes tested. Scalebar = 200 μm (bottom right).

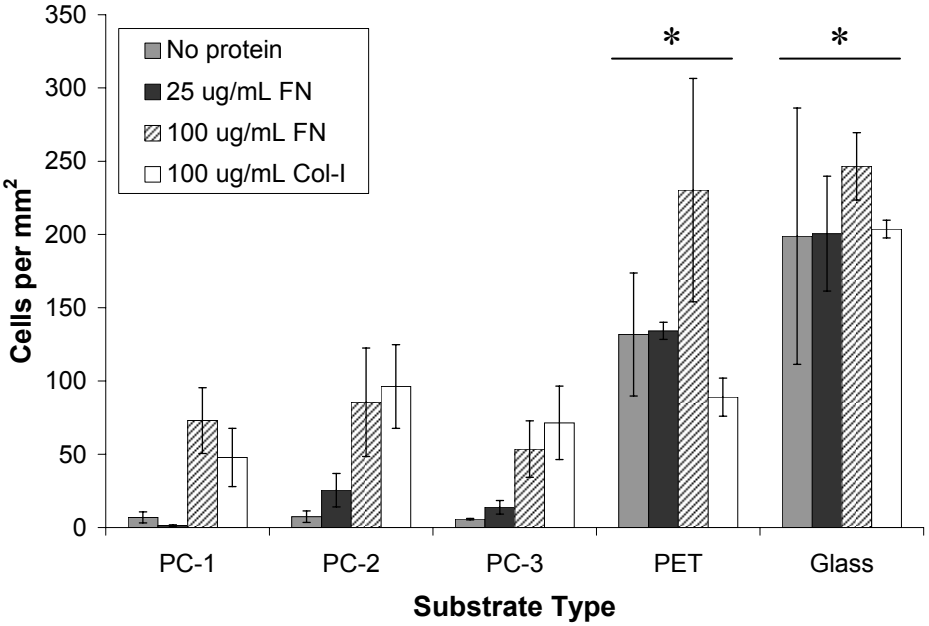

Figure 7.6. PAVEC adhesion on protein-coated membranes.

Cell counts per unit area for different protein-coated substrates. PET membrane and glass slides yielded highest numbers of adhered cells. Statistical significance (* $P < 0.01$) was detected between PET membrane and glass to all other membrane substrates.

7.2.2 Device Characterization

To ensure proper device operation during permeability tests, fluorescent video microscopy (Olympus IX-71) was used to test membrane reliability and fidelity (Figure 7.7). Top and bottom microchannels were first filled with 10 mM PBS with 0.05% (w/v) Pluronic F-68 (buffer) to prime the device. FITC-BSA (2 μg/mL in buffer) was manually injected into the top channel via syringe and allowed to permeate the membrane at the channel intersection. Permeation was a result of positive transmembrane pressure generated by flow in the top channel with no flow in the bottom channel. After less than a minute of permeation and noticeable accumulation of FITC-BSA in the bottom channel, flow was switched such that buffer was injected into the bottom channel while flow was ceased in the top channel. The accumulated dye molecules washed downstream as expected.

Furthermore, because of the switch in flows, transmembrane pressure from bottom to top channel resulted in permeation of buffer through the membrane into the top channel. This washed away FITC-BSA in the top channel in both the upstream and downstream directions from the intersection.

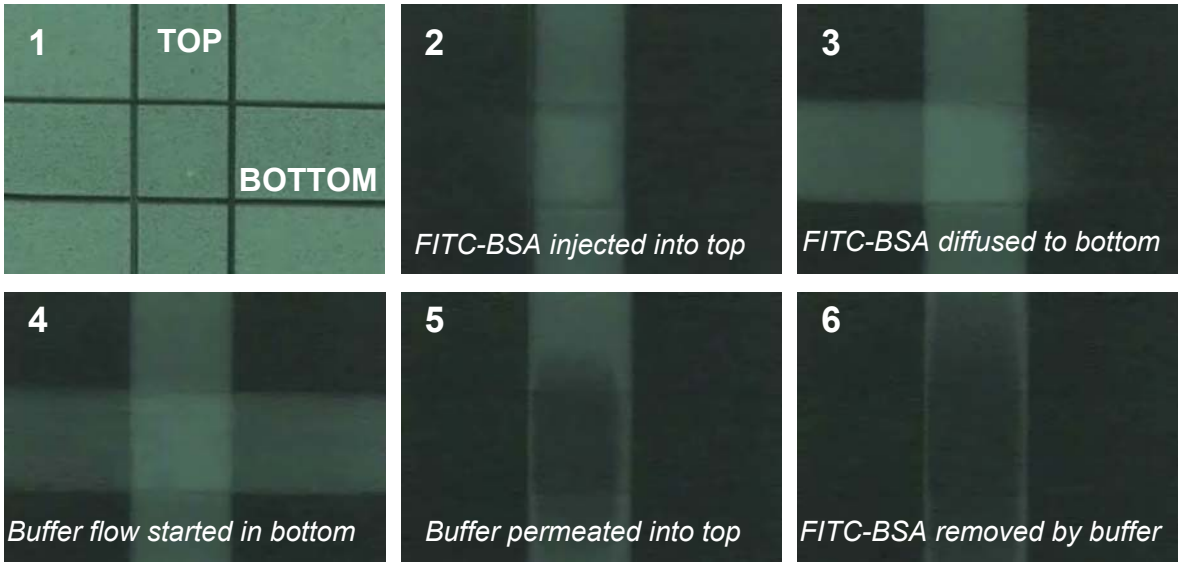

Figure 7.7. Fluorescent video microscopy demonstrating membrane operation.
(1) Phase contrast image of intersection. (2) FITC-BSA injected into top channel. (3) FITC-BSA permeated into bottom channel. (4) Flow switched to buffer flowing in bottom channel to wash permeated BSA downstream of intersection. (5) Buffer permeated membrane and (6) removed BSA in top channel.

7.2.3 Viability of Cultured Cells

Cells seeded and cultured in membrane microfluidic devices were perfused at flow rates of 100 μL/hr, which generated an average shear stress of ~0.15 dyn/cm^2, insignificant to detach cells or induce shear-related responses. Cells were monitored for viability and proliferation by calcein AM/ethidium homodimer-1 staining every 24 hours. Cells attached, spread, and proliferated to near confluence over 4-5 days of culture. Cells were 100% viable under these conditions for the duration of culture (Figure 7.8).

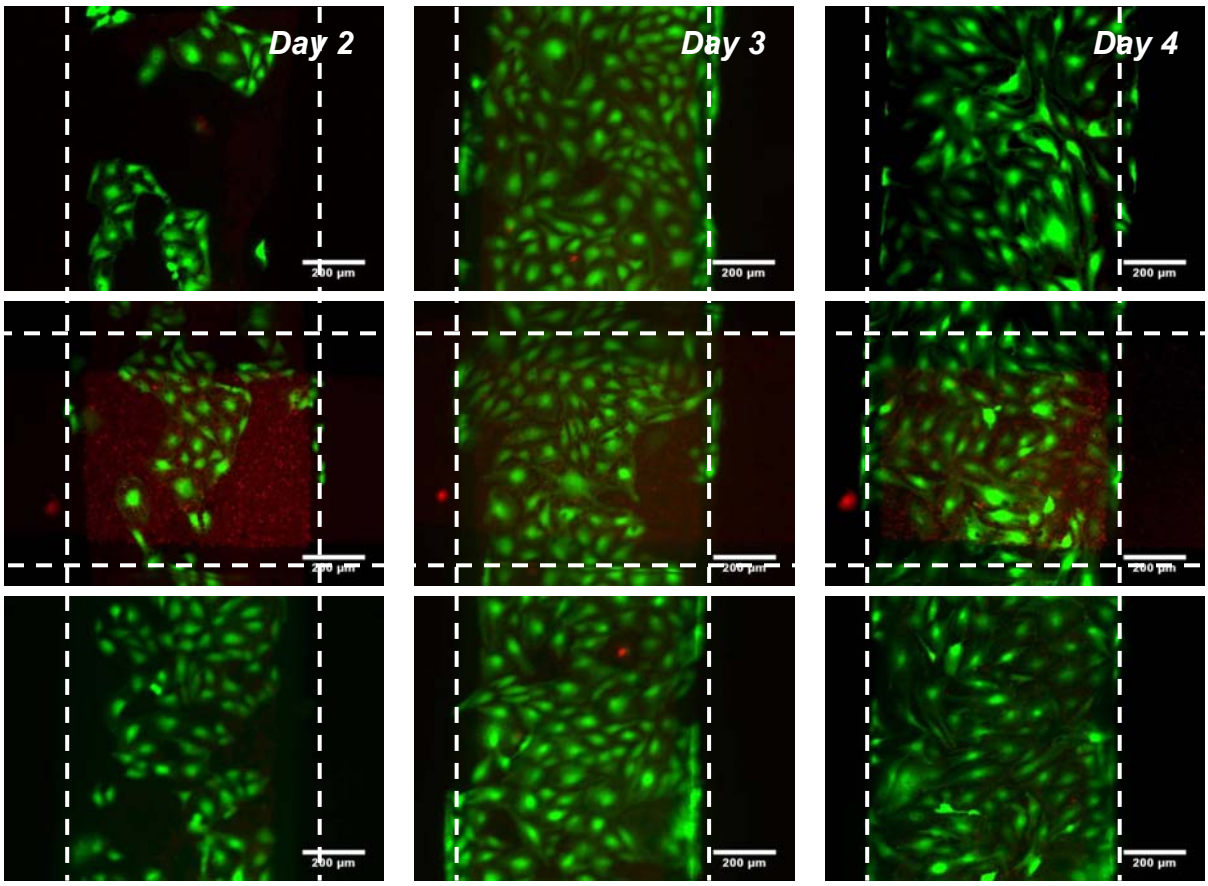

Figure 7.8. Calcein AM/ethidium homodimer-1 staining of live PAECs during perfusion culture.

Cells cultured by perfusion formed endothelial islands by day 2, reached 90% confluence by day 3, and confluence by day 4, with some regions lacking cell-cell contacts. Calcien AM (green) and ethidium homodimer (red). Dotted white lines delineate top and bottom channel walls. Top row = upstream of intersection. Middle row = intersection. Bottom row = downstream of intersection. Scalebar = 200 µm.

7.2.4 Permeability Measurements

Real-time permeability was measured using LIF detection, and calculated by applying a mixing model to translate measured fluorescence intensity into permeability coefficients via Darcy's law. A typical experiment involved flowing FITC-BSA into the top microchannel at a constant flow rate, and flowing buffer into the bottom microchannel over a range of flow rates in a stepwise manner (Figure 7.9). As bottom channel flow rate (Q_b) was

adjusted, measured fluorescence intensity changed to reflect corresponding changes in transmembrane pressure that led to differences in the amount of permeating FITC-BSA.

Each experimental run started with an injection (via syringe) of FITC-BSA into both top and bottom microchannels. For normalization purposes, fluorescence of this solution was measured at the detection point to establish maximum fluorescence for a particular run (t = 0-2.5 min of Figure 7.9). This corresponded to $\overline{C} = 1$ for v_b = 0 μL/min in Eq. (7.6). To measure background fluorescence, top and bottom channel flow rates were chosen to yield zero transmembrane pressure, which corresponded to no flow through membrane, or v_s = 0 by Eq. (7.1). For example, because L_t = 25 mm and L_b = 50 mm for our devices, the combination of v_t = 400 μL/min and v_b = 200 μL/min yielded zero transmembrane pressure according to Eq. (7.4) (non-zero but negligible transmembrane pressure in practice). This was captured in Figure 7.9 as the baseline fluorescence at time t = 3 min to 4.5 min where v_b = 200 μL/min yielded the lowest detectable fluorescence. Using these measurements as maximum and minimum markers for each run, we normalized all intensities to fall between $\overline{C} = 0$ and $\overline{C} = 1$.

Figure 7.9 also shows typical readings from LIF detection during the stepwise procedure where bottom channel flow rates were adjusted. As flow rates were changed (e.g., from 100 to 1 μL/min at t = 18 min, from 1 to 2 μL/min at t = 20 min, and from 2 to 5 μL/min at t = 23 min), detected fluorescence intensities changed accordingly through a transient stage before reaching a plateau region. At higher bottom channel flow rates, the transient stage was shorter in time. A 30-second average of an arbitrarily-chosen portion of the plateau region was taken as the representative intensity measurement at that flow rate (blue lines in Figure 7.9). Multiple cycles of the stepwise procedure with good repeatability

are possible during one experiment depending on the volume of syringes used. Figure 7.9 displays the second cycle of a two-cycle run, where the first cycle from t = 4.5 min to t = 16.5 min was truncated for clarity. As bottom channel flow rate increased, detected fluorescence intensity decreased. This was expected from Eq. (7.6) since higher v_b meant the permeated molecules were more diluted by the time it reached the detection point.

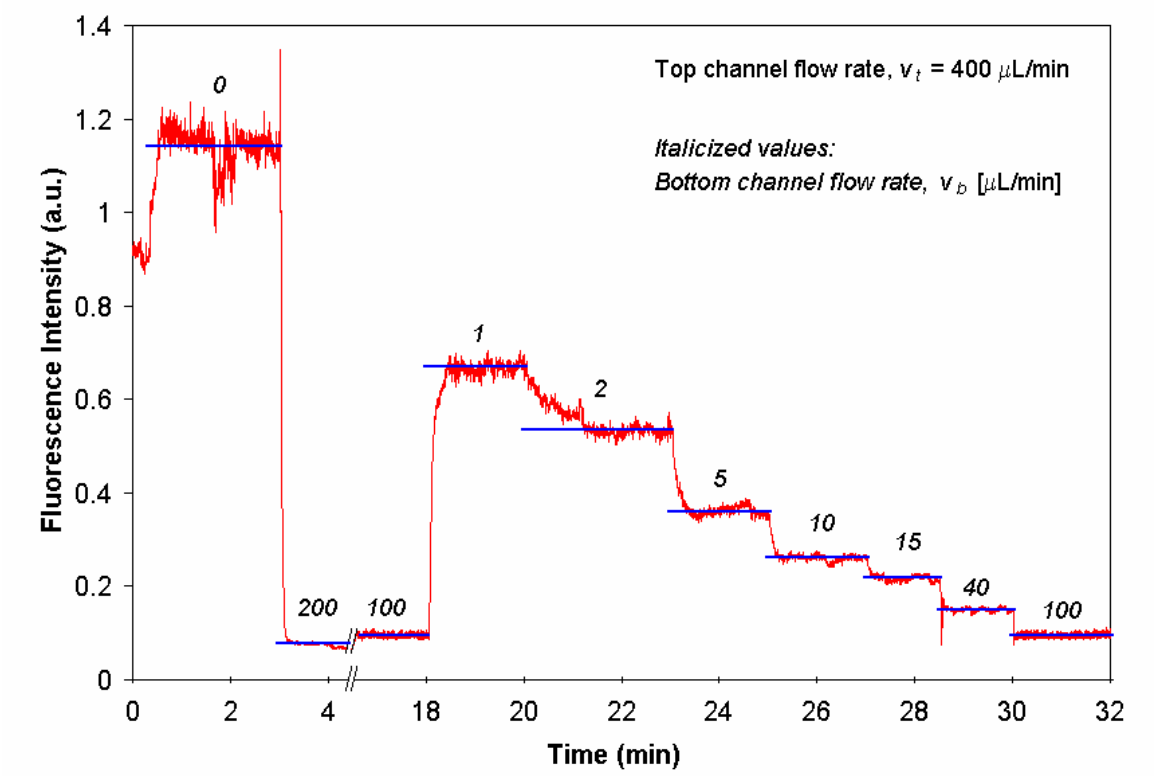

Figure 7.9. Fluorescence intensity versus time curve.

A typical real-time fluorescence intensity curve for predicting albumin permeability was generated via LIF detection at a prescribed location downstream of the intersection. Top channel flow rate was held constant (v_t = 400 μL/min) while bottom channel flow rate was ramped (v_b = 0 to 200 μL/min, italicized numbers) to create a stepwise curve. Blue lines represent average fluorescence values in the plateau region for each step. The length of the blue line represents the length of time in which the particular flow rate was applied.

Averaged fluorescence intensity measurements at plateau regions were normalized to maximum fluorescence intensity and plotted versus flow rate ratio, defined as $R = Q_t/Q_b$ (Figure 7.10). R can be considered simply as a replacement variable for bottom channel flow rate because Q_t is constant in the devised procedure. A curve-fitting procedure using Darcy's law and the mixing model (Eqs. (7.1) and (7.6)) was employed to extract a predicted permeability coefficient k from the experimental curve. Specifically, a theoretical value k_0 was guessed to produce superficial velocities and normalized concentrations at each data point on the curve (for each of n tested flow rate ratios), based on k_0, i.e.

$$v_{s,i} = \frac{k_0}{\mu}\frac{(\Delta p_T)_i}{\Delta z},\ i = 1, 2, \ldots, n \tag{7.8}$$

and

$$\overline{C}_{t,i} = \frac{v_{s,i} w}{v_{s,i} w + v_{b,i} h},\ i = 1, 2, \ldots, n \tag{7.9}$$

where $v_{s,i}$, $(\Delta p_T)_i$, $v_{b,i}$, and $\overline{C}_{t,i}$ were the superficial velocity, transmembrane pressure, bottom channel flow rate, and normalized concentrations for the i^{th} of n flow rate ratios. The theoretical value $\overline{C}_{t,i}$ from Eq. (7.9) was then compared to normalized fluorescence intensities from experiment, $\overline{C}_{e,i}$, at each flow rate ratio R_i, and a sum of squares of differences, $S(k_0)$, was determined by

$$S(k_0) = \sum_i \left(\overline{C}_{t,i} - \overline{C}_{e,i}\right)^2 \tag{7.10}$$

The k_0 value that yielded the minimum of $S(k_0)$ was considered the experimental permeability coefficient.

Figure 7.10 shows representative curves of normalized fluorescence intensities versus flow rate ratio for three experimental cases: (1) for the 1-μm pore size PET membrane alone (red line), (2) for PET membrane coated with 200 μg/mL FN (blue line); and (3) for fixed PAECs grown to confluence on FN-coated membrane (black line). All three curves showed trends that reflected those of the time curves, where increasing bottom channel flow rate (or decreasing R) led to decreasing fluorescence intensity. For a given flow rate ratio, the membrane alone was the most permeable (highest fluorescence intensity), followed by the FN-coated membrane, and the PAECs on FN-coated membrane (lowest fluorescence intensity), as expected. A theoretical curve was also plotted for the membrane alone, based on the cylindrical pore model of Eq. (7.2) (blacked dashed line of Figure 7.10). The theoretical curve matched the trend of the experimental measurements, but was found to lie between the experimental curves for membrane alone and FN-coated membrane. Dotted lines represent curve fits that led to predicted permeability coefficients for each of the experimental curves.

Permeability coefficients from curve fits were summarized and compared to several related results from the literature (Table 7.1). These other studies reported permeability coefficients as hydraulic conductivity L_p,

$$L_p = \frac{J_v}{S\Delta P} \tag{7.11}$$

where J_v was volume flux (cm^3/s), S was membrane surface area at intersection (cm^2), and ΔP was transmembrane pressure (cm H_2O), such that L_p had units ($cm \cdot s^{-1} \cdot cmH_2O^{-1}$). L_p is closely related to k, and this is apparent from rearranging Darcy's law to be:

$$\frac{k}{\mu \Delta z} = \frac{v_s}{\Delta P_T} \tag{7.12}$$

Since $v_s = J_v/S$,

$$L_p = \frac{k}{\mu \Delta z} \tag{7.13}$$

Thus, for the same fluid viscosity (μ= 0.001 N·s/m^2 for aqueous solutions at room temperature) and same membrane thickness Δz, L_p and k are interchangeable.

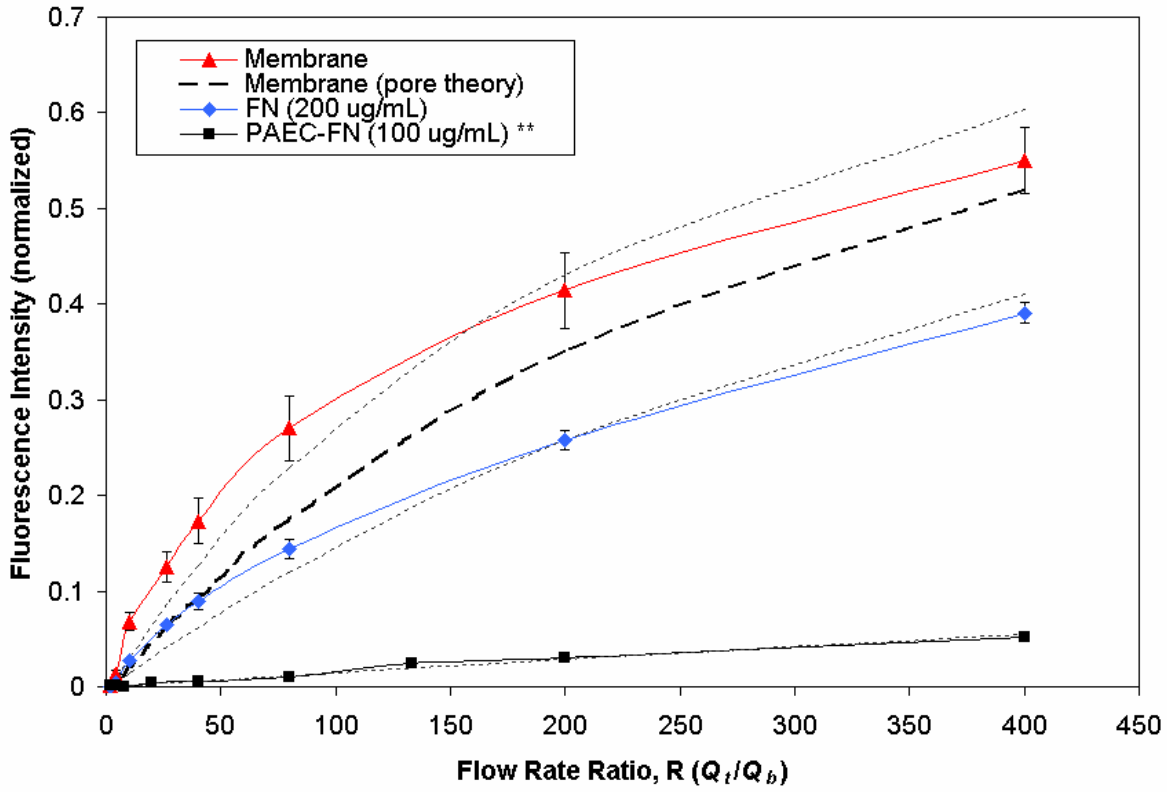

Figure 7.10. Normalized fluorescence intensity versus flow rate ratio.

Fluorescence intensity decreased with lower flow rate ratio (or higher Q_b). Membrane alone (red), FN-coated membrane (blue), and PAECs grown on FN-coated membrane (black solid). Theoretical curve for the membrane alone, using cylindrical pore model (black dashed), was found to lie between results from membrane alone and FN-coated membrane. Dotted lines are curve fits through experimental curves. Each curve represents results from one device. Error bars = SE; $n \geq 3$ measured plateau regions for each flow rate ratio. ** PAEC-FN data for n = 1 only.

PAECs grown on FN were exposed to shear of 25 dyn/cm^2. The various reports from literature were for permeability tests on ECs with and without shear. Comparisons show that our results for fixed PAECs grown on FN were approximately one order of magnitude higher than results for both fixed pulmonary artery ECs [171], as well as for live bovine aortic ECs (BAECs) after five hours of thrombin induction [85]. Permeability with cells was also one order of magnitude lower than without cells (FN-coated membrane). These results suggest that our method produces reasonable permeability values for sheared ECs, but more validations are needed to corroborate data between our system and others reported in the literature.

Table 7.1. Predicted permeability coefficients for experiments, compared to literature.

Case	***Permeability Coefficient, k*** (nm^2)	***Hydraulic Conductivity, Lp*** (10^{-6} $cm \cdot s^{-1} \cdot cmH_2O^{-1}$)
Membrane only, cylindrical pore model (dashed line)	393	---
Membrane only, experiment (red line)	550	---
Membrane + 200 ug/mL FN (blue line)	252	---
Membrane + 100 ug/mL FN + fixed PAECs, shear of 25 dyn/cm^2 (black solid line)	**21.1**	**20.6**
Membrane (PC) + gelatin + fixed pulmonary artery ECs, no shear (Turner, 1992)[171]	---	1.1
Membrane (PC) + gelatin + FN + live BAECs, no shear, thrombin added for 5 hrs (Sill, 1995)[85]	---	2.4
Membrane (PC) + gelatin + FN + live BAECs, shear of 10 dyn/cm^2, no thrombin (Sill, 1995)[85]	---	0.7

7.3 Discussion

Permeability is an important EC property that has been studied extensively for fundamental research as well as for pharmaceutical applications. Current experimental methods for measuring permeability involve testing endothelial barrier function through either static culture in well inserts, which lack the element of shear, or in large-scale shear flow systems that incorporate shear stress effects into experimental protocols, but are not practical for high-throughput studies. Microfluidics offers a potential solution: channel geometries are naturally suited for shear flow, and high-throughput experiments are possible via parallelized microfluidic networks. We designed, fabricated, and implemented a microfluidic membrane device for measuring permeability of endothelial monolayers, and performed cell-based and control experiments to validate the system. We found that the system performed as expected for control tests, but more experiments were needed to validate data from our work with those from existing literature.

Permeability of fixed ECs has been studied in the past to investigate the sealing effect of endothelial monolayers [84, 85, 171]. The sealing effect is a phenomenon where permeability decreases when a monolayer is exposed to a hydrostatic pressure gradient. These past reports discovered that sealing occurred for both fixed and unfixed cells, suggesting that the effect was not dependent on biological activity, but was instead a result of mechanical deformations in the monolayer leading to changes in volume flux through fluid passages. Preliminary work here was performed with fixed ECs partly to validate our microfluidic system with observations of the sealing phenomenon, as well as to avoid practical challenges inherent in live cell experimentation. With proper setup, such as the

addition of a temperature-controlled enclosure (Section 6.1.2.3), live cell studies can be performed without difficulty, and will likely be the focus of future work.

Permeability coefficients were one order of magnitude higher than reported hydraulic conductivity values. The most likely cause of this discrepancy was damage to the endothelial monolayer during sheared permeability testing. Non-confluent EC regions of the microchannel intersection were noticeable via fluorescence microscopy of immunostained cells after the experiment. The damage on the monolayer was likely more significant than the leaky junctions observed by Sill and co-workers [85], who noticed significant increase in permeability after five hours of thrombin induction, but still reported hydraulic conductivity lower than data obtained here (see Table 7.1). To ensure monolayer integrity before and after experimentation, it would be beneficial to stain fixed cells for cell-cell junctions (such as VE-cadherin for adherens junctions and occludin for tight junctions) to ensure intercellular connections were intact before and after experimentation.

The cylindrical pore model was a first-order approximation of the theoretical permeability expected through the membrane. Although the model was able to predict the same monotonic increase in permeability with increasing R, it underestimated the measured permeability value by approximately 28%. This discrepancy can be attributed to the simplicity of the model, and its inability to account for boundary layer effects on the membrane surface as a result of shear flow. Neeves and Diamond recently reported the use of a similar Darcy's law model to describe flux of ADP through a membrane device, and showed that boundary layer thickness due to shear flow in top and bottom channels were dependent on shear rate [165]. Tangential velocity across the membrane coupled with the presence of the boundary layer would render the two-dimensional Darcy's law model

inadequate for accurate predictions of permeability. Improvements to the model can be made, however, by accounting for boundary layer and other secondary effects through well documented filtration models in membrane theory [172].

Fouling of the membranes and PDMS surfaces were observed in preliminary testing due to surface adsorption of BSA. BSA is commonly used as a blocking agent to prevent undesirable non-specific binding of test proteins to hydrophobic surfaces, and is effective because of its own hydrophobic nature. However, fouling of labelled BSA in permeability tests would compromise the accuracy of the fluorescence intensity measurements because accumulating surface-bound BSA molecules would increase detected intensities of flowing analytes. To reduce fouling, Pluronic F68 was added to both buffer and FITC-BSA solutions. Pluronic additives were previously shown to reduce fouling of digital microfluidic devices with Teflon surfaces [173]. When 0.1% (w/v) Pluronic F68 was added to the flowing solutions in our experiments, fouling was eliminated on PDMS surfaces, and significantly reduced on PET membranes. To ensure Pluronic F68 was not toxic to ECs, PAECs were grown on tissue culture-treated polystyrene and cultured with 0.1% (w/v) Pluronic F68 added to supplemented M199 media (Section 5.1.2). PAECs remained viable for up to a week, with no noticeable changes in morphology. Thus, Pluronic F68 was used in all subsequent experiments, including for those reported in this chapter.

PET membranes were selected for this work because we demonstrated good adhesion and proliferation of ECs on these surfaces. However, during perfusion culture of ECs within microchannels, specific regions sometimes remained non-confluent. One reason may be non-uniformity during cell seeding, leaving small regions devoid of cells even as other regions have reached confluence. Another possible reason is non-uniformity of the FN

coating, in which case uniform seeding would have led to complete coverage of the surface, except that regions without FN did not allow initial attachment and spreading of cells, thus leaving these regions bare. Immunostaining of FN-coated surfaces in our work have shown evidence of non-uniform protein coatings. The advantage of using PET membranes, however, is the option to provide surface modifications to enhance protein adsorption. One report has shown that PET can be modified using 3-aminopropyltriethoxysilane (APTES) in conjunction with glutaraldehyde (GA) to provide an aldehyde group for covalent bonding with amine groups of proteins [174]. APTES-GA chemistry has previously been used to immobilize proteins via this imine linkage [175], and presumably this surface modification would allow for uniform immobilization of FN on our membranes to improve uniformity of endothelial proliferation.

Microchannels of 120-μm depth and 800-μm width were judiciously chosen to produce appropriate shear stresses over the range of practical flow rates, and to provide enough surface area for cell growth and enough volume for microscale culture. Shear stresses ranging from 1 to 100 dyn/cm^2 can be applied using flow rates from 16 to 1600 μl/min, well within the limits of the syringe pump. Depending on application, microchannel sizes can be easily modified to accommodate other experimental parameters of interest because of the convenience of soft lithography. In view of our results from Chapter 6, however, aspect ratios must be selected with caution to ensure cell monolayers are exhibiting normal behaviours in morphology and function.

In summary, the membrane-based microfluidic device appears to be suitable for endothelial permeability measurements based on validations from cell-based and control experiments. The device is flexible to the needs of the researcher because modifications can

be made to channel dimensions via soft lithography, and to the membrane surface via advanced surface chemistry. Live cells can be exposed to appropriate shear stresses, and throughput can be significantly increased with parallelization. However, more research is needed, with fixed and unfixed cells, to fully characterize the potential of this device.

Chapter 8

8 Conclusions and Recommendations

Microfluidic devices were designed, fabricated, and implemented for a series of investigations involving ECs. Of particular interest were ECs from the aorta and the aortic valve. Using simple microchannel designs, we (1) revealed previously unknown phenotypic differences between the two cell types, (2) discovered interesting phenomena in microchannels that may have important implications on future research directions, and (3) introduced a new application of microfluidics using established fabrication techniques. In the end, devices were employed for not only the current studies, but for other collaborative investigations as well, and this served as evidence that accessible microfluidic designs can have an impact on the cell biology community, if designed with the end user in mind.

Valve ECs were of interest to our current studies, so it was imperative to first obtain pure populations of these cells for proper experimentation. Isolation methods were optimized and two different purification procedures were tested for efficiency and economy.

In the end, the clonal expansion method proved to be the method of choice for producing pure populations of valve ECs.

With valve ECs and aortic ECs at our disposal, we studied their adhesion strength and cell spreading characteristics on various ECM proteins using a parallel microfluidic network. We found aortic ECs adhered strongly and spread well on both high coating concentrations of FN and Col-I, but valve ECs only adhered strongly and spread well on high concentrations of FN. The number of experimental conditions tested was substantial, but the use of microfluidic channels in parallel streamlined experimentation.

Valve and aortic ECs were further tested under shear flow, using macro- and microscale flow systems. Macroscale experiments with valve ECs grown on FN showed parallel alignment of cells with the direction of flow, in contrast to previous reports that observed perpendicular alignment of valve ECs on Col-I. The differences in morphological response were partially attributed to the ECM protein on which the cells were grown, and this was supported by a similar pattern of differential adherence. Interestingly, microscale experiments showed PAECs that aligned perpendicular to flow when sheared in microchannels. This phenomenon was observed on separate occasions, as evidenced by immunostaining and live-cell video microscopy. We speculated that perpendicular alignment of PAECs was a combination of a migratory response induced by shear stress gradients and a tendency for cells to elongate in the direction of migration. More research is necessary to test this hypothesis.

Finally, a microfluidic membrane device was designed and characterized for its potential use in measuring albumin permeability through endothelial monolayers. Using laser-induced fluorescence, we demonstrated detection of fluorescently-labelled albumin

molecules through a track-etched membrane sandwiched between PDMS channel layers. Permeability values were determined by Darcy's law, a mixing model, and a curve-fitting procedure. Permeability of several cases were measured, and results indicated that the membrane device was functional for control tests for permeability through membrane only and through a FN-coated membrane, but more experiments with fixed and unfixed cells were needed in order to validate the system for cell-based research.

In conclusion, the utility of microfluidics for endothelial cell biology was demonstrated through a series of experiments designed to reveal phenotypic differences between PAECs and PAVECs. The devices designed were simple and accessible for biologists, and proved that when microfluidic systems are designed with end user in mind, they offer a promising platform for studying endothelial cell biology.

Given the current results, there are a number of suggested directions that may be fruitful for future investigation:

1. *Adhesion and integrins*

   Based on differential adhesion of PAECs and PAVECs on FN and Col-I, we hypothesized above that expression of integrins, specifically $\alpha 2\beta 1$ for Col-I and $\alpha 5\beta 1$ for FN, were likely different between cell types. To test this hypothesis, one could block specific integrin function with antibodies against $\alpha 2\beta 1$ and $\alpha 5\beta 1$ for both cell types. Integrin blocking experiments would involve incubating cells with specific blocking antibodies to prevent integrin-mediated adhesion. These cells would then be injected into microchannels and subjected to the microfluidic adhesion assay to assess their adhesion properties after blocking.

2. *Shear stress in microchannels*

Microfluidic shear flow on PAECs showed perpendicular alignment, in contrast to results reported for PAECs sheared in macroscale PPFCs. To test whether this is cell type-dependent, similar experiments could be performed for PAVECs. In addition, we speculated that shear stress gradients may have induced a migratory response that led to lateral elongation. Microchannel geometries could be tested where height-to-width aspect ratios are decreased to reduce the portion of channel experiencing a shear stress gradient. To eliminate wall effects, micropatterned protein surfaces could be used in place of microchannels such that cells are constrained to similar patterns without side walls.

3. *Permeability*

More validation experiments with fixed cells are needed to fully characterize the usefulness of the membrane device. After validation, the system may be used to study permeability of live cells with and without chemical stimuli. For example, histamine and thrombin have been reported as factors that increase endothelial permeability [87]. As further validation of the system, histamine or thrombin can be introduced into the flowing buffer to stimulate an increase in permeability.

4. *Coculture*

Of the four major classes of endothelial cell studies discussed in the literature review, coculture was the only class that was not studied in this work. The membrane device is inherently suited to coculture studies because a membrane is available to separate two cell types from physical contact while allowing communication through chemical factors.

References

1. Aird, W.C., Phenotypic heterogeneity of the endothelium I. Structure, function, and mechanisms. *Circulation Research*, 2007. **100**(2): p. 158-173.

2. Aird, W.C., Phenotypic heterogeneity of the endothelium II. Representative vascular beds. *Circulation Research*, 2007. **100**(2): p. 174-190.

3. Thurston, G., P. Baluk, and D.M. McDonald, Determinants of endothelial cell phenotype in venules. *Microcirculation*, 2000. **7**(1): p. 67-80.

4. Simionescu, M., N. Simionescu, and G.E. Palade, Segmental differentiations of cell junctions in vascular endothelium - arteries and veins. *Journal of Cell Biology*, 1976. **68**(3): p. 705-723.

5. Aird, W.C., Endothelial cell heterogeneity. *Critical Care Medicine*, 2003. **31**(4): p. S221-S230.

6. Weinberg, P.D. and C.R. Ethier, Twenty-fold difference in hemodynamic wall shear stress between murine and human aortas. *Journal of Biomechanics*, 2007. **40**(7): p. 1594-1598.

7. Kerachian, M.A., et al., Isolation and characterization of human bone-derived endothelial cells. *Endothelium-Journal of Endothelial Cell Research*, 2007. **14**(2): p. 115-121.

8. Knook, D.L., N. Blansjaar, and E.C. Sleyster, Isolation and characterization of Kupffer and endothelial cells from rat-liver. *Experimental Cell Research*, 1977. **109**(2): p. 317-329.

9. Kuruvilla, L., T.R. Santhoshkumar, and C.C. Kartha, Immortalization and characterization of porcine ventricular endocardial endothelial cells. *Endothelium-Journal of Endothelial Cell Research*, 2007. **14**(1): p. 35-43.

10. Magid, R., et al., Optimization of isolation and functional characterization of primary murine aortic endothelial cells. *Endothelium-New York*, 2003. **10**(2): p. 103-109.

11. Simionescu, M. and N. Simionescu, Isolation and characterization of endothelial-cells from the heart microvasculature. *Microvascular Research*, 1978. **16**(3): p. 426-452.

12. Plendl, J., et al., Isolation and characterization of endothelial cells from different organs of fetal pigs. *Anatomy and Embryology*, 1996. **194**(5): p. 445-456.

13. Thi, M.M., et al., The role of the glycocalyx in reorganization of the actin cytoskeleton under fluid shear stress: A "Bumper-car" Model. *Proceedings of the National Academy of Sciences of the United States of America*, 2004. **101**(47): p. 16483-16488.

14. Alberts, B., et al., *Molecular Biology of the Cell*. 4th ed. 2002, New York: Garland Science.

15. Shyy, J.Y. and S. Chien, Role of integrins in endothelial mechanosensing of shear stress. *Circulation Research*, 2002. **91**(9): p. 769-775.

16. Wilhelmi, M., et al., Endothelial anatomy of the human heart: Immunohistochemical evaluation of endothelial differentiation. *Thoracic And Cardiovascular Surgeon*, 2002. **50**(4): p. 230-236.

17. Nugent, H.M. and E.R. Edelman, Tissue engineering therapy for cardiovascular disease. *Circulation Research*, 2003. **92**(10): p. 1068-1078.

18. Davies, P.F., Flow-mediated endothelial mechanotransduction. *Physiological Reviews*, 1995. **75**(3): p. 519-560.

19. Davies, P.F., et al., Scanning electron-microscopy in evaluation of endothelial integrity of fatty lesion in atherosclerosis. *Atherosclerosis*, 1976. **25**(1): p. 125-130.

20. Goode, T.B., et al., Aortic endothelial cell morphology observed insitu by scanning electron-microscopy during atherogenesis in rabbit. *Atherosclerosis*, 1977. **27**(2): p. 235-251.

21. Flaherty, J.T., et al., Endothelial nuclear patterns in canine arterial tree with particular reference to hemodynamic events. *Circulation Research*, 1972. **30**(1): p. 23-&.

22. Kwei, S., et al., Early adaptive responses of the vascular wall during venous arterialization in mice. *American Journal of Pathology*, 2004. **164**(1): p. 81-89.

23. Melkumyants, A.M., S.A. Balashov, and V.M. Khayutin, Endothelium dependent control of arterial diameter by blood-viscosity. *Cardiovascular Research*, 1989. **23**(9): p. 741-747.

24. Langille, B.L. and F. Odonnell, Reductions in arterial diameter produced by chronic decreases in blood-flow are endothelium-dependent. *Science*, 1986. **231**(4736): p. 405-407.

25. Langille, B.L., Arterial remodeling: Relation to hemodynamics. *Canadian Journal of Physiology and Pharmacology*, 1996. **74**(7): p. 834-841.

26. Traub, O. and B.C. Berk, Laminar shear stress - mechanisms by which endothelial cells transduce an atheroprotective force. *Arteriosclerosis Thrombosis and Vascular Biology*, 1998. **18**(5): p. 677-685.

27. Langille, B.L., M.A. Reidy, and R.L. Kline, Injury and repair of endothelium at sites of flow disturbances near abdominal aortic coarctations in rabbits. *Arteriosclerosis*, 1986. **6**(2): p. 146-154.

28. Dewey, C.F., et al., The dynamic-response of vascular endothelial-cells to fluid shear-stress. *Journal Of Biomechanical Engineering-Transactions Of The ASME*, 1981. **103**(3): p. 177-185.

29. Levesque, M.J. and R.M. Nerem, The elongation and orientation of cultured endothelial-cells in response to shear-stress. *Journal of Biomechanical Engineering-Transactions of the Asme*, 1985. **107**(4): p. 341-347.

30. Noria, S., et al., Transient and steady-state effects of shear stress on endothelial cell adherens junctions. *Circulation Research*, 1999. **85**(6): p. 504-514.

31. Viggers, R.F., A.R. Wechezak, and L.R. Sauvage, An apparatus to study the response of cultured endothelium to shear-stress. *Journal of Biomechanical Engineering-Transactions of the Asme*, 1986. **108**(4): p. 332-337.

32. Girard, P.R. and R.M. Nerem, Shear-stress modulates endothelial-cell morphology and f-actin organization through the regulation of focal adhesion-associated proteins. *Journal of Cellular Physiology*, 1995. **163**(1): p. 179-193.

33. Gupte, A. and J.A. Frangos, Effects of flow on the synthesis and release of fibronectin by endothelial-cells. *In Vitro Cellular & Developmental Biology*, 1990. **26**(1): p. 57-60.

34. Uematsu, M., et al., Regulation of endothelial cell nitric oxide synthase mRNA expression by shear stress. *American Journal of Physiology-Cell Physiology*, 1995. **38**(6): p. C1371-C1378.

35. Frangos, J.A., et al., Flow effects on prostacyclin production by cultured human-endothelial cells. *Science*, 1985. **227**(4693): p. 1477-1479.

36. Kuchan, M.J. and J.A. Frangos, Shear-stress regulates endothelin-1 release via protein-kinase-C and cGMP in cultured endothelial-cells. *American Journal of Physiology*, 1993. **264**(1): p. H150-H156.

37. Diamond, S.L., S.G. Eskin, and L.V. McIntire, Fluid-flow stimulates tissue plasminogen-activator secretion by cultured human-endothelial cells. *Science*, 1989. **243**(4897): p. 1483-1485.

38. Zhang, Z.H., Z.S. Xiao, and S.L. Diamond, Shear stress induction of C-type natriuretic peptide (CNP) in endothelial cells is independent of no autocrine signaling. *Annals of Biomedical Engineering*, 1999. **27**(4): p. 419-426.

39. Helmlinger, G., et al., Effects of pulsatile flow on cultured vascular endothelial-cell morphology. *Journal of Biomechanical Engineering-Transactions of the Asme*, 1991. **113**(2): p. 123-131.

40. Helmlinger, G., B.C. Berk, and R.M. Nerem, Pulsatile and steady flow-induced calcium oscillations in single cultured endothelial cells. *Journal of Vascular Research*, 1996. **33**(5): p. 360-369.

41. Mehta, D. and A.B. Malik, Signaling mechanisms regulating endothelial permeability. *Physiological Reviews*, 2006. **86**(1): p. 279-367.

42. Dudek, S.M. and J.G.N. Garcia, Cytoskeletal regulation of pulmonary vascular permeability. *Journal of Applied Physiology*, 2001. **91**(4): p. 1487-1500.

43. Lum, H. and A.B. Malik, Regulation of vascular endothelial barrier function. *American Journal of Physiology*, 1994. **267**(3): p. L223-L241.

44. Michel, C.C. and F.E. Curry, Microvascular permeability. *Physiological Reviews*, 1999. **79**(3): p. 703-761.

45. Youdim, K.A., A. Avdeef, and N.J. Abbott, In vitro trans-monolayer permeability calculations: Often forgotten assumptions. *Drug Discovery Today*, 2003. **8**(21): p. 997-1003.

46. Jo, H., et al., Endothelial albumin permeability is shear dependent, time-dependent, and reversible. *American Journal of Physiology*, 1991. **260**(6): p. H1992-H1996.

47. Butcher, J.T., C.A. Simmons, and J.N. Warnock, Review - Mechanobiology of the aortic heart valve. *Journal of Heart Valve Disease*, 2008. **17**(1): p. 62-73.

48. Liu, A.C., V.R. Joag, and A.I. Gotlieb, The emerging role of valve interstitial cell phenotypes in regulating heart valve pathobiology. *American Journal of Pathology*, 2007. **171**(5): p. 1407-1418.

49. Doran, A.C., N. Meller, and C.A. McNamara, Role of smooth muscle cells in the initiation and early progression of atherosclerosis. *Arteriosclerosis Thrombosis and Vascular Biology*, 2008. **28**(5): p. 812-819.

50. Butcher, J.T., et al., Unique morphology and focal adhesion development of valvular endothelial cells in static and fluid flow environments. *Arteriosclerosis Thrombosis and Vascular Biology*, 2004. **24**(8): p. 1429-1434.

51. Simmons, C.A., et al., Spatial heterogeneity of endothelial phenotypes correlates with side-specific vulnerability to calcification in normal porcine aortic valves. *Circulation Research*, 2005. **96**(7): p. 792-799.

52. Caro, C.G., Fitzgera.Jm, and R.C. Schroter, Arterial wall shear and distribution of early atheroma in man. *Nature*, 1969. **223**(5211): p. 1159-&.

53. *Pie: Virtual cardiac valves: 3d animation, cardiac valve model, mitral, aortic, tricuspid, pulmonary*. 2008 [cited December 7, 2008]; Available from: http://pie.med.utoronto.ca/PIE/PIE_whatWeDo_valves.html.

54. Thubrikar, M., *The Aortic Valve*. 1990, Boca Raton, Florida: CRC Press, Inc.

55. Weston, M.W., D.V. LaBorde, and A.P. Yoganathan, Estimation of the shear stress on the surface of an aortic valve leaflet. *Annals of Biomedical Engineering*, 1999. **27**(4): p. 572-579.

56. Yoganathan, A.P., Z.M. He, and S.C. Jones, Fluid mechanics of heart valves. *Annual Review of Biomedical Engineering*, 2004. **6**: p. 331-362.

57. Farivar, R.S., et al., Transcriptional profiling and growth kinetics of endothelium reveals differences between cells derived from porcine aorta versus aortic valve. *European Journal Of Cardio-Thoracic Surgery*, 2003. **24**(4): p. 527-534.

58. White, F.M., *Fluid Mechanics, 3rd ed.* 3rd ed. 1994, New York: McGraw-Hill, Inc.

59. Shah, R.K. and A.L. London, *Laminar Flow Forced Convection in Ducts*. 1978, New York: Academic Press.

60. Li, W., et al., Simultaneous generation of droplets with different dimensions in parallel integrated microfluidic droplet generators. *Soft Matter*, 2008. **4**(2): p. 258-262.

61. Beebe, D.J., G.A. Mensing, and G.M. Walker, Physics and applications of microfluidics in biology. *Annual Review Of Biomedical Engineering*, 2002. **4**: p. 261-286.

62. Resnick, N., et al., Fluid shear stress and the vascular endothelium: For better and for worse. *Progress in Biophysics & Molecular Biology*, 2003. **81**(3): p. 177-199.

63. Vankooten, T.G., et al., Development and use of a parallel-plate flow chamber for studying cellular adhesion to solid-surfaces. *Journal of Biomedical Materials Research*, 1992. **26**(6): p. 725-738.

64. Xiao, Y. and G.A. Truskey, Effect of receptor-ligand affinity on the strength of endothelial cell adhesion. *Biophysical Journal*, 1996. **71**(5): p. 2869-2884.

65. Usami, S., et al., Design and construction of a linear shear-stress flow chamber. *Annals of Biomedical Engineering*, 1993. **21**(1): p. 77-83.

66. Goldstein, A.S. and P.A. DiMilla, Comparison of converging and diverging radial flow for measuring cell adhesion. *Aiche Journal*, 1998. **44**(2): p. 465-473.

67. Goldstein, A.S. and P.A. DiMilla, Effect of adsorbed fibronectin concentration on cell adhesion and deformation under shear on hydrophobic surfaces. *Journal of Biomedical Materials Research*, 2002. **59**(4): p. 665-675.

68. Horbett, T.A., et al., Cell-adhesion to a series of hydrophilic-hydrophobic copolymers studied with a spinning disk apparatus. *Journal of Biomedical Materials Research*, 1988. **22**(5): p. 383-404.

69. Skarja, G.A., et al., Cone-and-plate device for the investigation of platelet biomaterial interactions. *Journal of Biomedical Materials Research*, 1997. **34**(4): p. 427-438.

70. Davies, P.F., et al., Influence of hemodynamic forces on vascular endothelial function - in vitro studies of shear-stress and pinocytosis in bovine aortic-cells. *Journal of Clinical Investigation*, 1984. **73**(4): p. 1121-1129.

71. Blackman, B.R., G. Garcia-Cardena, and M.A. Gimbrone, A new in vitro model to evaluate differential responses of endothelial cells to simulated arterial shear stress waveforms. *Journal of Biomechanical Engineering-Transactions of the Asme*, 2002. **124**(4): p. 397-407.

72. Bussolari, S.R., C.F. Dewey, and M.A. Gimbrone, Apparatus for subjecting living cells to fluid shear-stress. *Review of Scientific Instruments*, 1982. **53**(12): p. 1851-1854.

73. Schnittler, H.J., et al., Improved in-vitro rheological system for studying the effect of fluid shear-stress on cultured-cells. *American Journal of Physiology*, 1993. **265**(1): p. C289-C298.

74. Wechezak, A.R., R.F. Viggers, and L.R. Sauvage, Fibronectin and f-actin redistribution in cultured endothelial-cells exposed to shear-stress. *Laboratory Investigation*, 1985. **53**(6): p. 639-647.

75. Ruel, J., et al., Development of a parallel plate flow chamber for studying cell behavior under pulsatile flow. *ASAIO Journal*, 1995. **41**(4): p. 876-883.

76. Noria, S., et al., Assembly and reorientation of stress fibers drives morphological changes to endothelial cells exposed to shear stress. *American Journal of Pathology*, 2004. **164**(4): p. 1211-1223.

77. Davies, P.F., et al., Spatial relationships in early signaling events of flow-mediated endothelial mechanotransduction. *Annual Review of Physiology*, 1997. **59**: p. 527-549.

78. McCue, S., S. Noria, and B.L. Langille, Shear-induced reorganization of endothelial cell cytoskeleton and adhesion complexes. *Trends in Cardiovascular Medicine*, 2004. **14**(4): p. 143-151.

79. Tardy, Y., et al., Shear stress gradients remodel endothelial monolayers in vitro via a cell proliferation-migration-loss cycle. *Arteriosclerosis Thrombosis and Vascular Biology*, 1997. **17**(11): p. 3102-3106.

80. Chiu, J.J., et al., Effects of disturbed flow on endothelial cells. *Journal of Biomechanical Engineering-Transactions of the Asme*, 1998. **120**(1): p. 2-8.

81. Sprague, E.A., et al., Influence of a laminar steady-state fluid-imposed wall shear-stress on the binding, internalization, and degradation of low-density lipoproteins by cultured arterial endothelium. *Circulation*, 1987. **76**(3): p. 648-656.

82. Dieterich, P., et al., Quantitative morphodynamics of endothelial cells within confluent cultures in response to fluid shear stress. *Biophysical Journal*, 2000. **79**(3): p. 1285-1297.

83. Kuchan, M.J., H. Jo, and J.A. Frangos, Role of G-proteins in shear stress-mediated nitric-oxide production by endothelial-cells. *American Journal of Physiology*, 1994. **267**(3): p. C753-C758.

84. Suttorp, N., et al., Bacterial exotoxins and endothelial permeability for water and albumin in vitro. *American Journal of Physiology*, 1988. **255**(3): p. C368-C376.

85. Sill, H.W., et al., Shear-stress increases hydraulic conductivity of cultured endothelial monolayers. *American Journal of Physiology-Heart and Circulatory Physiology*, 1995. **37**(2): p. H535-H543.

86. Langeler, E.G. and V.W.M. Vanhinsbergh, Characterization of an in vitro model to study the permeability of human arterial endothelial-cell monolayers. *Thrombosis and Haemostasis*, 1988. **60**(2): p. 240-246.

87. Amerongen, G.P.V., et al., Transient and prolonged increase in endothelial permeability induced by histamine and thrombin - role of protein kinases, calcium, and rhoa. *Circulation Research*, 1998. **83**(11): p. 1115-1123.

88. Rubin, L.L., et al., A cell-culture model of the blood-brain-barrier. *Journal of Cell Biology*, 1991. **115**(6): p. 1725-1735.

89. Fillinger, M.F., et al., Coculture of endothelial cells and smooth muscle cells in bilayer and conditioned media models. *Journal of Surgical Research*, 1997. **67**(2): p. 169-178.

90. Kinard, F., et al., Compartmentalized coculture of porcine arterial endothelial and smooth muscle cells on a microporous membrane. *In Vitro Cellular & Developmental Biology-Animal*, 1997. **33**(2): p. 92-103.

91. Saunders, K.B. and P.A. Damore, An in vitro model for cell-cell interactions. *In Vitro Cellular & Developmental Biology-Animal*, 1992. **28A**(7-8): p. 521-528.

92. Komatsu, Y., et al., Regulation of endothelial production of C-type natriuretic peptide in coculture with vascular smooth muscle cells - role of the vascular natriuretic peptide system in vascular growth inhibition. *Circulation Research*, 1996. **78**(4): p. 606-614.

93. Redmond, E.M., P.A. Cahill, and J.V. Sitzmann, Perfused transcapillary smooth-muscle and endothelial-cell coculture - a novel in-vitro model. *In Vitro Cellular & Developmental Biology-Animal*, 1995. **31**(8): p. 601-609.

94. Redmond, E.M., P.A. Cahill, and J.V. Sitzmann, Flow-mediated regulation of endothelin receptors in cocultured vascular smooth muscle cells: An endothelium-dependent effect. *Journal of Vascular Research*, 1997. **34**(6): p. 425-435.

95. Redmond, E.M., P.A. Cahill, and J.V. Sitzmann, Flow-mediated regulation of G-protein expression in cocultured vascular smooth muscle and endothelial cells. *Arteriosclerosis Thrombosis and Vascular Biology*, 1998. **18**(1): p. 75-83.

96. Chiu, J.J., et al., Shear stress inhibits adhesion molecule expression in vascular endothelial cells induced by coculture with smooth muscle cells. *Blood*, 2003. **101**(7): p. 2667-2674.

97. Nackman, G.B., et al., Flow modulates endothelial regulation of smooth muscle cell proliferation: A new model. *Surgery*, 1998. **124**(2): p. 353-360.

98. Rainger, G.E., et al., A novel system for investigating the ability of smooth muscle cells and fibroblasts to regulate adhesion of flowing leukocytes to endothelial cells. *Journal of Immunological Methods*, 2001. **255**(1-2): p. 73-82.

99. Rainger, G.E. and G.B. Nash, Cellular pathology of atherosclerosis - smooth muscle cells prime cocultured endothelial cells for enhanced leukocyte adhesion. *Circulation Research*, 2001. **88**(6): p. 615-622.

100. Ziegler, T., et al., Coculture of endothelial, cells and smooth-muscle cells in a flow environment - an improved culture model of the vascular wall. *Cells and Materials*, 1995. **5**(2): p. 115-124.

101. Butcher, J.T. and R.M. Nerem, Valvular endothelial cells regulate the phenotype of interstitial cells in co-culture: Effects of steady shear stress. *Tissue Engineering*, 2006. **12**(4): p. 905-915.

102. Kantak, A.S., et al., Platelet function analyzer: Shear activation of platelets in microchannels. *Biomedical Microdevices*, 2003. **5**(3): p. 207-215.

103. Lu, H., et al., Microfluidic shear devices for quantitative analysis of cell adhesion. *Analytical Chemistry*, 2004. **76**(18): p. 5257-5264.

104. Gutierrez, E. and A. Groisman, Quantitative measurements of the strength of adhesion of human neutrophils to a substratum in a microfluidic device. *Analytical Chemistry*, 2007. **79**(6): p. 2249-2258.

105. Murthy, S.K., et al., Effect of flow and surface conditions on human lymphocyte isolation using microfluidic chambers. *Langmuir*, 2004. **20**(26): p. 11649-11655.

106. Plouffe, B.D., et al., Peptide-mediated selective adhesion of smooth muscle and endothelial cells in microfluidic shear flow. *Langmuir*, 2007. **23**(9): p. 5050-5055.

107. Plouffe, B.D., M. Radisic, and S.K. Murthy, Microfluidic depletion of endothelial cells, smooth muscle cells, and fibroblasts from heterogeneous suspensions. *Lab on a Chip*, 2008. **8**(3): p. 462-472.

108. Leclerc, E., Y. Sakai, and T. Fujii, Cell culture in 3-dimensional microfluidic structure of PDMS (polydimethylsiloxane). *Biomedical Microdevices*, 2003. **5**(2): p. 109-114.

109. Leclerc, E., Y. Sakai, and T. Fujii, Perfusion culture of fetal human hepatocytes in microfluidic environments. *Biochemical Engineering Journal*, 2004. **20**(2-3): p. 143-148.

110. Li, N.Z. and A. Folch, Integration of topographical and biochemical cues by axons during growth on microfabricated 3-D substrates. *Experimental Cell Research*, 2005. **311**(2): p. 307-316.

111. Rhee, S.W., et al., Patterned cell culture inside microfluidic devices. *Lab on a Chip*, 2005. **5**(1): p. 102-107.

112. Wei, C.W., J.Y. Cheng, and T.H. Young, Elucidating in vitro cell-cell interaction using a microfluidic coculture system. *Biomedical Microdevices*, 2006. **8**(1): p. 65-71.

113. Gray, B.L., et al., Microchannel platform for the study of endothelial cell shape and function. *Biomedical Microdevices*, 2002. **4**(1): p. 9-16.

114. Kovarik, M.L., et al., Fabrication of carbon microelectrodes with a micromolding technique and their use in microchip-based flow analyses. *Analyst*, 2004. **129**(5): p. 400-405.

115. Spence, D.M., et al., Amperometric determination of nitric oxide derived from pulmonary artery endothelial cells immobilized in a microchip channel. *Analyst*, 2004. **129**(11): p. 995-1000.

116. Oblak, T.D., P. Root, and D.M. Spence, Fluorescence monitoring of ATP-stimulated, endothelium-derived nitric oxide production in channels of a poly(dimethylsiloxane)-based microfluidic device. *Analytical Chemistry*, 2006. **78**(9): p. 3193-3197.

117. Song, J.W., et al., Computer-controlled microcirculatory support system for endothelial cell culture and shearing. *Analytical Chemistry*, 2005. **77**(13): p. 3993-3999.

118. Ismagilov, R.F., et al., Microfluidic arrays of fluid-fluid diffusional contacts as detection elements and combinatorial tools. *Analytical Chemistry*, 2001. **73**(21): p. 5207-5213.

119. Chueh, B.H., et al., Leakage-free bonding of porous membranes into layered microfluidic array systems. *Analytical Chemistry*, 2007. **79**(9): p. 3504-3508.

120. Huh, D., et al., Acoustically detectable cellular-level lung injury induced by fluid mechanical stresses in microfluidic airway systems. *Proceedings of the National Academy of Sciences of the United States of America*, 2007. **104**(48): p. 18886-18891.

121. Kuo, T.C., et al., Hybrid three-dimensional nanofluidic/microfluidic devices using molecular gates. *Sensors and Actuators a-Physical*, 2003. **102**(3): p. 223-233.

122. de Jong, J., R.G.H. Lammertink, and M. Wessling, Membranes and microfluidics: A review. *Lab on a Chip*, 2006. **6**(9): p. 1125-1139.

123. Hui, E.E. and S.N. Bhatia, Micromechanical control of cell-cell interactions. *Proceedings of the National Academy of Sciences of the United States of America*, 2007. **104**(14): p. 5722-5726.

124. Kane, B.J., et al., Liver-specific functional studies in a microfluidic array of primary mammalian hepatocytes. *Analytical Chemistry*, 2006. **78**(13): p. 4291-4298.

125. Tan, W. and T.A. Desai, Microscale multilayer cocultures for biomimetic blood vessels. *Journal Of Biomedical Materials Research Part A*, 2005. **72A**(2): p. 146-160.

126. Genes, L.I., et al., Addressing a vascular endothelium array with blood components using underlying microfluidic channels. *Lab on a Chip*, 2007. **7**(10): p. 1256-1259.

127. Sims, C.E. and N.L. Allbritton, Analysis of single mammalian cells on-chip. *Lab on a Chip*, 2007. **7**(4): p. 423-440.

128. Marcus, J.S., W.F. Anderson, and S.R. Quake, Microfluidic single-cell mRNA isolation and analysis. *Analytical Chemistry*, 2006. **78**(9): p. 3084-3089.

129. Ginsberg, S.D., RNA amplification strategies for small sample populations. *Methods*, 2005. **37**(3): p. 229-237.

130. Cheung, W., E.W.K. Young, and C.A. Simmons, Techniques for isolating and purifying porcine aortic valve endothelial cells. *Journal of Heart Valve Disease*, 2008: p. (in press).

131. Young, E.W.K., A.R. Wheeler, and C.A. Simmons, Matrix-dependent adhesion of vascular and valvular endothelial cells in microfluidic channels. *Lab on a Chip*, 2007. **7**(12): p. 1759-1766.

132. Johnson, C.M. and D.N. Fass, Porcine cardiac valvular endothelial-cells in culture - a relative deficiency of fibronectin synthesis invitro. *Laboratory Investigation*, 1983. **49**(5): p. 589-598.

133. Paranya, G., et al., Aortic valve endothelial cells undergo transforming growth factor-beta-mediated and non-transforming growth factor-beta-mediated transdifferentiation in vitro. *American Journal of Pathology*, 2001. **159**(4): p. 1335-1343.

134. Ugele, B. and F. Lange, Isolation of endothelial cells from human placental microvessels: Effect of different proteolytic enzymes on releasing endothelial cells from villous tissue. *In Vitro Cellular & Developmental Biology-Animal*, 2001. **37**(7): p. 408-413.

135. Song, L. and J.S. Pachter, Culture of murine brain microvascular endothelial cells that maintain expression and cytoskeletal association of tight junction-associated proteins. *In Vitro Cellular & Developmental Biology-Animal*, 2003. **39**(7): p. 313-320.

136. Miebach, S., et al., Isolation and culture of microvascular endothelial cells from gliomas of different who grades. *Journal of Neuro-Oncology*, 2006. **76**(1): p. 39-48.

137. Aird, W.C., Mechanisms of endothelial cell heterogeneity in health and disease. *Circulation Research*, 2006. **98**(2): p. 159-162.

138. Davies, P.F., A.G. Passerini, and C.A. Simmons, Aortic valve - turning over a new leaf(let) in endothelial phenotypic heterogeneity. *Arteriosclerosis Thrombosis and Vascular Biology*, 2004. **24**(8): p. 1331-1333.

139. Butcher, J.T., et al., Transcriptional profiles of valvular and vascular endothelial cells reveal phenotypic differences - influence of shear stress. *Arteriosclerosis Thrombosis And Vascular Biology*, 2006. **26**(1): p. 69-77.

140. Walker, G.M., H.C. Zeringue, and D.J. Beebe, Microenvironment design considerations for cellular scale studies. *Lab on a Chip*, 2004. **4**(2): p. 91-97.

141. Yu, H.M., et al., Diffusion dependent cell behavior in microenvironments. *Lab on a Chip*, 2005. **5**(10): p. 1089-1095.

142. Duffy, D.C., et al., Rapid prototyping of microfluidic systems in poly(dimethylsiloxane). *Analytical Chemistry*, 1998. **70**(23): p. 4974-4984.

143. Sinton, D., Microscale flow visualization. *Microfluidics And Nanofluidics*, 2004. **1**(1): p. 2-21.

144. Orr, A.W., et al., The subendothelial extracellular matrix modulates NK-kappa B activation by flow: A potential role in atherosclerosis. *Journal of Cell Biology*, 2005. **169**(1): p. 191-202.

145. Orr, A.W., et al., Mechanisms of mechanotransduction. *Developmental Cell*, 2006. **10**(1): p. 11-20.

146. Vesely, I., Heart valve tissue engineering. *Circulation Research*, 2005. **97**(8): p. 743-755.

147. Cuy, J.L., et al., Adhesive protein interactions with chitosan: Consequences for valve endothelial cell growth on tissue-engineering materials. *Journal Of Biomedical Materials Research Part A*, 2003. **67A**(2): p. 538-547.

148. Brody, S., et al., The effect of cholecyst-derived extracellular matrix on the phenotypic behaviour of valvular endothelial and valvular interstitial cells. *Biomaterials*, 2007. **28**(8): p. 1461-1469.

149. Hoerstrup, S.P., et al., Functional living trileaflet heart valves grown in vitro. *Circulation*, 2000. **102**(19): p. 44-49.

150. Steinhoff, G., et al., Tissue engineering of pulmonary heart valves on allogenic acellular matrix conduits - in vivo restoration of valve tissue. *Circulation*, 2000. **102**(19): p. 50-55.

151. Leyh, R.G., et al., Acellularized porcine heart valve scaffolds for heart valve tissue engineering and the risk of cross-species transmission of porcine endogenous retrovirus. *Journal of Thoracic and Cardiovascular Surgery*, 2003. **126**(4): p. 1000-1004.

152. Bhadriraju, K., et al., Activation of ROCK by RhoA is regulated by cell adhesion, shape, and cytoskeletal tension. *Experimental Cell Research*, 2007. **313**(16): p. 3616-3623.

153. Hazel, A.L. and T.J. Pedley, Vascular endothelial cells minimize the total force on their nuclei. *Biophysical Journal*, 2000. **78**(1): p. 47-54.

154. Nelson, C.M., et al., Emergent patterns of growth controlled by multicellular form and mechanics. *Proceedings Of The National Academy Of Sciences Of The United States Of America*, 2005. **102**(33): p. 11594-11599.

155. Frangos, J.A., L.V. McIntire, and S.G. Eskin, Shear-stress induced stimulation of mammalian-cell metabolism. *Biotechnology and Bioengineering*, 1988. **32**(8): p. 1053-1060.

156. McCann, J.A., et al., Non-uniform flow behavior in a parallel plate flow chamber alters endothelial cell responses. *Annals of Biomedical Engineering*, 2005. **33**(3): p. 328-336.

157. Chen, J.-H., *Effects of flow-induced shear stress on human umbilical cord perivascular (hucpv) derived mesenchymal stem cells*, in *Division of Engineering Science, Faculty of Applied Science and Engineering*. 2006, University of Toronto: Toronto. p. 46.

158. Wong, B., *Effects of flow-induced shear stress on human umbilical cord-derived mesenchymal stem cells*, in *Department of Mechanical & Industrial Engineering*. 2008, University of Toronto: Toronto.

159. Heo, Y.S., et al., Characterization and resolution of evaporation-mediated osmolality shifts that constrain microfluidic cell culture in poly(dimethylsiloxane) devices. *Analytical Chemistry*, 2007. **79**(3): p. 1126-1134.

160. Grasso, S., J.A. Hernandez, and S. Chifflet, Roles of wound geometry, wound size, and extracellular matrix in the healing response of bovine corneal endothelial cells in culture. *American Journal of Physiology-Cell Physiology*, 2007. **293**(4): p. C1327-C1337.

161. Vyalov, S., B.L. Langille, and A.I. Gotlieb, Decreased blood flow rate disrupts endothelial repair in vivo. *American Journal of Pathology*, 1996. **149**(6): p. 2107-2118.

162. Mehta, G., et al., Quantitative measurement and control of oxygen levels in microfluidic poly(dimethylsiloxane) bioreactors during cell culture. *Biomedical Microdevices*, 2007. **9**(2): p. 123-134.

163. Kim, L., et al., A practical guide to microfluidic perfusion culture of adherent mammalian cells. *Lab on a Chip*, 2007. **7**(6): p. 681-694.

164. Biganzoli, E., et al., Use of a caco-2 cell culture model for the characterization of intestinal absorption of antibiotics. *Farmaco*, 1999. **54**(9): p. 594-599.

165. Neeves, K.B. and S.L. Diamond, A membrane-based microfluidic device for controlling the flux of platelet agonists into flowing blood. *Lab on a Chip*, 2008. **8**(5): p. 701-709.

166. Piruska, A., et al., The autofluorescence of plastic materials and chips measured under laser irradiation. *Lab on a Chip*, 2005. **5**(12): p. 1348-1354.

167. Zeng, H.L., H.F. Li, and J.M. Lin, Chiral separation of dansyl amino acids by PDMS microchip gel monolithic column electrochromatography with gamma-cyclodextrin bonded in polyacrylamide. *Analytica Chimica Acta*, 2005. **551**(1-2): p. 1-8.

168. Llobera, A., et al., Multiple internal reflection poly(dimethylsiloxane) systems for optical sensing. *Lab on a Chip*, 2007. **7**(11): p. 1560-1566.

169. Wong, M.K.K. and A.I. Gotlieb, Invitro reendothelialization of a single-cell wound - role of microfilament bundles in rapid lamellipodia-mediated wound closure. *Laboratory Investigation*, 1984. **51**(1): p. 75-81.

170. Scheidegger, A.E., *The physics of flow through porous media*. 1974, Toronto, Canada: University of Toronto Press. 73-151.

171. Turner, M.R., Flows of liquid and electrical-current through monolayers of cultured bovine arterial endothelium. *Journal of Physiology-London*, 1992. **449**: p. 1-20.

172. Bhave, R.R., *Inorganic membranes: Synthesis, characteristics, and applications*. 1991, New York, NY: Van Nostrand Reinhold.

173. Luk, V.N., G.C.H. Mo, and A.R. Wheeler, Pluronic additives: A solution to sticky problems in digital microfluidics. *Langmuir*, 2008. **24**(12): p. 6382-6389.

174. Bui, L.N., et al., Surface modification of the biomedical polymer poly(ethylene-terephthalate). *Analyst*, 1993. **118**(5): p. 463-474.

175. Wang, Z.H. and G. Jin, Covalent immobilization of proteins for the biosensor based on imaging ellipsometry. *Journal of Immunological Methods*, 2004. **285**(2): p. 237-243.

176. Rosenthal, A.M. and A.I. Gotlieb, *Macrovascular endothelial cells from porcine aorta*, in *Cell culture techniques in heart and vessel research*, H.M. Piper, Editor. 1990, Springer-Verlag: Berlin, Germany. p. 117-129.

177. Gervais, T., et al., Flow-induced deformation of shallow microfluidic channels. *Lab on a Chip*, 2006. **6**(4): p. 500-507.

178. Gray, D.S., J. Tien, and C.S. Chen, Repositioning of cells by mechanotaxis on surfaces with micropatterned young's modulus. *Journal Of Biomedical Materials Research Part A*, 2003. **66A**(3): p. 605-614.

Appendix A. Endothelial Cell Isolation and Culture

A.1 Porcine Aortic Endothelial Cell Isolation (Enzyme Dispersion)

This isolation technique was provided by Mr. Dan Trcka from Dr. Lowell Langille's laboratory at the MaRS Research Centre, Toronto, Canada. The protocol was modified from the original procedure by Dr. Avrum Gotlieb [176].

Materials

6 or 8 porcine aortas, cut at slaughterhouse just below aortic arch. The aorta is taken directly from the organ line at the abattoir and placed into sterile fleaker containing PBS, 2% Pen-Strep, fungizone. Within 5-10 minutes transferred them to a second sterile fleaker in a room away from the abattoir floor. The aortas are transported to the lab within one hour at room temperature. (Each aorta provides 3-5, 35 mm dishes)

Reagents and Media

1. Blendzyme 2 (Roche) 11988433001
2. Phosphate-buffered saline (PBS)
3. Complete endothelial cell growth medium (Cell Applications Inc.)
4. Pencillin-Streptomycin (Invitrogen at#15070063)
5. Fungizone (Amphotericin B) (Invitrogen Cat#15290018)

Glassware and Dishes

1. 1 beaker (500 ml)
2. 4 sterile fleakers with cap (500 ml)
3. 4 Falcon tubes, conical bottom (50 ml)
4. 3 culture dishes, 150 mm
5. ~ 10 culture dishes, 35 mm
6. 1 canister sterile Pasteur pipettes
7. serological pipettes, 10 ml, 5 ml

Surgical Instruments

1. 1 long forceps (teeth) (for abattoir)
2. 1 regular scissors (for abattoir)
3. 2 fine surgical scissors
4. 4 hemostats
5. 2 fine forceps

6. 1 long forceps

Miscellaneous

1. Biobag (to dispose animal tissue)
2. Medical gloves
3. Timer
4. Test tube rack

Note: Sterilize surgical instruments, beaker, fleakers and lids individually by autoclaving

Procedure

1. Wipe down the safety cabinet using 70% ethanol. Set up for procedure.
2. Wash outside of fleaker before placing in hood.
3. With long forceps, remove each aorta individually from fleaker, place on bottom half of the culture dish 150 mm, trim adventitia thoroughly with fine scissors, and place adventitia on top half of dish for disposal later.
4. After vessel is well trimmed, place it in the beaker containing PBS.
5. Remove aortas individually from beaker, and clamp below the branch points so that you maximize the length of the vessel.
6. Cut vessel immediately below clamp. Set this extra piece aside to be discarded with adventitia.
7. Fill vessel with PBS, decant in a different container, fill once again, decant (~5 times). This will gently wash out any bloody cells.
8. Set vessel and clamp in upright position in either top half or bottom half of culture dish 150 mm.
9. Fill each vessel with enzyme solution (Blendzyme 2) (by pouring directly from Falcon Tube).
10. Allow vessels to stand undisturbed in the hood for 8-10 minutes (set timer)
11. In the meantime pipette 1 ml of growth medium into a 35 mm dish.
12. When time is up, decant all the enzyme into a sterile tube (to be discarded).
13. Using a pipette, fill each vessel with growth medium (EC Growth Medium) to a level just below its end.
14. Using a pipette aspirate the media in the vessel and using this medium, rinse the intima of the vessel progressing around its circumference. Be careful not to touch the tip of the pipette to the vessel itself.
15. After this rinsing aspirate the entire medium from the vessel. Now add this cell-medium suspension to one of the 35 mm dishes already prepared.
16. Put the dish in the incubator, 37 deg C, 5% CO_2.
17. Repeat steps 5-16 for the rest of the aortas.
18. Place all dishes on a tray and view under inverted microscope. You should see ~6 clumps of ~10-50 rounded cells/10x field. Initial attachment may already have occurred in the dishes plated first.

Feeding Cultures

These cultures should be fed 48 hours after initial plating.
Approximately ¾ of the "conditioned medium" should be left in the dish and new medium added to a total volume of 2.5 ml.
pH of the medium should be closely monitored and appearance of the cells too (must have cobblestone shape).

How to prepare the Enzyme

Resuspend the whole vial in 2 ml PBS. Make aliquots of 0.5 ml.
Keep them stored at -20 deg C.
To get 18 units/ml (working concentration), take 0.5 ml stock and dilute in 39 ml PBS.
(All this work has to be done inside the biosafety cabinet).

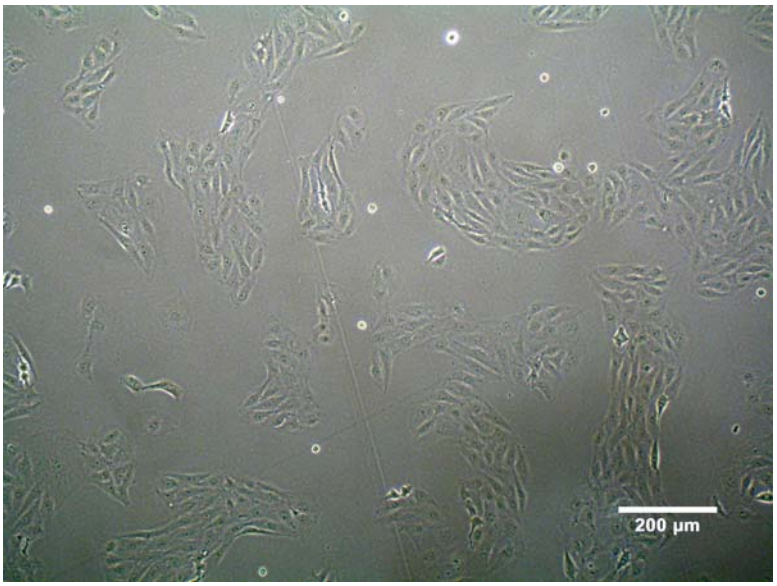

Figure A.1. PAEC (P2) 48 hours after initial seeding at 8000 cells/cm^2.

A.2 Porcine Aortic Valve Endohthelial Isolation

This isolation protocol was developed and refined by the author and Wing-Yee Cheung at the Cellular Mechanobiology Laboratory at the University of Toronto. The purpose is to isolate pure populations of valve endothelial cells from pig aortic valves, and maintain long-term viability with no interstitial cell contamination.

Reagents

1. Sterile PBS w/ Ca^{2+} Mg^{2+} (stored in 4 deg C fridge)
2. Sterile PBS w/o Ca^{2+} Mg^{2+} (stored in 4 deg C fridge)
3. Penicillin/Streptomycin (P/S) (Sigma #P4333, stored in -20 deg C)
4. Gelatin, 3% (w/v) (Sigma #G9391)
5. Fetal bovine serum (FBS) (Hyclone, Lot# KRA25245)
6. M199 basal media (Sigma #M5017)
7. EGM-2 BulletKit: EGM-2 basal media + SingleQuots (Lonza, Cedarlane, CC-3162)
8. Collagenase (Sigma #C0130)
    a. Reconstitute in PBS (Invitrogen #10010023, w/o Ca^{2+} and Mg^{2+}) to 600 U/mL
    b. Aliquot (~10 mL each) and store at -20 deg ^{o}C
9. Dispase (Invitrogen #17105-041)
    a. Take from stock bottle and reconstitute as needed.
    b. Reconstitute in PBS (Invitrogen #10010023, w/o Ca^{2+} and Mg^{2+}) to 10 mg/mL; typical amounts are 100 mg in 10 mL for stock solution.
    c. Store any remaining stock solution at -20 deg ^{o}C

Collagenase/Dispase Solution (can make solution day before isolation, or can store in -20 deg, 5 mL per 2 hearts – 6 valve leaflets)

1. 60 U/mL collagenase
2. 2.0 U/mL dispase

Supplemented M199 media

1. M199 basal media
2. 10% FBS
3. 1% P/S

Supplemented EGM-2 media

4. EGM-2 BulletKit
5. 20% FBS
6. 1% P/S

Equipment

1. Conical tubes, 15 mL
2. Scalpel
3. Dissecting scissors
4. Dissection tray
5. Biobags (available at the animal care facility for free, MSB basement)
6. Pipettor
7. Serological pipettes
8. Mini-Vortexer (VWR Scientific Products, Mississauga, ON)
9. ViCell Analyzer (Beckman Coulter), or hemocytometer
10. T-25 or T-75 tissue-culture treated flasks (for non-clonal expansion)
11. 5 X 96-well plates (for clonal expansion)

Procedure

Dissection and rinsing of leaflets

1. Prepare 3 conical tubes containing PBS w/ Ca^{2+} and Mg^{2+} + 1% P/S for rinsing.
2. Remove heart tissue from mid-heart to apex using scalpel.
3. Remove heart tissue from around the aortic valve using scalpel.
4. With the aortic valve in view, cut valve longitudinally between commissures of two leaflets, using either scalpel or scissors, to open the valve.
5. Rinse all leaflets with PBS w/ Ca^{2+} and Mg^{2+} + 1% P/S thoroughly with a pipette to clean off blood clots and other debris.
6. Excise leaflets by cutting near base, leaving a margin of valve tissue (about ¼ of length) near the annulus.
7. Rinse leaflets in the prepared conical tubes through 3 washes of PBS w/ Ca^{2+} and Mg^{2+} + 1% P/S, holding the leaflets in the final wash solution until ready for collagenase treatment.

Leaflet digestion and cell isolation

1. Incubate (at 37 deg C, 5% CO_2) all three leaflets from each heart together in 5 mL of collagenase/dispase digestion solution for **2.5 hours** in a conical tube. Place each conical tube on a rack in a horizontal position in the incubator.
2. After incubation, vortex conical tubes on Mini-Vortexer for 1 minute on "high" setting to dislodge endothelial cells from matrix while leaving matrix intact. This method has shown to limit excessive removal of subendothelial matrix debris.
3. Remove leaflet tissues from conical tubes, leaving only dislodged cells in suspension.
4. Centrifuge the cell solution at 7 min at 1150 rpm (284 x g).
5. Aspirate supernatant and resuspend pellet in 5 mL of supplemented EGM-2 media.
6. Keep cells on ice before plating.
7. Take 0.5 mL of resuspended solution to ViCell Analyzer for cell counting to determine approximate isolation yield and concentration. Similarly, can use 20 uL of cell solution for counting on hemocytometer.

Plating and Culturing

A. Clonal

1. Coat wells of 96-well plates with 3% (w/v) gelatin for 10 min. (50-100 uL, essentially, enough to cover the surface)
2. Perform serial dilution of cell suspension to reach cell concentration of 1 cell/mL.
3. In 5 separate 96-well plates, seed cells into wells by pipetting 200 uL of cell suspension per well. This equates to 0.2 cells/well, which is optimal for obtaining a high number of wells containing a single cell.
4. Culture at 37 deg C and 5% CO_2 for one week. Monitor regularly.
5. 1 wk after initial seeding, identify wells containing only EC colonies by morphological screening. For all wells identified as pure EC colonies, replace media with 100 uL of fresh supplemented EGM-2 media, and do so every 2 days until 70% confluence.
6. At 70% confluence, passage cells, and transfer to 24-well plates without mixing the colonies from separate wells.
7. Once in 24-well plates, feed every 2 days with supplemented M199 media.
8. Passage at 70% confluence; transfer to larger platform (6-well plate, then T-75).

B. Non-clonal

1. Coat tissue-culture treated flasks (T-25 or T-75, depending on total number of isolated cells) with 3% (w/v) gelatin for 10 min. Rule of thumb: Use 2.5 mL for T-25, and 7.5 mL for T-75.
2. Plate cells into flasks at 5000 cells/cm^2.
3. Culture at 37 deg C and 5% CO_2.
4. Feed cells with fresh supplemented EGM-2 media every 2 days until 70% confluence.
5. At 70% confluence, passage cells, and feed all subcultures with supplemented M199 media to reduce costs.

Cryopreservation

- stuff specific to ECs – use 70% M199 + 20% FBS + 10% DMSO sterile
- 1 mL of 1.5 x 10^6 cells/mL into each vial

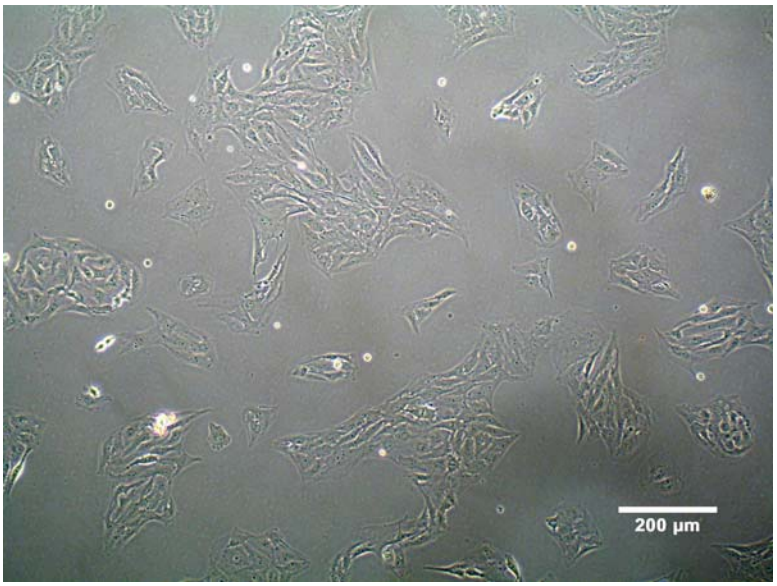

Figure A.2. PAVEC P3 – 48 hours after initial seeding at 8000 cells/cm^2.

Appendix B. Microfabrication by Soft Lithography

B.1 Master Fabrication Process for SU-8

This protocol was developed by Chris Moraes, with minor modifications.

Purpose

To process flow to microfabricate SU-8 molds. Parameters for various thicknesses and SU-8 types are provided in the accompanying SU-8 Fabrication Parameters excel file

Equipment Required

Cleanroom equipment – bench, spin coater, SU-8, swabs, masks, exposure unit, etc.

Process

1. Use glass slides with seed layers of SU-8 only.
2. Dehydration bake – hotplate, ~180 degrees, ~20-30 minutes
3. Let samples cool on cleanroom wipe
4. Pour SU-8 across sample, being careful not to introduce bubbles
    - If bubbles are excessive, try remove them with a needle. Be careful not to scratch the surface
5. Tilt sample to spread SU-8 over as much of the surface as possible.
6. Re-tilt to get the bulk of SU-8 back to the center, and mount in the spin coater
7. Spin at the appropriate parameters
8. While the sample is in the spin coater under vacuum, perform Edge-bead removal:
    - This prevents SU-8 reflow from causing significant variation across your sample
    - use mechanical EBR on the top surface (scrape ~2-3mm of the edges with a swab),
    - use chemical EBR on bottom surface – swab with acetone-soaked swab to remove SU-8 drip-offs
9. Use ONE hotplate only, initially set at 65 degrees.

10. Level the hotplate using the bubble level (found in the top 'cupboard' of the storage cabinet next to the profilometer in the cleanroom). This is important to keep uniformity across the sample

11. Keep sample on hotplate at 65 degrees for the appropriate time.

12. When time is up, set the hotplate to 95 degrees. Start timing after the readout shows 95+.

13. When time is up, set the hotplate to <<65 degrees, and wait to cool. When the readout is less than 65 degrees, remove the sample and place on a cleanroom wipe on the bench. Allow more time to cool to RT

14. Set the hotplate to 65 degrees again.

15. Expose in the aligner for appropriate time and settings.

    - Note: if using soft or hard contact, use the blank glass slide as the hard-mask backing, and place your mask directly on top of your sample before loading, ink side down.

16. Place samples on hotplate for the appropriate time

17. When time is up, set the hotplate to 95 degrees. Start timing after the readout shows 95+.

18. When time is up, set the hotplate to <<65 degrees, and wait to cool. For really thick samples with lots of SU-8 cross-linking, allow it to cool on hotplate all the way to room temperature. Up to ~150um structures, cool to 60 degrees, and then remove and allow to cool to RT on wipe on cleanroom bench.

19. WAIT OVERNIGHT BEFORE DEVELOPING. This gives the SU-8 film time to relax and it won't crack.

20. Develop for however long it takes – check at ~10 minute intervals for the first 30 minutes, and then 5 minute intervals after that. Replace developer every 10 minutes or so.

21. Hard-bake according to parameters.

    - If hard-bake temperature ramps are too steep, cracking in thick SU-8 has been observed. Be careful – use an oven at low T for a long time if necessary.

B.2 PDMS – Glass Hybrid Device Fabrication

1. Pour PDMS over masters in a 10:1 ratio of elastomer base and curing agent, and cure for at least 4 hours at 70 deg C. Once cured, carefully remove PDMS from SU-8 master using scalpel blade, taking care not to scratch SU-8 layer.

2. For the glass slides that are to be used as the bottom substrate, wash in piranha solution (70% sulfuric acid, 30% hydrogen peroxide), for 30 min.

3. Rinse piranha-washed glass slides in DI water and isopropyl alcohol, and spray with nitrogen. Do the same to the PDMS slabs with microchannel features that have been cured and removed from their masters. Make sure inlet and outlet ports have been cored out before proceeding.

4. Check for dust particles on slabs, and use scotch tape to remove any debris from surface.

5. Plasma treat glass slide and PDMS slab (channel feature side facing up) for 90 seconds in Harrick Plasma Cleaner on high radio frequency setting, 400 mTorr on PlasmaFlo Gas Flow Mixer.

6. Remove glass slide and PDMS slab from plasma cleaner and immediately bond.

Table B-1. SU-8 Fabrication Parameters

CODE	SU-8 Type	Spin Parameters				Pre-bake		Expose	Post-bake		Develop	Hard-bake	Thickness
		Spin #	Time (s)	RPM	ACL	65°C (min)	95°C (min)	Time (s)	65°C (min)	95°C (min)	Time (min)	Temp/Time	[Estimated] (Measured)
S-5-seed	SU-8-5	1	5	500	88								
		2	30	500	88								
		3	15	3000	528								
		4	30	3000	528	2	5	FLOOD-6	1	4	2	180°C/0.3 h	[7 um]
S-25-seed	SU-8-25	1	5	500	88								
		2	30	500	88								
		3	15	3000	528								
		4	30	3000	528	2	5	FLOOD-7	1	4	2	180°C/0.3 h	[7 um]
S-25-50	SU-8-25	1	5	500	88								
		2	30	500	88								
		3	5	1000	352								
		4	30	1000	352	5	15	SOFT-9	1	6	10	180°C/1 h	(48, 55 um)
S-50-100	SU-8-50	1	5	500	88								
		2	30	500	88								
		3	5	1000	352								
		4	33	1000	352	10	30	SOFT-30	2	15	~20	180°C/1 h	(120 um)
S-50-300	SU-8-50	1	5	500	88								
		2	30	500	88								
		3	5	1000	352								
		4	33	1000	352	10	30	PROCEED TO SPIN #5					
		5	5	500	88								
		6	30	500	88								
		7	5	1000	352								
		8	33	1000	352	10	45	SOFT-45	3	22	40*	75°C/3 days	(310 um)

Appendix C. Adhesion Study Supplemental Information

C.1 Theory

For fully developed laminar flow through a microchannel of rectangular cross-section, an analytical solution of the velocity profile has been derived. Shah and London [59] have presented both the exact solution involving Fourier series expansions, as well as a simple approximation to the velocity profile originally proposed by Purday. Because this approximation is in excellent agreement with classical experimental results, and is much easier to compute, we used it to estimate maximum velocity at the midplane of the microchannels, and shear stress on the microchannel surface.

For a microchannel of half-width $a = w/2$, and half-height $b = h/2$, the laminar velocity profile through a rectangular cross-section, as shown in Figure 5.1 of the main text, can be approximated by:

$$\frac{u}{u_m} = \left(\frac{m+1}{m}\right)\left(\frac{n+1}{n}\right)\left[1-\left(\frac{y}{b}\right)^n\right]\left[1-\left(\frac{z}{a}\right)^m\right] \tag{C.1}$$

and

$$\frac{u_{\max}}{u_m} = \left(\frac{m+1}{m}\right)\left(\frac{n+1}{n}\right) \tag{C.2}$$

where u, u_m, and u_{max} are the axial, mean, and maximum velocities, respectively, and m and n are empirical parameters. Wall shear stress on the bottom surface is given by

$$\tau_w = \mu\frac{du}{dy} \tag{C.3}$$

We differentiate Eq. (C.1) with respect to y and substitute $y = -b$ to obtain:

$$\frac{du}{dy} = u_m \left(\frac{m+1}{m} \right) \left(\frac{n+1}{n} \right) \left(\frac{n}{b} \right) \left[1 - \left(\frac{z}{a} \right)^m \right] \tag{C.4}$$

Recognizing that $u_m = Q/wh$ and $b = h/2$, where Q is the flow rate, we can substitute Eq. (C.4) into (C.3) and simplify to obtain

$$\tau_w = \frac{2\mu Q}{wh^2} \left(\frac{m+1}{m} \right) (n+1) \tag{C.5}$$

at $z = 0$ (i.e., center of channel width).

For aspect ratio $\alpha = h/w < 1/3$, $m = 1.7 + 0.5\alpha^{-1.4}$ and $n = 2$. Channel dimensions were measured to be $h = 58.5 \pm 4.2$ μm and $w = 516 \pm 6$ μm, which yields $\alpha = 0.113$, $m = 12.24$, and $u_{max}/u_m = 1.623$. This is ~8% larger than $u_{max}/u_m = 1.5$ for the parallel plate approximation. Also, substitution of m and n into Eq. (C.5) yields

$$\tau_w = \frac{6\mu Q}{wh^2} \left(\frac{m+1}{m} \right) = 1.082 \cdot \frac{6\mu Q}{wh^2} \tag{C.6}$$

Again, as expected, the shear stress is ~8% larger than for the parallel plate approximation of $\tau_w = 6\mu Q / wh^2$. For $\mu = 0.72 \times 10^{-3}$ kg/m·s, the shear stresses applied in the channels were 11, 110, and 220 dyn/cm^2.

C.2 Flow Characterization

As described in the main text, particle streak velocimetry [143] was used to measure velocities in each microchannel. Flow rates of 1.2 mL/hr and 2.4 mL/hr were chosen such that measurable lengths of sufficiently bright streaklines could be obtained. At higher flow rates, streaklines spanned more than 50% of the viewfield even with the shortest possible exposure time, and therefore could not be used as an accurate measure. Five separate images were collected per microchannel, all at $x = 15$ mm from the start of the main channel section.

In these velocimetry experiments, measured maximum velocities were u_{max} = 2.38 ± 0.19 mm/s for flow rate of Q = 1.2 mL/hr, and u_{max} = 4.55 ± 0.38 mm/s for Q = 2.4 mL/hr, less than 10% variability between channels within the same network. Measured maximum velocities were also consistent with theoretical predictions since Q = 1.2 mL/hr (or 0.15 mL/hr per channel) equated to u_m = 1.38 mm/s. Since u_{max}/u_m = 1.62, we have u_{max} = 2.24 mm/s, or roughly 6% difference with experiment. For Q = 2.4 mL/hr, theory predicted u_{max} = 4.48 mm/s, or less than 2% difference.

We considered the possible deformation of PDMS due to pressure-driven flow as discussed by Gervais et al. [177], and we assessed whether the deformation experienced under our experimental conditions had a significant effect on the measured velocities and the shear stress. For a conservative estimate of Young's modulus of E = 2 MPa for PDMS cured at a 10:1 base/curing agent ratio [177, 178], an applied flow rate of Q = 2.4 mL/hr resulted in less than 0.1% difference in the mean velocity from the beginning (x = 0) to the end (x = 30 mm) of the microchannel. Furthermore, at the highest flow rate used in the shear assay of Q = 240 mL/hr, mean velocity was predicted to differ by only 7.5% between ends of the channel. This confirms that the experimental conditions used, both for the velocimetry experiments and for the shear assay, were not significantly affected by PDMS deformation, and that there was good uniformity in shear stress from one end of the microchannel to the other.

C.3 Complementary Experiments – Dynamics of Cell Detachment

See Figure C.1 below.

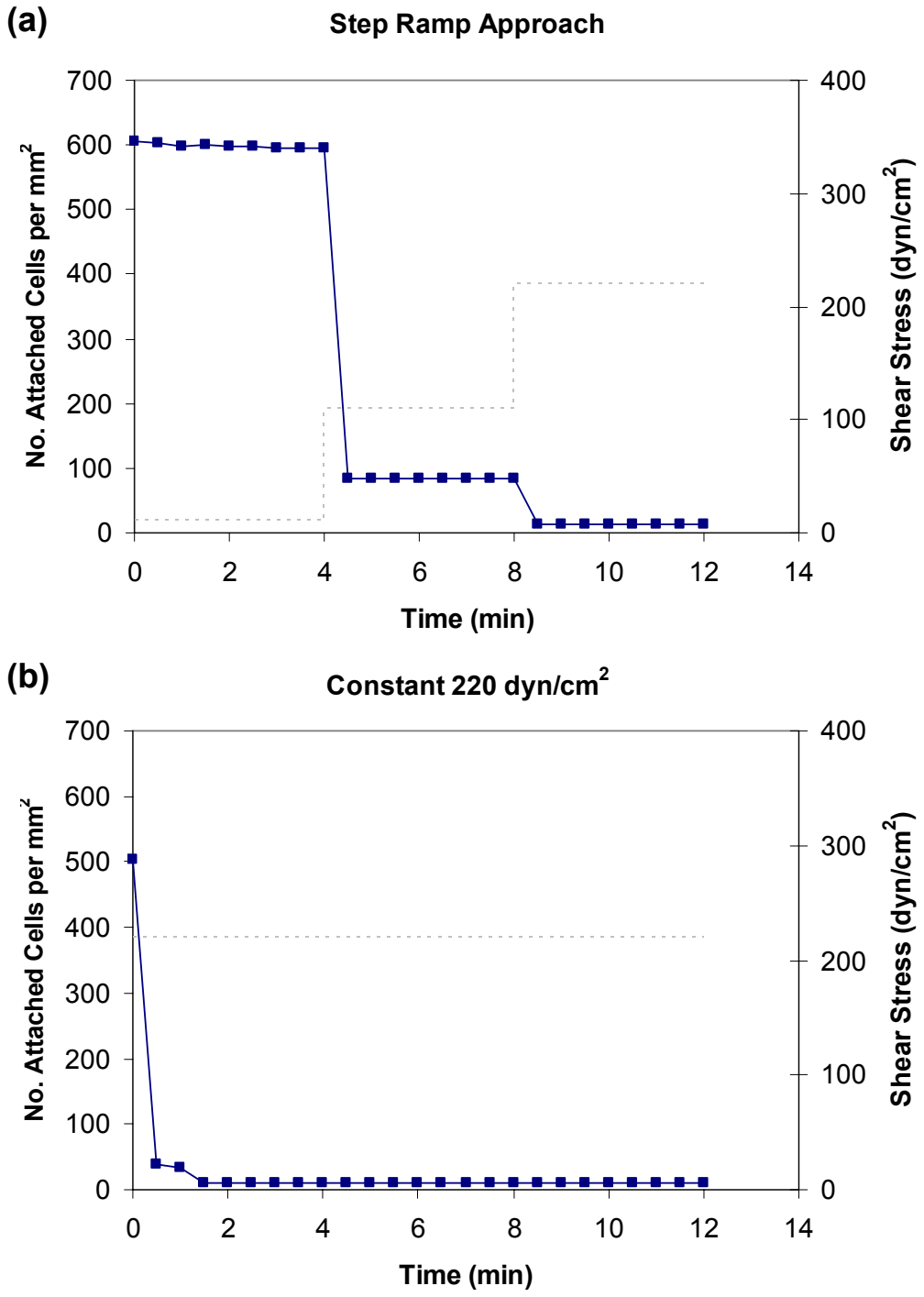

Figure C.1. Intermediate timepoint experiments for examining dynamics of cell detachment. PAVECs on FN at 50 μg/mL were used in both tests. Images were taken every 30 seconds over the 12-minute shear period. Squares = number of attached cells. Dotted line = shear stress applied. (a) Step ramp approach using 11, 110, and 220 dyn/cm^2 as in the experiments presented in the main text. (b) Constant 220 dyn/cm^2 applied for entire 12 minutes. Results confirm previous observations that cells detach abruptly upon exposure to each shear level.

Appendix D. Adhesion Assay Protocol

Materials

1. 10 million cells x 3 = 30 million cells = 6 T-75 flasks of confluent PAVECs/PAECs
2. Parallel microchannel system x 3
3. 1 mL syringe (BD) x 8
4. Needles, 18G and 21G, x 8 each
5. Microfluidic tubing
6. 15 mL and 50 mL conicals
7. Eppendorf tubes, 1.5 mL
8. T-75s, to be coated with gelatin

Equipment

1. Bio-safety cabinet
2. Hot plate
3. Incubator
4. Fluorescent microscope and camera
5. Hemacytometer
6. Syringe pump

Reagents

1. Hoechst nuclear dye – 10 mg/mL stock solution
2. CellTracker Green (Invitrogen #C2925) – 10 mM in DMSO, aliquoted in -20 deg C
3. 70% Ethanol
4. PBS w/ Mg^{2+} Ca^{2+}
5. PBS w/o Mg^{2+} Ca^{2+}
6. Protein of interest (Fibronectin, Collagen Type I, Collagen Type IV, Laminin)
7. M199 basal medium
8. M199 + 10% FBS + 1% P/S (PAVEC supplemented medium)
9. M199 + 5% FBS + 5% CS + 1% P/S (PAEC supplemented medium)
10. BSA, 1% (w/v)
11. Gelatin (for replating cells for next experiment)
12. Trypsin (0.05%) + EDTA (0.2 g)

Cell Adhesion in Parallel Microfluidic Channels

Procedure

1. CELLS (10 min):
    a. Prepare Hoechst live stain 1:5000, 2 uL in 10 mL of FSM
    b. Prepare CellTracker Green 1:2000, 5 uL in 10 mL of serum-free medium

2. CHANNELS (15 min): Rinse channels, 70% ethanol, let sit for 5 min x 2.

3. CELLS (30 min): Replace old media with Hoechst-added media to ALL cells to be used for FULL experiment, and incubate at 37 deg C.

4. CHANNELS (15 min): Rinse channels, PBS w/o Mg^{2+} Ca^{2+}, let sit for 5 min x 2.

5. CHANNELS (30 min): Remove PBS w/o by pumping in sterile air (from inside laminar flow hood), and further evacuate channels by evaporation using hot plate at 50 deg C. This permits detection of a protein-solution interface that can be drawn into the channels in the next step.

6. CELLS (10 min): Check cells for fluorescence under microscope. Aspirate media, and rinse with PBS w/ Mg^{2+} Ca^{2+}.

7. CELLS (30 min): Replace PBS with CellTracker Green serum-free media, and incubate at 37 deg C.

8. CHANNELS (15 min): Reconstitute protein of interest at the following concentrations for the eight available channels:
    i. 500 ug/ml Col IV
    ii. 50 ug/ml Col IV
    iii. 500 ug/ml LN
    iv. 50 ug/ml LN
    v. 500 ug/ml FN
    vi. 50 ug/ml FN
    vii. BSA BLOCK
    viii. BSA BLOCK

9. CHANNELS (10 min): Load protein into channels from outlet port, 15 uL droplets.

10. CHANNELS (30 min): Incubate at room temperature for desired adsorption time, in this case, for **30 minutes**.

11. CELLS (15 min): Check cells for fluorescence under microscope. Aspirate media, and rinse with PBS w/ Mg^{2+} Ca^{2+}. Check cells again for fluorescence under microscope.

12. CELLS (30 min): Replace PBS with regular full-supplemented media, and incubate at 37 deg C.

13. CHANNELS (10 min): Load using 1 mL syringe from inlet port 1% (w/v) BSA (equal to 10 mg/mL) into channels for blocking non-specific binding.

14. CHANNELS (30 min): Incubate 1% BSA at 37 deg C.

15. CELLS (15 min): Check cells for fluorescence under microscope.
16. CELLS (30 min): Prepare cell suspension:
    a. Trypsinize with 0.05% trypsin + 0.2 g EDTA at 37 deg C (10 min)
    b. Dilute 1:1 with regular fully-supplemented medium. Dislodge cells by squirting medium onto flask surface repeatedly. Transfer to conical and pipette up and down to obtain single cell suspension (5 min)
    c. Centrifuge at 1150 rpm for 7 min, and count cells with hemacytometer during this step (10 min)
    d. Aspirate supernatant and resuspend in fresh growth medium at desired cell seeding concentration (10 million cells/ml) (5 min)

17. CHANNELS (5 min): Flush channels clear of BSA using regular supplemented media appropriate for cell type.

***** CHANNEL PREPARATION COMPLETE *****

18. Load cell suspension into channels from inlet side (5 min).

19. Incubate cells in microchannel at 37 deg C for desired time for cell attachment. (2 hrs)

20. Capture images of cells using fluorescent microscope and camera; take images (Hoechst-blue and CTG-green channels) of five (5) separately marked locations per channel of interest (including BSA control). Apply shear force using syringe pump for desired shear stress ramping scheme. (1.5 hrs)

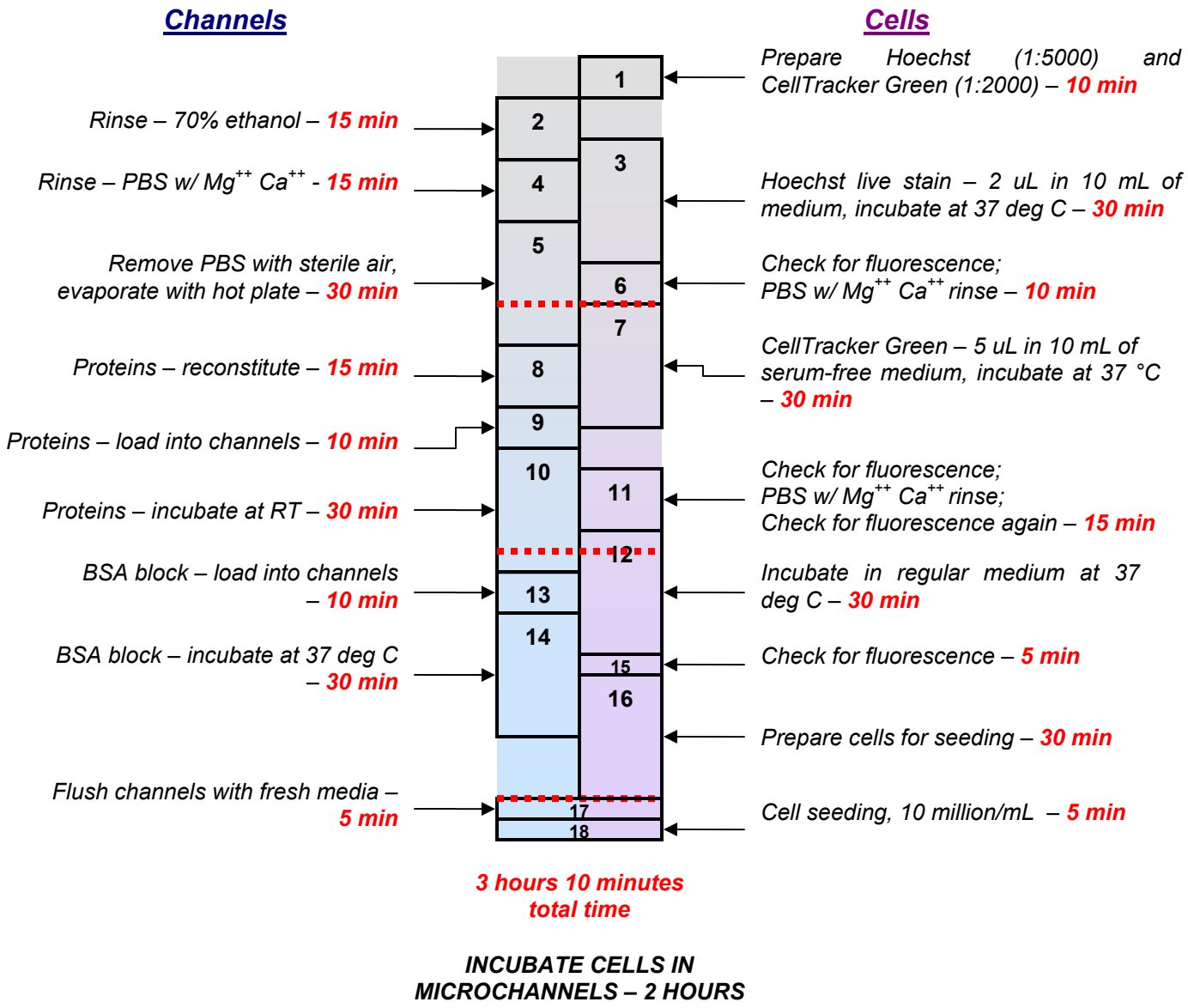
Channels
Cells
Rinse – 70% ethanol – 15 min
Rinse – PBS w/ Mg++ Ca++ - 15 min
Remove PBS with sterile air, evaporate with hot plate – 30 min
Proteins – reconstitute – 15 min
Proteins – load into channels – 10 min
Proteins – incubate at RT – 30 min
BSA block – load into channels – 10 min
BSA block – incubate at 37 deg C – 30 min
Flush channels with fresh media – 5 min
Prepare Hoechst (1:5000) and CellTracker Green (1:2000) – 10 min
Hoechst live stain – 2 uL in 10 mL of medium, incubate at 37 deg C – 30 min
Check for fluorescence; PBS w/ Mg++ Ca++ rinse – 10 min
CellTracker Green – 5 uL in 10 mL of serum-free medium, incubate at 37 °C – 30 min
Check for fluorescence; PBS w/ Mg++ Ca++ rinse; Check for fluorescence again – 15 min
Incubate in regular medium at 37 deg C – 30 min
Check for fluorescence – 5 min
Prepare cells for seeding – 30 min
Cell seeding, 10 million/mL – 5 min
1
2
3
4
5
6
7
8
9
10
11
12
13
14
15
16
17
18
3 hours 10 minutes total time
INCUBATE CELLS IN MICROCHANNELS – 2 HOURS

Appendix E. Recirculatory Microfluidics Parts List

Equipment

Masterflex L/S economy digital pump drive (Cole-Parmer, #7524-50)
Masterflex Easy-Load II pump heads (Cole-Parmer, #77202-60)

Materials

Masterflex L/S tygon food tubing (Cole-Parmer, #06419-13)
Female luer, 1/16" hose barb adapter (Cole-Parmer, #45500-00)
Male luer with lock ring, 1/16" hose barb adapter (Cole-Parmer, #45503-00)

Intramedic polyethylene tubing, Clay Adams, PE60, 0.76 mm ID × 1.21 mm OD
Intramedic polyethylene tubing, Clay Adams, PE190, 1.194 mm ID × 1.70 mm OD
Upchurch P-702 Low Pressure PEEK Union
Upchurch P-200 Flangeless ETFE ferrule (blue)

Note: If PE190 tubing has trouble fitting into ferrule, a new ferrule needs to be used (old one has been compression-fitted into the union after threading, compressing the tubing and the ferrule to give a good seal).

Note: PE60 is preferred for the barbed end. To fit it into the PEEK union, take 1.5 cm of PE190 and sleeve it over the end of the PE60 that goes into the union. The threading of the ferrule, PE190, and PE60 will give a perfect seal.

Procedure – Recirculatory flow in microchannels

1. Fabricate microchannel devices for recirculatory shear flow experiments by following the procedure from Appendix B. Note that for recirculatory flow and long-term culture, inlet/outlet ports and interconnect assemblies need to be designed properly to allow room for fittings and to ensure secure attachment of ports without leakages.

   Inlet/outlet ports made from PE190 tubing should be 3.5 cm in length before insertion into the PDMS channel slab to allow the lock nut and ferrule from the low-pressure union to fit onto the device. The longer port lengths also increase the volume of media available to the cells in culture, and this helps to mitigate the effects of evaporation.

   For interconnects, a more reliable method than using epoxy for securing inlet/outlet ports is to bond and cure a separate block of PDMS around the ports.

To do this:

i. Cut out a small block of PDMS (1 × 1 × 0.3 cm thick) for each reservoir.

ii. Use hole punch or other tool to remove material from center of block.

iii. Clean both the block and PDMS channel slab with scotch tape, and plasma treat both surfaces (90 seconds, 400 mTorr on the Harrick Plasma cleaner).

iv. Position the block such that the hole surrounds the location where the port is to be inserted, and bond by applying force.

v. Insert the port as usual, and then fill the hole within the block with uncured PDMS (or epoxy). Enough uncured PDMS should be added to fill the hole, envelope the port, and slightly bulge up from the surface of the block due to surface tension.

vi. Place entire device into the oven at 70 deg C, and cure overnight.

The result is a seamless block of cured PDMS surrounding each inlet/outlet port.

2. Culture cells directly within microchannels as follows:

i. Rinse all microchannels with 5 mL of 100% ethanol to wet PDMS and glass surfaces. 100% ethanol is a wetting fluid that will easily fill the microchannel space even in the presence hydrophobic surfaces. Since this is the first injection of liquid into a previously gas-filled channel, be cautious not to trap bubbles or introduce them during injection. If bubbles are present, keep flushing 100% ethanol until all bubbles have been removed.

ii. Rinse out 100% ethanol with 70% ethanol. This step is meant to sterilize the channel, and dilute the 100% ethanol from the previous rinse. Use 5 mL per channel.

iii. Rinse with PBS (without divalent cations) to flust out ethanol. Use 5 mL per channel.

iv. Inject in protein coating solution (fibronectin (FN), 250 ug/mL, at least 200 uL per channel). Note that a concentration of 250 ug/mL for a channel with dimensions of $L \times w \times h$ = 50 mm × 1.5 mm × 320 um is equivalent to ~ 8 ug/cm^2 (on all surfaces).

v. Incubate FN coating at room temperature (90 min).

vi. With 20 minutes left in the coating incubation, prepare cells into suspension by trypsinization (0.05% trypsin with EDTA, 5 minutes), centrifugation (1150 rpm or 284 × g, 7 min), and resuspension into 100,000 to 500,000

cells/mL. Note: When in doubt about cell concentration during resuspension (because of uncertainties with cell count), the conservative choice is a lower cell seeding density to reduce the chance of cell clumping and overcrowding.

vii. After 90-min FN incubation is completed, (manually) flush out FN solution at a low flow rate of ~ 1 mL/min using M199 supplemented media (0.5 mL, 30 sec).

viii. Inject in cell suspension, 200-300 uL, into channel.

ix. Incubate cells at 37 deg C, 5% CO_2. Monitor cells at 3 hrs after seeding, and feed for the first time at 6-8 hrs after seeding. Feed cells every 12 hours after the initial 8 hrs.

x. Monitor frequently, and grow to confluence.

3. Autoclave the Tygon tubing (both lengths), female and male luer adapters, the damper and the media reservoir (with caps).

4. Rinse the PE60 and PE190 intramedic tubing with 5-10 mL of 70% ethanol.

5. Assemble the tubing and fittings according to Figure E.1 below.

6. Add media into the reservoir and damper (quantity of media will vary depending on container size.) Once the accessories have been assembled according to Figure E.1, take the microdevice out of the incubator for final assembly.

7. Place lock nut and ferrule onto each inlet and outlet port of the device. Add media into the union(s) and allow it to wet through the union port to the other side. Screw in the union onto the device end first, merging the media together to prevent bubbles. Once all unions are in place, add more media into the unions, then screw in and tighten the lock nuts from the two ends of the tubing assembly.

8. Check the damper to ensure tight seals around the tubing and between the cap and damper container. Without a tight seal, pressure will not build up properly in the damper to force liquid through the outlet.

9. Hook up the system to the peristaltic pump, and adjust to desired flow rate.

10. Monitor cells as necessary (or at desired timepoints) simply by stopping the pump, and taking the entire system to the microscope without any disassembly. Cell morphology can be easily detected through the underlying glass substrate.

11. When checking the cells, be careful not to induce excessive gravity-driven flow into the microchannel. Because the pump is disconnected during this time, backflow from the reservoir can draw in air bubbles that could destroy the endothelial monolayer.

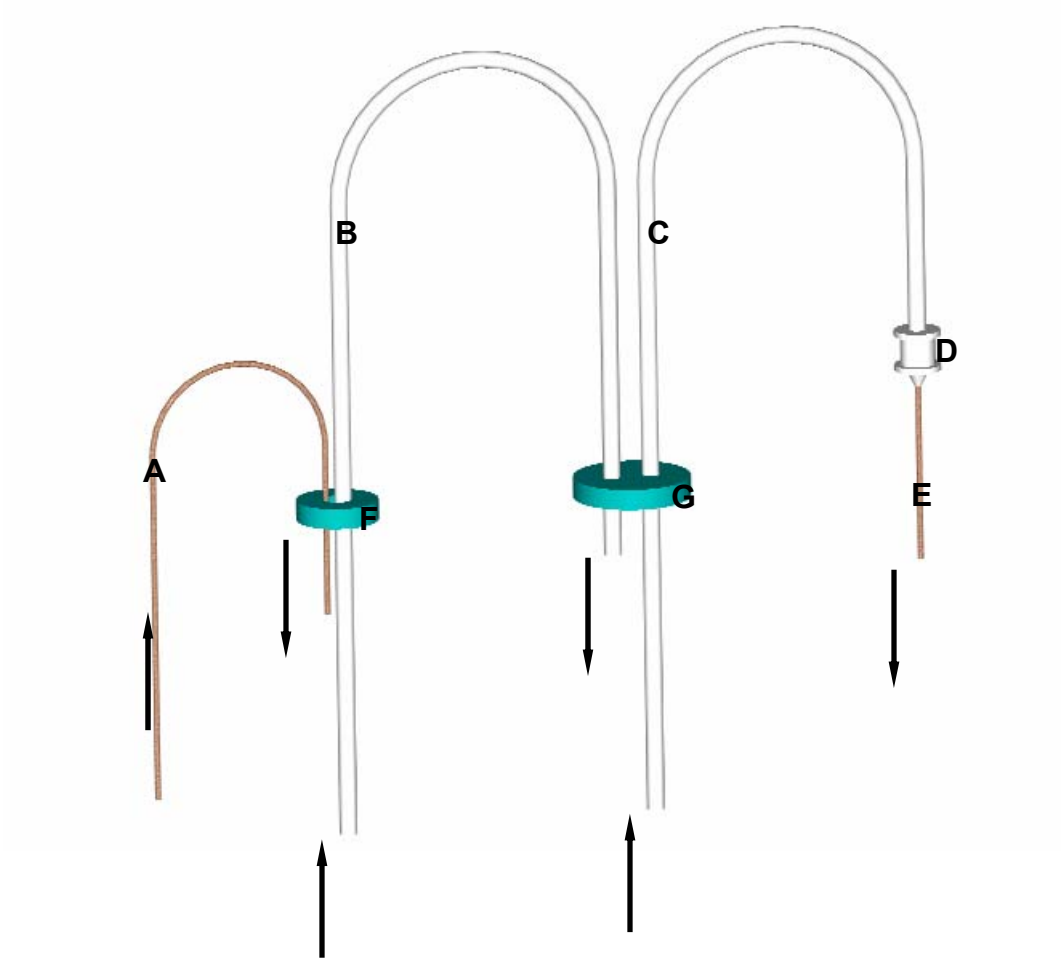

Figure E.1. Tubing assembly for recirculatory microfluidic flow system. (A and E) PE60 polyethylene tubing; (B and C) Masterflex L/S tygon food tubing; (D) Luer-lock adapter (male-to-female); (F) 15 mL conical tube cap; (G) 50 mL conical tube cap. Arrows indicate direction of media flow. E is connected to microchannel inlet, and inflow end of A is connected to microchannel outlet.

Appendix F. Membrane Device Fabrication

Purpose

To fabricate a microfluidic membrane device containing a PET membrane suitable for cell culture sandwiched between two PDMS channel layers. This procedure assumes you have prepared cured PDMS slabs ready for assembly.

Equipment

Spincoater – Laurell WS-400B-NPP-Lite
Nitrogen gas and spray gun
Vortexer
Scalpel
Scissors
Hole puncher (different sizes)

Materials (Assuming SU-8 masters are available)

BD cell culture inserts, 6-well plate, 1.0 um pore size (BD (VWR CA62406-171)
PDMS Sylgard 184
Glass slides – Corning 2947, 75 mm × 50 mm
Glass vial
Syringes (for PDMS dispensing)

Isopropyl alcohol (IPA)
Toluene
Deionized water for rinsing

Procedure

1. Make PDMS mortar by mixing toluene and uncured PDMS prepolymer in a 1:1 volume ratio inside a glass vial. PDMS prepolymer includes 10:1 volume ratio of base to curing agent.
   e.g. For 11 mL of total mortar, use 5 mL PDMS base, 0.5 mL curing agent, and 5.5 mL of toluene.
   Vortex the mortar in glass vial vigorously for at least 5 minutes. The mixture should change from looking like an emulsion of a viscous polymer and a runny solvent to looking homogeneous throughout (i.e. no convective eddies visible).

2. Clean 75 mm x 50 mm glass slides with soap and distilled water, rinse in IPA, and spray with N_2 gas until dry. Inspect glass slide for residue before use. Leave on clean wipe covered with Petri dish lid until ready for use.

3. First punch access holes into the "top" PDMS slab for inlets and outlets of ALL channels from top and bottom slabs. Then, using scotch tape of packing tape, remove dust and other particles from surfaces of PDMS slabs. Rinse slabs with distilled water, IPA, and spray with N_2 gas until dry. Leave on clean wipe covered with Petri dish lid.

4. Set spincoater settings to the following:

    i. 4 s, 1600 rpm, ACL 528
    ii. 60 s, 1600 rpm, ACL 528

5. Place glass slide on spincoater chuck, and add ~1 mL of PDMS mortar on the slide. Tilt slide to spread mortar across the slide. Reposition on chuck, apply vacuum, and start the spin. (1 mL is approximate: if you make 12 mL of mortar, you can expect to spin 12 mortar slides. It would be best to pipette 1 mL exactly on the slide, but this is not absolutely necessary.)

    Repeat for second glass slide.

6. Gently place one of the PDMS channel slabs on one of the glass slides. Start at one of the 50 mm edges, and mate the PDMS with the mortar layer using the tip of a tweezer to push the slab toward the glass without trapping any bubbles. Monitor the progression of the mortar-PDMS mating interface as you work from one edge to the other. The key is to ensure no bubbles are trapped, and that the PDMS slab does not move around excessively such that mortar seeps into the channel features.

    Repeat for second PDMS slab. Let both PDMS slabs sit in mortar for 1 minute. There is no need to add extra force on the slabs; their own weight is enough to generate a stamped mortar layer on the slab.

7. Carefully remove the PDMS slabs by peeling at one corner and slowly separating the slab from the glass with the help of a tweezer. Leave the two slabs with channel features and mortar layer facing up.

8. Using two tweezers, take an appropriately-sized PET membrane piece (cut out from insert) and carefully dip the four membrane edges into spun mortar. (You can use leftover mortar on the spincoated slides, in unstamped regions.)

9. Carefully place membrane in desired region of one PDMS slab.

10. Gently place the other PDMS slab on top of the membrane-containing slab. Again, start at one of the 50 mm edges, and mate the PDMS slabs using a tweezer to push the slabs together without trapping bubbles. When you reach the edge of the membrane, ensure mortar fully surrounds the edge and fills only the membrane regions outside of the channels. Continue to monitor the progression of the mortar interface as you

work from one edge to the other. Inspect to ensure no bubbles have been trapped. At this point, the PDMS slabs have sandwiched the membrane, and the slabs should not be moved or repositioned with respect to each other from this point forward.

NOTE: If a bubble is trapped near the membrane region and the PDMS slabs must be separated to remove the bubble, the device should be discarded. Attempting to reposition the slabs after separation will lead to seepage of mortar into channels, movement of membrane around mortar layer, and possible membrane pore occlusion.

11. If mating of the PDMS slabs is successful, plasma treat ONLY the glass slide for 90 seconds, and bond the plasma-treated glass surface with the untreated bottom PDMS slab. The underlying glass slide gives the device added support for subsequent steps, and prevents the slabs from excessive expansion and contraction during temperature cycling. Plasma treating the PDMS slabs will result in seepage of PDMS mortar into the channels.

    NOTE: This glass bottom is critical to ensure that the device does not expand or contract during heating and cooling. Expansion or contraction of the device leads to membrane buckling because of differences in thermal expansion coefficients between PDMS and PET. Membrane buckling results in cross-talk between top and bottom channels in regions outside of channel intersections.

12. Stack a 70-100 g weight (aluminum plate) on top of the device, covering the entire surface. Place the weight and device together into the oven and incubate at 70 deg C overnight.

13. After overnight curing of the mortar layer, remove device from oven and inspect for membrane tautness and proper curing of mortar. Add appropriate inlet and outlet tubing, and secure with epoxy.

Appendix G. Endothelial Cell Culture in Membrane Microdevices

1. Rinse all channels with 100% ethanol to wet all PDMS surfaces. 100% ethanol is a wetting fluid that will easily fill the microchannel space even in the presence of hydrophobic PDMS surfaces. Assume that membrane pores are filled with the ethanol during the rinse. Use 1 mL ethanol per channel.
2. Rinse out 100% ethanol with 70% ethanol. This step is meant to sterilize the channel, and dilute the 100% ethanol from the previous rinse. Use 5 mL per channel each time, alternating between top and bottom channel, and repeat once.
3. Rinse with PBS (without divalent cations) to flush out ethanol. Use 5 mL per channel each time, alternating between top and bottom channel, and repeat once.
4. Inject in protein coating solution (fibronectin (FN), 100 ug/mL, at least 200 uL per channel to be coated).
5. Incubate FN coating at room temperature (1 hr).
6. With 20 minutes left, prepare cells into suspension by trypsinization (0.05% trypsin with EDTA, 5 minutes), centrifugation (1150 rpm, 7 minutes), and resuspension into 500,000 cells/mL.
7. After the 1-hr FN incubation is completed, flush out FN solution on top channel and the remaining PBS solution in the bottom channel with M199 supplemented media. Use 0.5 mL media and flush out at a flow rate of ~1 mL/min.
8. Inject in cell suspension, 200 uL, in top channel.
9. Incubate cells for 6 hrs to allow for attachment and spreading. Check cell viability every 2 hrs.
10. Start perfusion of cells with syringe pump, at a flow rate of 30 ul/hr (0.5 ul/min). This corresponds to a shear of 0.03 dyn/cm^2, which should be negligibly small and not induce any shear stress-related cellular responses.

NOTE: During the entire channel preparation and cell seeding procedure, it is critical to ensure that bubbles are not generated. Bubbles can be inoculated into the channel during rinsing steps as needles are inserted and removed repeatedly. Bubbles left in the device during the procedure have the potential to expand during incubation, leading to possible cell loss and cell death. The purpose of the 100% ethanol in the first rinse is to reduce the likelihood of trapping bubbles, which may occur when a fluid with lower wetting properties (i.e. 70% ethanol or PBS) is injected into the air-filled PDMS device to start.